METROLOGY OF MERCURY MEASUREMENTS IN THE AIR

Jan Gačnik

Doctoral Dissertation
Jožef Stefan International Postgraduate School
Ljubljana, Slovenia

Supervisor: Asst. Prof. Jože Kotnik, Jožef Stefan Institute and Jožef Stefan International Postgraduate School, Ljubljana, Slovenia
Co-Supervisor: Prof. Dr. Milena Horvat, Jožef Stefan Institute and Jožef Stefan International Postgraduate School, Ljubljana, Slovenia

Evaluation Board:
Doc. Dr. Marko Štrok, Chair, Jožef Stefan Institute and Jožef Stefan International Postgraduate School, Ljubljana, Slovenia, Ljubljana, Slovenia
Prof. Dr. Uroš Cvelbar, Member, Jožef Stefan Institute and Jožef Stefan International Postgraduate School, Ljubljana, Slovenia
Dr. Warren Corns, Member, P S Analytical Ltd., Orpington, Kent, United Kingdom

MEDNARODNA PODIPLOMSKA ŠOLA JOŽEFA STEFANA
JOŽEF STEFAN INTERNATIONAL POSTGRADUATE SCHOOL

Jan Gačnik

METROLOGY OF MERCURY MEASUREMENTS IN THE AIR

Doctoral Dissertation

METROLOGIJA DOLOČANJA ŽIVEGA SREBRA V ZRAKU

Doktorska disertacija

Supervisor: Asst. Prof. Jože Kotnik

Co-Supervisor: Prof. Dr. Milena Horvat

Ljubljana, Slovenia, September 2022

"Everyone thinks of changing the world, but no one thinks of changing it himself."

— *Lev Nikolayevich Tolstoy*

Acknowledgments

First of all, I would like to thank my mentors Asst. Prof. Dr. Jože Kotnik and Prof. Dr. Milena Horvat for their supervision. They helped me with their advice, knowledge, experience and motivation when problems arose. They also taught me perseverance and careful analytical thinking, which is necessary for fruitful work in the field of analytical chemistry.

I am grateful to the members of the committee for the evaluation of the doctoral dissertation Doc. Dr. Marko Štrok, Prof. Dr. Uroš Cvelbar and Dr. Warren Corns for their valuable input in the shape of comments and corrections, which improved the quality of this thesis.

A good atmosphere at the workplace of the Department of Environmental Sciences, Jožef Stefan Institute was maintained by many colleagues, I thank them all. I would especially like to thank all the coworkers of the Inorganic Biogeochemistry group. I had the privilege of working with some great people in the mercury analysis laboratories, namely: Vesna Fajon, Dr. Ermira Begu, Dr. Igor Živković, Dr. Raghuraj Singh Chouhan, Dr. Ajda Trdin, Sabina Berisha, Adna Alilović, Polona Klemenčič, Saeed Waqar Ali, Sreekanth Vijayakumaran Nair, Teodor Daniel Andron and Dominik Božič. In the radiochemistry laboratories, I worked with colleagues who also helped me in one way or another: Asst. Prof. Dr. Radojko Jaćimović, Asst. Prof. Dr. Ljudmila Benedik and Klaudia Block-Łaszewska.

I would also like to thank the staff of the TRIGA reactor at the Reactor Infrastructure Centre of the Jožef Stefan Institute for their availability and cooperation. Those 12-hour sample irradiations were never a burden to you.

This research has been financially supported by: project no. 16ENV01 MercOx which has received funding from the EMPIR program co-financed by the Participating States and from the European Union's Horizon 2020 research and innovation program; project no. 689443 Integrated Global Observing Systems for Persistent Pollutants (IGOSP) funded by the European Commission in the framework of the program "The European network for observing our changing planet (ERA-PLANET)"; project no. 860497 GMOS-Train, which has received funding from the European Union's Horizon 2020 research and innovation program under the Marie Sklodowska-Curie; Slovenian Research Agency (ARRS), grant numbers P1-0143 and PR-52044.

Brez prijateljev bi bil čas doktorskega študija mnogo manj razgiban. Na tem mestu bi se rad zahvalil vsem prijateljem, predvsem pa prijateljski klapi "Dečki" – dolgotrajnim prijateljem s tradicijo.

Na koncu bi se rad zahvalil družini: mama Saša, pokojni oče Roman, brat Luka, stari starši ter ostala družina. Nikoli nisem niti za trenutek pomislil, da ne bi imel vaše popolne podpore pri mojem doktorskem delu, kar mi je bila ogromna opora.

Abstract

Atmospheric mercury (Hg) plays an important role in the biogeochemical Hg cycle. Hg species in the atmosphere are present in very low concentrations. While gaseous elemental mercury (GEM) is relatively inert, gaseous oxidized (GOM) and particulate-bound (PBM) mercury are highly reactive. These characteristics of atmospheric Hg species make the speciation measurements challenging, and instruments measuring atmospheric Hg species have been shown to be subject to bias and uncertainty. Most of the challenges originate from the sampling and calibration of the measurement instrumentation. Different sampling and calibration methods exist for atmospheric Hg, but their validation is often lacking or non-existent at ambient concentration levels. Additionally, the results obtained by different methods are commonly not comparable due to the lack of measurement traceability and uncertainty evaluation.

Traceability of GEM calibration has previously been established, though researchers still often use non-traceable GEM calibrations. Our first objective was to compare three different GEM calibration approaches: primary gas standard, calibration via reference material, and bell-jar calibration. The first two calibrations were traceable to the International System of Units (SI) and gave comparable results, while the latter calibration was not traceable to SI and gave statistically different results. Bell-jar calibration was shown to give 8% underestimated results compared to the SI traceable primary gas standard.

Sampling and calibration are the most challenging for reactive Hg species: GOM and PBM. Our second objective was to validate GOM sampling with KCl sorbent traps and KCl impinging solutions and an evaporative calibrator for GOM; validation was focused on ambient GOM concentration levels. Validation experiments at ambient concentration levels were mostly performed with the ^{197}Hg radiotracer. The results showed that KCl sorbent traps are feasible for ambient GOM sampling, showing low Hg^{II} losses (under 5%) and high specificity (negligible retention of Hg^{0}) under simulated sampling conditions. On the other hand, KCl impinging solutions were found to be unsuitable for ambient GOM sampling due to low specificity originating from Hg^{0} solubility and oxidation in the solution. The evaporative calibrator was not accurate and precise; its Hg^{II} output was concentration- and time-dependent; near-ambient Hg^{II} concentrations were the most problematic due to Hg^{II} adsorption. At the lowest $HgCl_2$ concentration tested (5.90 ng m^{-3}), the calibrator recovery (accuracy measure) was as low as 39.4%.

The results indicated that new GOM calibration methods are needed for ambient GOM concentrations. In our final work, we developed a calibration approach based on nonthermal plasma (NTP) oxidation of Hg^{0} to Hg^{II} species in the presence of a reaction gas. Validation work was done using the ^{197}Hg radiotracer. The obtained oxidation efficiencies with the corresponding expanded standard uncertainty values were 100.5 ± 4.7% (k = 2) for 100 pg of HgO, 96.8 ± 7.3% (k = 2) for 250 pg of $HgCl_2$, and 77.3 ± 9.4% (k = 2) for 250 pg of $HgBr_2$. The presence of each species was confirmed by temperature-programmed desorption quadrupole mass spectrometry (TPD-QMS). Since mercury analyzers detect mercury in

elemental form, we thermally reduced the produced Hg^{II} species to Hg^0. The quantitative thermal reduction was achieved with the Al_2O_3 catalyst.

The ^{197}Hg radiotracer was successfully applied for our work and was used for the first time for studies of atmospheric Hg. Radiotracer has been shown to be a more suitable validation tool than stable isotopes and isotope dilution methods due to its unique characteristics that allow validation for reactive Hg species at ambient concentration levels.

Povzetek

Atmosfersko živo srebro (Hg) ima pomembno vlogo v biogeokemičnem Hg ciklu. Specije Hg so v atmosferi prisotne v zelo nizkih koncentracijah. Medtem ko je plinasto elementarno živo srebro (GEM) relativno inertno, sta plinasto oksidirano živo srebro (GOM) in živo srebro, vezano na delce (PBM), zelo reaktivna. Zaradi teh značilnosti atmosferskih Hg specij so meritve speciacije zahtevne in dokazano je, da so instrumenti za merjenje atmosferskih Hg specij podvrženi pristranskosti in negotovosti. Večina izzivov izvira iz vzorčenja in kalibracije merilnih instrumentov. Obstajajo različne metode vzorčenja in umerjanja za atmosfersko Hg, vendar je njihova validacija pogosto pomanjkljiva ali sploh ne obstaja na ravneh koncentracije v okolju. Poleg tega rezultati, pridobljeni z različnimi metodami, običajno niso primerljivi zaradi pomanjkanja sledljivosti meritev in ocene merske negotovosti.

Sledljivost kalibracije za GEM je bila že vzpostavljena, a raziskovalci še vedno pogosto uporabljajo GEM kalibracije, ki niso sledljive. Naš prvi cilj je bil primerjati tri različne pristope za kalibracijo GEM: primarni plinski standard, kalibracijo prek referenčnega materiala in kalibracijo s t. i. "bell-jar" kalibratorjem. Prvi dve kalibraciji sta bili sledljivi do Mednarodnega sistema enot (SI) in sta dali primerljive rezultate, medtem ko slednja ni bila sledljiva do SI in je dala statistično različne rezultate. Pokazalo se je, da je bell-jar kalibracija dala 8 % podcenjene rezultate v primerjavi s SI sledljivim primarnim plinskim standardom.

Vzorčenje in kalibracija sta najzahtevnejša za reaktivne vrste Hg: GOM in PBM. Naš drugi cilj je bil validirati vzorčenje GOM s pastmi iz KCl sorbentov in raztopinami KCl ter evaporativni kalibrator za GOM; validacija je bila osredotočena na koncentracije GOM v okolju. Validacijski poskusi pri koncentraciji GOM v okolju so bili večinoma izvedeni s ^{197}Hg radioaktivnim sledilcem. Rezultati so pokazali, da so pasti iz KCl sorbentov primerne za vzorčenje GOM v okolju, saj kažejo nizke izgube Hg^{II} (pod 5 %) in visoko specifičnost (zanemarljivo zadrževanje Hg^0) v simuliranih pogojih vzorčenja. Po drugi strani pa je bilo ugotovljeno, da so raztopine KCl neprimerne za vzorčenje GOM v okolju zaradi nizke specifičnosti, ki izvira iz topnosti in oksidacije Hg^0 v raztopini. Evaporativni kalibrator ni bil točen in natančen, izhodna koncentracija Hg^{II} iz kalibratorja je bila odvisna od koncentracije in časa; koncentracije Hg^{II} v bližini koncentracijskih nivojev v okolju so bile najbolj problematične zaradi adsorpcije Hg^{II}. Pri najnižji testirani koncentraciji $HgCl_2$ (5,90 ng m^{-3}) je bil izkoristek kalibratorja (mera točnosti) le 39,4 %.

Zgoraj omenjeni rezultati so pokazali, da so potrebne nove metode umerjanja GOM za koncentracije GOM v okolju. V našem zaključnem delu smo razvili kalibracijski pristop, ki temelji na oksidaciji Hg^0 v Hg^{II} specije s pomočjo »netermalne plazme« (NTP) v prisotnosti reakcijskega plina. Validacijsko delo je bilo opravljeno z uporabo ^{197}Hg radioaktivnega sledilca. Dobljeni oksidacijski izkoristki s pripadajočimi razširjenimi standardnimi negotovostmi so bili 100,5 ± 4,7 % (k = 2) za 100 pg HgO, 96,8 ± 7,3 % (k = 2) za 250 pg $HgCl_2$ in 77,3 ± 9,4 % (k = 2) za 250 pg $HgBr_2$. Prisotnost vsake specije je bila potrjena s temperaturno programirano desorpcijo, povezano s kvadrupolno masno spektrometrijo (TPD-QMS). Ker analizatorji živega srebra zaznavajo živo srebro v elementarni obliki, smo

proizvedene Hg^{II} specije termično reducirali do Hg0. Kvantitativno termično redukcijo smo dosegli z Al_2O_3 katalizatorjem.

^{197}Hg radioaktivni sledilec je bil uspešno uporabljen v našem delu in se je nasploh prvič uporabil za atmosferske študije Hg. Izkazal se je kot primernejše validacijsko orodje od stabilnih izotopov in metod izotopskega redčenja zaradi svojih edinstvenih značilnosti, ki omogočajo validacijo za reaktivne zvrsti Hg pri ravneh koncentracije v okolju.

Contents

List of Figures

Abbreviations

AC	... activated carbon
AMDEs	... atmospheric mercury depletion events
APCI-MS	... atmospheric pressure chemical ionization-mass spectrometry
CEM	... cation exchange membrane
CRM	... certified reference material
CVAAS	... cold-vapor atomic absorption spectrometry
CVAFS	... cold-vapor atomic fluorescence spectrometry
DGM	... dissolved gaseous mercury
DOC	... dissolved organic carbon
DFT	... density functional theory
EPA	... Environmental Protection Agency
EPRI	... Electric Power Research Institute
GC-MS	... gas chromatography-mass spectrometry
GEM	... gaseous elemental mercury
GOM	... gaseous oxidized mercury
Hg	... mercury
Hg^{0}	... gaseous elemental mercury
Hg^{II}	... gaseous oxidized mercury
Hg-p	... particulate-bound mercury
ICP-MS	... inductively-coupled plasma-mass spectrometry
ID-ICP-MS	... isotope-dilution inductively-coupled plasma-mass spectrometry
IPS	... International Postgraduate School
JSI	... Jožef Stefan Institute
LOD	... limit of detection
MeHg	... methylmercury
MESA	... mercury speciation absorption method
MS	... mass spectrometry
NIST	... National Institute of Standards and Technology
NPL	... National Physics Laboratory
NTP	... nonthermal plasma
PBM	... particulate-bound mercury
RMAS	... Reno-Reactive Mercury Active System
RM	... reactive mercury
SI	... International System of Units
SRM	... standard reference material
TAM	... total atmospheric mercury
TGM	... total gaseous mercury
TPD-QMS	... temperature-programmed desorption quadrupole mass spectrometry
U.S. EPA	... United States Environmental Protection Agency
VSL	... Van Swinden Laboratory

Chapter 1

Introduction

Mercury (Hg) is a naturally occurring element that has been used in many applications for centuries. Human activities have led to a steady increase in Hg concentrations in the environment in recent decades. Due to its elevated concentrations and exposure to health risks, Hg is nowadays widely regarded as a pollutant of global concern. Therefore, the knowledge of the global Hg cycle is crucial for mitigating human impact and enforcing appropriate legislation (UN Environment, 2019). The biogeochemical Hg cycle begins with the emission of Hg into the atmosphere, where it exists in three main operationally defined species: gaseous elemental (Hg^0, GEM), gaseous oxidized (HgII, GOM) and particulate-bound (Hg-p, PBM) mercury. The fate of emitted species depends on their atmospheric lifetime: GEM persists in the atmosphere long enough for global transport before deposition, while GOM and PBM with short atmospheric lifetimes are deposited locally (Seth N. Lyman, Cheng, et al., 2020). Through deposition, Hg enters aquatic and terrestrial ecosystems, where it can enter the food web. The species of greatest concern in terms of entering the food web is methylmercury (MeHg) due to its bioaccumulation and neurotoxicity (UN Environment, 2019).

Although aquatic and terrestrial environments are where most of the neurotoxic MeHg is formed, the source of major perturbance to the natural Hg cycle comes from anthropogenic Hg emissions to the atmosphere. Anthropogenic Hg is most commonly emitted from fuel combustion, followed by processes such as cement and metal production. Due to the elevated Hg emissions, the slow natural process of sediment and soil burial does not have sufficient Hg removal capacity to counteract the increased Hg concentrations (Selin, 2009). The importance of atmospheric Hg is well recognized, but its species, reactions, transformations and deposition (shown in Figure 1.1) are still not well understood. Knowledge gaps often stem from the lack of adequate metrological infrastructure for atmospheric Hg speciation. Problems with the metrology of atmospheric Hg species have been highlighted by a number of scientific papers and authors. Most problems were found at the sampling/preconcentration (M. S. Gustin et al., 2015; Seth N. Lyman, Cheng, et al., 2020; Lynam & Keeler, 2002; McClure et al., 2014) or calibration (Dumarey et al., 2010; M. Gustin & Jaffe, 2010; Huber et al., 2006) of analytical procedures. Therefore, the focus of this thesis was on improving the metrology of atmospheric Hg and its speciation.

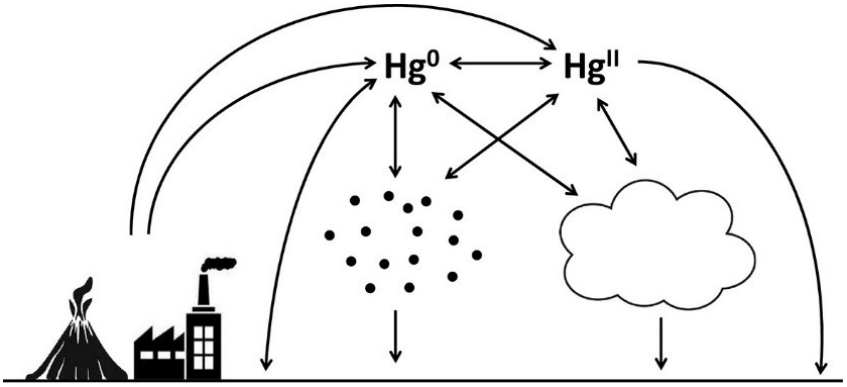

Figure 1.1: Atmospheric mercury and its diverse transformation and deposition pathways, through which Hg enters the terrestrial and aquatic systems. Adapted from Lyman et al., 2020.

First, we investigated calibration for GEM at different concentration levels and using different calibration approaches. Concentration levels ranging from ambient (2 ng m^{-3}) to emission (1 µg m^{-3}) concentrations were tested for SI-traceable calibration, calibration based on reference material, and calibration based on an empirical equation. The results are available in our article entitled "Comparability of calibration strategies for measuring mercury concentrations in gas emission sources and the atmosphere" (De Krom et al., 2021). Since most of the problems related to atmospheric Hg speciation are connected with GOM and PBM rather than GEM, the rest of our work was focused on GOM metrology. We began by investigating a promising commercially available calibration unit for GOM. Its performance was evaluated from the standpoint of validity and measurement uncertainty with emphasis on the use of concentration levels close to ambient concentrations. The results are presented in our article "Validating an Evaporative Calibrator for Gaseous Oxidized Mercury" (Gačnik, Živković, Ribeiro Guevara, Jaćimović, Kotnik, & Horvat, 2021). Since GOM sampling methods are known to introduce bias into the atmospheric Hg speciation measurements (Huang & Gustin, 2015a), we also tested sampling methods for GOM speciation. The GOM sampling methods tested in our work have not been previously reviewed, particularly for ambient air sampling. The results are summarized in our article "Behaviour of KCl sorbent traps and KCl trapping solutions used for atmospheric mercury speciation: stability and specificity" (Gačnik, Živković, Ribeiro Guevara, Jaćimović, Kotnik, De Feo, et al., 2021). Finally, we tried to solve the issues related to GOM calibration by developing a new calibration method. Repeatable amounts of Hg^{II} species (HgO, $HgCl_2$ and $HgBr_2$) were produced by oxidation of a known amount of Hg^0 using a nonthermal plasma in the presence of trace amounts of the reaction gas. The novel procedure and its potential for traceable GOM calibration are described in our work "Calibration Approach for Gaseous Oxidized Mercury Based on Nonthermal Plasma Oxidation of Elemental Mercury" (Gačnik et al., 2022).

The structure of the thesis will be presented in the following sequential order: the article on GEM calibration approaches in Section 0, followed by articles focused on the validation and performance of the commercially available GOM calibration (Section 3.2) and GOM sampling (Section 3.3). Since the article on our development of a novel GOM calibration was a product of knowledge gained from our previous work on the metrology of atmospheric Hg speciation, it is presented last in Section 0.

1.1 Atmospheric Mercury

Mercury is emitted to the atmosphere from natural and anthropogenic sources in the form of operationally defined GEM, GOM and PBM. Even though this is the commonly used division of species in the literature, the actual chemical composition of GOM and PBM remains unknown and subject to debate. Experimental observations using thermal desorption (Huang et al., 2017), studies of atmospheric mercury depletion events (Steffen et al., 2010) and modelling (Holmes et al., 2010; Holmes et al., 2009) indicate the presence of $HgCl_2$, $HgBr_2$, and to a lesser extent HgO and other species (e.g. mixed mercury halides and oxo complexes), but there is no universally accepted composition of GOM and PBM. The most abundant atmospheric Hg species is GEM, which comprises more than 95% of Hg in ambient air. It is relatively inert, which allows it to be transported over long distances. In contrast, GOM and PBM represent highly reactive species that are deposited locally rather than globally. Because GOM and PBM differ from GEM in their reactivity and characteristics, they are often considered together as reactive mercury (RM) (Ariya et al., 2015a). Organic species such as dimethyl mercury may be present in the atmosphere, but have not been experimentally confirmed and discussed as often as other species due to their rather short-lived nature due to rapid oxidation (Schroeder & Munthe, 1998). In the atmosphere, Hg undergoes a number of chemical and physical processes, which will be described in the following subsections.

Mercury enters the atmosphere through emission, undergoes chemical and physical interactions, and exits the atmosphere through a deposition. Therefore, the next subsections will be devoted to describing atmospheric Hg processes in the same sequence.

1.1.1 Mercury emission and reemission

Hg emissions are of natural or anthropogenic origin and can be further divided into primary and secondary emission sources. Primary emission sources transfer Hg from the lithosphere to the atmosphere, while secondary emission sources represent the reemission of Hg that was previously deposited to surface reservoirs (aquatic and terrestrial environments). While primary emissions increase the global Hg pool, secondary emissions serve as an exchange of Hg between the surface reservoirs and the atmosphere (Driscoll et al., 2013).

Natural sources of Hg emissions are volcanoes and geothermal sources, while the largest anthropogenic sources of Hg emissions originate from the combustion of fossil fuels (e.g. coal and biomass), ferrous and non-ferrous metal production, municipal waste incinerators, cement plants, chemical production plants (Pirrone et al., 2010), and artisanal-scale gold minining (Veiga et al., 2014). China is the largest contributor to anthropogenic emissions in the world due to the large extent of fossil fuel combustion resulting from its dramatic industrial growth (Fu et al., 2015). In general, anthropogenic activity contributing to Hg emissions is greater in the Northern Hemisphere than in the Southern Hemisphere. The combination of anthropogenic activity in the Northern Hemisphere and limited air exchange between the two hemispheres results in higher Hg concentrations in the Northern Hemisphere than in the Southern Hemisphere (Driscoll et al., 2013). Nevertheless, recent research in mountainous areas of South America suggests that a certain degree of air mass mixing between the hemispheres is possible (Koenig et al., 2022).

Secondary emission or re-emission results from Hg evasion from surface water, land, and vegetation. Model results showed that the majority of present-day Hg deposition is actually re-emitted surface Hg of anthropogenic origin, highlighting the importance of secondary emissions (Helen M. Amos et al., 2013). Re-emission of Hg to the atmosphere undergoes in the elemental form of Hg (GEM). The starting point for Hg re-emission from the surface water is the photochemical (Saiz-Lopez et al., 2018) and biotic (Lamborg et al.,

2021) reduction of divalent Hg forms to dissolved gaseous mercury (DGM) (Živković et al., 2022). Once DGM is produced, it can be emitted to the atmosphere. Similarly, mercury in soil and vegetation is reduced to elemental mercury before re-emission. Reduction in soil depends on Hg concentration, soil temperature, moisture, redox potential, and organic matter (C. D. Holmes et al., 2010; C. J. Lin et al., 2010; Moore & Castro, 2012). Reduction in vegetation is mostly due to photochemical reduction of divalent Hg complexes in leaves (Y. Liu et al., 2021; Yuan et al., 2019), though evidence of non-photochemical reduction at night has also been presented in the literature. However, the cause of the non-photochemical reduction and nocturnal evasion of Hg is still not known. In general, re-emission of Hg from vegetation depends on plant species and activities, atmospheric Hg concentration, and meteorological conditions (e.g. temperature, solar irradiation and relative humidity) (Y. Liu et al., 2021).

1.1.2 Chemical and physical interactions

The complexity of the processes that Hg undergoes in the atmosphere is shown in **Error! Reference source not found.**. Redox processes, partitioning between different phases, and adsorption/desorption have all been identified as processes affecting atmospheric Hg chemistry, but uncertainties remain for many of these processes, particularly those highlighted by the red text in **Error! Reference source not found.** (Si & Ariya, 2018). Compared to the illustration in the work of Si & Ariya (2018), we added the gas phase reduction of Hg^{II} due to the fact that more recent work demonstrated its importance (de Foy et al., 2016; Saiz-Lopez et al., 2018, 2019).

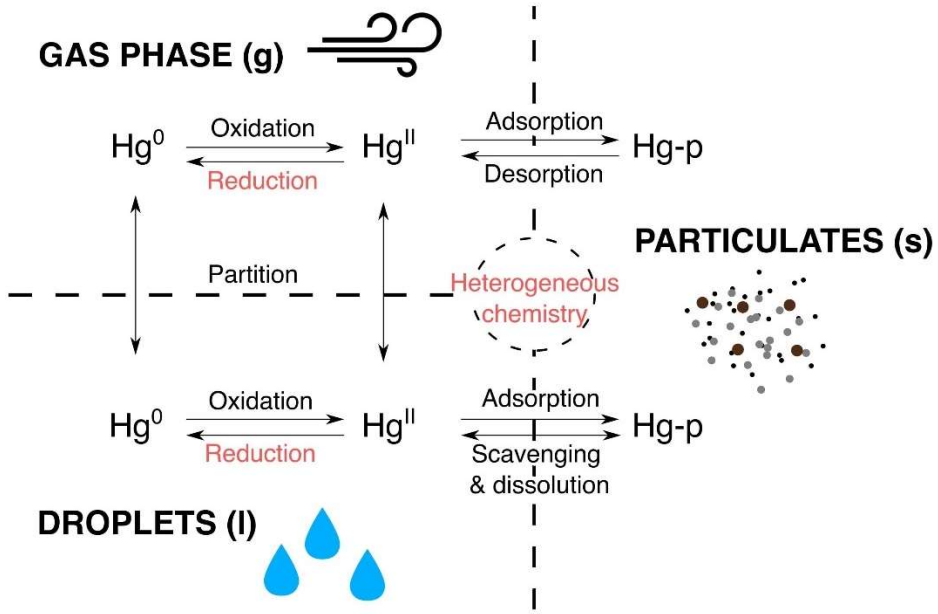

Figure 1.2: Complex chemical and physical interactions of atmospheric Hg. Red text indicates significant knowledge gaps. Adapted and modified from Si & Ariya (2018).

1.1.2.1 Gas phase redox processes

The gas phase oxidation of elemental mercury dictates its lifetime in the atmosphere since it serves as a mercury sink. The oxidation product of Hg^0, Hg^{II}, is water-soluble and can be deposited. As deposition is the exit of mercury from the atmosphere, the conversion of

Hg^0 to Hg^{II} and the knowledge of the conversion mechanism play a crucial role in understanding the biogeochemical Hg cycle (Seth N. Lyman, Cheng, et al., 2020).

In the field of atmospheric mercury redox chemistry, the accepted opinion regarding the predominant mechanism for Hg^0 to Hg^{II} oxidation has changed in recent decades. The once presumed dominant mechanism driven by ozone (O_3) (Engle et al., 2005; Sprovieri et al., 2005) and hydroxyl (OH) radical (Pal & Ariya, 2004) has been replaced by the halogen radical (chlorine and bromine) driven oxidation (Schmidt et al., 2016). The first evidence of oxidation initiated by halogen radicals was observed in atmospheric mercury depletion events (AMDEs) in polar regions (Ralf Ebinghaus et al., 2002; Lindberg et al., 2002; Sprovieri et al., 2005). Hg^0 concentrations were found to decrease significantly after the polar sunrise. During AMDEs, Hg^0 and O_3 concentrations were correlated – decreasing simultaneously. The reason for the depletion came from the oxidation of Hg^0 to Hg^{II} species by Br/Cl and BrO/ClO radicals. Though more evidence points towards oxidation mechanisms involving bromine, mechanisms involving chlorine and other complex and mixed oxo complexes have never been ruled out (Steffen et al., 2010). As in the Arctic, reactive halogen species (Laurier et al., 2003), most commonly Br (Yu et al., 2020), are thought to be the dominant oxidant for Hg^0 in the marine boundary layer. The marine boundary layer is a large reaction vessel for atmospheric mercury due to aerosols and high relative humidity, sunlight, and atmospheric oxidants (UN Environment, 2019). A common theme seems to be that although the prevalent oxidation mechanisms have been demonstrated in various experimental works and models, the dominant oxidants driving the Hg^0 oxidation are highly dependent on the altitude (atmospheric layer), region, and time of the day in question. Bieser et al. (2017) studied the effect of changing altitude on the composition of atmospheric Hg. The findings show that even though oxidation by Br is dominant in the upper troposphere, models cannot reproduce the experimental results in the lower troposphere without including OH and O_3 chemistry (Bieser et al., 2017). Similarly, recent atmospheric mercury models as well as stable isotope studies mostly incorporate both O_3/OH and halogen pathways for Hg^0 oxidation (Travnikov et al., 2017; Yu et al., 2020). Regional variability of dominant oxidation was demonstrated by comparing results obtained from marine, coastal, and inland areas (Ye et al., 2016). While at the marine site, the Hg^0 oxidation was dominated by Br, at the coastal and inland sites the oxidation was dominated by OH and O_3. Additionally, the authors attributed the diurnal variation of Hg^{II} concentration to changes in the dominant oxidation pathway (Ye et al., 2016). Articles focusing on the oxidants Br/Cl and O_3/OH are in the vast majority, but other oxidants such as hydrogen peroxide (H_2O_2) (Ye et al., 2016) and nitrite (NO_3) (Peleg et al., 2015) radicals were also proposed. These two radicals are especially important in the second step of the two-stage oxidation of Hg^0, where the first step is oxidation to HgBr (Horowitz et al., 2017).

Evidence for the opposite reaction, the gas phase reduction of Hg^{II} to Hg^0, was also theoretically confirmed. In their work, Saiz-Lopez et al. (2018) showed that photochemically induced reduction of Hg^{II} can significantly alter atmospheric Hg dynamics (Saiz-Lopez et al., 2018). Moreover, the same can be said for the reduction of monovalent mercury (Hg^I) to Hg^0, as recent work has shown that HgBr radicals can undergo photoreduction to Hg^0. In general, the reduction of Hg^{II}/Hg^I leads to an extended lifetime of atmospheric mercury and should be considered in addition to the Hg^0 oxidation (Saiz-Lopez et al., 2019). De Foy et al. (2016) performed field measurements in remote Tibet and found that their results are best reproduced by theoretical models when gas phase photoreduction of Hg^{II} is included.

In summary, the above examples illustrate how the generalization and notion of only one global atmospheric Hg^0 oxidation pathway is questionable. There are too many influencing factors such as seasonality, diurnal variations, vertical variability, and other

regional influences to treat Hg^0 oxidation uniformly across the planet. Br radicals might dictate the oxidation at the marine boundary level, upper troposphere, and polar regions, but this might not be the case at the continental boundary level and lower troposphere, where O_3 and OH radicals become important. Another factor that contributes to the uncertainty of redox pathways are the highly uncertain kinetics of chemical reactions (Seth N. Lyman, Cheng, et al., 2020). Also, the conditions under which the kinetic parameters were experimentally obtained are often not comparable to real atmospheric conditions (e.g. experimentally used Hg concentrations that are orders of magnitude higher than ambient Hg concentrations) (Ariya et al., 2015b; Subir et al., 2011).

1.1.2.2 Aqueous phase redox processes

In the category of aqueous phase redox processes we will take into account the research that was done on aerosols, clouds, and fog. Even though aerosols, clouds, and fog represent the aqueous phase, surfaces exist there. Consequently, the studies that include surface chemistry will be discussed under heterogeneous processes (Section 1.1.2.3) rather than in this subsection.

Oxidation of Hg^0 in the aqueous phase can potentially proceed via O_3 and OH radicals, similar to the gas phase oxidation (Gårdfeldt et al., 2001; John Munthe, 1992). In contrast to gas phase oxidation, aqueous Br is not believed to be the predominant oxidant of Hg^0 due to small kinetic rate constants (Z. Wang & Pehkonen, 2004). Aqueous Cl ($HOCl/OCl^-$) showed the potential to oxidize Hg^0, especially when the pH of atmospheric droplets is relatively high (above 5.0). Such conditions are realistic at night in the marine troposphere (C. Lin & Pehkonen, 1998). Hg^0 has poor solubility and high volatility, making it less susceptible to aqueous scavenging. Nonetheless, aqueous phase Hg^0 oxidation rates are higher than gas phase Hg^0 oxidation rates, indicating that aqueous oxidation should not be neglected and should be incorporated into atmospheric models (Subir et al., 2011).

More data are available on the aqueous reduction of Hg^{II} than on the aqueous oxidation of Hg^0. The reported reduction pathways can be divided into sulphite-driven reduction and photoreduction. The reduction of Hg^{II} by sulfite is believed to be an important process for atmospheric droplets. Such reduction can occur in the pH of 1-7 (Feinberg et al., 2015; Van Loon et al., 2000) and is independent of the composition of aqueous Hg^{II} species (Feinberg et al., 2015). Photoreduction of Hg^{II} as a consequence of HO_2 radical was previously reported (Pehkonen & Lin, 1998), but the same reduction mechanism was later shown to be unlikely under normal environmental conditions (Gårdfeldt & Jonsson, 2003). The emphasis in the identification of the photoreduction mechanism was shifted to organic compounds. Dicarboxylic acids and alkanethiols have been investigated for the photoreduction of Hg^{II} (Bash et al., 2014; Si & Ariya, 2011). A model using dicarboxylic acid photoreduction mechanisms better described the empirical results than using the HO_2 radical mechanism (Bash et al., 2014). In addition to dicarboxylic acids, Hg^{II} photoreduction by alkanethiols has been shown to be a plausible aqueous phase reduction mechanism. The photoreduction was mediated by the formation of organic Hg^{II}-thiol complexes (Si & Ariya, 2011). Recently, Yang et al. (2019) investigated the photoreduction of Hg^{II} in rainwater in the presence of halides and dissolved organic carbon (DOC). Even though halides form stable aqueous complexes, their work on equilibrium calculations showed that Hg^{II} forms Hg^{II}-DOC complexes rather than Hg-halide complexes after partitioning into aerosols. The reduction of Hg^{II}-DOC was observed, but it was too slow to be relevant. Additionally, halides have been shown to inhibit Hg^{II}-DOC reduction (Yang et al., 2019). There is some disagreement as to whether photoreduction of Hg^{II} occurs in the aqueous or gas phase. Saiz-Lopez et al. (2018) demonstrated that rainwater irradiation

experiments did not support aqueous phase Hg^0 reduction. In response to research showing the opposite results, the authors argued that data obtained from experiments conducted on aquatic systems are not applicable to atmospheric water (Saiz-Lopez et al., 2018).

1.1.2.3 Heterogeneous processes

Encyclopaedia Britannica defines heterogeneous reactions as "any of a class of chemical reactions in which the reactants are components of two or more phases (solid and gas, solid and liquid, two immiscible liquids) or in which one or more reactants undergo a chemical change at an interface" (Britanica, 1998). Although the definition is straightforward, the boundary between homogenous or heterogeneous processes in atmospheric mercury chemistry is often blurred. This is due to the fact that it is often difficult to distinguish whether a particular reaction pathway takes place in the gas/aqueous/particulate phase or in fact on the surfaces between these phases. The importance of heterogeneous processes was first highlighted in the review articles by Subir et al. (2012) and Ariya et al. (2015a), though some experimental work that indicated the presence of heterogeneous chemistry had been done prior to that (Calvert & Lindberg, 2005; Engle et al., 2005). The heterogeneous chemistry of atmospheric Hg begins with the adsorption of mercury species on atmospheric surfaces. After adsorption, mercury species may desorb, dissolve, or undergo surface-enhanced reactions. Because of their large surface area, aerosols are commonly used as examples of atmospheric surfaces. An aerosol is defined as "sol (a colloidal fluid system of two or more components) in which the dispersed phase is a solid, a liquid or a mixture of both and the continuous phase is a gas (usually air)" (IUPAC, 1997). Understanding the surface chemistry of Hg is complicated due to the large number of parameters that can influence aerosols (i.e. concentration, size distribution and meteorological conditions) (Si & Ariya, 2018). In the following paragraphs, the heterogeneous redox processes are discussed first, followed by gas-particle phase partitioning processes.

Initial work on heterogeneous redox processes focused on heterogeneous oxidation pathways. Calvert & Lindberg (2005) hypothesised that the oxidation of Hg^0 by O_3 can be heterogeneous and that the oxidation end-products can be dictated by aerosol composition (Calvert & Lindberg, 2005). Later, the hypothesis was confirmed experimentally by simulating atmospheric conditions in a reaction chamber. Using a reaction chamber, the authors observed oxidation of Hg^0 in the presence of organic aerosols (A. P. Rutter et al., 2012). The reverse redox process, reduction of Hg^{II}, was studied by Tong et al. (2013, 2014). The authors used a controlled laboratory reactor to study the heterogeneous reduction of Hg^{II}. Firstly, they examined the role of light (dark, UV, visible, and simulated solar radiation) and the composition of NaCl (changing the presence of iron complexes). Rather than the wavelength of light, the irradiance (power) of the light source was found to be the factor influencing the reduction of Hg^{II}. For the aerosol composition, Fe(III) showed the strongest inhibition of Hg^{II} reduction, most likely due to its ability to scavenge the available electrons that are required for Hg^{II} reduction (Tong et al., 2013). Secondly, they examined the influence of native fly ash composition (low/high carbon/sulfate content) and synthetic aerosol composition (analogous to fly ash substrates), again under different lighting conditions. In contrast to their first study, the authors found some statistically significant dependence of Hg^{II} reduction on the wavelength of light. Aerosol composition affected the Hg^{II} reduction rates: low carbon/sulfate content exhibited the fastest reduction rates among native fly ash aerosols (Tong et al., 2014). Further work on the heterogeneous Hg^{II} reduction was done by Deng et al. (2019), who demonstrated that the reduction is driven by light, positively correlated (promoted) with increased aerosol water content, and

negatively correlated (inhibited) with the presence of oxidative metal ions (Deng et al., 2019). Complementary to experimental data, work has been done using computational methods to elucidate the mechanism of heterogeneous Hg^{II} reduction (Tacey et al., 2016, 2018). Using density functional theory (DFT) calculations, the authors investigated the reduction pathways for different Hg^{II} species on iron and sodium chloride surfaces. The results indicated that many Hg^{II} species could be reduced to Hg^0 on iron and sodium chloride surfaces, though the connection to the effect of light and photochemistry was not clear (Tacey et al., 2016). The role of photons in the reduction mechanism was further looked into for the example of an environmentally relevant iron oxide surface: α-$Fe_2O_3(0001)$. Based on DFT calculations, photons play a role in the breaking of the Hg-X bond (X=Cl/Br) and in the desorption of the produced Hg^0 from the aerosol surface. However, in addition to photon energy, thermal energy assistance is required to enable bond breaking steps (Tacey et al., 2018). Overall, the increased amount of work on the heterogeneous Hg^{II} reduction in recent years demonstrates that this process should not be neglected in future models for atmospheric mercury cycling.

Gas-particulate partition is the consequence of the sorption processes of mercury to particles. Since adsorption of Hg^0 is assumed to be negligible, partitioning occurs mostly for Hg^{II} species (Seth N. Lyman, Cheng, et al., 2020). Amos et al. (2012) also studied gas-particle partitioning and showed that in cold environments with high aerosol levels, more than 90% of Hg^{II} was in the particulate fraction. In cold environments, less than 10% of Hg^{II} was in the particulate fraction (H. M. Amos et al., 2012). Similarly, the temperature dependence of Hg^{II} partitioning was observed at a majority of the sampling locations of the Atmospheric Mercury Network sites in North America (I. Cheng & Zhang, 2017). Gas-particle partitioning ratios have also been used as an indicator of local or regional Hg origin (G. S. Lee et al., 2016). In addition to the temperature dependence, the composition of aerosols also dictates their Hg chemistry. A study that used synthetic aerosols with different compositions showed that the chemical composition of the aerosol had a significant impact on the gas-particle partitioning of Hg^{II}. Aerosols containing $NaNO_3$, KCl and NaCl caused Hg^{II} to partition towards the particulate phase, while $(NH_4)_2SO_4$ and organic levoglucosan/adipic acid caused Hg^{II} to partition towards the gas phase (Andrew P. Rutter & Schauer, 2007). Malcolm et al. (2009) used denuders coated with KCl and NaCl for partitioning studies simulating the behaviour of sea salt aerosols. Both KCl- and NaCl-coated denuders retained similar Hg^{II} amounts, indicating that sea salt aerosols are effective scavengers of atmospheric Hg^{II} (Malcolm et al., 2009). Mao et al. (2021) used $(NH_4)_2SO_4$ and NH_4NO_3 to represent fine urban aerosols, while they used NaCl and Na_2SO_4 to represent sea salt aerosols in their Hg^{II} partitioning experiments. The authors used Hg^{II} uptake coefficients to estimate the reactivity of aerosol surfaces. Simulated sea salt aerosols were found to be more reactive than urban aerosols, with the highest Hg^{II} uptakes (N. Mao et al., 2021). In addition to the gas-particle phase partitioning, the presence of the aqueous phase can alter the partitioning of Hg species. After Mao et al. (2021) exposed dry surfaces to high relative humidity, the uptake of Hg^{II} increased due to the newly formed aqueous phase. Holmes et al. (2009) showed theoretically that Hg^{II} above the ocean partitions into sea salt aerosols rather than into the gas phase. With this, the authors concluded that sea salt aerosols are responsible for 95% of the rapid losses of Hg^{II} in the marine-boundary layer. The processes that can occur after uptake of Hg^{II} into the aqueous phase of aerosols are described in Section 1.1.2.2.

1.1.3 Mercury deposition

Mercury deposition is a major sink of atmospheric Hg, transferring Hg from the atmospheric reservoir to terrestrial and aquatic environments. There are two pathways for Hg deposition: dry and wet deposition. While a wet deposition is mostly associated with the deposition of oxidized and particulate-bound Hg species (Seth N. Lyman, Cheng, et al., 2020), all atmospheric Hg species can be deposited by dry deposition (Enrico et al., 2016).

1.1.3.1 Mercury wet deposition

Methods for evaluating wet deposition of mercury are generally simpler than those for dry deposition of mercury. Most commonly, Hg wet deposition is assessed by collecting precipitation and analyzing it using well-established spectrometric methods (X. Zhang et al., 2012).

Globally, the extent of wet deposition varies and is greater in the Northern Hemisphere and lower in the Southern Hemisphere and the Arctic (Sprovieri et al., 2017). Recent wet deposition data suggests that global wet deposition of Hg is decreasing (Y. Tang et al., 2018). The decrease is most likely due to the improved emission controls and the phase-out of commercial Hg products, leading to a decrease in anthropogenic Hg emissions (Y. Zhang et al., 2016). In the work of Weiss-Penzias et al. (2016), the concentration of SO_4^- in precipitation was used as an indicator of the level of anthropogenic emissions. Since the trends of analyzed Hg and SO_4^- in precipitation showed a temporal decrease in their concentration, this confirmed the linkage between the decrease in Hg wet precipitation and the decrease of anthropogenic emissions (Weiss-Penzias et al., 2016). Regionally, there are differences between urban and rural locations; wet Hg deposition tends to be higher in urban than rural sampling sites (Lynam et al., 2016; Zhou et al., 2018). Large variability in the amount of wet Hg deposition may indicate strong local influences from emissions (Lynam et al., 2016). Some researchers (Brunke et al., 2016; Zhou et al., 2018) observed a correlation between high total gaseous mercury concentration and elevated wet Hg deposition, while others did not (H. Mao et al., 2017). This suggests that Hg^{II} concentration could be a better predictor of Hg wet deposition (Bu et al., 2018).

In addition to global and regional differences, Hg wet deposition varies with the amount of precipitation. An increase in the precipitation can lead to high Hg wet deposition. As high precipitation events often occur at similar time periods of the year, this also introduces a seasonal dependence of Hg wet deposition (Chen et al., 2018). Warm seasons generally have more precipitation, leading to high Hg wet deposition (Chen et al., 2018; Lynam et al., 2016). However, this is not the only factor affecting seasonality since the availability of Hg^{II} species (Lynam et al., 2016) and the greater Hg^{II} removal efficiency of rain relative to snow (White et al., 2013) also increase the warm-season Hg wet precipitation. In contrast, some wet deposition monitoring studies have shown high winter and spring Hg wet precipitation (Ahn et al., 2011), indicating that the seasonal behaviour of Hg wet precipitation cannot be generalized to all areas.

1.1.3.2 Mercury dry deposition

Dry deposition is thought to contribute significantly to the global Hg cycle, but its magnitude is difficult to assess due to slow deposition rates and reemission (Mae Sexauer Gustin, 2011). Hg dry deposition is usually estimated using micrometeorological approaches, dynamic gas flux chambers, and surrogate surface approaches (Paige Wright et al., 2016). Micrometeorological approaches measure the vertical gradient of Hg species and then use a theoretical relation to describe the air-surface exchange of Hg (Paige Wright

et al., 2016). Air-surface Hg flux can also be estimated by placing dynamic gas flux chambers (sometimes called gas exchange chambers) over the surface of interest. The difference in Hg concentration between the inlet and outlet air for the chamber is used to estimate the Hg dry deposition flux (Millhollen et al., 2006; Stamenkovic & Gustin, 2009). Approaches for Hg dry deposition measurement using surrogate surface approaches can be divided into i) water/solution-based surfaces (Marsik et al., 2007; Sakata & Marumoto, 2004), ii) filter-based surfaces (Lai et al., 2011), iii) membrane-based surfaces (Huang & Gustin, 2015b; Lai et al., 2011), and iv) turf-based surrogate surfaces (Hall et al., 2017; Lynam et al., 2015).

The fact that there is a broad array of methods used for the estimation of Hg dry deposition creates uncertainty and comparability issues, which is manifested in frequent disagreements between measured and modelled data. It is also hard to draw clear conclusions about the factors influencing Hg dry deposition (L. Zhang et al., 2019). Since Hg dry deposition occurs predominantly as Hg^0 (Paige Wright et al., 2016), the majority of data are available for Hg^0 rather than Hg^{II} and particulate-bound Hg. Hg^0 dry deposition depends on the soil and vegetation type and the Hg^0 concentration. Studies conducted for tundra (Obrist et al., 2017), peat bog system (Enrico et al., 2016), and forest canopies (Paige Wright et al., 2016) have shown that Hg^0 is indeed the prevailing form of Hg that undergoes dry deposition. As for the oceans, reemission of Hg strongly outweighs dry Hg deposition and is therefore not often discussed (Ariya et al., 2015a).

1.2 Atmospheric Mercury Measurement Techniques

In the early years of atmospheric Hg research, most sampling and analysis for atmospheric Hg was done for gaseous elemental mercury (GEM), without knowing about the existence of other forms. Indications that precipitation Hg concentrations could not be described by GEM solubility implied that other atmospheric Hg species must exist (Fitzgerald & Gill, 1979), which started the field of atmospheric Hg speciation (Mae Sexauer Gustin, Dunham-Cheatham, Huang, et al., 2021). The three major atmospheric Hg forms - GEM, GOM and PBM - are operationally defined. The actual composition of the species that make up GOM and PBM is unknown.

The paragraphs follow the sequential order as the atmospheric Hg speciation steps: atmospheric mercury sampling, secondary sample treatment, and mercury detection. Problems of atmospheric mercury measurements and improvement attempts will be discussed in Section 1.3.

1.2.1 Atmospheric mercury sampling

Firstly, mercury species must be collected from the air and accumulated in a suitable medium that is compatible with further sample analysis. Since Hg species are present in the atmosphere at very low concentrations (especially for GOM and PBM), a pre-concentration step is required to accumulate a sufficiently large quantity of the species. This is a mandatory step to obtain mercury quantities that are above the limit of detection.

1.2.1.1 TGM sampling

TGM can be sampled manually or by automated sampling methods. Manual collection of TGM is achieved by drawing air through different types of quartz traps filled with sorbent materials at a known and fixed flow rate. Most often, sorbent is a type of gold material. The main goal of different gold materials is to provide a large gold surface area for the

collection of Hg through amalgamation. This unique property of Hg to form amalgams with certain transition metals is exploited for TGM collection. Variations of gold materials include coiled gold wire, gold nanostructures and high surface-area substrate coated with gold. The decision for a specific variation of the gold material depends mainly on the mass of mercury that is expected to be collected. The gold-wire approach is mostly used for short collection times (<1 h), while high surface area gold-coated substrates are used when extended periods of sampling (over 1 week) are required (Pandey et al., 2011; United States Environmental Protection Agency (U.S. EPA), 1999). An alternative to gold sorbent materials are sorbents based on impregnated activated carbon (AC) (Electric Power Research Institute (EPRI), 2015; Živković et al., 2020). In contrast to gold materials, AC does not suffer from the passivation of surfaces and is more durable. AC is often used for the removal of GEM from flue gas (S. J. Lee et al., 2004; Presto & Granite, 2007), but can also be used to sample more challenging air matrices. Many other materials can be used as sorbents for TGM, but their development and application has so far been mostly oriented toward Hg removal from flue gases (W. Liu et al., 2019; Xie et al., 2013; H. Xu et al., 2015). Nonetheless, gold materials remain the most commonly used sorbents, especially for ambient air TGM sampling.

Additionally, automated methods can be used for TGM sampling. At the end of the last century, different commercially available units emerged on the market. We will discuss only the units that are still used for TGM analysis in recent studies: the Tekran 2537 analyzer, the PS Analytical (PSA) analyzer, the Gardis analyzer, and the Lumex Zeeman atomic absorption analyzer. Tekran 2537 is by far the most commonly used unit (Kamp et al., 2018; Karthik et al., 2017; Mason et al., 2017; Obrist et al., 2017; Spolaor et al., 2018). It uses pre-filtered air that is passed through two alternating gold traps that collect GEM. Mercury is analyzed by thermal desorption and cold-vapour atomic fluorescence spectrometry (CVAFS) measurement (Tekran Inc., 1998). The mercury analyzer developed by PSA can also be used for TGM measurements (Petrov et al., 2020; Sasmaz et al., 2012). The instrument uses gold-coated silica traps, thermal desorption and CVAFS detection, similar to the Tekran 2537. The Gardis instrument also uses gold amalgamation but detects Hg using cold-vapour atomic absorption (CVAAS) instead of CVAFS (Unagar et al., 2021; Urba et al., 1995). The Lumex mercury analyzer is the only listed analyzer that does not use preconcentration of TGM, but instead analyzes the air directly. The unit uses atomic absorption spectrometry and Zeeman correction for mercury detection (Kalinchuk et al., 2018; Sprovieri et al., 2016). Since the Lumex analyzer can operate without a power supply and is portable, it can be considered a sensor-based method (Pandey et al., 2011).

1.2.1.2 GOM sampling

In the initial works, GOM was sampled with a high-flow refluxing chamber (mist chamber). High flow rates (15-20 L min^{-1}) of air were passed through a nebulizer nozzle to produce a nebulized mist that absorbed and collected GOM. The droplets containing GOM were then drained into the scrubber solution, which was a 0.5% HCl solution (Stratton & Lindberg, 1995). This type of GOM sampling is no longer used, so we will focus on the three main methods for GOM sampling shown in Figure 1.3: denuders, sorbent designs, and impinging solutions (impingers).

Denuders are divided into two types: tubular and annular denuders. Tubular denuders are quartz tubes coated with KCl. Annular denuders consist of two tube fractions, one outer and one inner tube. The outer tube is coated with KCl from the inside and the inner tube from the outside. KCl coating is used to retain GOM from the ambient air. The denuder sampling system is heated to 45 °C to prevent vapour condensation (Pandey et al., 2011). The used airflow values can vary, but in general, tubular denuders are used with

1 L min^{-1}, while annular denuders can be used with as high as 10 L min^{-1} airflow. The high airflow (higher sampled mass of GOM) and easier secondary treatment of annular than tubular denuders (thermal conversion versus liquid extraction) favoured the use of annular denuders (J. Munthe et al., 2001). Landis et al. (2002) developed and characterized annular denuders for GOM sampling in their work. Manual and automated sampling for GOM was developed (Landis et al., 2002); the automated system became the most widely used GOM sampling method in the following decades (Duan et al., 2017; B. Liu et al., 2010; Moore & Castro, 2012; L. Xu et al., 2015).

Sorbent designs can be trivially divided into i) designs using sorbent membranes enclosed in filter assemblies and ii) designs using sorbent materials enclosed in quartz traps ("sorbent traps"). Early use of sorbent membranes was reported by Ebinghaus et al. (1999) who used cation exchange membranes (CEM) and BrCl digestion to determine GOM in ambient air. More recently, the use of sorbent membranes has been promoted by the works of Mae Gustin and colleagues in their laboratories (Mae Sexauer Gustin et al., 2019; Mae Sexauer Gustin, Dunham-Cheatham, Zhang, et al., 2021; Huang & Gustin, 2015b). They have investigated the use of cation-exchange membranes, nylon membranes and other membrane materials (anion exchange, polyethersulfone, and polycarbonate materials) for GOM sampling (Dunham-Cheatham et al., 2020). Nylon membranes and especially cation exchange membranes remain the most commonly used membrane materials.

In contrast to sorbent membranes, sorbent trap materials for selective GOM sampling have so far only been applied for sampling high concentrations of GOM in flue gases. Sorbent materials for sorbent traps are most commonly based on KCl. Guidelines for speciated mercury measurements from the Electric Power Research Institute suggest the use of KCl crystal (Electric Power Research Institute (EPRI), 2015), while the Mercury Speciation Adsorption (MESA) method suggests the use of KCl impregnated soda lime sorbent (Prestbo & Bloom, 1995). Alternative sorbent materials were suggested by Tang et al. (2017) who evaluated selective adsorption characteristics of CaO, MgO, NaCl, and KCl surfaces using theoretical DFT calculations. They suggested that CaO might be the most prominent tested material for capturing GOM due to its predicted selectivity for $HgCl_2$ (H. Tang et al., 2017). The theoretical studies were further investigated with experimental tests for CaO sorbents. CaO synthesized via acetate monohydrate precursor (CaO-AcS) showed the most favourable results in terms of selectivity and adsorption capacity for $HgCl_2$ (H. Tang et al., 2019). Švehla et al. (2019) tested quartz wool, SiC and raw aluminium oxide for flue gas GOM sampling. Raw aluminium oxide showed the best GOM retention, though all materials also retained a significant amount of GEM. Interestingly, even just an empty tube retained around 80% of GOM, which indicates the strong adsorption properties of GOM (Švehla et al., 2019). Though many new sorbent materials are emerging, all of the above materials have so far been used only for flue gas GOM concentrations: work on the evaluation of sorbent traps for ambient GOM sampling is still needed.

Impinging solutions (impingers, also sometimes called "bubblers") were first introduced by Ontario Hydro Technologies in 1994, and the method for Hg species determination is called Ontario Hydro (OH) method (ASTM International, 2008). In 2004, EPA recognized the OH method as suitable for Hg speciation for flue gases from coal-fired sources (Ryan & Keeney, 2004). The method is based on the use of a number of impinging solutions. The number of impingers and solutions used as impinging solutions depends on the intended use. Modifications of the OH method that use up to 8 have been used in the literature (ASTM International, 2008). Initially, impingers that selectively capture GOM typically included 10% H_2O_2 in 5% HNO_3 (United States Environmental Protection Agency (U.S. EPA), 1996), but this impinging solution was later found to be insufficiently selective for GOM. 10% H_2O_2 in 5% HNO_3 solution was replaced by KCl solutions of different molarities,

which showed better selectivity. Following GOM selective impingers, $KMnO_4$ impingers are often used to capture GEM. The capturing system is usually completed with additional impingers that capture moisture and neutralize unwanted flue gasses, if necessary (Ippolito et al., 2011).

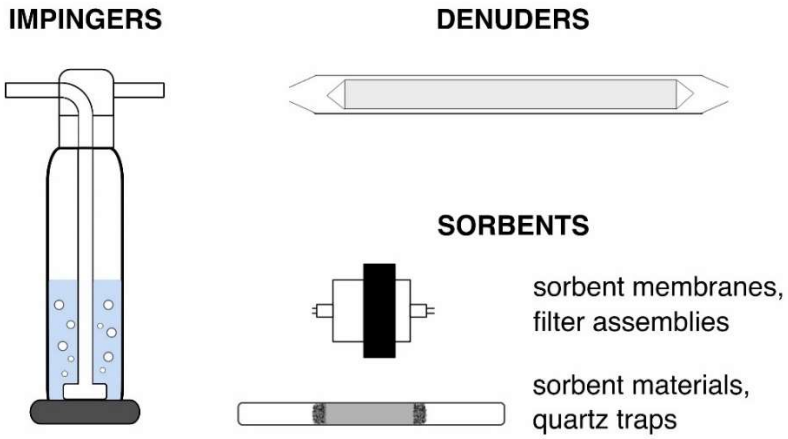

Figure 1.3: Illustration of the commonly used gaseous oxidized mercury sampling methods that include denuders, impingers and different sorbent designs.

1.2.1.3 PBM sampling

As was also the case for GOM, large volumes of air must be sampled through the collection material to ensure a sufficient amount of PBM for further sample processing. The methods usually consist of an accumulation media, a gas-flow control device, and a vacuum pump (Pandey et al., 2011). The accumulation medium can be a filter or a multiple-stage impactor. The most commonly used PBM sampling method are filters, which can be quartz-fiber, cellulose-acetate, glass-fibre and Teflon filters. Quartz-fiber filters are used for automated PBM sampling in the widely used Tekran speciation unit (Landis et al., 2002). PBM on filters can be digested by wet chemical methods or thermally reduced to Hg^0 before further analysis (Hui Zhang et al., 2019). Multiple-stage impactors sample PBM by particle size and can estimate the size distribution of PBM (Feddersen et al., 2012). Less commonly, gold-coated denuders are also used for PBM sampling (Lu & Schroeder, 1999).

In general, PBM sampling is one of the most challenging aspects of atmospheric Hg speciation. Problems arise in the effective separation of GOM and PBM, since both have adsorptive properties and behave very similarly. GOM and PBM are often considered together as reactive mercury (RM) precisely because of their similar behaviour. Issues related to PBM sampling will be discussed further in Section 1.3.1.

1.2.2 Secondary sample treatment

Mercury can be quantitatively detected by conventional detection methods only as elemental Hg (detection methods discussed in Section 1.2.3). Consequently, additional sample treatment is needed for GOM and PBM analysis to convert these species to the elemental form of mercury. Two main approaches are used for secondary sample treatment: wet acid digestion and thermo-reductive methods.

The wet acid digestion approach involves the use of a combination of acids and oxidants (including HCl, H_2SO_4, HNO_3, and the oxidants H_2O_2 and BrCl) and high temperature/microwaves. The exact combination of acids and conditions used varies with the sampling medium. For example, the Ontario Hydro method uses HNO_3 and H_2O_2 in

combination with conventional or microwave heating for the digestion of the GOM fraction in impinging solutions (ASTM International, 2008). Cation exchange membranes for GOM sampling are digested using BrCl, following the U.S. EPA method 1631 E (Huang et al., 2013; U.S. Environmental Protection Agency, 2002). The same procedure is also used for PTFE membranes used for PBM sampling (Mae Sexauer Gustin et al., 2019). In general, many filter- and membrane-based sampling methods for GOM and PBM use some form of wet digestion (Hui Zhang et al., 2019), though this is not the case for all materials (i.e. silica, nylon membranes, quartz filters) . Sorbent traps for flue gas Hg speciation in the MESA method were initially also wet-digested with acids (Prestbo & Bloom, 1995), although thermal reduction is nowadays the preferred choice (Electric Power Research Institute (EPRI), 2015; Živković et al., 2020). After digestion, the mercury in the solution is generally reduced to elemental mercury by $SnCl_2$ in a step often called the cold-vapour procedure. Elemental mercury is purged from the solution and can then be detected (Horvat et al., 1991). The wet digestion method is time-consuming, tedious and carries the risk of mercury loss through volatilization. It is also common to further dilute the resulting solution before the analysis, which lowers the sensitivity of the method (Pandey et al., 2011).

Thermo-reductive methods employ high temperatures (>500 °C) to reduce all mercury species to the elemental form, followed by conventional detection methods. Thermal reduction is commonly used for the secondary treatment of GOM captured by denuders and PBM captured by quartz filters in the automated atmospheric Hg speciation unit developed by Tekran (Landis et al., 2002). Additionally, qualitative analysis of oxidized mercury species captured on nylon membranes can be done by thermal desorption and subsequent spectrometric detection (Dunham-Cheatham et al., 2020). Hg on sorbent traps for mercury speciation in flue gases is also most commonly thermally reduced (Electric Power Research Institute (EPRI), 2015; Stergaršek et al., 2008; H. Zhang et al., 2015; Živković et al., 2020), though as previously stated, wet digestion can also be used if necessary (C. M. Cheng et al., 2009; Prestbo & Bloom, 1995). Thermal reduction is a faster and simpler alternative to the wet-digestion procedure, which also eliminates the possibility of contamination and generation of hazardous waste. Nevertheless, thermo-reductive methods can sometimes lead to lower (Lynam & Keeler, 2002) or higher (C. M. Cheng et al., 2009) yields compared to reference methods, likely due to the effects of matrix interferences that can affect the amalgamation process (Lynam & Keeler, 2002).

1.2.3 Detection of mercury

In this subsection, we review in detail the detection methods that are commonly used to date (CVAAS, CVAFS and mass spectrometry), while only briefly discussing less common detection methods.

1.2.3.1 Cold vapour atomic absorption/flouresence spectrometry

Of all mercury detection techniques, cold vapour atomic absorption spectrometry and cold vapour atomic fluorescence spectrometry are the most widely used techniques. The first use of CVAAS for mercury detection was reported back in 1964 (Poluektov et al., 1964). While CVAAS methods use the absorption of light by the target analyte and subsequent measurement of absorbance, CVAFS methods measure the emitted radiation of the excited mercury atoms as they return to their ground state – this radiation process is called fluorescence (Pandey et al., 2011). Figure 1.4 depicts a simplified scheme of the CVAAS and CVAFS instruments. In these instruments, the Hg^0 vapor obtained by the previously described processes (Section 1.2.2) is then transported to the detection cell. For Hg

determination, the CVAAS instrument measures absorbance at a wavelength of 253.7 nm, while the CVAFS instrument measures the emitted fluorescence at the same wavelength (Leopold et al., 2010). A comparison of the limits of detection (LODs) shows that CVAFS is advantageous to CVAAS (and also to the spectrometric methods discussed in the next paragraph), achieving up to one order of magnitude lower LOD values (Lasorsa et al., 2012). Nevertheless, both methods were found to have sufficient LODs (in the low pg m^{-3} range) for mercury measurements under normal ambient conditions (K. H. Kim & Kim, 2002).

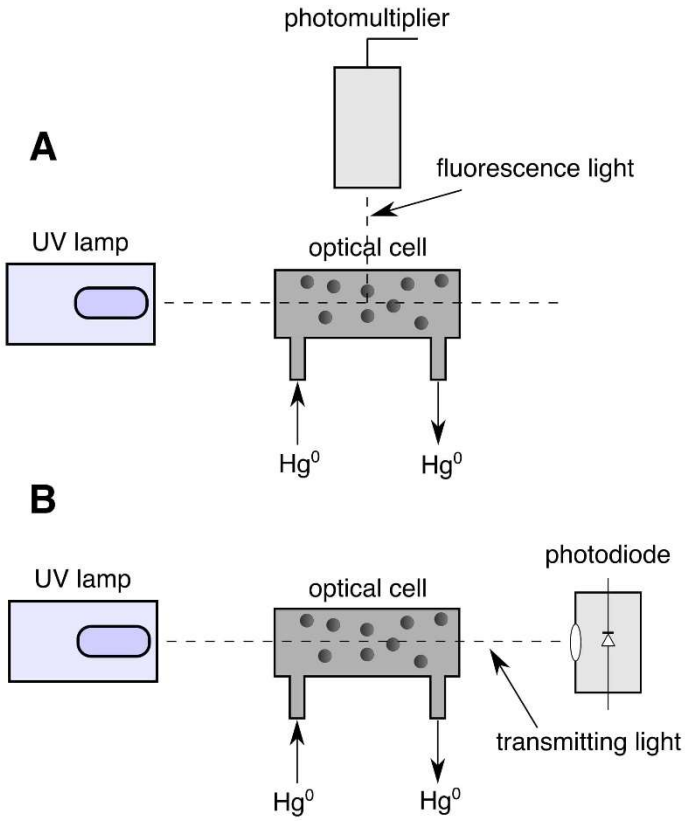

Figure 1.4: Simplified scheme of a) cold vapour atomic fluorescence spectrometry and b) cold vapour atomic absorbance spectrometry. Modified from: http://www.uwm.edu.pl (last access 4 July 2022).

1.2.3.2 Mass spectrometry

Mass spectrometry (MS) is also a viable detection method for atmospheric mercury, albeit used less frequently for airborne mercury than for other Hg-containing environmental matrices. Attempts to quantify atmospheric Hg species by MS are usually performed with inductively coupled plasma MS (ICP-MS). Amouroux et al. (1999) used gas chromatography (GC) coupled with ICP-MS to quantify atmospheric Hg^0. (Lynam et al., 2013) used isotope dilution and ICP-MS coupled with thermal desorption to quantify PBM. They achieved comparable results to conventional CVAFS detection (Lynam et al., 2013). Recent improvements in the sensitivity of mass spectrometric methods have led to an increasing number of attempts to analyze Hg^{II} species directly rather than by prior transformation of Hg species to Hg^0. Deeds et al. (2015) analyzed Hg^{II} species on particles by preconcentration and atmospheric pressure chemical ionization-mass spectrometry (APCI-MS). Using ACPI-MS, $HgCl_2$ and $HgBr_2$ species were identified in urban and indoor particulate mercury, though low temporal resolution and unwanted ion reactions limited

their work (Deeds et al., 2015). An improved APCI-MS methodology was also used for analysis and identification of Hg^{II} nanoparticles (Ghoshdastidar et al., 2020; Ghoshdastidar & Ariya, 2019). Gas chromatography coupled with mass spectrometry (GC-MS) was used by Jones et al. (2016) for the separation and identification of Hg^{II} species in ambient air. While mercury halides were successfully identified, this was not the case for other Hg^{II} species, such as $Hg(NO_3)_2$ and HgO (Jones et al., 2016).

1.2.3.3 Other detection methods

In the past, nuclear methods for the analysis of atmospheric mercury were mainly used for Hg bound to filter materials. Of nuclear methods, neutron activation analysis (Dams, 1992) and particle-included X-ray emission (Hacon et al., 1995) have been the most useful. Due to the higher LODs obtained with the aforementioned nuclear methods, these are used less commonly than CVAAS and CVAFS techniques for atmospheric Hg analysis (Pandey et al., 2011). Sensor-based atmospheric Hg detection methods have been available for a long time (Scheide & Taylor, 1975) but are not yet widely used. Sensor methods include piezoelectric sensors (Scheide & Taylor, 1975), nanomaterial-based sensors (Macagnano et al., 2017), coated printed circuit board sensors (Mazzolai et al., 2004), cavity ring-down spectrometry (Faïn et al., 2010), and more.

1.2.4 Stable and radioactive isotopes as validation tools

Due to the absence of certified reference material for airborne Hg species, measurement methodology is often validated using stable and radioactive isotopes as tracers. Stable Hg isotopes are also used to decipher the origin of atmospheric mercury and to trace Hg transformation processes that may occur in the atmosphere, but we will only discuss the use of stable isotopes as a validation tool.

Work with stable isotopes for validation of Hg measurement methodology typically relies on the use of isotope dilution and ICP-MS detection. These methods use mercury enriched in a certain stable isotope (i.e. ^{202}Hg) with a known isotopic composition. The enriched Hg material is then "diluted" with Hg from the sample (the isotopic composition is also known) and thus the amount of Hg from the sample can be determined. Isotope dilution ICP-MS has previously been successfully applied for validation of GEM calibrators (Long, Norris, Carney, Ryan, et al., 2020; Quétel et al., 2014, 2016). However, these validations were not performed at ambient GEM levels due to the high detection limits of the isotope dilution ICP-MS validation technique.

Radioactive Hg isotopes also show promise as validation tools, though they have not been used for atmospheric Hg studies so far. Their use was limited to the aquatic (Bratkič et al., 2017; Koron et al., 2012) and terrestrial part of the Hg cycle (Pérez Catán et al., 2007; Ribeiro Guevara et al., 2007). Since radioactive Hg isotopes do not occur naturally, they must be produced by irradiating natural Hg with neutrons. Irradiation is usually carried out with thermal neutrons in the nuclear reactor core. During irradiation, ^{197}Hg and ^{203}Hg are the most important produced radioisotopes due to their high specific activity and characteristic energy of emitted radiation. ^{197}Hg and ^{203}Hg are formed by the neutron capture reaction from ^{196}Hg and ^{202}Hg, respectively. The combination of the very favourable reaction of ^{196}Hg with neutrons and the use of ^{196}Hg-enriched elemental Hg (51.58 % of ^{196}Hg) enables low detection limits, fitting for ambient Hg concentration studies. Therefore, the ^{197}Hg radioisotope is more commonly used for validation studies than the ^{203}Hg radioisotope. Both radioisotopes and their characteristic radiation energies are detected by high-purity germanium detectors (Ribeiro Guevara et al., 2004; Ribeiro Guevara & Horvat, 2013). In comparison to stable isotopes and isotope dilution, radioactive isotopes have

certain advantages, such as: lower detection limits, straightforward detection methods, and the absence of blanks (no naturally occurring Hg radioisotopes). The most obvious disadvantage of radioisotopes is that they can only be produced with a nuclear reactor, which is often unavailable to researchers.

1.3 Metrological Difficulties

1.3.1 Atmospheric Hg species sampling

Sampling is likely the largest source of bias and uncertainty for atmospheric Hg speciation. Regarding GEM measurements, there is some debate about what is actually being sampled: GEM or TGM (GEM+GOM) or TAM (GEM+GOM+PBM). The conventional Tekran 2537 instrument is believed to measure TGM (Mae Sexauer Gustin et al., 2013). The same is true for the PSA 10.525 Sir Galahad, since both instruments operate on a similar principle, using a filter that removes particulates (Corns et al., 2009). TAM measurement requires a pyrolizer at the sample inlet, so that GOM and PBM both are converted to GEM (M. S. Gustin et al., 2015).

The majority of the uncertainty and bias in atmospheric Hg sampling comes from GOM and PBM sampling. Denuders for GOM sampling, which are widely used for automated GOM sampling, have been shown to be biased by underestimating GOM (Huang et al., 2013; McClure et al., 2014). Experimental work was conducted to study the effect of humidity (Huang & Gustin, 2015a; McClure et al., 2014) and ozone (S. N. Lyman et al., 2010; McClure et al., 2014) on the GOM capture efficiency of KCl denuders. It was concluded that the capture efficiency of these denuders is greatly reduced under high humidity conditions. Using water vapour spikes, the collection efficiency of GOM on KCl denuders was very low, and the GEM concentrations were consequently enhanced. This finding clearly indicated that GOM can transform into GEM under high humidity conditions (Huang & Gustin, 2015a). Lyman et al. (2010) studied the effect of ozone on the release of mercury halides from KCl denuders. The authors showed that denuders loaded with $HgCl_2$ and $HgBr_2$ lost 29-55% of these compounds when exposed to ozone in the 12-200 $\mu g\ m^{-3}$ range. GOM losses were positively correlated with ozone concentration. Such losses could lead to an overestimation of GEM in the presence of ozone for sampling systems that measure GEM downstream of the KCl denuder, since oxidized mercury species can be carried over from the denuders to the GEM collection part of the sampler. Additionally, the need to establish a traceable and stable calibration method for various oxidized Hg compounds has been pointed out (S. N. Lyman et al., 2010). In addition to the evidence of biased negative results, recent work has shown that there is a possibility for positive bias due to the binding of Hg-containing nanoparticles, which could present an artefact for GOM measurement (Ghoshdastidar et al., 2020). Another potential source of bias in the Tekran atmospheric Hg speciation system was shown by Feng et al. (2003), who observed approximately 30% losses of GOM surrogate ($HgCl_2$) on the Tekran impactor which is designed to remove coarse particles.

Alternatives to GOM sampling with denuders have been explored in an attempt to reduce sampling bias. A comparison between KCl-coated denuders, nylon membranes and CEM was done by Huang & Gustin (2015a). Similar findings for the inverse dependence of GOM yields on humidity and ozone concentrations were found for nylon membranes as for KCl-coated denuders, while CEM showed positive artefacts with increasing humidity (Huang & Gustin, 2015a). Nylon membranes are nowadays used predominantly in connection with thermal desorption and qualitative analysis of Hg^{II} species, since it has been proven that nylon membranes do not bind Hg^{II} species quantitatively. CEM are used

for quantitative analysis of Hg^{II} (Dunham-Cheatham et al., 2020). A combination of qualitative (nylon membranes) and quantitative (CEM) analysis was incorporated in the Reno-Reactive Mercury Active System (RMAS) (Mae Sexauer Gustin et al., 2016). Though the RMAS method of measuring reactive mercury species (GOM+PBM) has recently been updated and improved, the temporal resolution is still in the range of 1-2 weeks (Luippold et al., 2020), which is much lower than the conventional denuder method used in the Tekran instrument. Also, secondary sample treatment of cation exchange membranes requires wet digestion, which is tedious. Though RM sampling with cation exchange membranes has been a step forward in terms of more precise and accurate measurements, further development of materials is needed to enable simplification, automation and better temporal resolution of RM measurements. As such, sorbent trap materials that are thermally stable and enable thermal reduction of atmospheric Hg^{II} species could represent a feasible solution. Bu et al. (2018) demonstrated that capture efficiency for real samples was similar for CEM and different KCl-coated quartz sorbent traps, while denuders again showed significantly lower capture efficiency. Nevertheless, the use of sorbent trap materials has so far been aimed mostly at flue gas Hg determination (Švehla et al., 2019; H. Tang et al., 2017, 2019).

PBM sampling in the Tekran speciation system was also associated with artefacts. Gustin et al. (2013) demonstrated that GOM can be retained on the Tekran quartz fiber filter designed to collect PBM. Talbot et al. (2011) compared a manual PBM sampling method that uses Teflon filters with the automated Tekran PBM sampling. They found that Tekran PBM was on average 20% lower than manually measured PBM (Talbot et al., 2011). Wang et al. (2013) used three ways PBM sampling with quartz fiber filters: an open-faced filter pack, a five-stage impactor, and a Tekran filter. Sampling methods did not behave similarly under all conditions. and artefacts were observed for all tested PBM sampling methods (S. Wang et al., 2013). Overall, accurate quantification of PBM has proven to be one of the most difficult tasks of atmospheric mercury speciation. Problems include: i) variations in the size and distribution of PBM due to meteorological conditions, adsorption, nucleation gas-particle partitioning, and other physical/chemical processes (P. R. Kim et al., 2012; Andrew P. Rutter & Schauer, 2007), ii) ultra-low PBM concentrations, iii) formation of artefacts during sampling (Malcolm & Keeler, 2007; S. Wang et al., 2013), and iv) losses of PBM during longer sampling periods (Malcolm & Keeler, 2007).

1.3.2 Atmospheric Hg species calibration

Challenges also stem from the calibration of the used instruments and the uncertainty of such calibration. GEM- and GOM-specific calibrations exist, while PBM-specific calibration does not; therefore, PBM calibration will not be discussed in the following subsections. This points towards the need for PBM-specific calibration of atmospheric Hg speciation measurements.

1.3.2.1 GEM calibration

In the last decades, the most commonly used GEM calibration unit has been the so-called "bell-jar", which is a glass calibration vessel that contains saturated Hg vapor. In the calibration vessel, liquid mercury is kept at atmospheric pressure and controlled temperature. The equation for calculating the concentration of saturated Hg vapour was formulated using the measured Hg headspace concentration at different temperatures. The Hg headspace concentration was measured against certified reserence materials (CRMs) and Hg vapour produced from reduction of aqueous phase Hg standards. However, the

origin and validation of the equation were published much later than it was used (Dumarey et al., 2010). The predominant empirical equation used for the calculation of the saturated mercury vapour concentration goes as follows:

$$\gamma(Hg) = \frac{D}{T} = 10^{-(A+\frac{B}{T})} \quad (1.3.2.1)$$

where: γ(Hg) is the mass concentration of saturated mercury in the air inside the calibration vessel, in ng mL^{-1}; T is the temperature of the air inside the calibration vessel, in K; A is a constant equal to −8.134459741; B is a constant equal to 3240.871534 K; D is a constant equal to 3216522.61 K ng mL^{-1}. The above equation (Eq. 1.3.2.1) is also called the "Dumarey" equation (Dumarey et al., 2010). Calibration using this equation is based on injecting a known volume of mercury-saturated gas after the development of saturated mercury atmosphere in a glass calibration vessel. It is stated that approximately 2% uncertainty should be associated with the Dumarey equation (Dumarey et al., 2010). In contrast, the National Institute of Science and Technology (NIST) published a new Hg vapour pressure curve which differs from the Dumarey equation by 7% (Huber et al., 2006). The conclusions were that the Dumarey equation gives the best predictions at 1 atm air pressure (Gustin, 2010). De Krom et al. (2021) observed a 3.8% difference between their GEM calibrator and the bell-jar calibration. R. J. C. Brown & A. S. Brown (2008) investigated bell-jar thermodynamics using Hg vapour injections ranging from 0 to 12 ng over a temperature range of −5 °C to 35 °C. The kinetics were studied by using perturbations (removal of a large volume of Hg-saturated air) to the bell-jar apparatus. The conclusions were that without the application of corrections, large biases can be observed between the expected and actual mass concentrations of Hg-saturated injected air. These biases were explained by the temperature difference between the syringe and the vapour in the bell-jar. Since many users cool the bell jar to reduce the headspace Hg concentration thereby allowing larger syringe injection volumes, there can be large differences in the temperature of the bell-jar vapour and syringe, which leads to biases. On the other hand, kinetic factors have been found to be negligible if long enough time periods are used to re-establish equilibrium. A number of best practise guidiles for bell-jar use have been published (R. J. C. Brown & Brown, 2008), but will not be discussed here in detail.

Ultimately, the bell-jar calibration is traceable to the Dumarey equation. There is often confusion and disagreements regarding the use of the appropriate empirical equation. To ensure stability, comparability, and coherence for mercury vapour measurements, different authors sought to establish System of Units (SI) traceability for these measurements. Those efforts are described in the following paragraph.

A. S. Brown et al. (2008) used a dynamic mercury generator to accumulate a larger amount of mercury to provide a sufficient mass of mercury for weighing with a high-accuracy balance. The mass output of the GEM generator was captured on the adsorption tubes, and the retained Hg was determined gravimetrically. Next, the authors dosed smaller masses of GEM from the generator and the bell-jar apparatus and compared the responses. Since the results were comparable, this demonstrated the traceability of the bell-jar output to SI units; the SI unit of traceability being mass. However, the results were associated with large uncertainties due to the delicate gravimetric process and the complex technical nature of the experiment (Brown et al., 2008). Similar work in terms of SI traceability to mass has been done by isotope-dilution ICP-MS (ID-ICP-MS) (Quétel et al., 2014). Known amounts of mercury vapor from the bell-jar were introduced into the CRM, which was a liquid solution enriched in the ^{202}Hg isotope. Using a combination of the ^{202}Hg-enriched liquid phase and the bell-jar GEM (with natural isotopic composition), isotope-dilution of CRM was achieved. The authors also presented the traceability routes for the entire

measurement procedure. The results had a low relative uncertainty (<3%, k = 2) and were not in agreement with the Dumarey equation. The discrepancy between the Dumarey equation and their work was similar to the results of Huber et al. (2006) (5.8% difference). A drawback was the lack of measurements at other temperatures since only room temperature measurements in the range of 20 °C to 21 °C were made (Quétel et al., 2014). Quétel et al. (2016) then used a modified experimental setup to expand the range of measurements to temperatures different from room temperature. The method was validated using different sample-to-spike ratios for isotope dilution experiments. Even though the experiments were successful, the authors observed Hg contamination from the ambient laboratory air and higher expanded uncertainties than in their previous work (5.9% compared to <3%), due to the temperature incubation chamber (Quétel et al., 2016). ID-ICP-MS was also used for traceable calibration of the GEM generator developed by the National Institute of Standards and Technology (NIST). First, ID-ICP-MS itself was calibrated with SI traceable NIST standard reference material (SRM) 3133, and then the NIST GEM generator was calibrated with ID-ICP-MS, extending the SI traceability chain to the GEM generator (Long, Norris, Carney, & Ryan, 2020). In accompanying work (Long, Norris, Carney, Ryan, et al., 2020), secondary GEM generators intended for real-time calibration were calibrated with the NIST GEM generator. Thus, it was demonstrated that traceable calibrations of real-time measurements are possible. Both works used GEM concentrations ranging from 0.5 to 40 µg m^{-3}, which is reasonable for flue gas Hg calibration but too high for ambient Hg concentration calibration. The authors suggested that an alternative robust laser absorption spectrometry (LAS) technique could simplify the calibration (Long, Norris, Carney, & Ryan, 2020; Long, Norris, Carney, Ryan, et al., 2020), and to that end, Srivastava & Hodges (2018) developed a new LAS technique. They used a high-resolution LAS method to achieve SI traceability for the NIST GEM generator. Traceability was achieved by modelling observations from first principles (ab initio) and from the overall low measurement uncertainty (Srivastava & Hodges, 2018). Finally, the ID-ICP-MS and LAS methods were compared: the agreement between the methods was good. LAS was less uncertain compared to ID-ICP-MS (0.4% vs. 0.9% relative combined standard uncertainty) for the tested GEM concentration range (41-287 µg m^{-3}) (Srivastava et al., 2021). Another realization of SI traceability via gravimetry was done with a mercury vapour generator based on an improved diffusion method (Ent et al., 2014). Up to 18 diffusion cells with characterized diffusion rates were filled with liquid Hg (approximately 80 g) and kept in the same housing, each of them surrounded by a similar nitrogen flow pattern. The combined Hg vapor flow from these cells was guided from the Hg vapor generator through the "roof" of the housing. Mass differences before and after the outlet of Hg were measured with a high-resolution mass comparator. Even though this system enabled very stable and low Hg vapor levels, traceability to SI units was insufficient due to the high uncertainty of the gravimetric process (Ent et al., 2014). The uncertainty of the mercury vapor generator was reduced by de Krom et al. (2021), who improved diffusion cells and used an advanced mercury loss weighing procedure. Relative expanded uncertainties (k=2) amounted to 3% for 0.1-2.1 µg m^{-3} of Hg and 1.8% for 5-100 µg m^{-3} of Hg (de Krom et al., 2021). It is worth noting that the concentration levels studied are still two orders of magnitude above the ambient Hg concentration.

1.3.2.2 GOM calibration

The calibration methods that were so far used for GOM calibration can be divided into two major groups: "wet-gas" and "dry-gas" calibration. Wet-gas calibration usually involves generation of humidified Hg^{II} gas by combining a nebulized aqueous Hg^{II} solution (commonly $HgCl_2$ or $HgBr_2$ solutions in acidic media) with a carrier gas (Saxholm et al.,

2020). Dry-gas calibrations principally use the permeation of solid Hg^{II} salts (commonly solid $HgCl_2$ or $HgBr_2$) (S. Lyman et al., 2016).

Schmäh (2007) patented a wet-gas calibration system (HovaCAL®, IAS GmbH) that generates a humidified gas from the chosen solution by vaporizing it and combining it with N_2 gas (or other instrument-grade gases). By precise measurements of the liquid and gas flow, the concentration of Hg^{II} in the output calibration gas can be calculated (Schmäh, 2007). The intended use of the HovaCAL unit is for the calibration of mercury continuous emission monitoring in flue gases (U.S. Environmental Protection Agency, 2017). The system requires very precise control of temperature and flowrate and is additionally prone to vibrations – all of which are difficult to control in field measurements. Moreover, impurities of Hg^0 are a known problem that introduces uncertainty to such calibration (Dunham et al., 2010). A wet-gas calibration system similar to HovaCAL was developed by Optoseven Ltd. and VTT Ltd., and was described by Saxholm et al. (2020). The authors claim that the characteristics of the calibration unit are fast response time, wide use of concentration ranges, and minimal adsorption of Hg^{II}. The unit has shown promise for traceable GOM calibration but has so far only been fully validated for use at high concentrations (>1 µg m^{-3}). Though some satisfactory linearity tests have been performed at near-ambient GOM concentrations (Petrov et al., 2020), this does not serve as a complete and sufficient validation of the calibration unit. Tekran also offers an oxidative gas generator (Tekran Model 3400-CAL, modified for $HgCl_2$ generation) that uses the Hg^0 output of the Tekran 3400-CAL and combines it with nebulized HCl solution to oxidize Hg^0 to $HgCl_2$. Again, the unit is only intended for calibration at flue gas GOM concentration (Tekran, n.d.).

The most common dry-gas methods for GOM calibration are permeation tube designs. A method for GOM generation using permeation tubes was first reported by Lyman et al. (2010), who modified the solid $HgCl_2$ permeation vial setup used by Swartzendruber et al., (2009) to generate HgX_2 (X=Cl/Br). Generally, solid HgX_2 is placed in a Teflon tube and capped with Teflon plugs. The permeability (sublimation) of HgX_2 is controlled by temperature or by adjusting the permeable area of the permeation tube (S. N. Lyman et al., 2010). After the initial use of permeation tubes for denuder validation tests (S. N. Lyman et al., 2010; McClure et al., 2014), attempts were also made to establish their use for GOM calibration. With the intent to use permeation tubes for GOM calibration, Lyman et al. (2016) developed a novel calibration unit for Hg atmospheric species using a special design of permeation oven. The permeation oven housed permeation tubes containing $HgCl_2$ and $HgBr_2$. Permeation rates were determined using a pyrolysis unit by converting all of these species to Hg^0 prior to CVAFS detection. The exhibited achieved stable permeation rates that were high enough to achieve gravimetric verification but also emitted relatively high amounts of Hg^0 simultaneously with $HgCl_2$ and $HgBr_2$. Therefore, an independent, traceable, and reliable source of Hg^{II} compounds was not completely achieved (S. Lyman et al., 2016). Characterization of the permeation tube output was attempted by gravimetry to achieve SI traceability, but gravimetric results were highly variable not in agreement with results from GOM analyzers (Seth N. Lyman, Gratz, et al., 2020). Dry-gas calibration was also introduced by Thermo Fisher Scientific, who developed a Mercury Chloride Generator (Oxidizer) that generates $HgCl_2$ by mixing Cl_2 gas with Hg^0 to produce $HgCl_2$. For the Cl_2 source, the unit uses a gas cylinder (900 ppm of Cl_2 in N_2), while the Hg^0 comes from their own Model 81i elemental Hg generator (Thermo Fisher Scientific, 2014). No report on the validation work of the Thermo Fisher Scientific generator is available in the literature.

Chapter 2

Aims and Hypothesis

Atmospheric mercury speciation is crucial to ensure better understanding of the processes that govern the biogeochemical Hg cycle. Knowledge of such processes is often limited by the highly uncertain and biased measurements of atmospheric Hg species. In this thesis, we first wanted to examine whether the currently used sampling and calibration methods for atmospheric Hg speciation are sufficiently accurate and precise. Furthermore, we aimed to contribute to the analytical infrastructure of atmospheric Hg measurements by developing new or improved sampling and calibration methods.

Hg species are present in the atmosphere in very low concentrations, which is especially true for GOM and PBM. We hypothesized that the tested sampling and calibration methods might behave differently if examined under different meteorological conditions and concentration levels. We assumed that the use of the ^{197}Hg radiotracer would enable experiments at ambient concentration levels, as it was previously shown that the radiotracer is highly selective and sensitive (Ribeiro Guevara et al., 2007). Since the current metrological infrastructure for atmospheric Hg speciation is known to be unreliable and inaccurate (Jaffe et al., 2014), we wanted to test new methods for GOM sampling and calibration. These include GOM sampling using sorbent trap designs or impinging solutions (not previously tested for ambient concentrations) and calibration based on nonthermal plasma oxidation of elemental Hg to Hg^{II} species. By developing new sampling and calibration methods, we intended to establish the foundation for SI traceable speciated measurements of atmospheric Hg. Only clear statements of measurement uncertainty can demonstrate traceability, so we aimed to thoroughly evaluate the measurement uncertainty of the developed methods.

Hypotheses:

i) ^{197}Hg radiotracer can enable validation of existing calibrations and sampling procedures at ambient Hg concentration levels.
ii) Losses and interconversions of Hg species during atmospheric sampling are largely dependent on sampling and atmospheric conditions.
iii) Evaporative calibrator is not suitable for calibrations at ambient Hg concentrations.
iv) Quantitative oxidation of elemental Hg by non-thermal plasma provides a good basis for the development of SI traceable calibration for GOM and enables lower measurement uncertainty as compared to conventional calibration techniques.
v) Evaporative calibrators and non-thermal plasma calibration are suitable for loading sorbent traps with Hg^{II} of known isotopic composition, which can then be used to calibrate stable isotope measurements of Hg^{II} species in the atmosphere.

Chapter 2

Scientific Publications

This dissertation consists of four publications. The order in which they are presented is chronological and follows the general content of the dissertation. The first publication compares different GEM calibration strategies (0). The second (3.2) and third (3.3) publications focus on the evaluation of existing calibration and sampling methods for GOM, respectively. The last publication is a result of work on the development of a novel GOM calibration approach (0).

3.1 Manuscript 1: Comparability of Calibration Strategies for Measuring Mercury Concentrations in Gas Emission Sources and the Atmosphere

De Krom I., Bavius W., Ziel R., McGhee E. A., Brown R. J. C, Živković I., Gačnik J., Fajon V., Kotnik J., Horvat M., Ent H. (2021). Atmospheric Measurement Techniques, 14, 2317-2326.

The most wide-spread calibration for gaseous elemental mercury in recent decades has been the bell-jar calibration. Calibration works on the principle of Hg^0 vapor saturation. The concentration of Hg^0 vapor that is drawn from the bell-jar for calibration is calculated using an equation that describes the dependence of Hg^0 vapor on temperature. Since the used equations in the liteture are empirical, there are disagreements about which equation is correct (Huber et al., 2006; Quétel et al., 2016). Newly developed GEM calibrations exist, and comparative studies are needed for their evaluation and validation.

In the presented study, we compared three different calibration strategies: i) bell-jar calibration, ii) gravimetrically verified calibration based on Hg^0 diffusion, and iii) calibration based on NIST SRM 3133. The Hg^0 permeation method was developed at the Van Swinden Laboratory (VSL), while the NIST SRM 3133 calibration is routinely used at the Jožef Stefan Institute (JSI). Both calibrations are traceable to SI units (VSL calibration directly, JSI calibration indirectly through generation of Hg^0 from an aqueous solution), unlike bell-jar calibration. Since the output of the VSL Hg^0 permeation calibrator (also called the primary gas standard) was previously well characterized (Ent et al., 2014), it was used as a reference value for comparisons. Mercury from different calibrations was sampled with sorbent traps (carbon and gold sorbent traps). Sorbent traps were chosen as a suitable medium for use as a transfer standard. Background and flue gas GEM amounts ranging from 2 to 1000 ng were used for comparison studies.

The first comparison was for the 2-10 ng Hg range. Amasil™ (gold-impregnated silica) sorbent traps loaded with the primary gas standard were analyzed by VSL and also by the National Physics Laboratory (NPL). Both laboratories used a PSA Sir Galahad analyzer that was calibrated with the bell-jar. The second comparison was for the 10-1000 ng Hg range. Gold and carbon traps loaded with the primary gas standard were analyzed by JSI using a Lumex mercury analyzer. In this case, the analyzer was calibrated using NIST SRM 3133.

The comparison results show that the bell-jar GEM output is approximately 8% lower than the output of the primary gas standard. The observed difference in our work is similar to that reported by Srivastava & Hodges (2018). The NIST 3133 calibration was in good agreement with the primary gas standard: only 1.3% discrepancies were found, which was within measurement uncertainty.

Sorbent of the primary gas standard with sorbent traps was found to be suitable for obtaining transfer standards with a reproducibility standard deviation of 3%. The use of sorbent traps as transfer standards can be convenient for the establishment of metrological traceability of mercury equipment used in the field. The comparison results imply that both SI traceable calibrations gave comparable results within their measurement uncertainty, while the bell-jar gave significantly different results. Based on this, our work shows that the use of Dumarey equation gives a negative bias of approximately 8%.

I contributed to the manuscript by performing Hg^0 calibration based on NIST SRM 3133, preparing tables and finalizing the final draft of the manuscript.

Atmos. Meas. Tech., 14, 2317–2326, 2021
https://doi.org/10.5194/amt-14-2317-2021
© Author(s) 2021. This work is distributed under
the Creative Commons Attribution 4.0 License.

Atmospheric Measurement Techniques

Comparability of calibration strategies for measuring mercury concentrations in gas emission sources and the atmosphere

Iris de Krom[1], Wijnand Bavius[1], Ruben Ziel[1], Elizabeth A. McGhee[2], Richard J. C. Brown[2], Igor Živković[3], Jan Gačnik[3], Vesna Fajon[3], Jože Kotnik[3], Milena Horvat[3], and Hugo Ent[1]

[1]VSL, Department of Chemistry, Mass, Pressure and Viscosity, Thijsseweg 11, 2629 JA Delft, the Netherlands
[2]Environment Department, National Physical Laboratory, Hampton Road, Teddington, TW11 0LW, UK
[3]Jozef Stefan Institute, Department of Environmental Sciences, Jamova Cesta 39, 1000 Ljubljana, Slovenia

Correspondence: Iris de Krom (idekrom@vsl.nl)

Received: 5 August 2020 – Discussion started: 21 September 2020
Revised: 28 January 2021 – Accepted: 7 February 2021 – Published: 25 March 2021

Abstract. A primary mercury gas standard was developed at Van Swinden Laboratory (VSL) to establish an International System of Units (SI)-traceable reference point for mercury concentrations at emission and background levels in the atmosphere. The majority of mercury concentration measurements are currently made traceable to the empirically determined vapour pressure of mercury. The primary mercury gas standard can be used for the accurate and precise calibration of analytical systems used for measuring mercury concentrations in air. It has been especially developed to support measurements related to ambient air monitoring (1–2 ng m^{-3}), indoor and workplace-related mercury concentration levels according to health standards (from 50 ng m^{-3} upwards) as well as stationary source emissions (from 1 µg m^{-3} upwards).

The primary mercury gas standard is based on diffusion according to ISO 6154-8. Calibration gas mixtures are obtained by combining calibrated mass flows of nitrogen and air through a generator holding diffusion cells containing elemental mercury. In this paper, we present the results of comparisons between the primary gas standard and mercury calibration methods maintained by NPL (National Physical Laboratory in the United Kingdom), a National Metrology Institute (NMI), and the Jozef Stefan Institute (JSI), a Designated Institute (DI). The calibration methods currently used at NPL and JSI are based on the bell-jar calibration apparatus in combination with the Dumarey equation or a NIST (National Institute of Standards and Technology in the United States) reference material. For the comparisons, mercury was sampled on sorbent traps to obtain transfer standards with levels between 2 and 1000 ng with an expanded uncertainty not exceeding 3 % ($k = 2$). The comparisons performed show that the results for the primary gas standard and the NIST reference material are comparable, whereas a difference of −8 % exists between results traceable to the primary gas standard and the Dumarey equation.

1 Introduction

Mercury is a global pollutant and in its many chemical forms highly toxic to human, animal and environmental health. Mercury occurs naturally in the environment, and in addition human activities have increased the atmospheric mercury concentration up to 500 % above natural levels (Global mercury assessment, 2018a, b). Reliable and comparable measurement results of mercury concentration levels in the environment are key to underpinning global efforts to control and reduce the mercury emissions, to meeting the obligations of legislation and to protecting human health.

The majority of measurements of mercury concentrations are currently traceable to the empirically determined equations describing the saturated vapour pressure of mercury, usually via a bell-jar calibration apparatus (A. S. Brown et al., 2008; R. J. C. Brown et al., 2008a). This apparatus allows a saturated concentration of mercury vapour in air to develop in a confined space in equilibrium with ambient conditions, from which a known amount of mercury can be removed for calibration purposes. Several empirical equations are available, e.g. the Dumarey and the, more recently pro-

Published by Copernicus Publications on behalf of the European Geosciences Union.

posed, Huber equations (Dumarey et al., 1979, 1985, 2010; Huber et al., 2006). The agreement between these equations is unsatisfactory, with vapour pressures from different equations differing by more than 7 % at 20 °C (Brow et al., 2010; Quétel et al., 2014). To remove the dependency of mercury concentration measurements from these empirical equations and to provide stability and comparability, a primary mercury gas standard has been developed by VSL (Van Swinden Laboratory, National Metrology Institute in the Netherlands) to provide metrological traceability to the International System of Units (SI) (Ent et al., 2014; de Krom et al., 2020). The SI-traceable primary gas standard, working according to ISO 6145-8 (2005), can be used for the calibration of instruments and the certification of mercury gas generators. Furthermore, sorbent traps can be spiked with known amounts of mercury from the primary gas standard using pumped sampling, according to ISO 16017-1 (2000). The transfer standards obtained can be used as certified reference materials to calibrate field instruments or for comparisons such as mandatory for calibration and testing laboratories to show their conformity assessment under ISO/IEC 17025 (2017). Such a comparison can only be successful if it allows participants to validate their measurement procedures with respect to SI-traceable standards as required by ISO/IEC 17043 (2010).

Measurements of mercury concentrations in air are typically carried out using a pump to sample air at a monitoring location, at a known rate for a known time, onto an adsorption tube (Pirrone et al., 2013; Pandey et al., 2011). The trapping of mercury is usually performed with a sorbent tube using gold to form an amalgam and trap the mercury. To increase the surface area available, the gold is often dispersed on silica or a similar support (Brown et al., 2011, 2017). Mercury in this adsorption tube is then thermally desorbed and measured. Furthermore, in 2019 a new technical specification was adopted in Europe, which describes the use of gold amalgamation traps for sampling and determination of mercury compounds in flue gas (NVN-CEN/TS 17286, 2019). This technical specification is based on the United States Environmental Protection Agency (US EPA) 30B method (EPA, 2017). That method in turn uses carbon sorbent traps for the determination of total gaseous mercury emissions from coal-fired combustion sources. The sorbent traps contain carbon typically activated with iodine or another halogen (Živković et al., 2020).

To demonstrate the robustness and comparability of transfer standards obtained with the primary gas standard, in this paper we present the results of comparisons with current calibration methods maintained, using the bell jar in combination with the Dumarey equation or the NIST (National Institute of Standards and Technology in the United States) liquid standard reference material (SRM 3133) for calibration of the equipment. For the comparisons, gold sorbent tubes and carbon sorbent tubes were sampled with the primary mercury gas standard to obtain transfer standards. For the first comparison, between NPL (National Physical Laboratory in the United Kingdom) and VSL, gold sorbent tubes have been sampled with mercury amounts between 2 and 10 ng. Calibration of the analysers was performed with injections from the bell jar in combination with the Dumarey equation. During the second comparison, between JSI (Jozef Stefan Institute in Slovenia) and VSL, amounts between 10 and 1000 ng were sampled and the NIST SRM 3133 was used to calibrate the analyser used.

2 Materials and methods

2.1 Primary mercury gas standard

The primary gas standard has been developed as an elemental mercury (Hg^0) gas generator to establish metrological traceability of mercury concentration measurement results, based upon a gravimetric approach, for ambient air levels as well as higher concentrations (Ent et al., 2014; de Krom et al., 2020).

The working principle of the primary mercury vapour generator is based on diffusion according to ISO 6145-8 (2005). Specially developed stainless-steel diffusion cells are filled with approximately 2 mL of Hg^0. The Hg^0 vapour diffuses from the cell through a capillary. To obtain several diffusion ranges, cells with different capillary diameters are used, e.g. 33 and 3 mm. By weighing the diffusion cells at regular time intervals on a high-resolution analytical balance (AX1006 mass comparator with a Mettler AT1005 balance, Mettler, Switzerland), the Hg^0 mass flow rate (diffusion) is determined gravimetrically. The characterisation of different diffusion cells has been described previously by de Krom et al. (2020).

In the dynamic mercury gas generator, the cells are housed in a diffusion chamber. The diffusion chamber is temperature (20.0 ± 0.1 °C) and pressure (105.0 ± 0.1 kPa) controlled. At the bottom a nitrogen flow of 500 mL min^{-1} enters the diffusion chamber. All of the flow, also enriched by mercury vapour, is then guided out of the diffusion chamber through an aperture at the top. Standard Hg^0 gas mixture concentrations are prepared by mixing the Hg^0 vapours in nitrogen with flows, between 1 and 20 L min^{-1}, of matrix gas, e.g. purified air. Using diffusion cells with a capillary of 3 mm in diameter, mercury concentrations between 0.1 and 2.1 µg m^{-3} can be obtained with an expanded uncertainty of 3 %. Diffusion cells with a capillary of 33 mm in diameter can generate mercury concentrations between 5 and 100 µg m^{-3} with an uncertainty of 1.8 %. In this project both types of diffusion cell have been used to obtain the primary mercury gas standard.

2.2 Preparation of transfer standards

Transfer standards are prepared via pumped sampling of known volumes of the primary mercury gas standard for a known time onto sorbent traps according to ISO 16017-1 (2000) using a specially designed multi-sampling mani-

fold, made up of six thermal mass flow controllers (MFCs) operating in sucking mode. Each MFC is connected to a three-way valve. All valves are controlled with a timer that allows them to switch simultaneously. The sampling is done under controlled environmental conditions.

The mercury amount collected onto the sorbent material can be calculated using Eq. (1).

$$m_{\mathrm{Hg}} = \frac{\overline{q}_{\mathrm{m}}\,(\mathrm{Hg})\, t\, q_{\mathrm{v}}\,(\mathrm{sample})}{q_{\mathrm{v}}\,(\mathrm{air})} \quad (1)$$

m_{Hg} is the mercury amount on the sorbent material in ng, $\overline{q}_{\mathrm{m}}\,(\mathrm{Hg})$ is the mercury diffusion rate from the diffusion cell(s) in ng min^{-1}, t is the sampling time in minutes, $q_{\mathrm{v}}\,(\mathrm{sample})$ is the pumped sampling flow in L min^{-1} and $q_{\mathrm{v}}\,(\mathrm{air})$ is the total gas flow in L min^{-1} through the generator to obtain the primary mercury gas standard. As an example, the standard measurement uncertainty associated with a mercury amount of 10.5 ng, obtained using three diffusion cells with a capillary of 3 mm in diameter, can be calculated from Eq. (1) using the law of propagation of uncertainty of the Guide to the expression of Uncertainty in Measurement (GUM) (BIPM et al., 2008). In Table 1 the uncertainty budget belonging to the mercury amount is shown. The expanded uncertainty is 0.3 ng ($k = 2$), which is equivalent to a relative expanded uncertainty of 3 %.

2.3 First comparison: 2–10 ng mercury

Amasil sorbent tubes (PS Analytical, UK) with a specific area of 100 m^2 g^{-1} have been used in this study. The sorbent material used in these tubes is gold-coated silica. The primary gas standard is obtained using two diffusion cells with a capillary of 3 mm in diameter (diffusion rate of 2.92 $\pm$ 0.09 ng min^{-1}, $k = 2$). Different system flow rates are used to obtained different mercury concentrations ($x\,(\mathrm{Hg})$) (Table 2). The sorbent tubes were sampled, during three different rounds (in May, July and September 2017), with five different amounts (approximately 2, 4, 6, 8 and 10 ng) using a sample flow of 0.5000 ± 0.0018 L min^{-1} ($k = 2$) for all sorbent tubes. During round 1 (May 2017), five sorbent tubes per amount were sampled simultaneously, two were analysed by NPL and three were analysed by VSL. Thereafter, two tubes per amount were sampled simultaneously in round 2 (July 2017) and round 3 (September 2017), which were analysed by NPL (Table 2). Both laboratories calibrated the analyser using injections from a bell jar in combination with the Dumarey equation.

Analysis of samples took place at NPL using a PS Analytical Sir Galahad II analyser (PS Analytical, UK) with a fluorescence detector, using NPL's procedure, accredited by UKAS to ISO/IEC 17025 (2017), which is in accordance with the published reference method EN 15852 (2010) (NPL's manual variant of EN 15852 has been shown to be equivalent to the automatic reference method within the uncertainty of the analytical determination; Brown et al., 2012). The instrument was calibrated prior to analysis using a gas-tight syringe, making multiple injections of known amounts of mercury vapour from the bell jar onto the permanent trap of the analyser, across the range of expected sample concentrations. Sampled adsorption tubes were placed in the remote port of the instrument and heated to 900 °C, desorbing the mercury onto a permanent trap. Subsequent heating of this trap then desorbed the mercury onto the detector for final measurement. Samples are desorbed three times to ensure all the mercury has been removed. It is assumed that the third desorption is equal to the blank level of the tube, and this response is taken off the response of the first and second desorptions, which are then added together to provide a total analytical response. Quality control injections are made in between samples to ensure that the analyser is not drifting outside a specified range. A conservative estimate of the relative expanded analysis uncertainty is between 8 % and 10 %. The main components of this uncertainty come from the uncertainty in the response from the adsorption tube during desorption, the repeatability of the instrument response and residual instrument drift (R. J. C. Brown et al., 2008b).

At VSL a PS Analytical 10.525 Sir Galahad (PS Analytical, UK) is used to analyse the sorbent tubes. For calibration a commercially available bell jar has been used for comparison between the primary mercury gas standard and the Dumarey equation. The Tekran® Model 2505 (Tekran, USA) mercury vapour calibration unit is based on the bell-jar principle. Since the saturation vapour pressure of mercury is a function of temperature, the exact volume injected and temperature of the mercury-saturated air need to be set in order for the bell jar to determine the mercury injection amount based on the Dumarey equation (R. J. C. Brown et al., 2008a; Dumarey et al., 1979, 1985). Injections, by use of a gas-tight syringe, between 100 and 800 µL have been used (including a zero-linearity check point) to calibrate the analyser in the range of 1.3 to 10.5 ng.

2.4 Second comparison: 10–1000 ng mercury

Gold sorbent tubes have been used for the 10, 50, 100 and 500 ng samples and carbon traps for the 1000 ng samples. Commercially available gold-coated silica (Brooks Rand Instruments, US) and in-house prepared gold-coated high-grade corundum sand (mass fraction gold of 9.6 %) have been used in this study to prepare gold traps. Clean quartz tubes (i.d. 5 mm) were filled with gold-coated silica or corundum (20 mm length) and fixed with quartz wool. Carbon traps were prepared by filling clean quartz tubes (i.d. 5 mm) with 20 mm length of iodinated activated carbon (AIC-500 from Apex Instruments, US) and fixed with quartz wool. For this comparison three or four sorbent tubes were sampled simultaneously at five different levels according to Table 3 using the diffusion cells with a capillary of 3 or 33 mm in diameter (diffusion rates of 4.23 or 218.5 ng min^{-1} respectively). The air flow through the system was kept constant at

Table 1. Uncertainty budget for mercury amount sampled onto sorbent materials ($k = 1$) calculated from Eq. (1) using the law of propagation of uncertainty according to the GUM.

Measurand	Value	Distribution	Standard uncertainty	Sensitivity coefficient	Uncertainty contribution
$\overline{q}_m$(Hg cell 18)	1.37 ng min^{-1}	Normal	0.03 ng min^{-1}	2.490 min	0.075 ng
$\overline{q}_m$(Hg cell 19)	1.44 ng min^{-1}	Normal	0.04 ng min^{-1}	2.490 min	0.110 ng
$\overline{q}_m$(Hg cell 20)	1.41 ng min^{-1}	Normal	0.04 ng min^{-1}	2.490 min	0.090 ng
t	75.000 min	Normal	0.015 min	0.140 ng min^{-1}	0.002 ng
q_v(sample)	0.1002 L min^{-1}	Normal	0.0004 L min^{-1}	150.094 ng L^{-1} min	0.037 ng
q_v(air)	3.018 L min^{-1}	Normal	0.008 L min^{-1}	−3.489 ng L^{-1} min	−0.029 ng
m_{Hg}	10.5 ng	Normal	0.17 ng		

Table 2. Parameters used to sample sorbent tubes from the primary mercury gas standard for the first comparison.

Round	System flow rate (L min^{-1}) ($U, k = 2$)	x(Hg) (µg m^{-3}) ($U, k = 2$)	Sampling time (min) ($U, k = 2$)	Mercury amount per tube (ng) ($U, k = 2$)
1	20.01 (0.12)	0.146 (0.04)	28.00 (0.03)	2.04 (0.06)
	10.03 (0.06)	0.291 (0.09)	28.00 (0.03)	4.07 (0.13)
	10.00 (0.06)	0.292 (0.09)	42.00 (0.03)	6.12 (0.19)
	5.901 (0.017)	0.494 (0.15)	33.50 (0.03)	8.28 (0.26)
	5.901 (0.017)	0.494 (0.15)	42.00 (0.03)	10.38 (0.32)
2	14.98 (0.09)	0.195 (0.06)	21.00 (0.03)	2.04 (0.06)
	10.00 (0.06)	0.292 (0.09)	28.00 (0.03)	4.08 (0.13)
	10.00 (0.06)	0.292 (0.09)	42.00 (0.03)	6.12 (0.19)
	6.022 (0.017)	0.484 (0.15)	34.00 (0.03)	8.23 (0.26)
	6.022 (0.017)	0.484 (0.15)	42.00 (0.03)	10.17 (0.32)
3	15.04 (0.09)	0.194 (0.06)	21.00 (0.03)	2.04 (0.06)
	9.99 (0.06)	0.292 (0.09)	28.00 (0.03)	4.08 (0.13)
	9.99 (0.06)	0.292 (0.09)	42.00 (0.03)	6.13 (0.19)
	5.995 (0.017)	0.486 (0.15)	34.00 (0.03)	8.26 (0.26)
	6.021 (0.017)	0.484 (0.15)	42.00 (0.03)	10.16 (0.32)

3.00 ± 0.02 L min^{-1} ($k = 2$) to obtain a mercury concentration of 1.41 ± 0.04 and 71.4 ± 0.9 µg m^{-3} respectively. Other parameters, i.e. the diffusion cells, sample flow and sampling time, were changed during the different entries to demonstrate the variability of the primary mercury gas standard setup.

The sorbent tubes were analysed directly after sampling by JSI at VSL in November 2018. The amount of mercury on the carbon traps was determined using mercury analyser RA-915M with a PYRO-915+ thermal decomposition attachment (Lumex Scientific, St. Petersburg, Russia) that is based on differential Zeeman atomic absorption spectrometry. Iodinated activated carbon and quartz wool from the carbon trap were quantitatively transferred to a quartz boat and mercury was released from the sample by combustion in the thermal decomposition unit at 700 °C. The system was calibrated by spiking a known amount of NIST SRM 3133 standard solution (1000 ng) to iodinated activated carbon and determining the corresponding signal using the same procedure as for the sample. The signal of procedural blanks (average value 1.9 ng) was subtracted from the corresponding sample (standard) signal.

The amount of mercury on the gold traps was determined using mercury analyser RA-915M with a modification of the PYRO-915+ to allow direct desorption of mercury from the gold trap in the thermal decomposition unit. The system was calibrated by reducing a known amount of NIST SRM 3133 standard solution (10–500 ng) with tin(II) chloride solution, quantitative purging of the obtained Hg^0 gas onto a gold trap (EPA, 2002), and its desorption in the thermal decomposition unit (Shulupov et al., 2004). The signal of procedural blank was always within the instrumental noise and could not be subtracted from the corresponding sample (standard) signal.

The uncertainty of the analytical procedure was estimated using the law of propagation of uncertainty (BIPM et al., 2008). Estimated relative standard uncertainty of the calibra-

Table 3. Parameters used to sample sorbent tubes from the primary mercury gas standard for the second comparison.

Entry	Diffusion flow rate ($ng\,min^{-1}$) ($U, k = 2$)	Sample flow rate ($L\,min^{-1}$) ($U, k = 2$)	Sampling time (min) ($U, k = 2$)	Mercury amount per tube (ng) ($U, k = 2$)
1	4.23 (0.13)	0.1002 (0.0004)	75.00 (0.03)	10.5 (0.3)
2	4.23 (0.13)	0.1999 (0.0007)	37.50 (0.03)	10.5 (0.3)
3	4.23 (0.13)	0.1999 (0.0007)	37.50 (0.03)	10.5 (0.3)
4	4.23 (0.13)	0.4997 (0.0017)	75.00 (0.03)	52.6 (1.7)
5	4.23 (0.13)	0.4997 (0.0017)	150.00 (0.03)	105 (3)
6	214.3 (2.4)	0.0499 (0.0002)	14.00 (0.03)	49.8 (0.7)
7	214.3 (2.4)	0.1003 (0.0004)	15.00 (0.03)	107.3 (1.5)
8	214.3 (2.4)	0.4997 (0.0017)	15.00 (0.03)	535 (8)
9	214.3 (2.4)	0.5000 (0.0018)	15.00 (0.03)	537 (8)
10	214.3 (2.4)	0.5000 (0.0018)	15.00 (0.03)	537 (8)
11	214.3 (2.4)	0.5000 (0.0018)	15.00 (0.03)	537 (8)
12	214.3 (2.4)	0.5000 (0.0018)	15.00 (0.03)	537 (8)
13	214.3 (2.4)	0.5001 (0.0018)	30.00 (0.03)	1070 (15)
14	214.3 (2.4)	0.1004 (0.0004)	150.00 (0.03)	1074 (15)

tion was calculated from the contributions of the NIST SRM 3133 (0.24 %, $k = 1$), uncertainties of pipettes used for spiking and preparation of NIST SRM 3133 dilutions, and the uncertainty of the volume due to possible temperature changes. The estimated relative standard uncertainty of the calibration ranged from 0.5 % to 0.6 % ($k = 1$) for 1000 and 10 ng spikes respectively. The relative expanded uncertainty of the whole analytical procedure was usually 2.5 %–3 % ($k = 2$) and included effects such as sampling repeatability as the greatest contribution and effects due to calibration and recovery.

3 Results

3.1 First comparison: 2–10 ng mercury

For the first comparison Amasil sorbent tubes were sampled in three rounds with amounts between 2 and 10 ng of mercury. Two tubes sampled simultaneously per level, as well as blank tubes, were sent to NPL for analysis after each sampling for each of the three rounds. Directly after round 1 three tubes were analysed by VSL for each sampling level. Both VSL and NPL calibrated their analyser with injections from the bell jar and the mercury amount is calculated using the Dumarey equation. This approach enables one to determine the difference between the primary mercury gas standard and the Dumarey equation. After calibration of the equipment the mercury amount on the tubes is verified against the Dumarey equation (Fig. 1).

The blank tubes were not sampled with mercury but have been returned to NPL to check for contamination during transport and storage. The recovery of all the blank tubes analysed during the three rounds is below 0.1 ng. The repeatability and reproducibility standard deviation have been calculated according to ISO 5725-2 (2019). Based on the results of NPL the repeatability standard deviation of the sampling (within rounds) is 2.2 %, and the reproducibility standard deviation (over three rounds, with the exception of the 6 ng samples) is 3 %. For the 6 ng samples the reproducibility standard deviation is 6.7 %. The reproducibility standard deviation of the verification results is equal to the uncertainty of the mercury amount (Table 1), except for the 6 ng samples. This reproducibility standard deviation is below the uncertainty of the analysis, which is ≤ 10 %. The verification results obtained during round 1 by NPL and VSL are comparable for the 4, 6, 8 and 10 ng samples. The difference between the results is well within the uncertainty of the analysis. For the 2 ng samples the result of Entry 1.1 is comparable with the NPL verification results; however, the results for Entries 1.2 and 1.3 are not (Fig. 1). In general, the verification of the samples shows results below the reference value with a few exceptions. The average difference between the reference values and the verification results is -8 % with a standard deviation of 6 %. This implies there is a difference between the primary mercury gas standard and the Dumarey equation of -8 %. Based upon these results, measurement results based upon the Dumarey equation have a -8 % measurement bias.

3.2 Second comparison: 10–1000 ng mercury

During the second comparison three or four sorbent tubes were sampled simultaneously at VSL and analysed directly at VSL. For the verification the average recovery of the three or four sorbent tubes is reported (Fig. 2). During the verification the analysers are calibrated with the NIST liquid reference material (SRM 3133). For Entries 1–5 (10, 50 and 100 ng; Table 3) the diffusion cells with a capillary of 3 mm in diameter have been used. The diffusion cells with a capil-

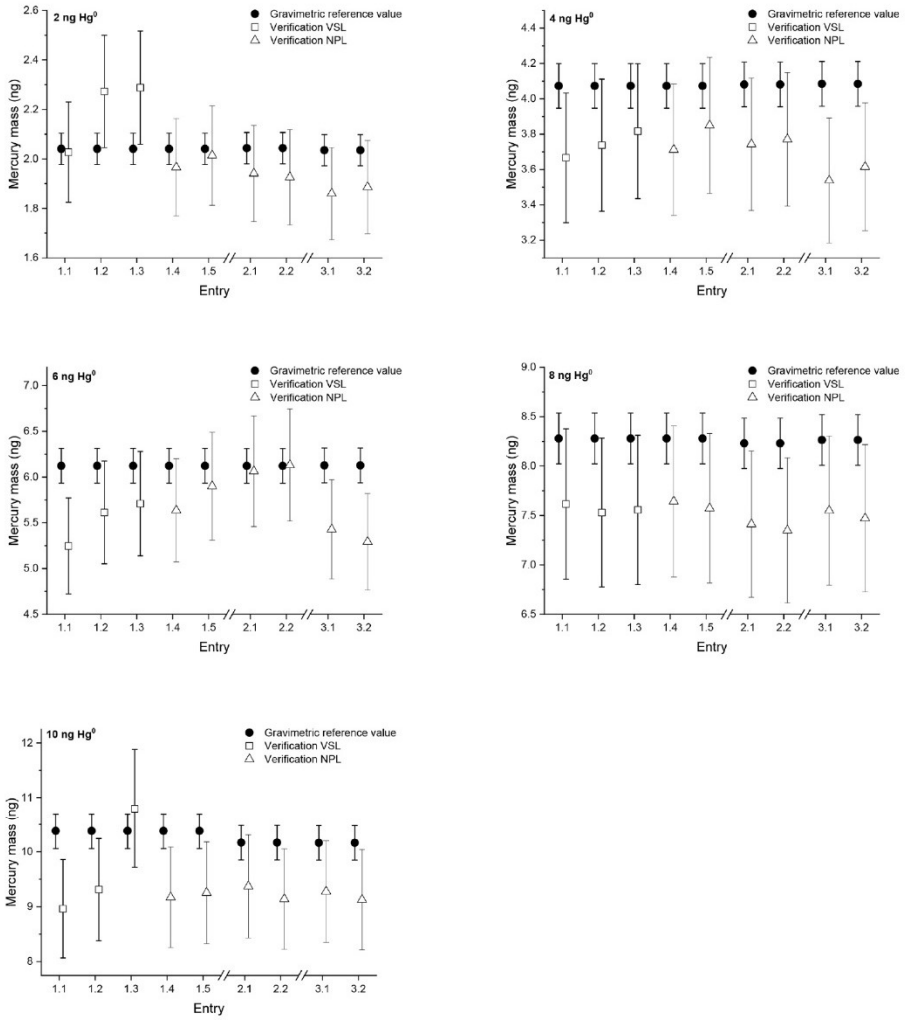

Figure 1. Verification results of the first comparison with mercury amounts of approximately 2, 4, 6, 8 and 10 ng on sorbent tubes. The open squares and triangles are the results from the measurements calibrated using the Dumarey equation. The closed circles are the reference values determined gravimetrically. The error bars indicate the expanded uncertainty for the reference values (ng) ($k = 2$) and the verification values (ng) ($k = 2$). Entries 1.1, 1.2 and 1.3 show the verification results of VSL from the first round. The verification results of NPL in the first round are Entries 1.4 and 1.5, in the second round 2.1 and 2.2 and in the third round 3.1 and 3.2.

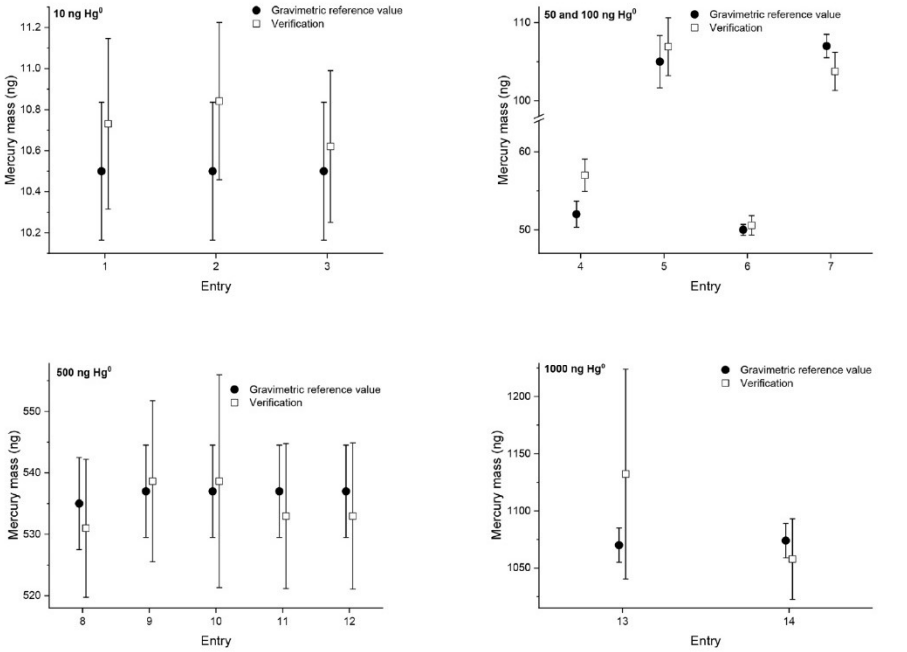

Figure 2. Verification results of the second comparison with mercury amounts of approximately 10, 50, 100, 500 and 1000 ng on sorbent tubes. The open squares are the verification results. The closed circles are the reference values determined gravimetrically. The error bars indicate the expanded uncertainty for the reference value (ng) ($k = 2$) and the verification value (ng) ($k = 2$).

lary of 33 mm in diameter have been used for sampling the other entries (Entries 6–14; 50, 100, 500 and 1000 ng; Table 3). As such, for sampling the sorbent tubes with 50 and 100 ng, both types of diffusion cells have been used.

The repeatability and reproducibility standard deviations of the 10 and 500 ng samples have been calculated according to ISO 5725-2 (2019). Repeatability standard deviations of 0.8 % for both levels have been obtained, and the reproducibility standard deviation is 1.3 % and 0.9 % for the 10 and 500 ng samples respectively. For the samples obtained using the diffusion cells with a capillary of 3 mm in diameter an average difference, between the reference values and the verification results, of +3.6 % has been obtained, except for Entry 4. In that case the reference value and verification result do not overlap, with a difference of +9.6 %. For the samples obtained using the diffusion cells with a capillary of 33 mm in diameter the difference between the reference values and the verification results is very small, just +0.1 %. The average difference between all the reference values and verification results is +1.3 % with a standard deviation of 3 %.

4 Discussion

In contrast to the primary mercury gas standard described in this work (based on diffusion according to ISO 6145-8, 2005), gaseous elemental mercury generators available on the market are based on the dilution of a saturated mercury atmosphere to obtain mercury concentrations according to ISO 6145-9 (2009). For many years different vapour pressure–temperature relationships for the computation of the output of such generators have been described and compared. Approximately 30 years ago the Dumarey equation was established which corresponds to the least-squares best fit of results obtained for measurements of mercury mass concentration in air at saturation (Dumarey et al., 2010). Huber et al. (2006) described a correlation based on fitting a thermodynamically constrained model over a wide temperature range

to numerous mercury vapour pressures. However, at room temperature (22 °C) the Dumarey equation yields a value which is 6.4 % lower compared to the Huber equation.

More recently results using SI-traceable mass spectroscopy to determine gaseous elemental mercury concentrations have been reported by Quétel et al. (2016) and Srivastava and Hodges (2018). Quétel et al. (2016) reported mercury concentration values nearly 3 % and 10 % higher compared to predictions (at 20 °C) based on the Huber equation and Dumarey correlations respectively. The comparison performed by Srivastava and Hodges (2018) showed that their measurement results are equivalent within their experimental uncertainty to the Huber equation and Quétel method. Furthermore, the mercury vapour pressure value predicted from the Dumarey equation is 8.5 % below the value based on the results from Srivastava and Hodges.

Based on the results from the two comparisons described in this paper, similar conclusions can be drawn. The primary mercury gas standard and the NIST SRM 3133 are comparable within 1.3 %. In contrast, the output of the Dumarey equation, used in the first comparison, shows a difference of approximately −8 % compared to the primary mercury gas standard. This discrepancy is outside the uncertainty range for the Dumarey equation (4 %; $k = 2$) and the primary gas standard (3 %; $k = 2$).

In extension to the comparisons highlighted in this work, future intercomparisons between the primary mercury gas standard and the primary measurement method based on laser absorption spectroscopy (LAS) (Srivastava et al., 2020) are planned.

5 Conclusion

The work described in this paper describes the comparison between mercury calibration methods maintained by two National Metrology Institutes (NMIs) and a Designated Institute (DI), using the bell jar in combination with the Dumarey equation or NIST SRM 3133 for the calibration of the equipment. The results of the comparisons show that robust mercury transfer standards can be obtained via sampling of the primary mercury gas standard with a reproducibility standard deviation 3 %, which is equal to the uncertainty of the mercury amount sampled onto the sorbent materials. Transfer standards containing gold or carbon as sorbent material can be prepared with levels between 2 and 1000 ng with a relative expanded uncertainty 3 %.

Based on the method used for the calibration of the analyser, a difference of −8 % has been obtained between the primary mercury gas standard, the Dumarey equation and a difference of +1.3 % when using NIST SRM 3133 to calibrate the analysers. This implies that the primary mercury gas standard and NIST SRM 3133 are comparable within their measurement uncertainty, whereas a difference of approximately 8 % exists between measurement results based on these two versus the output of the Dumarey equation. Based upon this work it should be emphasized that measurement results based on the Dumarey equation have a negative bias of approximately 8 %.

The transfer standards obtained with the primary mercury gas standard proved to be useful for establishing metrological traceability to the SI units and can be used for the calibration of mercury equipment used in the field, e.g. analysers, bell jars and gas generators. Furthermore, such transfer standards can be used to benchmark the results of laboratories involved in mercury measurements, e.g. by proficiency tests. The obtained results enable traceable mercury measurement results in emission sources and the atmosphere. These measurements are of fundamental importance for reducing the mercury burden on the environment to comply with related regulation and protect human health.

Data availability. The data used in this paper can be found on Zenodo https://doi.org/10.5281/zenodo.4616620 (de Krom, 2021).

Author contributions. IdK led the methodology, investigation, and writing of the original draft and provided the visualization and supervised the project. WB, RZ, and EAM did the investigation with IZ, JG, VF, and JK. RJCB provided the methodology and helped with the writing, reviewing and editing of the paper together with IZ, MH, and HE. HE also conceptualized the project.

Competing interests. The authors declare that they have no conflict of interest.

Acknowledgements. Warren Corns is thanked for providing iodinated activated carbon. This project 19NRM03 SI-Hg has received funding from the EMPIR programme co-financed by the Participating States and from the European Union's Horizon 2020 research and innovation programme.

Financial support. This research has been supported by the EMPIR programme co-financed by the Participating States and from the European Union's Horizon 2020 research and innovation programme (grant no. 19NRM03 SI-Hg).

Review statement. This paper was edited by Saulius Nevas and reviewed by Seth Lyman and one anonymous referee.

References

BIPM, IEC, IFCC, ILAC, ISO, IUPAC, and OIML: Guide to the expression of uncertainty in measurement JCGM 100:2008, GUM 1995 with Minor Corrections (BIPM), ISO, Geneva, Switzerland, 2008.

Brown, A. S., Brown, R. J. C., Corns, W. T., and Stockwell, P. B.: Establishing SI traceability for measurements of mercury vapour, Analyst, 133, 946–953, https://doi.org/10.1039/B803724H, 2008.

Brown, A. S., Brown, R. J. C., Dexter, M. A., Corns, W. T., and Stockwell, P. B.: A novel automatic method for the measurement of mercury vapour in ambient air, and comparison of uncertainty with established semi-automatic and manual methods, Anal. Methods, 2, 954–966, https://doi.org/10.1039/C0AY00058B, 2010.

Brown, R. J. C., Brown, A. S., Corns, W. T., and Stockwell, P. B.: Accurate calibration of mercury vapour indicators for occupational exposure measurements using a dynamic mercury vapour generator, Instrum. Sci. Technol., 36, 611–622, https://doi.org/10.1080/10739140802448309, 2008a.

Brown, R. J. C., Brown, A. S., Yardley, R. E., Corns, W. T., and Stockwell, P. B.: A practical uncertainty budget for ambient mercury vapour measurement, Atmospheric Environment, 42, 2504-2517, https://doi.org/10.1016/j.atmosenv.2007.12.012, 2008b.

Brown, R. J. C., Kumar, Y., Brown, A. S., and Kim, K. H.: Memory effects on adsorption tubes for mercury vapor measurement in ambient air: elucidation, quantification, and strategies for mitigation of analytical bias, Environ. Sci. Technol., 45, 7812–7818, https://doi.org/10.1021/es201454u, 2011.

Brown, R. J. C., Kumar, Y., Brown, A. S., Dexter, M. A., and Corns, W. T.: Field comparison of manual and semi-automatic methods for the measurement of total gaseous mercury in ambient air and assessment of equivalence, J. Environ. Monit., 14, 657–665, https://doi.org/10.1039/C2EM10719H, 2012.

Brown, R. J. C., Braysher, E. C., McGhee, E. A., Goddard, S. L., Ent, H., Kim, K. H., and Nielsen, J.: Characterising and reducing the blank response from mercury vapour sorbent tubes, Anal. Methods, 9, 2654–2659, https://doi.org/10.1039/C7AY00451F, 2017.

de Krom, I.: Comparability of calibration strategies for measuring mercury concentrations in gas emission sources and the atmosphere, Zenodo, https://doi.org/10.5281/zenodo.4616620, 2021.

de Krom, I., Bavius, W., Ziel, R. P., Efremov, E., van Meer, D., van Otterloo, R. P., van Andel, I., van Osselen, D., Heemskerk, M., Corns, W. T., and Ent, H.: Primary mercury gas standard for the calibration of mercury measurements, Measurement, 169, 108351, https://doi.org/10.1016/j.measurement.2020.108351, 2020.

Dumarey, R., Heindryckx, R., Dams, R., and Hoste, J.: Determination of volatile mercury compounds in air with the coleman mercury analyzer system, Anal. Chim. Acta, 107, 159–167, https://doi.org/10.1016/S0003-2670(01)93206-4, 1979.

Dumarey, R., Temmerman, E., Dams, R., and Hoste, J.: The accuracy of the vapour-injection calibration method for the determination of mercury by amalgamation/cold-vapour atomic absorption spectrometry, Anal. Chim. Acta, 170, 337–340 https://doi.org/10.1016/S0003-2670(00)81759-6, 1985.

Dumarey, R., Brown, R. J. C., Corns, W. T., Brown, A. S., and Stockwell, P. B.: Elemental mercury vapour in air: the origins and validation of the "Dumarey equation" describing the mass concentration at saturation, Accred. Qual. Assur., 15, 409–414, https://doi.org/10.1007/s00769-010-0645-1, 2010.

EN 15852:2010: Ambient air quality – Standard method for the determination of total gaseous mercury, CEN, Brussels, Belgium, 2010.

Ent, H., van Andel, I., Heemskerk, M., van Otterloo, R. P., Bavius, W., Baldan, A., Horvat, M., Brown, R. J. C., and Quétel, C. R.: A gravimetric approach to providing SI traceability for concentration measurement results of mercury vapor at ambient air levels, Meas. Sci. Technol., 25, 115801, https://doi.org/10.1088/0957-0233/25/11/115801, 2014.

EPA: Method 1631, Revision E: Mercury in water by oxidation, purge and trap, and cold vapor atomic fluorescence spectrometry, available at: https://www.epa.gov/sites/production/files/2015-08/documents/method_1631e_2002.pdf (last access: 18 March 2021), 2002.

EPA: Method 30B – mercury sorbent trap procedure, available at: https://www.epa.gov/sites/production/files/2017-08/documents/method_30b.pdf (last access: 18 March 2021), 2017.

Global mercury assessment 2018: https://wedocs.unep.org/bitstream/handle/20.500.11822/27579/GMA2018.pdf (last access: 18 March 2021), 2018a.

Global mercury assessment 2018: https://www.unenvironment.org/resources/publication/global-mercury-assessment-2018 (last access: 18 March 2021), 2018b.

Huber, M. L., Laesecke, A., and Friend, D. G.: Correlation for the vapor pressure of mercury, Indust. Eng. Chem., 45, 7351–7361, https://doi.org/10.1021/ie060560s, 2006.

ISO 16017-1:2000: Indoor, ambient and workplace air – Sampling and analysis of volatile organic compounds by sorbent tube/thermal desorption/capillary gas chromatography – Part 1: Pumped sampling, ISO, Geneva, Switzerland, 2000.

ISO 6145-8:2005: Gas analysis – Preparation of calibration gas mixtures using dynamic volumetric methods – Part 8: Diffusion method, ISO, Geneva, Switzerland, 2005.

ISO 6145-9:2009 Gas analysis – Preparation of calibration gas mixtures using dynamic volumetric methods – Part 9: Saturation method, ISO, Geneva, Switzerland, 2009.

ISO 5725-2:2019: Accuracy (trueness and precision) of measurement methods and results – Part 2: Basic method for the determination of repeatability and reproducibility of a standard measurement method, ISO, Geneva, Switzerland, 2019.

ISO/IEC 17043:2010: Conformity assessment – General requirements for proficiency testing, ISO, Geneva, Switzerland, 2010.

ISO/IEC 17025:2017: General requirements for the competence of testing and calibration laboratories, ISO, Geneva, Switzerland, 2017.

NVN-CEN/TS 17286:2019: Stationary source emissions – Mercury monitoring using sorbent traps, CEN, Brussels, Belgium, 2019.

Pandey, S. K., Kim, K. H., and Brown, R. J. C.: Measurement techniques for mercury species in ambient air, TrAC, Trends Anal. Chem., 30, 899–917, https://doi.org/10.1016/j.trac.2011.01.017, 2011.

Pirrone, N., Aas, W., Cinnirella, S., Ebinghaus, R., Hedgecock, I. M., Pacyna, J., Sprovieri, F., and Sunderland, E. M.: Toward the next generation of air quality monitoring: mercury, Atmos. Environ., 80, 599–611, https://doi.org/10.1016/j.atmosenv.2013.06.053, 2013.

Quétel, C. R., Zampella, M., Brown, R. J. C., Ent, H., Horvat, M., Paredes, E., and Tunc, M.: International system of units traceable results of Hg mass concentration at saturation in air from

a newly developed measurement procedure, Anal. Chem., 86, 7819–7827, https://doi.org/10.1021/ac5018875, 2014.

Quétel, C. R., Zampella, M., and Brown, R. J. C.: Temperature dependence of Hg vapour mass concentration at saturation in air: New SI traceable results between 15 and 30 °C, Trends Anal. Chem., 85, 81–88, https://doi.org/10.1016/j.trac.2015.12.010, 2016.

Shulupov, S., Pogarev, S., Ryzhov, V., Mashyanov, N., and Stroganov, A.: Zeeman atomic absorption spectrometer RA-915+ for direct determination of mercury in air and complex matrix samples, Fuel Proc. Techn., 85, 473–485, https://doi.org/10.1016/j.fuproc.2003.11.003, 2004.

Srivastava, A. and Hodges, J. T.: Development of a high-resolution laser absorption spectroscopy method with application to the determination of absolute concentration of gaseous elemental mercury in air, Anal. Chem., 90, 6781–6788, https://doi.org/10.1021/acs.analchem.8b00757, 2018.

Srivastava, A., Long, S. E., Norris, J. E., Bryan, C. E., Carney, J., and Hodges, J. T.: Comparison of primary laser spectroscopy and mass spectrometry methods for measuring mass concentration of gaseous elemental mercury, Anal. Chem, 93, 1050–1058, https://doi.org/10.1021/acs.analchem.0c04002, 2020.

Živković, I., Berisha, S., Kotnik, J., Jagodic, M., and Horvat, M.: Traceable determination of atmospheric mercury using iodinated activated carbon traps, Atmosphere, 11, 780, https://doi.org/10.3390/atmos11080780, 2020.

3.2 Manuscript 2: Validating an Evaporative Calibrator for Gaseous Oxidized Mercury

Gačnik J., Živković I., Ribeiro Guevara S., Jaćimović R., Kotnik J., Horvat M. (2021). Sensors, 21, 2501

Calibration approaches for gaseous oxidized mercury are very limited, especially with regard to calibration at ambient concentration levels. Commercially available calibrators are mostly aimed at flue gas GOM calibration and are not validated for use at low concentration levels. This is also the case for the newly developed GOM calibration unit described by Saxholm et al. (2020). The developed calibrator uses the evaporation of an aqueous Hg^{II} solution and mixing it with a carrier gas to obtain a Hg^{II} reference gas that can be used for GOM calibration. Even though recent work has shown linearity of calibrator output even at near-ambient concentrations (Petrov et al., 2020), linearity alone is not a sufficient indicator of validity. Further validation of the calibrator feasibility for use at different concentration levels is needed.

In this paper, we attempted to validate the GOM calibration unit developed by Saxholm et al. (2020) for use at different concentration levels. We compared the expected output of the calibration unit (as stated by the manufacturer) with the actual output observed in validation experiments. Since the focus of our work was on ambient GOM concentrations, we used the ^{197}Hg radiotracer which enabled highly sensitive and selective measurements. Additionally, we performed speciation measurements of the calibrator output to determine if the output contained unwanted GEM in addition to GOM. For speciation, we used impinging solutions to separate GEM and GOM. The stability of the calibrator output was also tested to see how the unit behaves over long operation times. Since we expected that there would be some degree of GOM adsorption to the tubing inside or outside of the calibrator, we applied washing procedures for the tubing. Washing solutions were comprised of HCl and HNO_3 to effectively remove all adsorbed GOM. By doing so, we could potentially evaluate the absorption levels and attempt to reduce it. The manufacturers of the unit speculated that the calibrator could produce gaseous $HgBr_2$ in addition to $HgCl_2$, so we performed all of the aforementioned experiments with both Hg^{II} species.

The results of our paper showed that the behaviour of the tested GOM calibration unit changed significantly when going from high to low GOM concentrations. Recoveries (ratios of actual to expected calibrator outputs) were around 90% for the concentrations above 1000 ng m^{-3} of $HgCl_2$, and low relative amounts of GEM were found in the output. This was not the case for concentrations under 1000 ng m^{-3} of $HgCl_2$, since recoveries dropped as low as 39.4% when the lowest $HgCl_2$ concentration (5.90 ng m^{-3}) was used. Additionally, the relative GEM amount increased when switching to low $HgCl_2$ concentrations. A clear, time-dependent output of the calibrator output was observed at all concentration levels; output consistently increased over the tested 4-day operation periods. The revealed discrepancies between the theoretical and actual calibrator output were attributed to the adsorption of $HgCl_2$ on Teflon tubing. The results using $HgBr_2$ showed that $HgBr_2$ is even more problematic due to higher adsorptive properties than $HgCl_2$. Due to unsatisfactory results, even at the highest concentration levels, we abandoned the idea that the calibration unit could be used for $HgBr_2$ gas.

Using the adsorption results for $HgCl_2$, we applied an adsorption isotherm to calculate the thermodynamic properties of $HgCl_2$ adsorption onto Teflon tubing. Langmuir isotherm gave the best fit and using it we calculated the adsorption enthalpy (ΔH_{ads}); a ΔH_{ads} value of -12.33 kJ mol^{-1} was obtained. The negative value of ΔH_{ads} suggested that adsorption of

$HgCl_2$ is an exothermal process, which is consistent with the observations that high temperatures inhibit $HgCl_2$ adsorption. Finally, we tried to minimize the adsorption by saturating the adsorption sites with high $HgCl_2$ concentrations before using low $HgCl_2$ concentrations. The attempt was unsuccessful since adsorption of $HgCl_2$ was found to be reversible rather than irreversible.

The newly developed GOM calibrator can be used for calibration of flue gas GOM if the recovery correction is included. The recovery correction brings an additional component to the estimation of calibrator uncertainty which must be accounted for. For ambient GOM concentration levels, the calibrator is not feasible because adsorption becomes too large of a factor for reliable GOM calibrations. This is the case for both $HgCl_2$ and $HgBr_2$ calibration gas. Our results point towards the need for a newly designed or improved GOM calibration that would be suitable for ambient GOM concentrations, not only for flue gas concentrations.

My contribution to the present manuscript was in performing the experimental part of calibrator validation tests and the adsorption evaluation. I also participated in the calculation of thermodynamic parameters (adsorption isotherms and adsorption enthalpy), preparation of tables and figures, and in the writing of the manuscript.

sensors

MDPI

Article

Validating an Evaporative Calibrator for Gaseous Oxidized Mercury

Jan Gačnik [1,2], Igor Živković [2], Sergio Ribeiro Guevara [3], Radojko Jaćimović [2], Jože Kotnik [2] and Milena Horvat [1,2,*]

[1] Jožef Stefan International Postgraduate School, Jamova Cesta 39, 1000 Ljubljana, Slovenia; jan.gacnik@ijs.si
[2] Department of Environmental Sciences, Jožef Stefan Institute, Jamova Cesta 39, 1000 Ljubljana, Slovenia; igor.zivkovic@ijs.si (I.Ž.); radojko.jacimovic@ijs.si (R.J.); joze.kotnik@ijs.si (J.K.)
[3] Laboratorio de Análisis por Activación Neutrónica, Centro Atómico Bariloche, Av. Bustillo km 9.5, Bariloche 8400, Argentina; ribeiro@cab.cnea.gov.ar
* Correspondence: milena.horvat@ijs.si; Tel.: +386-1-588-53-55

Abstract: Understanding atmospheric mercury chemistry is the key for explaining the biogeochemical cycle of mercury and for improving the predictive capability of computational models. Increased efforts are being made to ensure comparable Hg speciation measurements in the air through establishing metrological traceability. While traceability for elemental mercury has been recently set, this is by no means the case for gaseous oxidized mercury (GOM). Since a calibration unit suitable for traceable GOM calibrations based on evaporation of $HgCl_2$ solution was recently developed, the purpose of our work was to extensively evaluate its performance. A highly specific and sensitive ^{197}Hg radiotracer was used for validation over a wide range of concentrations. By comparing experimental and calculated values, we obtained recoveries for the calibration unit. The average recoveries ranged from 88.5% for 1178 ng m^{-3} $HgCl_2$ gas concentration to 39.4% for 5.90 ng m^{-3} $HgCl_2$ gas concentration. The losses were due to the adsorption of oxidized Hg on the inner walls of the calibrator and tubing. An adsorption isotherm was applied to estimate adsorption enthalpy (ΔH_{ads}); a ΔH_{ads} value of -12.33 kJ mol^{-1} was obtained, suggesting exothermal adsorption. The results of the calibrator performance evaluation suggest that a newly developed calibration unit is only suitable for concentrations of $HgCl_2$ higher than 1 µg m^{-3}. The concentration dependence of recoveries prevents the system from being used for calibration of instruments for ambient GOM measurements. Moreover, the previously assessed uncertainty of this unit at µg m^{-3} level (2.0%, k = 2) was re-evaluated by including uncertainty related to recovery and was found to be 4.1%, k = 2. Calibrator performance was also evaluated for $HgBr_2$ gas calibration; the recoveries were much lower for $HgBr_2$ gas than for $HgCl_2$ gas even at a high $HgBr_2$ gas concentration (>1 µg m^{-3}). As $HgBr_2$ is often used as a proxy for various atmospheric HgBr species, the suitability of the unit for such calibration must be further developed.

Keywords: gaseous oxidized mercury; traceability; calibration; ^{197}Hg radiotracer

check for updates

Citation: Gačnik, J.; Živković, I.; Ribeiro Guevara, S.; Jaćimović, R.; Kotnik, J.; Horvat, M. Validating an Evaporative Calibrator for Gaseous Oxidized Mercury. *Sensors* **2021**, *21*, 2501. https://doi.org/10.3390/s21072501

Academic Editor: Eduard Llobet

Received: 23 February 2021
Accepted: 1 April 2021
Published: 3 April 2021

Publisher's Note: MDPI stays neutral with regard to jurisdictional claims in published maps and institutional affiliations.

Copyright: © 2021 by the authors. Licensee MDPI, Basel, Switzerland. This article is an open access article distributed under the terms and conditions of the Creative Commons Attribution (CC BY) license (https://creativecommons.org/licenses/by/4.0/).

1. Introduction

Mercury is present in the atmosphere in different forms as a result of anthropogenic activities and natural processes. When in air, mercury can be carried long distances across the hemisphere and deposited into terrestrial and aquatic environments, where it is taken into the food web or re-emitted into air [1]. Atmospheric Hg fractions are operationally defined as gaseous elemental mercury (GEM, Hg^0), gaseous oxidized mercury (GOM, Hg^{2+}), particulate-bound mercury (PBM, Hg-p), and total gaseous mercury (TGM). Since the atmosphere is the major pathway for global Hg transport, understanding the atmospheric Hg cycle is of great importance. Hg speciation is, therefore, a critical parameter of understanding the Hg atmospheric cycle [2].

Even though GEM is the most abundant atmospheric Hg form, PBM and especially GOM are also crucial in the atmospheric Hg cycle, as they serve as atmospheric mercury

sink [2–4]. Since GOM and PBM are more soluble and have shorter lifetimes than GEM, the knowledge of their wet and dry deposition and their occurring oxidation patterns is required. Method calibration, quantification of interferences and fundamental research on the speciation and behavior of these species are also still needed [4,5].

The results obtained for oxidized mercury species in the air are largely dependent on the method used for separating different mercury species/fractions [6,7]. Moreover, due to the absence of common calibration of the instruments, the results cannot be directly compared. Reliable comparisons of such data present a great challenge for researchers [2,7–9]. Metrological traceability of atmospheric Hg measurements needs to be ensured in order to achieve comparable data, starting at the traceable calibration of the analytical instrument. The International Vocabulary of Metrology (VIM) defines metrological traceability as a "property of a measurement result whereby the result can be related to a reference through a documented unbroken chain of calibrations, each contributing to the measurement uncertainty" [10]. Recently, there has been progress in ensuring SI traceability of GEM calibrations. SI traceability was achieved by Ent et al. [11], with a mercury vapor generator based upon an improved diffusion method that exploited gravimetric analysis to achieve traceability to the SI unit (mass) [11]. Živković et al. [12] loaded iodinated activated carbon (AC) traps by reducing NIST SRM 3133 and by directly spiking the said SRM (Standard Reference Material®). The results showed that traceable Hg^0 calibration of an iodinated AC trap can be achieved by direct SRM spiking. Quétel et al. used calibration based upon isotope dilution ICP-MS in the liquid phase, combined with automated handling of the air samples, to achieve SI traceability [13,14]. Isotope dilution ICP-MS was also used to calibrate the GEM generator developed by National Institute of Standards and Technology (NIST). NIST SRM 3133 (Mercury Standard Solution) was used for calibrating the ICP-MS method. Since NIST SRM 3133 is traceable to SI units, an unbroken chain of traceability to SI units was achieved [15]. Srivastava et al. [16] applied a high-resolution absorption spectroscopy method to achieve SI traceability for the GEM measurement. SI traceability was achieved by modeling the observations from the first principles (ab initio) and from the overall low measurement uncertainty [16]. Even though SI traceable GEM calibrations are now available, bell-jar calibration with mercury vapor is still widely used [17]. The empirical equation, which describes the relationship between the saturated Hg vapor and the temperature, is not universally agreed upon, which questions the comparability of the obtained data [8,17–20].

To date, the literature offers no SI traceable calibrations for GOM. In the last decade, a system produced by Tekran® (Tekran 2537A) has been the most widely used one for Hg speciation [21–24]. It is usually calibrated with the elemental Hg obtained from a bell-jar apparatus or with its internal calibration, which is performed using a mercury permeation tube that is located in a temperature-controlled chamber within the instrument itself [25]. In addition to lacking traceable calibrations, atmospheric Hg speciation systems are known to be dependent on the sampling method, meteorological conditions, and air quality (i.e., high humidity and high ozone concentration) [9,26,27].

Direct calibration with the gaseous Hg^{2+} species instead of Hg^0 is needed to obtain reliable measurements. Lyman et al. [28] developed a novel calibration unit for Hg atmospheric species using a special design of a permeation oven. The newly developed calibrator achieved stable permeation rates that were high enough to achieve gravimetric verification while emitting relatively high amounts of Hg^0 together with $HgBr_2$ and $HgCl_2$. These amounts were not quantitatively determined; hence, an independent, traceable, and reliable source of Hg compounds was not completely achieved [28]. Recently, efforts have been made to validate the permeation calibration via gravimetric methods. The permeation rates measured by the Tekran 1130 unit, dual-channel system, and gravimetric measurements were not always in agreement, so traceability to the mass has not yet been established [29]. A novel calibration method for the $HgBr_2$ species was implemented by McClure et al. [30]; the authors constructed a permeation tube with $HgBr_2$ crystals inside the tube. Schaedlich et al. [31] patented a calibration system (Hovacal®, IAS GmbH, Oberusel,

Germany) that generates humidified gas from the chosen solution. For the purpose of GOM calibration, $HgCl_2$ solutions of different concentrations can be used [31]. The system requires precise control of the temperature, as well as the flowrate, and is additionally prone to vibrations–all of which are hard to control in field measurements. Moreover, Hg^0 impurities are a known problem, as they introduce uncertainty to such calibration [32]. All GOM generation systems discussed in the introduction are shown and compared in Table 1.

Table 1. Comparison of GOM calibration systems.

Authors	Principle of Operation	Species	Concentration Level
Lyman et al. [28] McClure et al. [30]	permeation	$HgCl_2/HgBr_2$ $HgBr_2$	<1 ng m^{-3} 1 ng m^{-3}
Schaedllich et al. [31] (Hovacal®, IAS GmbH)	liquid evaporation	$HgCl_2$	N/A, used mostly for > 1 µg m^{-3}
Saxholm et al. [33] (Optoseven Ltd. & VTT Ltd.)		$HgCl_2/HgBr_2$ (not yet tested)	>1 µg m^{-3}, potential for ng m^{-3} levels

Recently, Optoseven Ltd., together with VTT Ltd., developed a portable gas generator suitable for generating gaseous Hg^{2+} species within the framework of the MercOx project (MercOx 16ENV01, Metrology for oxidized mercury). An evaporation method was applied to generate oxidized mercury gas. $HgCl_2$ solution of a known concentration is injected into the flow of the carrier gas (e.g., nitrogen) and is evaporated in an evaporation chamber at over 120 °C to form $HgCl_2$ gas. More information regarding the calibration unit is available elsewhere [33]. The calibration unit was previously tested for >1000 ng m^{-3} $HgCl_2$ gas concentrations. Although the flue gas GOM concentrations are in the range of 1000 ng m^{-3} [34,35], the ambient GOM concentrations range from 1–300 pg m^{-3} [36–38], and calibrators also need to be validated for such concentration levels. Petrov et al. [39] evaluated the performance of the calibration unit for the ng m^{-3} to µg m^{-3} concentration range and observed satisfactory results. While the authors obtained great stability, response time, and linearity, the validity of the output still has to be evaluated, especially for low gas concentrations [39]. To enable low concentration validation, stable [40–43] and radioactive [44–48] mercury isotopes can be used. While stable mercury isotopes and isotope dilution mass spectrometry (IDMS) are more commonly used, radioactive Hg isotopes have proven to be advantageous in situations where contamination and detection limits are problematic. Low detection limits can be achieved with radioactive ^{197}Hg due to the high specific activity, which can be obtained by the irradiation of ^{196}Hg-enriched elemental mercury with thermal neutrons (thermal (n,γ) cross section of 3080 barns for ^{196}Hg, one of the highest of all nuclides [49]). To the best of our knowledge, no work has been done on validating the calibration unit for low Hg concentrations. Our objective was to test the calibration unit over longer periods of constant operation and different concentration levels. Speciation measurements of Hg^{2+} and Hg^0 would also be addressed together with the adsorption of Hg^{2+} on the inner parts of the calibration unit and tubing.

2. Materials and Methods

2.1. Chemicals and Instruments

Chemicals used in our work: 95%–97% H_2SO_4 (for analysis, Merck, Darmstadt, Germany), 65% HNO_3 (for analysis, Supelco, Darmstadt, Germany), 30% HCl (suprapur, Merck, Darmstadt, Germany), 47% HBr (for analysis, Merck, Darmstadt, Germany), KCl (suprapur, Merck, Darmstadt, Germany), $KMnO_4$ (for analysis, max. 0.000005% Hg, Merck, Darmstadt, Germany), $HgCl_2$ (≥99.5% purity, Sigma-Aldrich, Darmstadt, Germany), NIST SRM 3133: Mercury (Hg) Standard Solution (National Institute of Standards and Technology, Gaithersburg, MD, USA), ^{196}Hg enriched elemental Hg (enriched to 51.58% ^{196}Hg, Isoflex, San Francisco, CA, USA), and Type I purified water (electrical resistivity 18.2 MΩ

cm; Milli-Q water, Merck, Darmstadt, Germany). Instruments used in our work: high-purity germanium (HPGe) well-type detector (model GCW6023/S, Canberra Industries Inc., Meriden, CT, USA), cold vapor atomic absorption spectrometer (Model Hg-201 Semi-Automated Mercury Analyzer, Sanso Seisakusho Co., Ltd., Tokyo, Japan), and a liquid evaporative generator for oxidized mercury (Optoseven Ltd. & VTT Ltd., Espoo, Finland).

The Optoseven liquid evaporative generator is a portable calibration unit for oxidized mercury. The flowchart of the Optoseven liquid evaporative generator is shown in Figure 1. First, the $HgCl_2$ calibration solution is prepared by dissolving a known amount of Hg^{2+} salt and by adding an adequate amount of HNO_3 and HCl (0.1% v/v for both acids). The $HgCl_2$ solution is pumped by an automatic syringe pump, which can produce precise and low liquid flow rates. The solution is mixed with carrier gas (dry, clean gas, e.g., nitrogen) in the evaporator. The thermal mass flow controller ensures a known mass flow rate of the carrier gas into the evaporator. All parts of the evaporator are covered with a chemically inert polytetrafluoroethylene (PTFE). In the evaporator, the nozzle mixes the carrier gas and the $HgCl_2$ solution; it then sprays the mixture into the evaporation chamber, which is kept at a temperature of >120 °C. Here, the $HgCl_2$ vapor is formed, which is the final output of the generator [33].

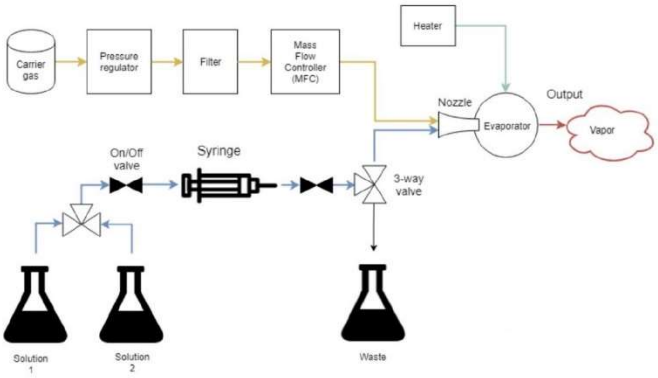

Figure 1. The flowchart of the liquid evaporative generator developed by Optoseven Ltd. and VTT Ltd.

The output $HgCl_2$ gas concentration is calculated by applying Equations (1) and (2).

$$c_{HgCl_2} = \frac{c_{sol}\, Q_{sol}}{Q_{gas} + Q_w} \quad (1)$$

$$Q_w = \frac{Q_{sol}\, R\, T}{M_{H_2O}\, p} \quad (2)$$

where:

$CHgCl_2$ is the concentration of $HgCl_2$ in the output gas [ng m^{-3}],
C_{sol} is the concentration of $HgCl_2$ in the calibration solution [ng L^{-1}],
Q_{sol} is the flowrate of $HgCl_2$ in the calibration solution [mL min^{-1}],
Q_{gas} is the flowrate of the carrier gas [L min^{-1}],
Q_w is the flowrate of water [L min^{-1}],
R is the gas constant [J K mol^{-1}],
T is the temperature [K],
M_{H2O} is the molar mass of water [kg mol^{-1}],
p is the pressure [Pa].

2.2. Production of the ^{197}Hg Radiotracer

Elemental Hg, enriched to 51.58% in the ^{196}Hg isotope (natural abundance is 0.15%), was used for production of the ^{197}Hg radiotracer. Two milliliters of enriched ^{196}Hg in 2% HNO_3 acid (v/v) solution was sealed into a quartz ampoule and irradiated for 12 h in the central channel (CC) of the 250 kW TRIGA Mark II research reactor of the Jožef Stefan Institute (JSI), Ljubljana, Slovenia. The sample was irradiated in neutron flux of 10^{13} cm^{-2} s^{-1} and the ^{197}Hg radionuclide was induced by ^{196}Hg(n,γ)^{197}Hg reaction. After irradiation, the Hg solution was transferred from the irradiated vial and diluted to appropriate Hg concentrations for subsequent experiments. In these experiments, solutions and gases of HgX_2 (X = Cl$^-$, Br$^-$) species were used; their concentrations are given as Hg concentrations in the following paragraphs and not as HgX_2 concentrations if not explicitly stated otherwise.

2.3. Determining ^{197}Hg by Using a HPGe Detector

To obtain standards for gamma measurement, triplicates of a standard solution (8 mL, 2% HNO_3 (v/v)) were transferred into glass vials. The standard solution was always diluted so that the obtained activity was similar to the activity of the measured sample. The activity (γ-rays and X-rays) of the standards in the vials was measured using a HPGe well-type detector.

Using Genie 2000 Gamma analysis software, the activity of ^{197}Hg in the samples was determined by a peak area comparison of the characteristic γ-ray and X-ray emissions for ^{197}Hg ($t_{1/2}$ = 2.671 d, two doublet peaks: 67.0 + 68.8 keV and 77.3 + 78.1 keV). All of the obtained activities were re-calculated to a reference time by applying an equation derived from the exponential law of radioactive decay. The exact equations that were used for the calculation of the activity and recovery are available in the Supplementary Material [44,48,50].

The recoveries discussed in the results section were obtained by comparing the activities of the impinger solution samples (impinger solutions retained $HgCl_2$ gas output of the calibrator–described in detail in the following sections) to the activities of the standard solutions (theoretical, 100% recovery values). To know exactly which activity level corresponded to which $HgCl_2$ concentration, we connected the activities of the $^{197}HgCl_2$ standard solutions to their concentration by CV-AAS measurement (calibration against NIST SRM 3133) [51]. The determined concentration for the stock $HgCl_2$ solution was 93.3 μg mL^{-1} of Hg. CV-AAS measurement was performed before and after irradiation to show that there was no difference in the $HgCl_2$ concentration before and after irradiation. From the $HgCl_2$ solution concentration, we calculated the $HgCl_2$ gas concentration in the calibrator output by applying Equations (1) and (2).

In our work, the solutions and gases of HgX_2 (X = Cl$^-$, Br$^-$) species were used; their concentrations are given as Hg concentrations in the following paragraphs and not as HgX_2 concentrations if not explicitly stated otherwise.

2.4. Calibrator Time Response Tests

2.4.1. Calibrator Time Response Tests Using $HgCl_2$ Gas

To obtain a time-dependent result of the output from the calibrator, it was continuously operating for a period of four workdays (up to 75 h, including continuous operation overnight). Since continuous monitoring of the calibrator output was not possible due to the use of the ^{197}Hg radiotracer, discrete measurements of the calibrator output were performed each day. In order to capture the calibrator output, a three-impinger setup was used as shown in Figure 2. This setup represents a considerable simplification of the Ontario Hydro (OH) method [52]. The setup was comprised of two KCl impingers (100 mL of 1 mol L^{-1} KCl solution) and one $KMnO_4$ impinger (100 mL of 10% $KMnO_4$ (w/v) in 20% H_2SO_4 (v/v) solution) downstream of the former. The KCl impingers were used for capturing Hg^{2+} while the Hg^0 that passed through them was retained in the $KMnO_4$ impinger [52].

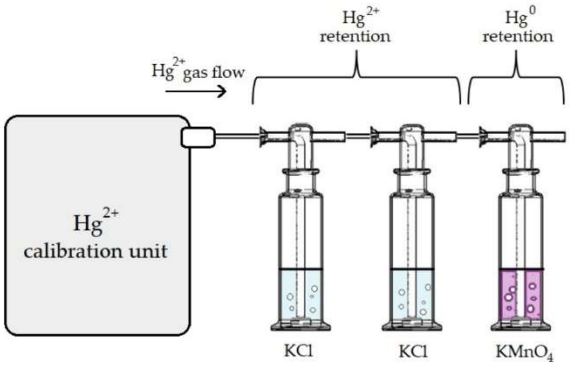

Figure 2. The three-impinger setup used for capturing the $HgCl_2$ gas output of the calibration unit (objects not shown to scale).

The $^{197}HgCl_2$ calibration solution for the Optoseven calibrator was prepared in 0.1% HCl (v/v) + 0.1% HNO_3 (v/v) (in agreement with the work of Saxholm et al. [33]); the $HgCl_2$ concentration depended on the concentration level that was tested, and it ranged from 0.467 ng mL^{-1} to 93.3 ng mL^{-1}, expressed as Hg. The exact composition of the $[HgCl_x]^{2-x}$ species present in the calibration solution was calculated and will be presented in the results and discussion section.

The calibrator was tested for the following conditions: a $^{197}HgCl_2$ solution intake of 0.07 mL min^{-1}, an N_2 carrier gas flow of 5 L min^{-1}, and an evaporation chamber temperature of 125 °C.

Prior to collecting the calibrator output, the calibrator was operated for 1 h for preconditioning in order to achieve a stable temperature in the evaporation chamber. The first discrete measurement taken during the first day was marked as $t = 0$. For a single discrete measurement, the output of the calibrator was collected for 10–20 min, depending on the activity of the radiotracer at the time of collection (a more decayed radiotracer required longer collection times). Eight milliliter aliquots of the impinger solutions were taken for gamma well measurement. Additionally, the ^{197}Hg that was adsorbed into the impinger surfaces was thoroughly cleaned with 10 mL of 10% HNO_3 (v/v) + 5% HCl (v/v) acid solution. Previous tests showed that this was the optimal acidic solution to quantitatively remove all oxidized Hg from the surfaces (results not shown). Eight milliliter aliquots of this washing solution were also taken for gamma measurement in the HPGe well-type detector.

During the 72 h of continuous calibrator operation, discrete measurements of the calibrator output were performed up to three times per workday. Some experiments had to be terminated before the 72 h had finished, due to the power supply malfunction of the calibrator. When the calibrator output was not being collected for discrete measurements, two $KMnO_4$ impingers were used for ^{197}Hg retention to avoid radioactive contamination.

2.4.2. Calibrator Time Response Tests Using $HgBr_2$ Gas

The preparation of standards, calculation of results, and experimental procedure were performed in the same way as described above. The only difference was that for the calibration solution, $^{197}Hg^{2+}$ in 0.1 HBr (v/v) + 0.1 HNO_3 (v/v) was used (two $HgBr_2$ calibration solution concentrations were used, 5.60 and 93.3 ng mL^{-1} expressed as Hg).

2.5. Hg^{2+} Species Adsorption Experiments

To evaluate any potential adsorption of $HgCl_2$ and $HgBr_2$ into the calibrator tubing, a two-impinger setup was used, which is a modification of the previously described setup in Figure 2. Since the speciation of the output was not the goal in these experiments, only two consecutive $KMnO_4$ impingers (prepared as described above) were used to capture the calibrator output. The permanganate solution retained all the present Hg species [53]; therefore, KCl impingers were not required. The scheme of the complete adsorption evaluation setup is shown in Figure 3.

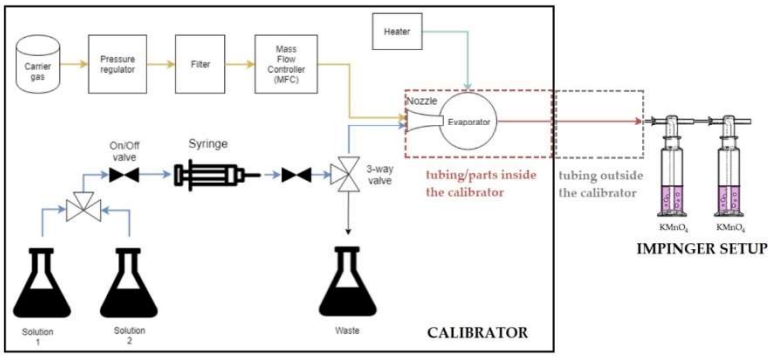

Figure 3. The scheme of the adsorption evaluation setup. Dashed lines show the parts of the setup where the adsorption was evaluated. Adsorption on the tubing/instrument parts inside the calibrator is marked by the red dashed lines, while adsorption on the tubing outside the calibrator is marked by grey dashed lines.

Since the initial purpose of the calibrator was to be used for $HgCl_2$ gas production, more attention was given to this species. To quantify the extent of adsorption, the conditions for capturing the output had to be adjusted. First, the cumulative adsorption of all tubing (inside and outside the calibrator) was evaluated to obtain the whole mass balance. Completely clean tubing inside the calibration unit and outside the calibration unit was used. Without prior preconditioning, the collection of gas output with the two-impinger setup began immediately when the production of HgX_2 gas started. The collection of output lasted for 20 min. When the collection stopped, the calibrator was immediately switched from the production of HgX_2 gas to the cleaning protocol (an injection of a blank into the carrier gas–no formation of $^{197}HgX_2$ gas) for 1 h to remove the $^{197}HgX_2$ adsorbed on the tubing inside the calibrator. The temperature of the calibrator evaporation chamber was 125 °C, and the HgX_2 gas concentration was 1178 ng m^{-3}. The ^{197}Hg on the tubing outside the calibrator was cleaned with 45 mL 10% HNO_3 (v/v) + 5% HCl (v/v) acid solution, and 8 mL aliquots were taken for gamma measurement. Eight milliliter aliquots of the impinger solutions were also taken for gamma measurement. Additionally, the ^{197}Hg that was adsorbed into the impinger surfaces was thoroughly cleaned with 10 mL of 10% HNO_3 (v/v) + 5% HCl (v/v) acid solution. Eight milliliter aliquots of this washing solution were also taken for gamma measurement.

By skipping the cleaning protocol (an injection of a blank into the carrier gas), we could additionally evaluate the adsorption on the tubing only outside the calibrator. All other experimental parameters were the same as in the paragraph above. Two different temperatures of the calibrator evaporation chamber (125 °C and 180 °C) and two different $HgCl_2$ gas concentrations (70.7 and 1178 ng m^{-3}) were tested. $HgBr_2$ adsorption on tubing outside the calibrator was not evaluated.

3. Results and Discussion

To simplify the discussion, the results will for $HgCl_2$ gas will be shown first and then the results for $HgBr_2$ gas. As the calibrator is intended for $HgCl_2$ gas production, most of our efforts were aimed at experiments using $HgCl_2$ gas.

3.1. Results Using $HgCl_2$ Gas

First, we calculated the exact composition of the $HgCl_x^{2-x}$ species present in the calibrator standard solution. The calculation was done by using the total concentration of chloride ions, the total concentration of mercury, as well as the equilibrium constants for the formation of the $HgCl_x^{2-x}$ species obtained from the work of Ciavatta and Grimaldi [54]. The full calculation is available in the Supplementary Material. Chloride concentration was always at least three orders of magnitude higher than the total mercury concentration; therefore, mercury concentration did not influence the calculated results. The obtained composition was 0.12% of $HgCl^+$, 99.6% of $HgCl_2$, and 0.27% of $HgCl_3^-$. Since $HgCl_2$ was clearly the most abundant species, we will discuss the results in terms of $HgCl_2$. Since water evaporates during the formation of $HgCl_2$ calibration gas, the $HgCl_2$ concentration changes, and based on the calculation, the relative abundance of HgCl species vastly changes during this process.

3.1.1. Calibrator Time Response Tests

Figure 4 presents the results obtained by the time response tests. Full results are presented in Supplementary Material.

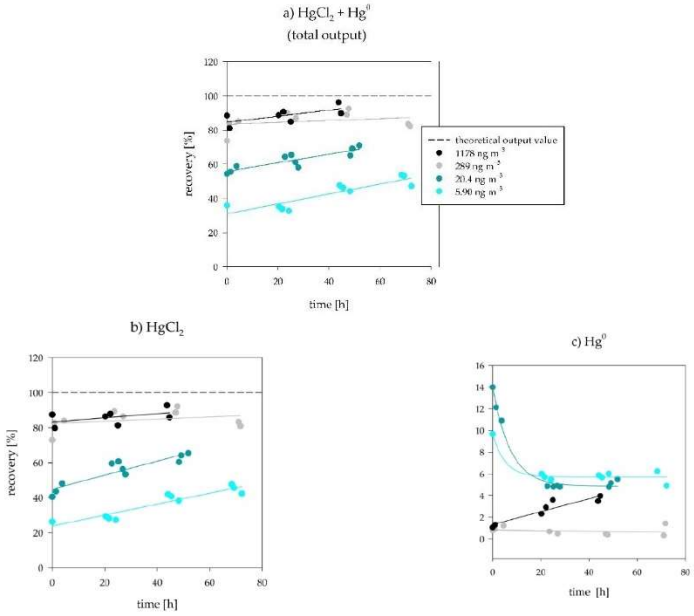

Figure 4. The concentration-dependent response of the $HgCl_2$ calibrator output during four days of continuous operation. (**a**) shows $HgCl_2$ plus Hg^0 (total calibrator output), (**b**) shows $HgCl_2$, and (**c**) shows the Hg^0 values. The straight line at 100 percent shows a 100% recovery value, to which the experimentally obtained values were compared. The experiment with 1178 ng m^{-3} concentration had to be finished after 40 h of operation due to a power supply malfunction.

For the 1178 ng m^{-3} $HgCl_2$ gas concentration experiments, the initial measurement points started at a recovery of 81% and reached a maximum recovery of 96% after 45 h. For the 289 ng m^{-3} $HgCl_2$ gas concentration experiments, the initial measurement points started at a recovery of 74% and reached a maximum recovery of 93% after 48 h (Figure 4a). The absolute percentages of the Hg^0 present in the calibrator output were between 1.2% and 4.4% for 1178 ng m^{-3} and between 0.3% and 1.7% for 289 ng m^{-3} (Figure 4c). Evidently, the recovery is dependent on the $HgCl_2$ gas concentration (Figure 4b). At lower $HgCl_2$ gas concentrations, considerably lower recoveries were obtained. For the 20.4 ng m^{-3} $HgCl_2$ gas concentration experiments, the initial measurement points started at a recovery of 54% and reached a maximum recovery of 71% after 52 h. For the 5.90 ng m^{-3} $HgCl_2$ gas concentration experiments, the initial measurement points started at a recovery value as low as 36% and reached a maximum recovery of 54% after 68 h (Figure 4a). The absolute percentages of the Hg^0 present in the calibrator output were between 7.3% and 26% for 20.4 ng m^{-3} and between 10% and 27% for 5.90 ng m^{-3} (Figure 4c).

Through all the concentration levels, the cumulative calibrator output ($HgCl_2$ + Hg^0) showed an increase with time since the beginning of calibrator operation. The increase was found to be linear with a similar slope, except for the 289 ng m^{-3} concentration (gray color in Figure 4a). If we were to exclude the last two measurements of the 289 ng m^{-3} experiment, the observed linear slope would be similar to the other gas concentrations. The fraction of Hg^0 was higher when using low concentrations than when using high concentrations, especially when considering Hg^0 relative to the whole calibrator output (the relative Hg^0 values are available in the Supplementary Material). A decrease of Hg^0 values with time was observed in four out of the five time-trends. The formation of Hg^0 within the calibrator might have contributed towards the Hg^{2+} + Hg^0 $\rightleftharpoons$ $Hg_2{}^{2+}$ comproportionation [55]. Unfortunately, the methods for $Hg_2{}^{2+}$ analysis and proof of existence in the calibration solution or in the gas are non-existent for the tested concentration levels. Low recoveries and formation of Hg^0 might also be due to the lack of check-valves after liquid injection: remaining Hg^{2+} liquid in the tubing could partition to Hg^0 resulting in losses as shown by the work of Sabri et al. [56]. Even though the findings of Sabri et al. are to be considered, we note that the chemistry of Hg^{2+} in monoethylene glycol is not directly comparable to the chemistry of Hg^{2+} in aqueous solutions.

On the basis of the time response test results, the linearity of the calibrator output was calculated. The results are shown in Figure 5.

While the linear regression resulted in a good correlation coefficient (R^2 = 0.9985), the slope of the experimental regression (k = 76.267) failed to match the theoretical slope (k = 84.835). Since biased low calibrator outputs were observed in the results above, the discrepancy between two slopes was to be expected. Petrov et al. [39] also observed great linearity of the calibrator output for the ng m^{-3} to μg m^{-3} $HgCl_2$ gas concentrations, which is in agreement with the results observed in our work. Even though the difference between the theoretical and experimental slope (Figure 5) might seem minimal, this does not reveal anything about the validity of the calibrator output. As seen previously in Figure 4, recoveries were as low as 32.7% at the beginning of calibrator operation (for the lowest $HgCl_2$ gas concentration), which questions the validity of the calibration unit for low $HgCl_2$ gas concentrations, even though the linearity of the output is observed. The obtained results illustrate that the linearity of the response by itself is not enough to be certain about the validity of the calibrator output.

It is well known that $HgCl_2$ gas tends to adsorb into various surfaces. Therefore, the hypothesis was that consistently low output values could be attributed to the adsorptive nature of $HgCl_2$, which would result in losses on the tubing both inside and outside of the calibrator. The results and discussion regarding the stated hypothesis are shown in the next section of the manuscript.

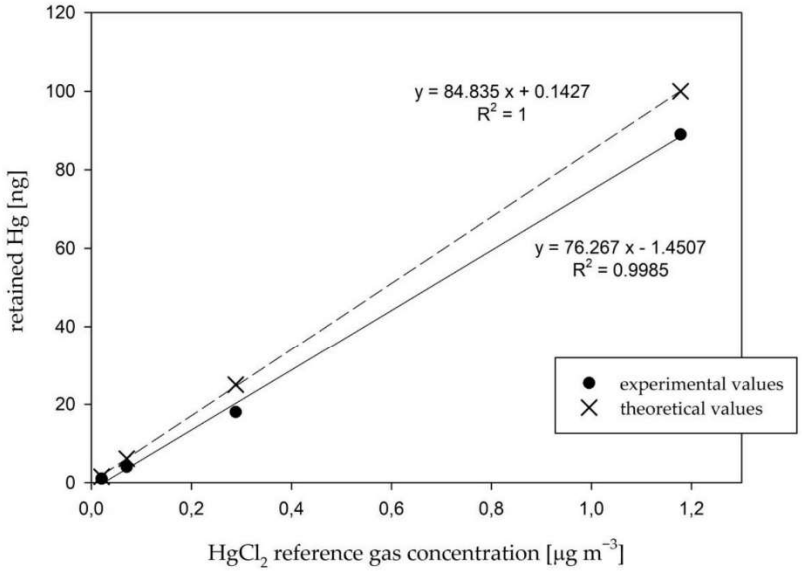

Figure 5. The linearity of the calibrator response at different $HgCl_2$ gas concentrations (from 5.90 to 1178 ng m^{-3}). Each data point represents a measurement at time 2 h after the calibrator start-up for four different $HgCl_2$ gas concentrations. Comparison is shown for theoretical and experimentally determined response.

3.1.2. $HgCl_2$ Adsorption

First, we performed a duplicate measurement of $HgCl_2$ adsorption on combined tubing outside and inside of the calibrator. The experiment is described in detail in Section 2.4. The results are presented in Table 2.

Table 2. The adsorption of the tubing inside and outside the calibration unit. A 70.7 ng m^{-3} $HgCl_2$ gas concentration and a 125 °C calibrator evaporation chamber temperature were used.

	Tubing Inside the Calibrator [%]	Tubing Outside the Calibrator [%]	Two-Impinger Setup [%]	Sum [%]
replicates	13.2	41.6	46.1	101
	16.3	45.5	43.6	105
average	14.7	43.6	44.8	103

The experiment was performed to show that complete mass balance can be achieved if we combine the $HgCl_2$ that reached the two-impinger setup with the adsorbed $HgCl_2$ on the tubing. Table 2 shows that the assumption was correct, since a 103% average mass balance was obtained. This was a considerable increase in the mass balance in comparison to the results for the calibrator time response tests in the previous section. The missing percentage of $HgCl_2$ was, therefore, attributed to the adsorption of the tubing inside the calibrator. Since the experimental conditions had to be adjusted to enable adsorption measurements, we stress that these results (103% mass balance) are not comparable with the results obtained from the time response experiments (in the previous section). Additional experiments were performed to evaluate the influence of the concentration as well as the calibrator evaporation chamber temperature on $HgCl_2$ adsorption. Only the influence

of adsorption on the tubing outside the calibrator was evaluated, since it was less time-consuming. The results are presented in Table 3.

The extent of the adsorption varied over different experimental conditions but usually ranged from 15.8% to 18.8%. The exception to this was the experiment with the 125 °C evaporation chamber temperature and the $HgCl_2$ gas concentration of 70.7 ng m^{-3}; these values ranged from 43.1% to 47.1%, which was considerably higher. These higher values can be attributed to the fact that the lower temperature of the evaporation chamber resulted in a lower gas temperature; consequently, more adsorption on the tubing surfaces occurred. For the 1178 ng m^{-3} $HgCl_2$ gas concentration experiment, the effect of the temperature was not as significant.

Table 3. The $HgCl_2$ adsorption of the tubing outside the calibrator in dependence on $HgCl_2$ gas concentration and the temperature of the calibrator evaporation chamber.

$HgCl_2$ Gas Concentration	Temperature of the Calibrator Evaporation Chamber [°C]	Tubing Outside the Calibrator [%]	Two-Impinger Setup [%]	Sum [%]
70.7 ng m^{-3}	125	47.1	43.7	90.7
		43.1	35.4	78.5
	180	18.8	61.8	80.6
1178 ng m^{-3}	125	16.9	63.1	80.1
		15.8	76.9	92.8
	180	16.3	74.3	90.6
		17.1	73.6	90.7

3.1.3. Efforts to Minimize $HgCl_2$ Adsorption

Adsorption was clearly a recurring problem. We tried to solve it in two different ways: with the use of monolithic ceramics and with the saturation of the tubing surfaces with high $HgCl_2$ gas concentrations:

(a) Use of monolithic boron nitride for tubing.

For the monolithic ceramic, we tested BN (boron nitride). The monolithic boron nitride (BN) tubing was tested due to the fact that BN is one of the most chemically resistant materials (possibly eliminating chemisorption of $HgCl_2$) [57]. Absorption into the Teflon tubing was compared to adsorption into the BN tubing by simply exposing both of these tubes to the same $HgCl_2$ gas concentration and then washing the tubing with 10% HNO_3 (v/v) + 5% HCl (v/v) acid solution. Adsorption was still present to an extent, even after using BN; therefore, we concluded that $HgCl_2$ adsorption is most probably a combination of chemisorption and physisorption, since BN is known to enhance physisorption [57].

(b) Saturation of adsorption sites.

Using high $HgCl_2$ gas concentrations could in a way precondition the system for the use of low $HgCl_2$ gas concentration. The active sites on tubing surface would be fully occupied; therefore, $HgCl_2$ adsorption could in theory be minimal. The whole experimental procedure was the same as described in Section 2.4.1. The only difference was that for this experiment, a mixture of cold $HgCl_2$ (without a ^{197}Hg radiotracer) and hot $HgCl_2$ (with a ^{197}Hg radiotracer) was used as a calibration solution for the formation of $HgCl_2$ gas. Cold $HgCl_2$ was used solely to saturate the tubing surfaces, while hot $HgCl_2$ was used for detection (cold $HgCl_2$ was not considered when calculating the recovery). After 24 h, the calibration solution (a combination of cold and hot $HgCl_2$) was replaced with hot $HgCl_2$ only. Therefore, the gas was switched from the initial high saturating concentration to a low concentration of $HgCl_2$.

Recovery values of 100% (calculated as described in previous sections) were compared to the actual calibrator output obtained from the ^{197}Hg radiotracer activity. The results of

the experiment for behavior of the calibrator under saturating conditions are shown in Figure 6.

The output of the calibrator reached the plateau value (Figure 6) when using a high conc. cold + low conc. hot $HgCl_2$. The hypothesis was that after occupying all adsorption places with a high $HgCl_2$ concentration, the calibrator output would stay at the same level when switching to a low conc. hot $HgCl_2$ only. As the adsorption places would hypothetically stay occupied, that would assure minimal adsorption even when changing to a low $HgCl_2$ concentration. Evidently, this was not the case, as the recoveries fell shortly after switching to a low conc. hot $HgCl_2$ (Figure 6), meaning that the adsorption of $HgCl_2$ was not permanent but collapsed shortly after. Hg^0 started rising after switching to low $HgCl_2$ concentrations. In fact, the recovery values and Hg^0 fraction approached the values obtained in Figure 4 (5.90 ng m^{-3}, light blue data points in the first measurement day).

The clear conclusion was that the method of preconditioning (saturating) the tubing of the setup prior to the use of low $HgCl_2$ concentrations in order to lower the effect of adsorption is inefficient. Adsorption in this case proved to be a dynamic process that competed with desorption rather than an irreversible one.

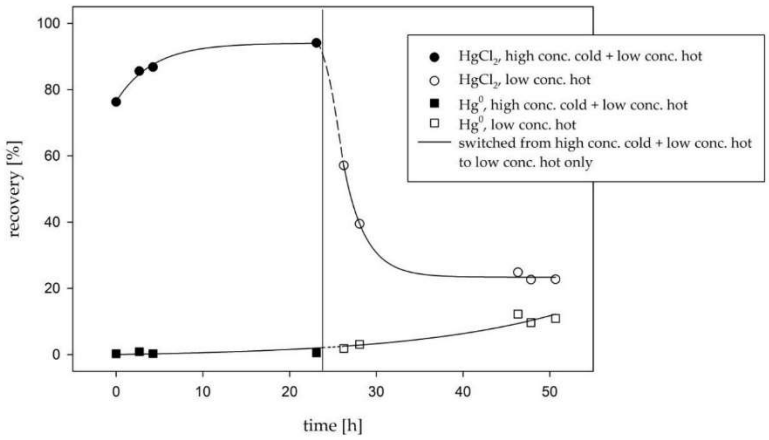

Figure 6. The characterization of the calibrator output when using high $HgCl_2$ concentrations (a combination of cold and hot $HgCl_2$) and after switching from high to low $HgCl_2$ concentrations (hot $HgCl_2$ only). The data points labelled "high conc. cold + low conc. hot" were obtained while the gas was comprised of a cold Hg (12.6 µg m^{-3}, "saturating" concentration) and a hot Hg (5.90 ng m^{-3}, low concentration) mixture. The data points labelled "low conc. hot" were obtained while the gas was comprised of only a hot Hg (low concentration). The continuous lines connecting the data points are estimations of the time trend using different regressions, and the dashed lines are extrapolations of the said regressions.

3.2. Results Using $HgBr_2$ Gas

3.2.1. Calibrator Time Response Tests

Similar to $HgCl_2$, we calculated the exact composition of the $HgBr_x^{2-x}$ species present in the calibrator standard solution. The calculation was performed in the same way as for $HgCl_x^{2-x}$, the exception being that the equilibrium constants for the formation of the $HgBr_x^{2-x}$ species were obtained from the work of Hepler and Olofsson [58]. The obtained composition was 98.4% of $HgBr_2$ and 1.58% of $HgBr_3^-$. Since $HgBr_2$ was clearly the most abundant species, we will discuss the results in terms of $HgBr_2$ only. Again, the water evaporates during the formation of $HgCl_2$ calibration gas, meaning that the $HgBr_2$ concentration changes, and the calculated composition vastly changes during this process.

The time response test results for the $HgBr_2$ gas are shown in Table 4.

The calibrator output for $HgBr_2$ rose slowly in comparison to the same gas concentrations for $HgCl_2$. To compare, the experiment with the 1178 ng m^{-3} $HgCl_2$ gas concentration resulted in a maximum recovery value of 96% while for the same concentration, the $HgBr_2$ experiment only resulted in a maximum recovery value of 30%. Considering the low starting values of the output, plus the fact that the $HgBr_2$ output values increased slowly, the full time-trends for $HgBr_2$ were not further investigated. To explain the results, we again proposed the hypothesis that the low recoveries were a result of $HgBr_2$ adsorption on the tubing both inside and outside the calibrator.

Table 4. The calibrator output composition during a time-trend experiment using 70.7 and 1178 ng m^{-3} $HgBr_2$ gas concentration. Columns "KCl 1," "KCl 2," and "$KMnO_4$" represent the first KCl impinger ($^{197}HgBr_2$ retention), the second KCl impinger ($^{197}HgBr_2$ retention, breakthrough), and $KMnO_4$ impinger ($^{197}Hg^0$ retention), respectively, and are presented as recovery percentages.

$HgBr_2$ Gas Concentration	Time [h]	KCl 1 [%]	KCl 2 [%]	$KMnO_4$ [%]	Sum [%]
70.7 ng m^{-3}	0	9.55	0.05	0.27	9.87
	1.50	10.3	0.42	0.12	10.8
	3.66	11.8	0.07	0.62	12.5
1178 ng m^{-3}	0	18.7	3.29	2.01	24.0
	1	27.4	0.07	1.97	29.5
	3	26.3	0.55	2.22	29.1

3.2.2. $HgBr_2$ Adsorption on the Outside and Inside Tubing of the Calibrator Combined

A duplicate measurement of $HgBr_2$ adsorption on the combined tubing outside and inside the calibrator was made due to the time-consuming nature of the experiment. Mass balances of 100% and 101% were obtained for $HgBr_2$. For $HgBr_2$, no adsorption experiments for tubing outside the calibrator were made (for $HgCl_2$ they were), but since complete mass balance was obtained by the experiment for combined adsorption on tubing outside and inside the calibrator, the presence of such adsorption can be attributed with high certainty.

When comparing $HgBr_2$ and $HgCl_2$ adsorption, the extent of adsorption seemed to be much greater for $HgBr_2$ than for $HgCl_2$. The only relevant physicochemical characteristic that separates these two species is their solubility. $HgCl_2$ is more soluble in water (6.57 g of $HgCl_2$ per 100 mL of water at 20 °C) than $HgBr_2$ (0.56 g of $HgBr_2$ per 100 mL of water at 20 °C). The dependence of adsorption on solubility is described by the Lundelius rule, which is used to predict (semi-quantitatively) the effect of the chemical character of the solute on its adsorption on surfaces. The rule states that there is an inverse relationship between solute solubility and adsorption, since the solute-solid surface binding competes with the solute-solvent attraction [59].

3.3. Thermodynamics of $HgCl_2$ Adsorption

Based upon the data obtained in the above described results, the adsorption isotherm was calculated. The previous literature mostly focuses on the adsorption isotherms for $HgCl_2$ adsorption on activated carbon [60,61], which is not applicable to our experiments. Therefore, we had to choose the most suitable isotherm for our case ($HgCl_2$ adsorption on Teflon tubing surfaces). The Langmuir adsorption isotherm was chosen, as it is most often used to describe chemisorption, which is thought to be the predominant adsorption type at higher $HgCl_2$ gas temperatures [62]. Additionally, the Langmuir model resulted in the best fit for our data.

The concentration of all available adsorption sites was calculated based on the assumption that for the highest gas concentration time-trend (1178 ng m^{-3}), all adsorption sites would be occupied. The concentration of the adsorbed $HgCl_2$ was obtained from the adsorption experiments described above. The temperature of the $HgCl_2$ gas was assumed to be the same as the temperature of the evaporation chamber (a high gas flow and a short

tubing length resulted in minimal cooling of the gas). Figure 7 presents the Langmuir adsorption isotherm for $HgCl_2$ adsorption on Teflon tubing at 125 °C.

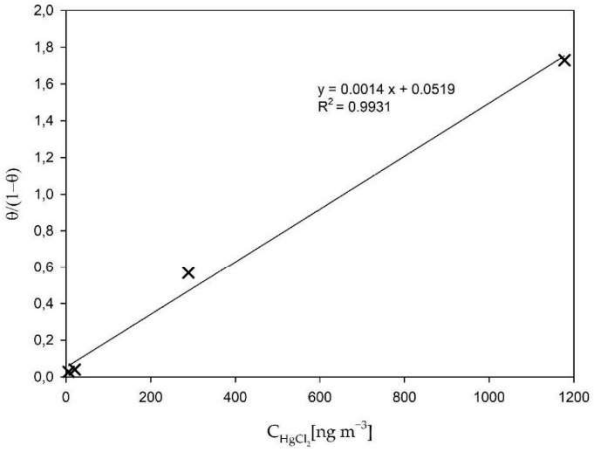

Figure 7. The Langmuir adsorption isotherm for $HgCl_2$ adsorption on Teflon tubing: 125 °C. θ presents the occupancy of adsorption sites, while C_{HgCl2} presents $HgCl_2$ gas concentration.

From the slope ($k_{125°C}$ = 0.0014 m^3 ng^{-1}) of the above presented Langmuir isotherm adsorption, the equilibrium constant at 125 °C ($K_{eq,125°C}$) can be calculated by using Equation (3) [63]:

$$K_{eq} = k\, M_{ads} \tag{3}$$

M_{ads} is the molecular weight of the adsorbate (in our case $HgCl_2$). The Langmuir isotherm was similarly applied for adsorption experiments at 180 °C. From the obtained slope ($k_{180°C}$ = 0.0022 m^3 ng^{-1}), the adsorption equilibrium constant at 180 °C ($K_{eq,180°C}$) was also calculated using Equation (3). From the two temperatures and their corresponding adsorption equilibrium constants, the adsorption enthalpy (ΔH_{ads}) for $HgCl_2$ adsorption on Teflon tubing was calculated using van't Hoff equation Equation (4) [63]:

$$\frac{d}{dT} lnK_{eq} = \frac{\Delta H^{\theta}}{RT^2} \tag{4}$$

The obtained value for adsorption enthalpy was $\Delta H_{ads} = -12.33$ kJ mol^{-1}. The negative value of the enthalpy suggests that the observed adsorption is an exothermal process. Lower temperatures would, therefore, promote adsorption, while higher temperatures would suppress it. This is in line with results observed by other authors [59,63,64].

The ΔH_{ads} value that was obtained in our work is not an exact value but more likely an estimation, due to the fact that some simplifications (the constant value of gas temperature and the estimation of the number of all adsorption sites) were used in order to be able to obtain ΔH_{ads}. Additionally, only two data points were available for calculation of Langmuir isotherm at 180 °C, therefore we could only assume that Langmuir isotherm is also best fitting isotherm for 180 °C adsorption from the fact that it was the case for the 125 °C isotherm.

3.4. Re-Estimation of the Uncertainty Budget for the Calibration Unit

On the basis of obtained results, the uncertainty budget for the calibration unit was re-estimated in accordance with Guide to the Expression of Uncertainty in Measurement

(GUM) [65]. Overall, the uncertainty budget of the Optoseven calibrator was previously estimated to be 2.02% (k = 2) at 10 μg m^{-3} $HgCl_2$ gas concentration [33]. By combining 2.02% with the uncertainty component of the recovery values obtained in our work, we calculated the new overall uncertainty values (k = 2), which were 4.10, 5.31, 6.35, and 12.1% for 1178, 289, 20.4, and 5.90 ng m^{-3} gas concentrations, respectively. The equations used for the calculation of the total uncertainty of the calibrator are presented in the Supplementary Material. We acknowledge that the concentration used for the uncertainty budget evaluation by the instrument providers (10 μg m^{-3}) is not in the same range as our concentrations. Nevertheless, this was the only data on the uncertainty of the calibration unit that were available to us. Dilutions of the standard solutions (for low gas concentrations) that were performed in addition to what was already considered by the calibrator manufacturers were not included in these calculations, since their contribution was negligible.

Whether or not the calculated uncertainty is acceptable for field measurement is still not clear. It can be concluded that the calibration unit and its uncertainty is suitable for flue gas GOM concentrations (>1 μg m^{-3}). The concentration dependence of recoveries prevents the system to be used for calibration of instruments for ambient GOM measurements.

4. Conclusions

The ^{197}Hg radiotracer has proven to be suitable for studying the characteristics of calibrators because it enabled us to closely follow the processes that limit the use of calibrators based on evaporation, especially for low GOM concentrations. The calibrator could be used for high concentration GOM calibrations, but the recovery and its contribution to the uncertainty must be considered. The recoveries have been shown to be even lower if we replace $HgCl_2$ with $HgBr_2$, suggesting that different GOM calibration systems will need to be developed (since $HgBr_2$ is commonly used as a proxy for all atmospheric HgBr species). In the future, similar calibration units will need to address the adsorption problem in order to provide calibration with ambient GOM levels or, alternatively, to change the principle of operation of the unit. Given that most GOM measurement systems are based on pre-concentration traps/denuders due to low concentrations, it is necessary to develop a calibration system that will be compatible with this pre-concentration method and will have uncertainty that will minimally contribute to the overall uncertainty.

Supplementary Materials: The following are available online at https://www.mdpi.com/article/10.3390/s21072501/s1: Equation S1; Equation S2; Equation S3; Equation S4; Table S1: calibrator output composition during the time-trend experiment using 1178 ng m^{-3} $HgCl_2$ gas concentration; Table S2: calibrator output composition during the time-trend experiment using 289 ng m^{-3} $HgCl_2$ gas concentration; Table S3: calibrator output composition during the time-trend experiment using 20.4 ng m^{-3} $HgCl_2$ gas concentration; and Table S4: calibrator output composition during the time-trend experiment using 5.90 ng m^{-3} $HgCl_2$ gas concentration.

Author Contributions: Conceptualization, J.G., S.R.G., J.K. and M.H.; Funding acquisition, M.H.; Methodology, J.G., I.Ž., S.R.G. and R.J.; Project administration, M.H.; Supervision, J.K. and M.H.; Validation, J.G. and I.Ž.; Writing—original draft, J.G.; Writing—review & editing, J.G., I.Ž. and M.H. All authors have read and agreed to the published version of the manuscript.

Funding: Project 16ENV01 MercOx which has received funding from the EMPIR program co-financed by the Participating States and from the European Union's Horizon 2020 research and innovation program; Slovenian Research Agency (ARRS), grant number P1-0143; Metrology Institute of the Republic of Slovenia (MIRS), contract number C3212-10-000071 (6401-5/2009/27).

Institutional Review Board Statement: Not applicable.

Informed Consent Statement: Not applicable.

Data Availability Statement: Data is contained within the article or Supplementary Material.

Acknowledgments: The authors would like to thank the TRIGA reactor staff at the Reactor Infrastructure Centre of the JSI for their availability and cooperation at all times. We would also like to thank

Jarkko Makkonen and Timo Rajamäki for supplying us with the calibrator and for operational advice. Financial support from the project Integrated Global Observing Systems for Persistent Pollutants (IGOSP) funded by the European Commission in the framework of program "The European network for observing our changing planet (ERA-PLANET)", Grant Agreement: 689443 is also acknowledged.

Conflicts of Interest: The authors declare no conflict of interest.

References

1. UN Environment. *Global Mercury Assessment 2018*; United Nations Environment Programme: Nairobi, Kenya, 2019.
2. Lyman, S.N.; Cheng, I.; Gratz, L.E.; Weiss-Penzias, P.; Zhang, L. An updated review of atmospheric mercury. *Sci. Total Environ.* **2020**, *707*, 135575. [CrossRef]
3. Holmes, C.D.; Jacob, D.J.; Mason, R.P.; Jaffe, D.A. Sources and deposition of reactive gaseous mercury in the marine atmosphere. *Atmos. Environ.* **2009**, *43*, 2278–2285. [CrossRef]
4. Ariya, P.A.; Amyot, M.; Dastoor, A.; Deeds, D.; Feinberg, A.; Kos, G.; Poulain, A.; Ryjkov, A.; Semeniuk, K.; Subir, M.; et al. Mercury Physicochemical and Biogeochemical Transformation in the Atmosphere and at Atmospheric Interfaces: A Review and Future Directions. *Chem. Rev.* **2015**, *115*, 3760–3802. [CrossRef] [PubMed]
5. Selin, N.E. Global Biogeochemical Cycling of Mercury: A Review. *Annu. Rev. Environ. Resour.* **2010**, *34*, 43–63. [CrossRef]
6. Gustin, M.S.; Dunham-Cheatham, S.M.; Zhang, L. Comparison of 4 Methos for Measurement of Reactive, Gaseous Oxiize, an Particulate Bound Mercury. *Environ. Sci. Technol.* **2019**, *53*, 14489–14495. [CrossRef] [PubMed]
7. Gustin, M.S.; Dunham-Cheatham, S.M.; Huang, J.; Lindberg, S.; Lyman, S.N. Development of an Understanding of Reactive Mercury in Ambient Air: A Review. *Atmosphere* **2021**, *12*, 73. [CrossRef]
8. Gustin, M.; Jaffe, D. Reducing the uncertainty in measurement and understanding of mercury in the atmosphere. *Environ. Sci. Technol.* **2010**, *44*, 2222–2227. [CrossRef]
9. Gustin, M.S.; Huang, J.; Miller, M.B.; Peterson, C.; Jaffe, D.A.; Ambrose, J.; Finley, B.D.; Lyman, S.N.; Call, K.; Talbot, R.; et al. Do we understand what the mercury speciation instruments are actually measuring? Results of RAMIX. *Environ. Sci. Technol.* **2013**, *47*, 7295–7306. [CrossRef] [PubMed]
10. The International Bureau of Weights and Measures (BIPM). *International Vocabulary of Metrology-Basic and General Concepts and Associated Terms (VIM)*; JCGM 200; Joint Committee for Guides in Metrology: Paris, France, 2012.
11. Ent, H.; Van Andel, I.; Heemskerk, M.; Van Otterloo, P.; Bavius, W.; Baldan, A.; Horvat, M.; Brown, R.J.C.; Quétel, C.R. A gravimetric approach to providing SI traceability for concentration measurement results of mercury vapor at ambient air levels. *Meas. Sci. Technol.* **2014**, *25*, 115801. [CrossRef]
12. Živković, I.; Berisha, S.; Kotnik, J.; Jagodic, M.; Horvat, M. Traceable determination of atmospheric mercury using iodinated activated carbon traps. *Atmosphere* **2020**, *11*, 780. [CrossRef]
13. Quétel, C.R.; Zampella, M.; Brown, R.J.C.; Ent, H.; Horvat, M.; Paredes, E.; Tunc, M. International system of units traceable results of Hg mass concentration at saturation in air from a newly developed measurement procedure. *Anal. Chem.* **2014**, *86*, 7819–7827. [CrossRef] [PubMed]
14. Quétel, C.R.; Zampella, M.; Brown, R.J.C. Temperature dependence of Hg vapour mass concentration at saturation in air: New SI traceable results between 15 and 30 °C. *TrAC-Trends Anal. Chem.* **2016**, *85*, 81–88. [CrossRef]
15. Long, S.E.; Norris, J.E.; Carney, J.; Ryan, V.; Mitchell, G.D.; Dorko, W.D. Traceability of the output concentration of mercury vapor generators. *Atmos. Pollut. Res.* **2020**, *11*, 639–645. [CrossRef]
16. Srivastava, A.; Hodges, J.T. Development of a High-Resolution Laser Absorption Spectroscopy Method with Application to the Determination of Absolute Concentration of Gaseous Elemental Mercury in Air. *Anal. Chem.* **2018**, *90*, 6781–6788. [CrossRef]
17. Dumarey, R.; Brown, R.J.C.; Corns, W.T.; Brown, A.S.; Stockwell, P.B. Elemental mercury vapour in air: The origins and validation of the "Dumarey equation" describing the mass concentration at saturation. *Accredit. Qual. Assur.* **2010**, *15*, 409–414. [CrossRef]
18. Brown, R.J.C.; Brown, A.S. Accurate calibration of mercury vapour measurements. *Analyst* **2008**, *133*, 1611–1618. [CrossRef] [PubMed]
19. Harvey, A.H. Estimation of the enhancement factor for mercury in air. *Int. J. Thermophys.* **2010**, *31*, 297–307. [CrossRef]
20. Huber, M.L.; Laesecke, A.; Friend, D.G. Correlation for the vapor pressure of mercury. *Ind. Eng. Chem. Res.* **2006**, *45*, 7351–7361. [CrossRef]
21. Ambrose, J.L. Improved methods for signal processing in measurements of mercury by Tekran® 2537A and 2537B instruments. *Atmos. Meas. Tech.* **2017**, *10*, 5063–5073. [CrossRef]
22. Brooks, S.; Ren, X.; Cohen, M.; Luke, W.; Kelley, P.; Artz, R.; Hynes, A.; Landing, W.; Martos, B. Airborne Vertical Profiling of Mercury Speciation near Tullahoma, TN, USA. *Atmosphere* **2014**, *5*, 557–574. [CrossRef]
23. Slemr, F.; Weigelt, A.; Ebinghaus, R.; Kock, H.H.; Bödewadt, J.; Brenninkmeijer, C.A.M.; Rauthe-schöch, A.; Weber, S.; Hermann, M.; Becker, J.; et al. Atmospheric mercury measurements onboard the CARIBIC passenger aircraft. *Atmos. Meas. Tech.* **2016**, *9*, 2291–2302. [CrossRef]
24. Xu, L.; Chen, J.; Yang, L.; Niu, Z.; Tong, L.; Yin, L.; Chen, Y. Chemosphere Characteristics and sources of atmospheric mercury speciation in a coastal city, Xiamen, China. *Chemosphere* **2015**, *119*, 530–539. [CrossRef] [PubMed]
25. Landis, M.S. Development and Characterization of an Annular Denuder Methodology for the Measurement of Divalent Inorganic Reactive Gaseous Mercury in Ambient Air. *Environ. Sci. Technol.* **2002**, *36*, 3000–3009. [CrossRef] [PubMed]

26. Huang, J.; Gustin, M.S. Uncertainties of gaseous oxidized mercury measurements using KCL-coated denuders, cation-exchange membranes, and nylon membranes: Humidity influences. *Environ. Sci. Technol.* **2015**, *49*, 6102–6108. [CrossRef] [PubMed]
27. Huang, J.; Miller, M.B.; Weiss-Penzias, P.; Gustin, M.S. Comparison of gaseous oxidized Hg measured by KCl-coated denuders, and nylon and cation exchange membranes. *Environ. Sci. Technol.* **2013**, *47*, 7307–7316. [CrossRef]
28. Lyman, S.; Jones, C.; O'Neil, T.; Allen, T.; Miller, M.; Gustin, M.S.; Pierce, A.M.; Luke, W.; Ren, X.; Kelley, P. Automated calibration of atmospheric oxidized mercury measurements. *Environ. Sci. Technol.* **2016**, *50*, 12911–12927. [CrossRef]
29. Lyman, S.N.; Gratz, L.E.; Dunham-cheatham, S.M.; Gustin, M.S.; Luippold, A. Improvements to the Accuracy of Atmospheric Oxidized Mercury Measurements. *Environ. Sci. Technol.* **2020**, *54*, 13379–13388. [CrossRef]
30. McClure, C.D.; Jaffe, D.A.; Edgerton, E.S. Evaluation of the KCl denuder method for gaseous oxidized mercury using HgBr2 at an in-service AMNet site. *Environ. Sci. Technol.* **2014**, *48*, 11437–11444. [CrossRef]
31. Schaedlich, F.R.; Schneeberger, D.R. Calibration Gas Delivery Apparatus. U.S. Patent 7,713,742 B2, 11 May 2010.
32. Dunham, G.; Mibeck, B.; Schulz, R.; Wilmoth, S. Catalyst for Generating Oxidized Mercury for Testing Mercury Continuous Emission Monitors (CEM). U.S. Patent 7,829,047 B2, 8 November 2010.
33. Saxholm, S.; Rajamäki, T.; Hämäläinen, J.; Hildén, P. Dynamic calibration method for reactive gases. *Meas. Sci. Technol.* **2020**, *31*, 034001.
34. Zhao, S.; Duan, Y.; Chen, L.; Li, Y.; Yao, T.; Liu, S.; Liu, M.; Lu, J. Study on emission of hazardous trace elements in a 350 MW coal-fired power plant. Part 1. Mercury. *Environ. Pollut.* **2017**, *229*, 863–870. [CrossRef] [PubMed]
35. Mlakar, T.L.; Horvat, M.; Vuk, T.; Stergaršek, A.; Kotnik, J.; Tratnik, J.; Fajon, V. Mercury species, mass flows and processes in a cement plant. *Fuel* **2010**, *89*, 1936–1945. [CrossRef]
36. Zhou, H.; Hopke, P.K.; Zhou, C.; Holsen, T.M. Ambient mercury source identification at a New York State urban site: Rochester, NY. *Sci. Total Environ.* **2019**, *650*, 1327–1337. [CrossRef]
37. Castro, M.S.; Moore, C.; Sherwell, J.; Brooks, S.B. Dry deposition of gaseous oxidized mercury in Western Maryland. *Sci. Total Environ.* **2012**, *417–418*, 232–240. [CrossRef]
38. Ambrose, J.L.; Lyman, S.N.; Huang, J.; Gustin, M.S.; Jaffe, D.A. Fast time resolution oxidized mercury measurements during the reno atmospheric mercury intercomparison experiment (RAMIX). *Environ. Sci. Technol.* **2013**, *47*, 7285–7294. [CrossRef]
39. Petrov, P.; Rajamäki, T.; Corns, W.T.; Goenaga-Infante, H. Evaluating the performance of oxidized Hg reference gas generators in the range ng m−3 to µg m−3 by improved coupling with ICP-MS. *Atmos. Environ. X* **2020**, *8*, 100090.
40. Long, S.E.; Norris, J.E.; Carney, J.; Ryan, J.V. Provision of primary NIST traceability to support vapor phase mercury emissions monitoring of combustion sources using isotope dilution inductively coupled plasma mass spectrometry. *Atmos. Pollut. Res.* **2020**, *11*, 909–919. [CrossRef]
41. Lynam, M.M.; Klaue, B.; Keeler, G.J.; Blum, J.D. Using thermal analysis coupled to isotope dilution cold vapor ICP-MS in the quanti fi cation of atmospheric particulate phase mercury. *J. Anal. At. Spectrom.* **2013**, *28*, 1788–1795. [CrossRef]
42. Štrok, M.; Anabelle, P.; Hintelmann, H. Comptes Rendus Geoscience The mercury isotope composition of Arctic coastal seawater. *C. R. Geosci.* **2015**, *347*, 368–376. [CrossRef]
43. Mazur, M.E.E.; Eckley, C.S.; Mitchell, C.P.J. Susceptibility of Soil Bound Mercury to Gaseous Emission As a Function of Source Depth: An Enriched Isotope Tracer Investigation. *Environ. Sci. Technol.* **2015**, *49*, 9143–9149. [CrossRef]
44. Ribeiro Guevara, S.; Jereb, V.; Arribére, M.A.; Pérez Catán, S.; Horvat, M. The production and use of $^{197}Hg^{g}$ radiotracer to study mercury transformation processes in environmental matrices. *RMZ-Mater. Geoenviron. J.* **2004**, *51*, 1928–1931.
45. Koron, N.; Bratkič, A.; Ribeiro Guevara, S.; Vahčič, M.; Horvat, M. Mercury methylation and reduction potentials in marine water: An improved methodology using ^{197}Hg radiotracer. *Appl. Radiat. Isot.* **2012**, *70*, 46–50. [CrossRef]
46. Žižek, S.; Ribeiro Guevara, S.; Horvat, M. Validation of methodology for determination of the mercury methylation potential in sediments using radiotracers. *Anal. Bioanal. Chem.* **2008**, *390*, 2115–2122. [CrossRef]
47. Ribeiro Guevara, S.; Queimaliños, C.P.; Diéguez, M.d.C.; Arribére, M. Methylmercury production in the water column of an ultraoligotrophic lake of Northern Patagonia, Argentina. *Chemosphere* **2008**, *72*, 578–585. [CrossRef]
48. Ribeiro Guevara, S.; Horvat, M. Stability and behaviour of low level spiked inorganic mercury in natural water samples. *Anal. Methods* **2013**, *5*, 1996–2006. [CrossRef]
49. Shibata, K. Evaluation of neutron nuclear data on mercury isotopes. *J. Nuclear Sci. Technol.* **2016**, *53*, 1595–1607. [CrossRef]
50. Ribeiro Guevara, S.; Žižek, S.; Repinc, U.; Catán, S.P.; Jačimović, R.; Horvat, M. Novel methodology for the study of mercury methylation and reduction in sediments and water using ^{197}Hg radiotracer. *Anal. Bioanal. Chem.* **2007**, *387*, 2185–2197. [CrossRef]
51. Akagi, H. Analytical methods for evaluating human exposure to mercury due to gold mining. In Proceedings of the Health and Environmental Effects of Mercury due to Mining Operations, Manila, Philipines, 26–27 November 1997; pp. 131–141.
52. Wang, S.; Zhang, L.; Wu, Y. Mercury emission and speciation of coal-fired power plants in China. *Atmos. Chem. Phys.* **2010**, *10*, 1183–1192. [CrossRef]
53. Kho, F.; Pham, G.H. Absorption kinetics of mercury (II) chloride into water and aqueous sodium chloride solution. *Fuel Process. Technol.* **2018**, *174*, 78–87. [CrossRef]
54. Ciavatta, L.; Grimaldi, M. Equilibrium Constants of Mercury (II) Chloride Complexes. *J. Inorg. Nucl. Chem.* **1968**, *30*, 197–205. [CrossRef]
55. Kozin, L.F.; Hansen, S.C. *Mercury Handbook: Chemistry, Applications and Environmental Impact*; Guminski, C., Ed.; Royal Society of Chemisty: Cambridge, UK, 2013; ISBN 9781849734097.

56. Sabri, Y.M.; Ippolito, S.J.; Tardio, J.; Morrison, P.D.; Bhargava, S.K. Studying mercury partition in monoethylene glycol (MEG) used in gas facilities. *Fuel* **2015**, *159*, 917–924. [CrossRef]
57. Bernard, S.; Salameh, C.; Miele, P. Boron nitride ceramics from molecular precursors: Synthesis, properties and applications. *Dalton Trans.* **2016**, *45*, 861–873. [CrossRef]
58. Hepler, L.G.; Olofsson, G. Mercury: Thermodynamic Properties, Chemical Equilibria, and Standard Potentials. *Chem. Rev.* **1975**, *75*, 585–602. [CrossRef]
59. Lyubchik, S.; Lyubchik, A.; Lygina, O.; Lyubchik, S.; Fonsec, I. Comparison of the Thermodynamic Parameters Estimation for the Adsorption Process of the Metals from Liquid Phase on Activated Carbons. In *Thermodynamics-Interaction Studies-Solids, Liquids and Gases*; Moreno-Piraján, J.C., Ed.; IntechOpen: London, UK, 2011.
60. Musmarra, D.; Karatza, D.; Lancia, A.; Prisciandaro, M.; Di Celso, G.M. A comparison among different sorbents for mercury adsorption from flue gas. *Chem. Eng. Trans.* **2015**, *43*, 2461–2466.
61. Lin, H.Y.; Yuan, C.S.; Chen, W.C.; Hung, C.H. Determination of the adsorption isotherm of vapor-phase mercury chloride on powdered activated carbon using thermogravimetric analysis. *J. Air Waste Manag. Assoc.* **2006**, *56*, 1550–1557. [CrossRef]
62. Ie, I.R.; Chen, W.C.; Yuan, C.S.; Hung, C.H.; Lin, Y.C.; Tsai, H.H.; Jen, Y.S. Enhancing the adsorption of vapor-phase mercury chloride with an innovative composite sulfur-impregnated activated carbon. *J. Hazard. Mater.* **2012**, *217–218*, 43–50. [CrossRef] [PubMed]
63. Ghosal, P.S.; Gupta, A.K. Determination of thermodynamic parameters from Langmuir isotherm constant-revisited. *J. Mol. Liq.* **2017**, *225*, 137–146. [CrossRef]
64. Mananghaya, M.; Yu, D.; Santos, G.N.; Rodulfo, E. Adsorption of mercury(II) chloride and carbon dioxide on graphene/calcium oxide (0 0 1). *Korean J. Mater. Res.* **2016**, *26*, 298–305. [CrossRef]
65. The International Bureau of Weights and Measures (BIPM). *Evaluation of Measurement Data-Guide to the Expression of Uncertainty in Measurement*; JCGM 100; Joint Committee for Guides in Metrology (JCGM): Paris, France, 2008.

Supplementary materials

Validating an evaporative calibrator for gaseous oxidized mercury

Jan Gačnik, [1,2] Igor Živković, [2] Sergio Ribeiro Guevara, [3] Radojko Jaćimović, [2] Jože Kotnik, [2] and Milena Horvat [1,2,*]

[1] Jožef Stefan International Postgraduate School, Jamova cesta 39, 1000 Ljubljana, Slovenia
[2] Jožef Stefan Institute, Department of Environmental Sciences, Jamova cesta 39, 1000 Ljubljana, Slovenia
[3] Laboratorio de Análisis por Activación Neutrónica, Centro Atómico Bariloche, Av. Bustillo km 9.5, 8400 Bariloche, Argentina
* Correspondence: milena.horvat@ijs.si; Tel.: +386-1-588-53-55

Equation S1

$$A_{0,sample} = \frac{A_{sample} * \lambda}{e^{-\lambda * t_{passed}} * [1 - e^{-\lambda * t_{measurement}}]}$$

Equation S2

$$R = \frac{A_{0,sample}}{A_{0,std.}} * \frac{m_{Hg,std.}}{m_{Hg,sample}} * f_{dillution} * 100$$

where:
$A_{0,\,sample}$ is the sample activity at the reference time t=0 [Bq],
$A_{0,\,std}$ is the standard activity at the reference time t=0 [Bq],
A_{sample} is the sample activity at the time of measurement [Bq],
λ is the decay constant [s^{-1}]
$t_{1/2}$ is the half-life of ^{197}Hg [s],
t_{passed} is the time passed since reference time t=0 until the start of measurement [s],
$t_{measurement}$ is the time passed during the measurement [s],
R is the recovery [%],
$m_{Hg,std.}$ is the mass of Hg used for the standard [pg],
$m_{Hg,sample}$ is the mass of Hg used for the sample, assuming 100% recovery [pg],
$f_{dillution}$ is the dilution factor in case the sample and standard were not diluted in the same way.

Equation S1 was applied to calculate both A_0 (activity at reference time) of the sample and A_0 of the standard. The recoveries were calculated using Equation S2.

Equation S3

$$u(R_m) = R_m \times \sqrt{\left(\frac{s_{obs}^2}{n \times C_{obs}^2}\right) + \left(\frac{u(C_{calc})}{C_{calc}}\right)^2}$$

where:
$u(R_m)$ is the uncertainty of the mean recovery,
R_m is the mean recovery,
S_{obs} is the standard deviation of the observed values,
C_{obs} is the observed gas concentration,
n is the number of observed values,
$u(C_{calc})$ is the uncertainty of the calculated (theoretical) gas concentration obtained from the manufacturer,
C_{calc} is the calculated (theoretical) gas concentration.

The standard uncertainty of mean recovery was then incorporated into the combined standard uncertainty by Equation S4. As all other relevant uncertainty components were already included in the calculation of calibrator the uncertainty by the manufacturer; only the uncertainty of the mean recovery had to be added to get the new evaluation of total uncertainty.

Equation S4

$$U = 2\,u_c = 2\sqrt{{u_{cal}}^2 + {u_{Rm}}^2}$$

Where:
U is the expanded uncertainty with a coverage factor k = 2,
u_{cal} is the standard uncertainty of the calibrator obtained from manufacturer,
u_{Rm} is the standard uncertainty of the mean recovery,
u_c is combined standard uncertainty of the calibrator.

Text S1. The calculation of the concentration of $HgCl_x^{2-x}$ and $HgBr_x^{2-x}$ species present in the calibrator standard solution.

As the calculation was the same for the $HgCl_x^{2-x}$ and $HgBr_x^{2-x}$ species (the only exception were the values of constants), we will only demonstrate the calculation for the $HgCl_x^{2-x}$ species. Four values of equilibrium constants (k) for the formation of the $HgCl_x^{2-x}$ species and the complex formation constant (β) were obtained from the literature (also for $HgBr_x^{2-x}$) [1, 2].

$$k_1 = \frac{[HgCl^+]}{[Hg^{2+}][Cl^-]} \qquad k_2 = \frac{[HgCl_2]}{[HgCl^+]\,[Cl^-]} \qquad k_3 = \frac{[HgCl_3^-]}{[HgCl_2][Cl^-]} \qquad k_4 = \frac{[HgCl_4^{2-}]}{[HgCl_3^-][Cl^-]} \qquad \beta = \frac{[HgCl_2^{2-}]}{[Hg^{2+}][Cl^-]^4}$$

where:
$\log k_1 = 6.72$, $\log k_2 = 6.51$, $\log k_3 = 1.00$, $\log k_4 = 0.97$, $\log \beta = 15.2$

The total concentration of Hg ($[Hg_T]$) and Cl ($[Cl_T]$) species was known; therefore, two additional equations were obtained:

$$[Hg_T] = [Hg^{2+}] + [HgCl^+] + [HgCl_2] + [HgCl_3^-] + [HgCl_4^{2-}]$$

$$[Cl_T] = [HgCl^+] + 2\left[HgCl_2\right] + 3\left[HgCl_3^-\right] + 4[HgCl_4^{2-}] + [Cl^-]$$

Since we had 7 equations (equations for k_1, k_2, k_3, k_4, β, $[Hg_T]$ and $[Cl_T]$) and 6 variables ($[Hg^{2+}]$, $[HgCl^+]$, $[HgCl_2]$, $[HgCl_3^-]$, $[HgCl_4^{2-}]$ and $[Cl^-]$), the analytical solution for this system of equations was obtainable. Using the described system, we could then calculate the concentration of all $HgCl_x^{2-x}$ species for each $[Hg_T]$ (which varied over the conducted experiments). As already mentioned in the manuscript, the total chloride concentration exceeded the total mercury concentration by over 3 orders of magnitude; therefore, varying the total Hg concentration did not result in considerably different calculated values of $HgCl_x^{2-x}$.

A similar calculation was also performed for the formation of $HgBr_x^{2-x}$.

Table S1. The calibrator output composition during the time-trend experiment using 1178 ng m^{-3} $HgCl_2$ gas concentration. Columns "KCl 1," "KCl 2," and "$KMnO_4$" represent the first KCl impinger ($^{197}HgCl_2$ retention), the second KCl impinger ($^{197}HgCl_2$ retention, breakthrough), and $KMnO_4$ impinger ($^{197}Hg^0$ retention), respectively, and are presented in relative terms as a percentage of the whole e mass balance (% of X for convenience).

time passed since calibrator start-up [h]	mass balance, X [%]	KCl 1 [% of X]	KCl 2 [% of X]	$KMnO_4$ [% of X]
0	88.5	97.4	1.41	1.19

1.00	81.0	96.8	1.63	1.60
20.2	88.7	95.4	2.04	2.60
22.1	90.7	95.2	1.61	3.21
25.0	84.9	94.1	1.63	4.23
43.7	96.2	94.6	1.76	3.62
44.7	89.8	93.9	1.69	4.40

Table S2. The calibrator output composition during the time-trend experiment using 289 ng m^{-3} $HgCl_2$ gas concentration. Columns "KCl 1," "KCl 2," and "$KMnO_4$" represent the first KCl impinger ($^{197}HgCl_2$ retention), the second KCl impinger ($^{197}HgCl_2$ retention, breakthrough), and the $KMnO_4$ impinger ($^{197}Hg^0$ retention), respectively, and are presented in relative terms as a percentage of the whole mass balance (% of X for convenience).

time passed since calibrator start-up [h]	mass balance, X [%]	KCl 1 [% of X]	KCl 2 [% of X]	$KMnO_4$ [% of X]
0.0	73.7	98.4	0.57	1.04
0.83	83.6	98.0	0.92	1.11
4.50	85.1	97.8	0.81	1.42
23.6	90.0	98.5	0.76	0.74
27.0	86.9	99.0	0.45	0.54
47.0	89.0	99.1	0.43	0.50
47.7	92.5	99.3	0.29	0.41
71.0	83.5	99.1	0.59	0.36
71.7	82.3	98.0	0.28	1.72

Table S3. The calibrator output composition the during time-trend experiment using 20.4 ng m^{-3} $HgCl_2$ gas concentration. Columns "KCl 1", "KCl 2," and "$KMnO_4$" represent first KCl impinger ($^{197}HgCl_2$ retention), the second KCl impinger ($^{197}HgCl_2$ retention, breakthrough), and the $KMnO_4$ impinger ($^{197}Hg^0$ retention), respectively, and are presented in relative terms as a percentage of the whole mass balance (% of X for convenience).

time passed since calibrator start-up [h]	mass balance, X [%]	KCl 1 [% of X]	KCl 2 [% of X]	$KMnO_4$ [% of X]
0.00	54.4	73.3	0.98	25.7
1.42	55.6	77.5	0.78	21.8
3.75	58.9	80.4	1.06	18.5
22.7	64.3	90.5	1.98	7.56
25.2	65.4	90.8	1.90	7.34
26.8	61.2	90.6	1.35	8.05
27.9	58.1	88.0	3.74	8.27
48.3	65.1	90.8	1.83	7.35
49.1	69.2	90.8	1.75	7.44
51.8	70.9	83.5	8.71	7.77

Table S4. The calibrator output composition during the time-trend experiment using 5.90 ng m^{-3} $HgCl_2$ gas concentration. Columns "KCl 1," "KCl 2," and "$KMnO_4$" represent the first KCl impinger ($^{197}HgCl_2$ retention), the

second KCl impinger ($^{197}HgCl_2$ retention, breakthrough), and the $KMnO_4$ impinger ($^{197}Hg^0$ retention), respectively, and are presented in relative terms as a percentage of the whole mass balance (% of X for convenience).

time passed since calibrator start-up [h]	mass balance, X [%]	KCl 1 [% of X]	KCl 2 [% of X]	$KMnO_4$ [% of X]
0.0	35.9	69.7	3.37	26.9
20.3	35.3	79.2	3.75	17.0
21.6	33.8	79.2	3.99	16.8
24.2	32.7	78.2	5.10	16.7
44.1	47.7	85.5	2.26	12.3
45.4	46.3	85.2	2.62	12.2
48.2	44.2	63.3	3.00	13.6
68.4	53.8	86.9	1.48	11.6
69.2	53.2	84.4	1.32	14.3
72.2	47.2	87.6	2.01	10.4

References:

1. L. G. Hepler and G. Olofsson, "Mercury: Thermodynamic Properties, Chemical Equilibria, and Standard Potentials," Chem. Rev., vol. 75, no. 5, pp. 585–602, 1975, doi: 10.1021/cr60297a003.
2. L. Ciavatta and M. Grimaldi, "Equilibrium Constants of Mercury (II) Chloride Complexes," J. Inorg. Nucl. Chem., vol. 30, no. Ii, pp. 197–205, 1968.

3.3 Manuscript 3: Behavior of KCl Sorbent Traps and KCl Trapping Solutions Used for Atmospheric Mercury Speciation: Stability and Specificity

Gačnik J., Živković I., Ribeiro Guevara S., Jaćimović R., Kotnik J., De Feo G., Dexter M. A., Corns W. T., Horvat M. (2021). Atmospheric Measurement Techniques, 14, 6619-6631

The sampling of gaseous oxidized mercury is the largest source of bias and uncertainty for ambient GOM analysis. Currently, the widely used ambient GOM sampling by denuders is being replaced by other sampling methods, such as cation-exchange membranes. Even though sorbent membranes are advantageous over denuders from the standpoint of sampling losses, their temporal resolution is low (1-2 weeks). Since all currently used GOM sampling methods have certain drawbacks, the investigation of alternative sampling methods is needed. As such, sorbent traps and impinging solutions have potential for ambient GOM sampling, but have so far mostly been used only for flue gas sampling.

In our presented article, we evaluated sorbent traps and impinging solutions for ambient GOM sampling from the perspective of stability and specificity. For sorbent traps, we tested KCl crystal, quartz wool impregnated with KCl, and KCl crystal with Al_2O_3. A 1 mol L^{-1} KCl solution was tested as the impinging solution.

Sorbent traps were tested for specificity by exposing the sorbent material to Hg^0. We used fresh and reused sorbents to evaluate the potential effect of reuse on specificity. Since sorbents must be GOM selective, retention of GEM must be as low as possible. This turned out to be true for all three fresh sorbents (negligible GEM retention), while some GEM retention was observed while testing KCl crystal and KCl crystal with Al_2O_3. Specificity tests for sorbent traps have shown that fresh (never used before) sorbent materials should always be the preferred choice. Sorbent trap stability tests were done by loading a known amount of Hg^{II} on the sorbent, exposing it to the airflow, and monitoring the Hg^{II} losses during half-hour intervals. Stability tests were conducted under a wide variety of experimental conditions: $HgCl_2$/$HgBr_2$ species, high/low concentration, calibrator/spike Hg^{II} loading, and high/low airflow. Overall, the Hg^{II} stability was good for all tested conditions, with under 3% losses observed in most experiments. We observed concentration dependence of Hg^{II} losses, the highest relative losses were observed when using low Hg^{II} concentrations. The effects of the other tested experimental conditions were statistically insignificant.

KCl impinging solution was tested for specificity by evaluating the solubility and oxidation of Hg^0 in the solution. Firstly, a Hg^0 solubility experiment was conducted by purging a known flow with a known amount of Hg^0 through the KCl solution. To ensure that no Hg^0 oxidation occurred and that the retained Hg^0 was only due to solubilization of Hg^0, the reductant $SnCl_2$ was added. Hg in solution and Hg^0 that passed through the solution were measured, and the results were used to calculate Henry's law constant. The value of the constant was 0.0093, which can be used for future estimations of Hg^0 solubility in KCl solution. A similar test, but without the reducing agent $SnCl_2$, was used to study the oxidation of Hg^0 in the KCl solution. For nitrogen and air matrices, Hg^0 oxidation was found to be 2.9% and 3%, respectively. At the end, the results from Hg^0 solubility and oxidation were used in the predicted bias calculation. We predicted that GOM overestimation bias of up to 3000% could originate from the Hg^0 solubility and oxidation in KCl impinging solutions. The predicted bias is highly dependent on the GEM:GOM ratio and the concentration considered. At flue gas Hg concentrations with relatively higher

GOM fraction, the bias is small, while this is not the case for ambient air Hg concentrations. The stability of Hg^{II} in the KCl solution was also checked: no losses were observed, which indicated that Hg^{II} is stable in the solution.

All tested KCl sorbent traps materials were found to be suitable for sampling ambient GOM. The sorbent traps exhibited good selectivity (negligible Hg^0 retention) and stability (small Hg^{II} losses) for Hg^{II} species. KCl impinging solutions were not selective due to the Hg^0 solubility and oxidation in the solution, which could lead to large biases. Due to the lack of selectivity, our results suggest that KCl impinging solutions are not a suitable medium for the preconcentration of ambient GOM. Further comparison work for GOM sampling with denuders, membranes, and sorbent traps is needed. The development of a traceable source of Hg^{II} species could provide a much-needed tool for unambiguous validation of GOM sampling methods.

In the present manuscript, I participated in all experimental work related to KCl sorbent traps. I also participated in preparation of figures and tables, statistical analyses, and in the writing of the manuscript.

Atmos. Meas. Tech., 14, 6619–6631, 2021
https://doi.org/10.5194/amt-14-6619-2021
© Author(s) 2021. This work is distributed under
the Creative Commons Attribution 4.0 License.

Atmospheric Measurement Techniques
Open Access
EGU

Behavior of KCl sorbent traps and KCl trapping solutions used for atmospheric mercury speciation: stability and specificity

Jan Gačnik[1,2], Igor Živković[2], Sergio Ribeiro Guevara[3], Radojko Jaćimović[2], Jože Kotnik[1,2], Gianmarco De Feo[4], Matthew A. Dexter[4], Warren T. Corns[4], and Milena Horvat[1,2]

[1]Jožef Stefan International Postgraduate School, Jamova Cesta 39, 1000 Ljubljana, Slovenia
[2]Department of Environmental Sciences, Jožef Stefan Institute, Jamova Cesta 39, 1000 Ljubljana, Slovenia
[3]Laboratorio de Análisis por Activación Neutrónica, Centro Atómico Bariloche,
Av. Bustillo km 9.5, 8400 Bariloche, Argentina
[4]P S Analytical Ltd, Arthur House, Main Road, Orpington, Kent, BR5 3HP, UK

Correspondence: Milena Horvat (milena.horvat@ijs.si)

Received: 25 May 2021 – Discussion started: 15 June 2021
Revised: 30 August 2021 – Accepted: 2 September 2021 – Published: 13 October 2021

Abstract. Atmospheric mercury speciation is of paramount importance for understanding the behavior of mercury once it is emitted into the atmosphere as gaseous elemental mercury (GEM), gaseous oxidized mercury (GOM) and particulate-bound mercury (PBM). GOM and PBM can also be formed in the atmosphere; their sampling is the most problematic step in the atmospheric mercury speciation. GOM sampling with speciation traps composed of KCl sorbent materials and KCl trapping solutions are commonly used sampling methods, although the research conducted with them at ambient air concentrations is limited. The results of the specificity test demonstrated that the KCl sorbent traps are highly specific when using new traps, while their specificity drops dramatically when they are reused. The results of the stability test indicated that the highest Hg^{2+} losses (up to 5.5 % of Hg^{2+} loss) occur when low amounts of Hg^{2+} (< 1 ng) are loaded, due to a reduction of Hg^{2+} to Hg^0. KCl trapping solutions have also been considered as a selective trapping media for GOM in atmospheric samples. A dimensionless Henry law constant was experimentally derived and was used to calculate the solubility of elemental Hg in KCl solution. The degree of GEM oxidation was established by purging elemental Hg calibration gas into a KCl solution and determining the GOM trapped using aqueous-phase propylation liquid–liquid extraction and gas chromatography–atomic fluorescence spectrometry (GC-AFS) measurement. A positive GOM bias was observed due to the solubility and oxidation of GEM in KCl trapping solutions, strongly suggesting that this approach is unsuitable for atmospheric mercury speciation measurements.

1 Introduction

Since the 19th century, human activities have led to a 450 % increase in the concentration of mercury in the atmosphere (United Nations Environment Programme, 2019). In order to achieve comparability of atmospheric mercury speciation worldwide, the analytical methodology needs to be well understood in the terms of metrology and the conversion processes that may occur during the analysis. Uncertainties and lack of knowledge already appear in the sampling phase of the analytical procedure (Jaffe et al., 2014; Gustin et al., 2013).

First, the mercury species must be collected from the air and accumulated in a medium suitable for further analysis. Because some species of Hg are present in the atmosphere at very low concentrations, a highly selective preconcentration step is required to accumulate sufficient quantity of the species for analysis. The collection of total gaseous mercury (TGM) is achieved by drawing air through different types of quartz traps filled with gold materials at a known and fixed flow rate. Types of gold materials include coiled gold wire, gold nanostructures and high specific-surface-area substrate coated with gold (U.S. EPA, 1999). The decision to use a particular gold material depends primarily on the mass of mercury to be collected. For gaseous oxi-

Published by Copernicus Publications on behalf of the European Geosciences Union.

dized mercury (GOM), the main sampling and preconcentration methods are KCl-coated denuders (Bu et al., 2018), KCl impinging solutions (impingers, adaptations of the Ontario Hydro method (ASTM International, 2016) and KCl sorbent traps (U.S. EPA, 2017; Prestbo and Bloom, 1995). Cation-exchange (CEM) or nylon membranes collect reactive mercury (RM – sum of GOM and PBM) but can also be used for GOM sampling if polytetrafluoroethylene (PTFE) membranes (PBM collection) are placed upstream (Bu et al., 2018; Huang et al., 2013; Gustin et al., 2021). Various types of filters (quartz-fiber, cellulose-acetate, glass-fiber and Teflon filters) are most commonly used for particulate-bound mercury (PBM) sampling (Zhang et al., 2019).

It is generally accepted that all forms of gaseous mercury are collected on gold traps and the measurement represents TGM (Dumarey, 1985; Shafawi et al., 1999). However, there is disagreement concerning whether the applied sampling protocols are optimal for GOM (Gustin and Jaffe, 2010).

Most problems with sampling of atmospheric mercury are related to GOM and PBM. Accurate quantification of PBM has proven to be one of the most difficult tasks of atmospheric mercury speciation. Problems include (i) meteorological conditions, adsorption, nucleation, gas–particle partitioning and other physical/chemical processes; (ii) ultralow concentrations of PBM; (iii) formation of artifacts during sampling; and (iv) loss of PBM during longer sampling periods (Wang et al., 2013). Recently, research has focused on GOM sampling and its dependence on ambient conditions. Various studies of KCl-coated denuders have demonstrated that there is a clear dependence of collection efficiency on relative humidity (McClure et al., 2014; Huang and Gustin, 2015) and on the presence of ozone (McClure et al., 2014; Lyman et al., 2010). The collection efficiency has been found to be inversely dependent on ozone concentration and relative humidity, dropping as low as 13 % in some cases (Wang et al., 2013; McClure et al., 2014; Huang and Gustin, 2015). Experiments using water vapor spikes found that not only was the efficiency for GOM collection on KCl-coated denuders very low under high-humidity conditions, but also gaseous elemental mercury (GEM) concentrations were increased. This observation made it clear that under conditions of high humidity, GOM can be converted to GEM (or detected as such) (Huang and Gustin, 2015). Underestimated GOM and overestimated GEM due to processes occurring during denuder sampling have been confirmed by Lyman et al. (2016). In addition to denuders, the effectiveness of CEM and nylon membranes at different relative humidity levels was also studied. Humidity introduced a positive GOM bias for CEM while lowering the collection efficiency of nylon membranes. Nylon membrane passivation occurred with ozone exposure (Huang and Gustin, 2015). Gustin et al. (2019) compared different measurement methods for atmospheric Hg speciation. The results demonstrated that GOM and RM, measured with nylon membranes, were approximately 50 % lower than GOM and RM measured with CEM (Gustin et al., 2019). In addition to CEM and nylon membranes, various materials have been tested as membrane materials. CEM and polyethersulfone membrane (PES) have been shown to be the most quantitative sorbents. Nylon was best for identifying GOM compounds by thermal desorption. Other materials such as anion-exchange membranes, polycarbonate and polypropylene materials have obtained unsatisfactory results (Dunham-Cheatham et al., 2020). A three-membrane system (CEM + nylon + PTFE membranes) was recently applied with an attempt to distinguish between PBM and GOM. It was demonstrated that PTFE membranes retain mostly PBM, while CEM and nylon membranes retain RM if used without an upstream-placed PTFE membrane or GOM if used with an upstream-placed PTFE membrane (Gustin et al., 2021).

Various authors have studied the behavior of membranes and denuders as GOM/RM sampling methods, but less work has been done on the behavior of KCl sorbent traps and KCl trapping solutions for mercury atmospheric measurements. Initial experiments on KCl sorbent trap valuation were performed by the authors of the mercury speciation adsorption method (MESA) used for flue gas sampling (Prestbo and Bloom, 1995). The authors determined the species stability of KCl sorbent traps during storage, matrix effects, breakthrough and artifact formation (Prestbo and Bloom, 1995). Although several KCl sorbent trap behavior studies have been performed for flue gas sampling (EPRI, 2015), no studies have been conducted on their use for atmospheric mercury speciation measurements. KCl trapping solutions are commonly used for Hg speciation in flue gas (ASTM International, 2016), but the selectivity and suitability for GOM in atmospheric mercury measurements have not been previously investigated. Therefore, the aim of this work was to focus on gathering information on the behavior of KCl sorbent traps and KCl trapping solutions under different sampling conditions that would complement the aforementioned work and improve knowledge of the processes that may occur during atmospheric Hg speciation.

2 Methodology

All chemicals and instruments that were utilized in the following experiments are listed in the Supplement (Tables S1 and S2).

2.1 Production of ^{197}Hg radiotracer

To allow experiments using low Hg amounts (under 1 ng), radioactive ^{197}Hg tracer was used as it has been demonstrated to be advantageous in cases where contamination and detection limit are problematic (Ribeiro Guevara et al., 2004; Koron et al., 2012; Ribeiro Guevara and Horvat, 2013). Mercury labeled with radioactive ^{197}Hg was used for all KCl sorbent trap experiments. Mercury enriched to 51.58 % in ^{196}Hg iso-

tope (only 0.15 % of ^{196}Hg isotope is naturally present) was used to produce ^{197}Hg ($t_{1/2} = 2.671$ d) via a neutron capture reaction (n,γ). A total of 2 mL of a 2 % HNO_3 (v/v) solution of enriched mercury was sealed into quartz ampoules. Quartz ampoules were then irradiated in the central channel of the TRIGA Mark II (250 kW) reactor core channel (JSI, Ljubljana, Slovenia). High neutron flux (approximately 10^{13} cm^{-2} s^{-1} at thermal power of 250 kW) in the center of the reactor core caused the nuclear neutron capture reaction in solution to produce ^{197}Hg during irradiation. Prior to irradiation, Hg concentration of the solution was determined by cold vapor atomic absorption spectrometry (CV AAS). The Hg concentration measured (93.3 µg mL^{-1} of Hg) was the reference for Hg amounts that were used in all experiments. HgX_2 (X = Cl$^-$, Br$^-$) solutions and gases were used in the presented work; to clarify, all Hg-related concentrations that will be presented in the paper will refer to Hg concentrations and not to HgX_2 concentrations if not explicitly stated otherwise. After irradiation, the Hg solution was transferred from the irradiated vial and diluted to appropriate Hg concentrations for subsequent experiments.

2.2 Determining ^{197}Hg using an HPGe detector

The activity of radiotraced Hg in solutions was measured by means of a well-type HPGe detector (model GCW6023/S, Canberra Industries Inc., Meriden, CT, USA), while in gold traps and non-liquid samples the activity was measured using a coaxial-type HPGe detector (model 7229P, Canberra Industries Inc., Meriden, CT, USA). All activity measurements were relative to standards obtained from the irradiated solution in each experimental run, considering the Hg concentration as described in the previous paragraph. The ^{197}Hg activity was determined by evaluating γ-ray and X-ray emissions; experimental samples were measured in the same geometry as the standards. To obtain standards for well-type detector, triplicates of a Hg radiolabeled solution (8 mL, 2 % HNO_3 (v/v)) were transferred into glass vials. The standard solution was always diluted so that the activity was similar to the activity of the measured sample. The ^{197}Hg activity of the standards in the vials was measured using a well-type detector. Standards for the coaxial-type detector were obtained by $^{197}Hg^{2+} \rightarrow {}^{197}Hg^0$ reduction, performed in an impinger with a $SnCl_2$ solution (100 mL, 2 % $SnCl_2$ (w/v) and 0.5 % HCl (v/v)), which was purged for 10 min with N_2 carrier gas (purity 4.7, flow rate of 1 L min^{-1}). Purged $^{197}Hg^0$ was transferred to a gold trap by the carrier gas to obtain a measurement standard. The absence of Hg^0 breakthrough was confirmed by placing an additional gold trap downstream the main gold trap. Similar to liquid samples, standards for the coaxial-type gamma detector were made in triplicate. Any time that new gold traps were prepared, new triplicate standards were also prepared following the same procedure. Gold traps were prepared in quartz tubes (170 mm long, 6 mm inner diameter) by placing 15 mm in length of the absorbing material, which was fixed in place by quartz wool. Absorbing material was prepared by dissolving 1 g of $HAuCl_4 \cdot xH_2O$ (gold chloride hydrate) in 10 mL of Milli-Q water where 10 g of Al_2O_3 (corundum, 0.60–0.85 mm grain size) was added. The solution was then evaporated in an automatic rotary evaporator, and the remaining material was heated to 500 °C for 4 h in an argon atmosphere. In order to reuse gold traps, they were heated to 300 °C for 30 s, which released the bounded $^{197}Hg^0$. Complete release of ^{197}Hg was confirmed by evaluation of ^{197}Hg remains in the HPGe detector.

The evaluation of the characteristic γ-ray and X-ray emissions associated with ^{197}Hg decay (two doublet peaks: 67.0 + 68.8 and 77.3 + 78.1 keV) was performed by computing peak areas using Genie 2000 Gamma analysis software. All activities were referred to a reference time by applying an equation derived from the exponential law of radioactive decay. The specific equations that were used for the calculation of the activity and recovery are available in the Supplement (Eqs. S1 and S2) (Ribeiro Guevara and Horvat, 2013; Koron et al., 2012; Ribeiro Guevara et al., 2007).

2.3 Specificity of KCl sorbent traps and experimental design

A scheme of the experimental setup for testing KCl sorbent trap specificity is depicted in Fig. 1. Firstly, Hg^{2+} (ranging from 0.1 to 1 ng) was reduced to Hg^0 in the impinger using $SnCl_2$ solution (100 mL, 2 % $SnCl_2$ (w/v) and 0.5 % HCl (v/v)). Hg^0 was then purged out with N_2 carrier gas (flow rate of 1 L min^{-1}) for 10 min, passed through various types of KCl sorbent traps (described below) and captured at the end by a gold trap.

Three different types of KCl sorbent traps were used: KCl crystal, quartz wool impregnated with KCl, and KCl crystal + Al_2O_3 catalyst. The latter was considered for an application that will be discussed in future work. Briefly, Al_2O_3 is intended to catalyze the reduction of Hg^{2+} to Hg^0 in the next step of the analysis. All sorbent traps were prepared in quartz tubes (170 mm long, 6 mm inner diameter). In design 1, KCl crystal was 15 mm long and fixed using quartz wool. In design 2, quartz wool impregnated with KCl was 70 mm long. Quartz wool impregnated with KCl was prepared by soaking quartz wool in 1 mol L^{-1} KCl for 24 h, draining the excess solution and drying at 130 °C for 24 h. In design 3, the KCl crystal was 5 mm long and the Al_2O_3 catalyst part was 65 mm long. All three types of sorbent traps were tested new (no heating of the traps) and reused (traps heated to ≈ 600 °C three times prior to the experiment), resulting in six variations tested.

To determine the amount of Hg^0 collected on the KCl sorbent traps, the traps were leached with 20 mL of 10 % HNO_3 (v/v) + 5 % HCl (v/v) solution and ^{197}Hg in leachate was measured. In our research, it has previously been found that this acid mixture completely leaches Hg from KCl sorbent

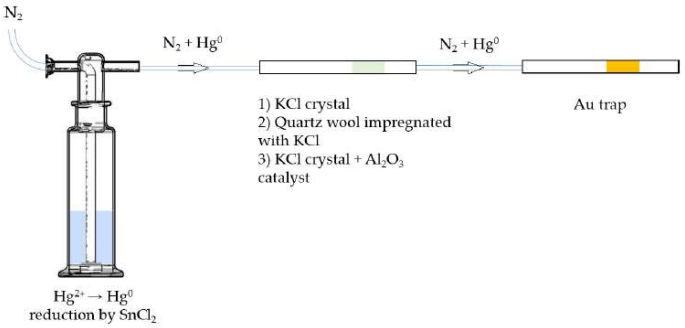

Figure 1. Scheme of the experimental setup for testing the extent of undesirable Hg^0 retention on three different KCl sorbent trap designs (not depicted to scale).

traps. Radiolabeled Hg^0 on gold sorbent traps was also measured.

2.4 Stability of Hg^{2+} loading on KCl sorbent traps and experimental design

In order to test Hg^{2+} stability on KCl sorbent traps, the traps were exposed to ambient airflow for 30 min periods after loading with radiolabeled Hg. Potential formation of Hg^0 was captured downstream of the KCl sorbent trap by an Au trap. After each 30 min exposure period, the radiolabeled Hg^0 activity in the Au trap was measured. KCl sorbent traps were loaded with radiolabeled Hg^{2+} again (to simulate the sampling process where new Hg^{2+} is constantly adsorbed); the procedure was repeated 4 to 5 times. To assure that no Hg^{2+} breakthrough occurred and that the measured losses only comprised of Hg^0, an additional KCl crystal trap was placed between the KCl sorbent trap and the Au trap to filter the potential Hg^{2+} breakthrough. The Hg^{2+} on the KCl trap filter was always below the detection limit of the gamma detector, so these results will not be presented in the results and discussion section. Since this KCl trap filter was always free of Hg, it was later checked only from time to time as a control. Figure 2 depicts a diagram of all conditions studied in the stability tests.

Two types of Hg^{2+} loadings were tested. The first type was a direct spike of Hg^{2+} onto the sorbent traps. The second type of loading was performed using an Optoseven evaporative gas calibrator. This instrument enabled Hg^{2+} loading by evaporating the Hg^{2+} solution and injecting it into a carrier gas (Saxholm et al., 2020; Gačnik et al., 2021). The calibration gas was comprised of 0.07 mL min^{-1} of Hg^{2+} solution (Hg^{2+} concentration dependent on the concentration level tested) and 5 L min^{-1} of carrier gas N_2. The calibration gas was formed in the evaporator at 125 °C. The obtained calibration gas had a Hg^{2+} concentration of 1178 ng m^{-3} for high-concentration tests and 5.90 ng m^{-3} for low-concentration tests. Previous studies have found that the output of the calibrator is concentration dependent; these findings were taken into account when calculating the expected calibrator output (Gačnik et al., 2021). Two Hg^{2+} species were tested for stability, $HgCl_2$ and $HgBr_2$. For Hg^{2+} spikes, a 4 % HCl (v/v) +3 % HNO_3 (v/v) solution was used for $HgCl_2$, and a 4 % HBr (v/v) +3 % HNO_3 (v/v) solution was used for $HgBr_2$. Compounds and their concentrations were chosen based on the composition of NIST 3177 standard reference material (Mercuric Chloride Standard Solution). Using equilibrium calculations described in the work of Gačnik et al. (2021), we confirmed that the spiking solutions contained only $HgCl_2$ and $HgBr_2$ without other Hg_xCl_x or Hg_xBr_x species (Gačnik et al., 2021). In the cases where Hg^{2+} was loaded using the Optoseven calibrator, a 0.1 % HCl (v/v) +0.1 % HNO_3 (v/v)

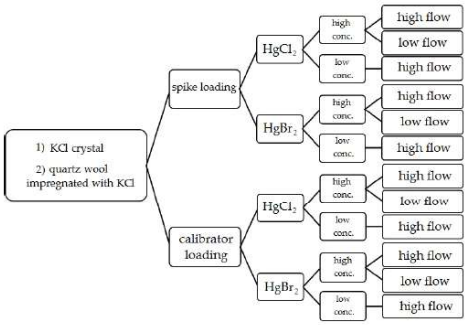

Figure 2. Variations of performed experimental conditions for Hg^{2+} stability on KCl sorbent traps during exposure in ambient airflow.

solution was used for $HgCl_2$ and 0.1 % HBr (v/v) +0.1 % HNO_3 (v/v) for $HgBr_2$. In addition to two loading types and two Hg species, two different KCl sorbent trap materials were tested: KCl crystal and quartz wool impregnated with KCl. Each trap material was then tested under different experimental conditions: high concentration (> 50 ng)/low concentration (< 1 ng) and high airflow (400 mL min^{-1})/low airflow (100 mL min^{-1}). All variations of experimental conditions, trap types, Hg species and loading types were performed following the Fig. 2 diagram.

2.5 Solubility of elemental Hg in KCl trapping solutions and experimental design

The solubility of elemental Hg in the 1 mol L^{-1} KCl trapping solution was established using a method based on the Henry law constant determination. From the dimensionless Henry law constant (HLC), the amount of elemental Hg that would be collected in the KCl solution can be predicted. This approach was applied to a seawater matrix by Andersson et al. (2008).

The system consisted of an extractor stripper vessel composed of a jacketed borosilicate glass cylinder. This is represented schematically in Fig. 3. During the experiment, water at known temperature was pumped through the jacket from a temperature-controlled bath. The capacity of the extractor vessel was 1 L. At the bottom of the vessel there was an injection port connected to the argon carrier gas. The gas was bubbled inside the vessel through a glass frit on the bottom of the vessel. The gas was produced from a mass flow meter at known flow. Two holes, one on the bottom and one on the top, allow the measurement of the temperature of both the solvent and the headspace. At the top of the vessel, the pressure was measured using an absolute pressure meter.

The mercury which is purged from the vessel was collected using a heated gold trap. Before and after every experiment, the recovery of the gold traps was checked to ensure that mercury collection was quantitative. The mercury extracted was compared to the mass of Hg injected as an indication of the success of the experiment and absence of oxidized mercury which would otherwise be trapped in solution. The KCl also included 11 mL L^{-1} of reductant solution (20 % (w/v) $SnCl_2$ in 10 % (v/v) HCl), used to avoid oxidation.

Elemental mercury (Hg^0) vapors were injected from a bell jar into the gas flow of the extractor vessel. The bell jar had a thermometer where the temperature was checked before the gas was pulled via a gastight syringe. The temperature and volume of gas are known, and therefore the mass of mercury injected could be calculated using the Dumarey equation (Dumarey et al., 2010). To make a correction on the measured mass flow and calculate the real flow, the vapor pressure must be known. The vapor pressure of 1 mol L^{-1} of KCl at 5 °C was assumed to be the same as water (Lide, 2007). The recovery of the spiked mercury into the extraction

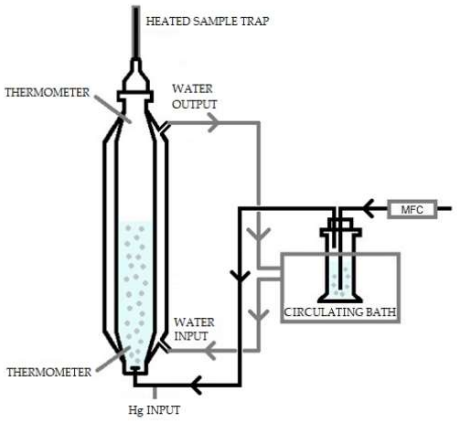

Figure 3. Henry law extractor stripping vessel arrangement.

vessel was checked after the experiments. The recovery is a good indication of the success of the experiment and of the absence of oxidized mercury.

The gas coming out from the vessel was collected using heated gold traps for fixed intervals of time. These gold traps were then analyzed to determine the mass of Hg released during each time interval. For this experiment, the volume of KCl in the vessel, the pressure, the measured gas flow rate, the exact interval of each extraction time and the temperature must be precisely determined. The calculation of dimensionless HLC was performed according to the method presented by Andersson et al. (2008), which is provided in the Supplement (Eqs. S3–S12). The value of the gold trap blank was subtracted from the mass of Hg measured for every extraction. This improved the linearity of the data providing a better measurement of the dimensionless HLC. The first point of the extraction typically deviated slightly from linearity because it included the signal rise time from the point of Hg vapor injection. During the signal rise period the test solution is not under equilibrium, and therefore the first point was ignored. Additionally, the final extraction points if considered to be close to the quantification limit are ignored as the uncertainty is higher, which can affect the linear regression.

2.6 Oxidation of elemental Hg in KCl trapping solutions and experimental design

The experimental arrangement for studying the selectivity of the KCl trapping solution is depicted in Fig. 4. A PSA 10.536 elemental Hg generator was used to generate a continuous stream of calibration gas of known concentration (nominally 20 µg m^{-3}) and flow rate. This is a considerably higher concentration of elemental Hg than ambient air concentration

as the original scope of this work was to study the Hg concentration range in flue gases. The total flow generated was $5\,L\,min^{-1}$, and both nitrogen and air (from an in-house air compressor, classified to ISO 8573-1:2010) (International Organization for Standardization, 2010) were studied. A slipstream flow of $0.5\,L\,min^{-1}$ was pulled through the test impingers using a vacuum pump and mass flow controller arrangement. An impinger solution of 100 mL of $1\,mol\,L^{-1}$ KCl was used as the test solution maintained at 5 °C in a water chiller bath. An empty impinger and an impinger of silica gel were also included to ensure that the gas going to the mass flow controller was dry. All tests were conducted over a 2 h period, during which an absolute mass of mercury of 1200 ng was passed through the impinger train. The KCl trapping solution was then analyzed by GC-AFS with aqueous-phase propylation liquid–liquid extraction to determine the oxidized Hg.

The same apparatus was used to test the stability of oxidized Hg in the KCl trapping solution. In this case a known mass of $HgCl_2$ was added to the KCl solution. The apparatus was then run using the same conditions as described above but without elemental Hg being introduced. In this experiment, the concentration of oxidized Hg should remain the same after the 2 h period of sampling. A concentration decrease would be indicative of $HgCl_2$ being reduced. After running the test, the KCl trapping solution was then analyzed by GC-AFS with aqueous-phase propylation liquid–liquid extraction to determine the oxidized Hg.

2.7 Determination of oxidized Hg in KCl trapping solution and experimental design

The KCl solution was propylated in the presence of an acetic acid–acetate buffer. This converts Hg^{2+} to dipropyl mercury. The derivatized mercury was then transferred and concentrated in an organic phase for injection into the GC-AFS instrument. To a 100 mL sample, 5 mL of buffer (0.5 M acetic acid) was added. The pH was then adjusted to 3.9. To this solution 500 µL of 2,2,4-trimethylpentane and 1 mL of the alkylation reagent were added. The solution was then shaken vigorously for 10 min and the trimethylpentane phase transferred to a GC vial. The sample was dried over anhydrous sodium sulfate and then analyzed by GC-AFS. Calibration was achieved by preparing mixed organometallic and Hg^{2+} standards and a blank, subjecting them to the same sample preparation. An injection volume of 2 µL was used in the splitless mode of operation with the injector at 250 °C. The GC temperature program used is summarized in the Supplement (Table S3). The eluent emerging from the column was thermally treated at 800 °C to breakdown organomercury compounds to elemental Hg before introduction to the AFS detector.

Table 1. Hg^0 retention on various KCl sorbent trap designs, and comparison of new and reused designs. Results are presented in percentage of the initially purged Hg^0 amount. Less than 1 ng of Hg was used.

Trap description	New/ reused	Retained Hg^0 (%)	Mass balance (%)
KCl crystal + Al_2O_3 catalyst	New	0.00	99.1
		0.00	96.7
	Reused	11.5	102
		18.0	101
		23.8	101
		9.46	101
KCl crystal	New	0.13	95.9
		0.14	102
		0.20	96.2
	Reused	4.10	95.4
		7.12	92.7
		2.41	94.5
Quartz wool impregnated with KCl	New	0.05	98.2
		0.23	109
		0.23	93.3
	Reused	0.35	100
		0.10	101
		0.64	100

3 Results and discussion

3.1 Specificity of KCl sorbent traps

The aim of this study was to determine the extent of unwanted retention of Hg^0 on KCl sorbent traps. This was achieved by transferring a known amount of Hg^0 in the carrier gas through a Hg^{2+} specific sorbent trap (where Hg^0 retention is unwanted). The results of the experiment are shown in Table 1. The column "retained Hg^0" represents Hg^0 retained on the KCl sorbent trap. The column "mass balance" represents the sum of Hg^0 on the KCl sorbent trap and Hg^0 on a gold trap. All values are shown as percentages relative to the Hg amount that was purged through the system. As previously mentioned, Hg^{2+} breakthrough was never present since it was negligible.

It can be observed that trap designs containing KCl crystals (KCl crystal + Al_2O_3 catalyst and KCl crystal traps) retained much more Hg^0 when reused, which is not desirable; Hg^{2+} specificity is required. The amount retained also varied greatly for reused sorbent traps. Since the KCl has a melting point of 770 °C, this could mean that the morphology of KCl has changed at experimental temperatures (≈ 600 °C) approaching the melting point. The morphological change could potentially explain the increased Hg^0 binding when using reused KCl sorbent traps. Traps that were unused prior

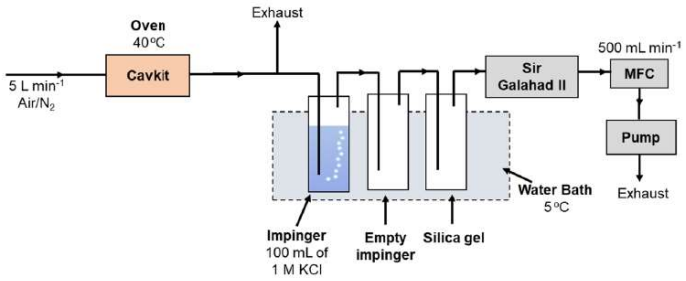

Figure 4. Experimental arrangement for KCl trapping experiments.

to the experiment ("new" traps) always retained very small amounts of Hg^0 (< 0.3 % for all designs). Mass balances were quantitative in all cases; therefore, these results can be trusted with a high level of confidence. From these findings, it can be concluded that new traps perform better than reused traps, and, therefore, to prevent the formation of artifacts only new traps should be used. It is not necessary to correct the measured values for the obtained recovery as losses are regularly lower than the variability of the recovery (standard deviation up to 4 %, losses up to 0.2 %).

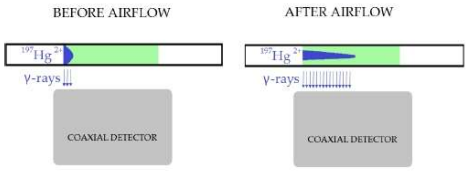

Figure 5. Effect of radiotracer distribution change along the trap on the activity measurement after exposure of KCl sorbent traps to airflow (not depicted to scale).

3.2 Stability of Hg^{2+} loading on KCl sorbent traps

Exposure of the loaded sorbent trap to airflow changed the geometry of the radiolabeled Hg^{2+} loading. This affected the measurement as depicted in Fig. 5, resulting in biasing the results. This effect was presumed based on the fact that mass balance was always considerably above 100 %. The figure illustrates a sorbent trap that is placed over a coaxial-type gamma detector before and after exposure to airflow. The airflow shifted the distribution of the radiolabeled Hg^{2+} along the trap. Prolonged exposure to the airflow caused greater shifts. Due to geometrical effects, the detection system has higher detection efficiency for a radioactive source on the axis of the detector than a source at the same distance from the detector surface but far from the axis. Therefore, a distribution of the radiolabeled Hg extended to the axis of the detector generates a higher recording on the detection systems than a distribution compacted to the detector border, with the same activity. Measurement after exposure to the airflow would therefore result in greater apparent sample activity than measurement prior to exposure to airflow. Due to this observation, it was not possible to verify the overall mass balance. On the other hand, this did not affect the measurement of Hg losses (Hg^0) captured on the Au trap, as Hg forms a strong amalgam with Au. Therefore, only the measured losses are presented in the tables below.

The results of the stability tests are shown in the figures below (Figs. 6, 7, 8 and 9). Full results are available in the Supplement (Tables S4, S5, S6 and S7). Losses are presented as a percentage relative to the cumulative amount of Hg that was spiked up to that time period. Some results have four time periods (marked with an asterisk in the figures), while others have five time periods due to time constraints of each measurement day.

The clear trend observed in the tables presented was that the relative losses were in almost all cases higher in the low-concentration experiments (5.54 % max. losses) than in high-concentration experiments (2.79 % max. losses, under 1 % in most cases). In addition, the first interval (0–0.5 h) had statistically significant maximum relative losses during the whole stability test (Kruskal–Wallis test, $p < 0.001$; pairwise multiple comparison procedures (Dunn's method), $p < 0.05$ for 0–0.5 h period against other periods). Because the variation in low/high airflow did not cause significant differences in the overall Hg^{2+} losses (paired t test, $p = 0.471$), the low airflow tests were omitted in the low-concentration stability tests. The $HgCl_2$ / $HgBr_2$ and calibrator/spike loading variations also did not cause any significant differences in Hg^{2+} losses during the stability tests.

Longer sampling times are often used for low concentrations of Hg^{2+} (the amount of Hg^{2+} collected from the ambient atmospheric samples is in the order of picograms); therefore, some losses of GOM will be observed most of the time. Losses depend not only on the parameters tested

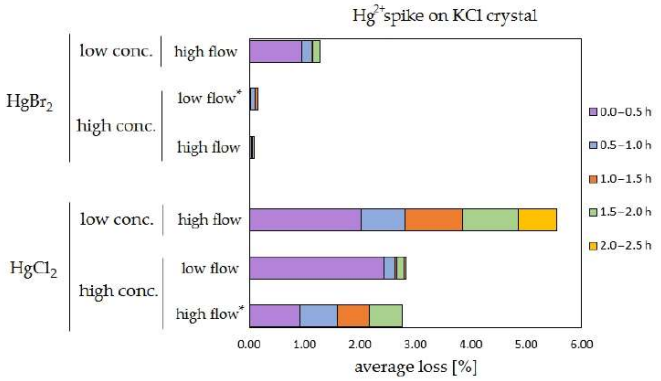

Figure 6. Results of the stability test for the $^{197}Hg^{2+}$ (radiotracer) spike on KCl crystal. Low concentrations were loaded with less than 1 ng Hg per time period, and high concentrations were loaded with more than 50 ng of Hg per time period. Low airflow experiments were performed with 100 mL min^{-1} airflow, while high airflow experiments were performed with 400 mL min^{-1} flow. Asterisks mark the results that only have the first four time periods.

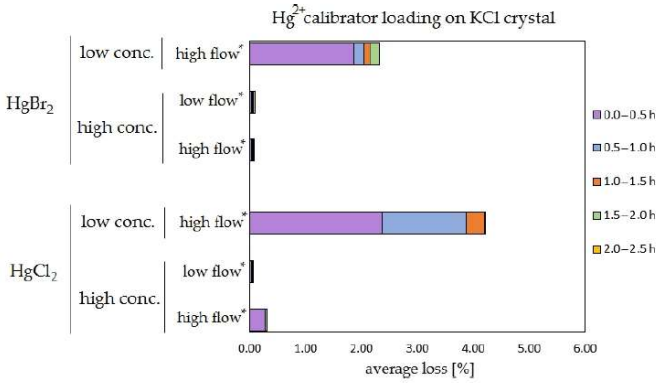

Figure 7. Results of the stability test for the calibrator loading of $^{197}Hg^{2+}$ (radiotracer) on KCl crystal. Low concentrations were loaded with less than 1 ng Hg per time period, and high concentrations were loaded with more than 50 ng of Hg per time period. Low airflow experiments were performed with 100 mL min^{-1} airflow, while high airflow experiments were performed with 400 mL min^{-1} flow. Asterisks mark the results that only have the first four time periods.

in our work, but also on meteorological conditions (e.g. humidity, presence of ozone, temperature). In Hg speciation measurements, reduction of Hg^{2+} to Hg^0 during sampling may result in a positive bias for Hg^0 (GEM) and a negative bias for Hg^{2+} (GOM) measurement. The considerations mentioned above should be considered carefully, particularly when longer sampling times are required.

3.3 Solubility of elemental Hg in KCl trapping solutions using the dimensionless Henry law constant

Using the experimental data taken from one of the tests using 1 mol L^{-1} KCl at 5 °C, the mass of Hg released during each 2 min interval is depicted graphically in Fig. 10. The natural logarithm of the mass of the Hg released during each interval was plotted to provide the α term using the slope (see

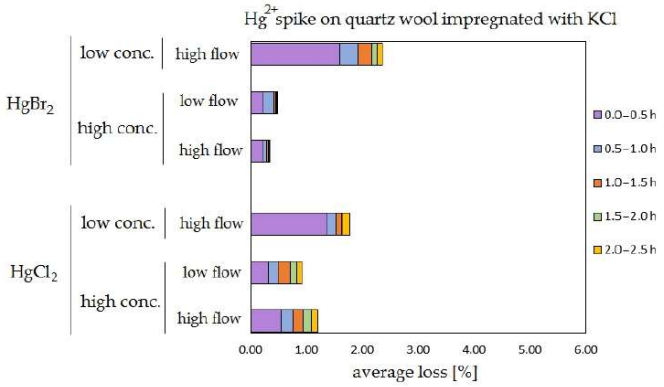

Figure 8. Results of the stability test for the $^{197}Hg^{2+}$ (radiotracer) spike on quartz wool impregnated with KCl. Low concentrations were loaded with less than 1 ng Hg per time period, and high concentrations were loaded with more than 50 ng of Hg per time period. Low airflow experiments were performed with 100 mL min^{-1} airflow, while high airflow experiments were performed with 400 mL min^{-1} flow.

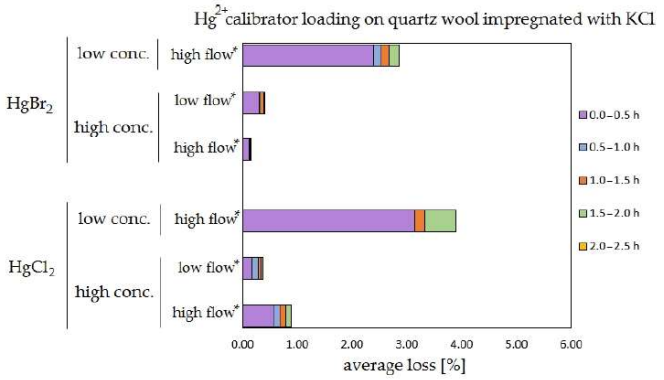

Figure 9. Results of the stability test for the calibrator loading of $^{197}Hg^{2+}$ (radiotracer) on quartz wool impregnated with KCl. Low concentrations were loaded with less than 1 ng Hg per time period, and high concentrations were loaded with more than 50 ng of Hg per time period. Low airflow experiments were performed with 100 mL min^{-1} airflow, while high airflow experiments were performed with 400 mL min^{-1} flow. Asterisks mark the results that only have the first four time periods.

Fig. 11). The slope was established using a linear regression weighting the errors in $\ln(m_{Hg}(n))$ using the calculated expanded uncertainty with a coverage factor $k = 2$.

As depicted in Fig. 11, plotting the logarithm of the Hg mass extracted against the extraction number gives a linear relationship that allows the calculation of the dimensionless HLC. A combined dimensionless HLC was found to be 0.1713 with an expanded uncertainty ($k = 2$) of 0.0093 (calculation and derivation of needed equations is located in the Supplement, Eqs. S3–S12). The dimensionless HLC can be used to calculate the elemental mercury concentration collected in the KCl solution at equilibrium conditions.

3.4 Oxidation of elemental Hg in KCl trapping solution

The oxidation of elemental mercury found for the nitrogen and air matrices was 2.9 % and 3.0 % respectively. When the KCl trapping blank solution was tested, it was found to be below the GC-AFS method detection limit (1 pg). Impurities present in the KCl trapping solution appear to oxidize a small percentage of the elemental Hg vapor which was con-

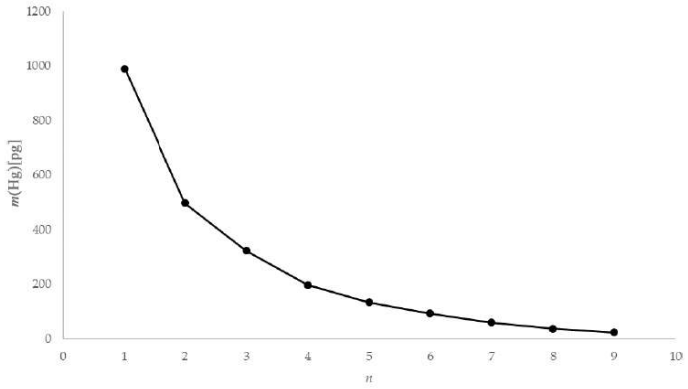

Figure 10. Example m(Hg) against extraction number (n) for 1 mol L^{-1} KCl at 5 °C.

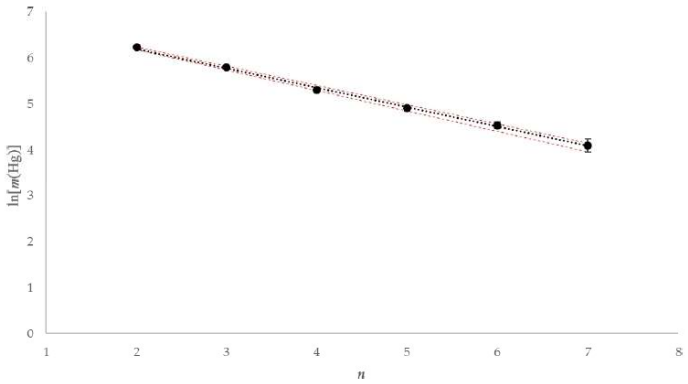

Figure 11. Example ln[m(Hg)] against extraction number (n) and linear regression for KCl at 5 °C (red error bars $\pm 1\ u_c$ [$k = 1$]).

tinuously introduced during the test. As a negligible difference was found when comparing air and nitrogen, it is reasonable to assume that this oxidation was not due to aerial oxidation. The results indicate that the KCl solution will also collect a small quantity of elemental Hg due to its solubility; this elemental Hg was observed in the chromatograms, as depicted in the Supplement (Fig. S1). This was not observed in standard solutions or blanks. The elemental Hg response was not quantified because the procedure used is not considered quantitative for elemental Hg, as this species does not undergo derivatization.

3.5 Retention of oxidized Hg in KCl trapping solution

In this test, bubbling the KCl solution spiked with $HgCl_2$ with nitrogen or air for the 2 h sampling period gave a recovery of 102.3 % and 101.8 %, respectively, indicating that no $HgCl_2$ was lost from the KCl solution. The slight increase is within the measurement uncertainty of the propylation GC-AFS.

3.6 Predicted bias calculation using KCl trapping solution at atmospheric Hg speciation concentrations

The experimental data indicate that GEM oxidation (Sect. 3.4) and GEM solubilization (Sect. 3.3) will occur in

KCl trapping solutions. The combination of these two factors will produce a positive bias which can be predicted using Eq. (1):

$$\text{Predicted GOM bias (\%)} = \frac{\text{GEM}_{\text{oxid}} + \text{GEM}_{\text{sol}}}{\text{GOM}_{\text{native}}} \times 100\,\%. \quad (1)$$

For example, if a $1\,m^3$ ambient air sample containing $2\,ng\,m^{-3}$ GEM and $0.002\,ng\,m^{-3}$ GOM (GOM_{native}) was sampled through a 1000 mL KCl solution, the bias can be predicted as follows: by applying the dimensionless HLC obtained from the presented work and using the equations available in the Supplement, the calculated contribution due to solubility (GEM_{sol}) will be $0.012\,ng\,m^{-3}$. Oxidation of 3 % of GEM was found in the KCl trapping solution. This equates to GEM_{oxid} of $0.060\,ng\,m^{-3}$ for this example. The apparent gas concentration in the KCl solution would be the summation of soluble GEM ($0.012\,ng\,m^{-3}$), oxidized GEM ($0.060\,ng\,m^{-3}$) and the native GOM ($0.002\,ng\,m^{-3}$), equating to $0.074\,ng\,m^{-3}$ rather than the expected $0.002\,ng\,m^{-3}$. From this simple calculation using Eq. (1), a GOM bias of 3500 % can be predicted due to the solubility and oxidation of GEM in the KCl solution. The bias depends on the GEM : GOM ratio – the higher the percentage of GOM relative to GEM, the lower the bias will be. For example, a similar calculation as above but with $1.980\,ng\,m^{-3}$ GEM and $0.02\,ng\,m^{-3}$ GOM results in 456 % bias instead of 3500 %. The calculated biases show that KCl trapping solutions are not appropriate for ambient GOM sampling, while they are still a valid choice for flue gas sampling (high GOM concentrations).

4 Conclusions

KCl sorbent traps exhibit good stability for most of the experimental conditions tested in this work. When KCl sorbent traps are used for ambient Hg concentration, the extent of GOM losses can reach up to 5.5 % (2 % to 3 % on average). When calculating the overall uncertainty of the atmospheric Hg speciation, these losses should be taken into account as the sampling uncertainty. Reuse of KCl sorbent traps resulted in large reduction in their specificity. Because the reuse of KCl-coated denuders (for ambient GOM sampling) is also common practice, a similar reduction in specificity could also occur for KCl-coated denuders. As denuders are the most commonly used means of sampling GOM, this poses a potential challenge which should be addressed.

The ^{197}Hg radiotracer proved to be a suitable tool for studying the metrology and processes occurring during atmospheric mercury speciation. In the future, the ^{197}Hg radiotracer could be applied for verifying other GOM sampling methods such as denuders and different membrane filters.

KCl trapping solutions cannot be considered truly selective for GOM measurements for atmospheric mercury speciation measurements. GEM will be captured in the solution due to both oxidation and solubilization producing a large bias in the GOM measurement.

Data availability. Data are contained within the article (Table 1) and the Supplement (Tables S1–S7, Fig. S1).

Supplement. The supplement related to this article is available online at: https://doi.org/10.5194/amt-14-6619-2021-supplement.

Author contributions. The conceptualization was done by JG, SRG, JK, WTC, and MH; funding was acquired by MH; the methodology was done by JG, IŽ, RJ, GDF, MAD, and SRG; the project was administered by MH; the work was supervised by JK, WTC, and MH; the validation of the analytical procedure was done by MAD, JG, RJ, and IŽ; the original draft was written by JG and WTC; the review writing and editing was done by JG, IŽ, MAD, and MH.

Competing interests. The contact author has declared that neither they nor their co-authors have any competing interests.

Disclaimer. Publisher's note: Copernicus Publications remains neutral with regard to jurisdictional claims in published maps and institutional affiliations.

Special issue statement. This article is part of the special issue "Research results from the 14th International Conference on Mercury as a Global Pollutant (ICMGP 2019), MercOx project, and iGOSP and iCUPE projects of ERA-PLANET in support of the Minamata Convention on Mercury (ACP/AMT inter-journal SI)". It is not associated with a conference.

Acknowledgements. Financial support from the project Integrated Global Observing Systems for Persistent Pollutants (IGOSP) funded by the European Commission in the framework of program "The European network for observing our changing planet (ERA-PLANET)", grant agreement 689443, is also acknowledged. The authors would like to thank the TRIGA reactor staff at the Reactor Infrastructure Centre of the JSI for their availability and cooperation at all times. We would also like to thank Jarkko Makkonen and Timo Rajamäki for supplying us with the calibrator and for operational advice. The authors would like to thank Ingvar Wängberg at IVL Sweden for their initial guidance and providing detailed information regarding the extractor vessel apparatus.

Financial support. This research has been supported by the European Commission, Horizon 2020 Framework Programme (ERA-PLANET (grant no. 689443)), the European Metrology Programme for Innovation and Research (grant no. 16ENV01), the Javna Agencija za Raziskovalno Dejavnost RS (grant nos. P1-0143 and PR-

52044), and the Urad Republike Slovenije za Meroslovje (grant no. C3212-10-000071).

Review statement. This paper was edited by Daniela Famulari and reviewed by two anonymous referees.

References

Andersson, M. E., Gårdfeldt, K., Wängberg, I., and Strömberg, D.: Determination of Henry's law constant for elemental mercury, Chemosphere, 73, 587–592, https://doi.org/10.1016/j.chemosphere.2008.05.067, 2008.

ASTM International: ASTM D6784-16, Standard Test Method for Elemental, Oxidized, Particle-Bound and Total Mercury in Flue Gas Generated from Coal-Fired Stationary Sources (Ontario Hydro Method), available at: http://www.astm.org (last access: 15 April 2021), 2016.

Bu, X., Zhang, H., Lv, G., Lin, H., Chen, L., Yin, X., Shen, G., Yuan, W., Zhang, W., Wang, X., and Tong, Y.: Comparison of Reactive Gaseous Mercury Collection by Different Sampling Methods in a Laboratory Test and Field Monitoring, Environ. Sci. Technol. Lett., 5, 600–607, https://doi.org/10.1021/acs.estlett.8b00439, 2018.

Dumarey, R.: Comparison of the collection and desorption efficiency of activated charcoal, silver, and gold for the determination of vapor-phase atmospheric mercury, Anal. Chem., 57, 2644–2646, 1985.

Dumarey, R., Brown, R. J. C., Corns, W. T., Brown, A. S., and Stockwell, P. B.: Elemental mercury vapour in air: The origins and validation of the "Dumarey equation" describing the mass concentration at saturation, Accredit. Qual. Assur., 15, 409–414, https://doi.org/10.1007/s00769-010-0645-1, 2010.

Dunham-Cheatham, S. M., Lyman, S., and Gustin, M. S.: Evaluation of sorption surface materials for reactive mercury compounds, Atmos. Environ., 242, 117836, https://doi.org/10.1016/j.atmosenv.2020.117836, 2020.

Electric Power Research Institute (EPRI): Guidelines for Speciated Mercury Field Measurements, Palo Alto, California, USA, 2015.

Gačnik, J., Živković, I., Guevara, S. R., Jaćimović, R., Kotnik, J., and Horvat, M.: Validating an evaporative calibrator for gaseous oxidized mercury, Sensors, 21, 2501, https://doi.org/10.3390/s21072501, 2021.

Gustin, M. and Jaffe, D.: Reducing the uncertainty in measurement and understanding of mercury in the atmosphere, Environ. Sci. Technol., 44, 2222–2227, https://doi.org/10.1021/es902736k, 2010.

Gustin, M. S., Huang, J., Miller, M. B., Peterson, C., Jaffe, D. A., Ambrose, J., Finley, B. D., Lyman, S. N., Call, K., Talbot, R., Feddersen, D., Mao, H., and Lindberg, S. E.: Do we understand what the mercury speciation instruments are actually measuring? Results of RAMIX, Environ. Sci. Technol., 47, 7295–7306, https://doi.org/10.1021/es3039104, 2013.

Gustin, M. S., Dunham-Cheatham, S. M., and Zhang, L.: Comparison of 4 Methos for Measurement of Reactive, Gaseous Oxize, an Particulate Bound Mercury, Environ. Sci. Technol., 53, 14489–14495, https://doi.org/10.1021/acs.est.9b04648, 2019.

Gustin, M. S., Dunham-Cheatham, S. M., Zhang, L., Lyman, S., Choma, N., and Castro, M.: Use of Membranes and Detailed HYSPLIT Analyses to Understand Atmospheric Particulate, Gaseous Oxidized, and Reactive Mercury Chemistry, Environ. Sci. Technol., 55, 893–901, https://doi.org/10.1021/acs.est.0c07876, 2021.

Huang, J. and Gustin, M. S.: Uncertainties of gaseous oxidized mercury measurements using KCl-coated denuders, cation-exchange membranes, and nylon membranes: Humidity influences, Environ. Sci. Technol., 49, 6102–6108, https://doi.org/10.1021/acs.est.5b00098, 2015.

Huang, J., Miller, M. B., Weiss-Penzias, P., and Gustin, M. S.: Comparison of gaseous oxidized Hg measured by KCl-coated denuders, and nylon and cation exchange membranes, Environ. Sci. Technol., 47, 7307–7316, https://doi.org/10.1021/es4012349, 2013.

International Organization for Standardization: ISO 8573-1:2010 Compressed air – Part 1: Contaminants and purity classes, available at: https://www.iso.org/standard/46418.html (last access: 28 March 2021), 2010.

Jaffe, D. A., Lyman, S., Amos, H. M., Gustin, M. S., Huang, J., Selin, N. E., Levin, L., Ter Schure, A., Mason, R. P., Talbot, R., Rutter, A., Finley, B., Jaeglé, L., Shah, V., McClure, C., Ambrose, J., Gratz, L., Lindberg, S., Weiss-Penzias, P., Sheu, G. R., Feddersen, D., Horvat, M., Dastoor, A., Hynes, A. J., Mao, H., Sonke, J. E., Slemr, F., Fisher, J. A., Ebinghaus, R., Zhang, Y., and Edwards, G.: Progress on understanding atmospheric mercury hampered by uncertain measurements, Environ. Sci. Technol., 48, 7204–7206, https://doi.org/10.1021/es5026432, 2014.

Koron, N., Bratkič, A., Ribeiro Guevara, S., Vahčič, M., and Horvat, M.: Mercury methylation and reduction potentials in marine water: An improved methodology using ^{197}Hg radiotracer, Appl. Radiat. Isot., 70, 46–50, https://doi.org/10.1016/j.apradiso.2011.07.015, 2012.

Lide, D. R.: CRC Handbook of Chemistry and Physics, 88th edn., edited by: Lide, D. R., Taylor & Francis, Bosa Roca, USA, 2007.

Lyman, S., Jones, C., O'Neil, T., Allen, T., Miller, M., Gustin, M. S., Pierce, A. M., Luke, W., Ren, X., and Kelley, P.: Automated calibration of atmospheric oxidized mercury measurements, Environ. Sci. Technol., 50, 12911–12927, https://doi.org/10.1021/acs.est.6b04211, 2016.

Lyman, S. N., Jaffe, D. A., and Gustin, M. S.: Release of mercury halides from KCl denuders in the presence of ozone, Atmos. Chem. Phys., 10, 8197–8204, https://doi.org/10.5194/acp-10-8197-2010, 2010.

McClure, C. D., Jaffe, D. A., and Edgerton, E. S.: Evaluation of the KCl denuder method for gaseous oxidized mercury using $HgBr_2$ at an in-service AMNet site, Environ. Sci. Technol., 48, 11437–11444, https://doi.org/10.1021/es502545k, 2014.

Prestbo, E. M. and Bloom, N. S.: Mercury Speciation Adsorption (Mesa) Method for Combustion Flue Gas: Methodology, Artifacts, Intercomparison, and Atmospheric Implications, Water Air Soil Pollut., 80, 145–158, https://doi.org/10.1007/BF01189663, 1995.

Ribeiro Guevara, S. and Horvat, M.: Stability and behaviour of low level spiked inorganic mercury in natural water samples, Anal. Methods, 5, 1996–2006, https://doi.org/10.1039/c3ay26496c, 2013.

Ribeiro Guevara, S., Jereb, V., Arribére, M. A., Pérez Catán, S., and Horvat, M.: The production and use of ^{197}Hg ^{g} radiotracer to study mercury transformation processes in environmental matrices, RMZ Mater. Geoenvironment J., 51, 1928–1931, 2004.

Ribeiro Guevara, S., Žižek, S., Repinc, U., Catán, S. P., Jaćimović, R., and Horvat, M.: Novel methodology for the study of mercury methylation and reduction in sediments and water using ^{197}Hg radiotracer, Anal. Bioanal. Chem., 387, 2185–2197, https://doi.org/10.1007/s00216-006-1040-y, 2007.

Saxholm, S., Rajamäki, T., Hämäläinen, J., and Hildén, P.: Dynamic calibration method for reactive gases, Meas. Sci. Technol., 31, 034001, https://doi.org/10.1088/1361-6501/ab4d68, 2020.

Shafawi, A., Ebdon, L., Foulkes, M., Stockwell, P., and Corns, W.: Determination of total mercury in hydrocarbons and natural gas condensate by atomic fluorescence spectrometry, Analyst, 124, 185–189, https://doi.org/10.1039/a809679a, 1999.

United Nations Environment Programme: Global mercury assessment 2018, available at: https://www.unep.org/resources/publication/global-mercury-assessment-2018 (last access: 9 April 2021), 2019.

United States Environmental Protection Agency (U.S. EPA): IO Compendium Method IO-5: Compendium of Methods for the Determination of Inorganic Compounds in Ambient Air: Sampling and Analysis for Vapor and Particle Phase Mercury in Ambient Air Utilizing Cold Vapor Atomic Fluorescence Spectrometry (CVAFS), available at: https://www.epa.gov/esam/epa-io-inorganic-compendium-method-io-5-sampling-and-analysis-vapor-and-particle-phase-mercury (last access: 15 February 2021), 1999.

United States Environmental Protection Agency (U.S. EPA): Method 30A – Determination Of Total Vapor Phase Mercury Emissions From Stationary Sources (Instrumental Analyzer Procedure), available at: https://www.epa.gov/emc/method-30a-mercury-instrumental-procedure (last access: 20 February 2021), 2017.

Wang, S., Holsen, T. M., Huang, J., and Han, Y.-J.: Evaluation of various methods to measure particulate bound mercury and associated artifacts, Atmos. Chem. Phys. Discuss., 13, 8585–8614, https://doi.org/10.5194/acpd-13-8585-2013, 2013.

Zhang, H., Fu, X., Wang, X., and Feng, X.: Measurements and Distribution of Atmospheric Particulate-Bound Mercury: A Review, Bull. Environ. Contam. Toxicol., 103, 48–54, https://doi.org/10.1007/s00128-019-02663-5, 2019.

Supplement of Atmos. Meas. Tech., 14, 6619–6631, 2021
https://doi.org/10.5194/amt-14-6619-2021-supplement
© Author(s) 2021. CC BY 4.0 License.

Atmospheric Measurement Techniques Open Access EGU

Supplement of

Behavior of KCl sorbent traps and KCl trapping solutions used for atmospheric mercury speciation: stability and specificity

Jan Gačnik et al.

Correspondence to: Milcna Horvat (milcna.horvat@ijs.si)

The copyright of individual parts of the supplement might differ from the article licence.

Table S1: Chemicals used in the presented work

Description	Purity / type	Producer
65 % nitric acid	For analysis	Supelco, Darmstadt, Germany
30 % hydrochloric acid	Suprapur	Merck, Darmstadt, Germany
47 % hydrobromic acid	For analysis	Merck, Darmstadt, Germany
Tin (II) chloride dihydrate ($SnCl_2 \cdot 2H_2O$)	For analysis, max. 0.000001 % Hg	Merck, Darmstadt, Germany
Gold (III) chloride hydrate ($HAuCl_4 \cdot xH_2O$)	99.995 % trace metal basis	Merck, Darmstadt, Germany
Elemental mercury	99.9999 % Suprapur	Merck, Darmstadt, Germany
Sodium tetrapropylborate	/	Merck, Darmstadt, Germany
Acetic acid	Puriss.	Merck, Darmstadt, Germany
Ammonium acetate	LiChropur	Merck, Darmstadt, Germany
2,2,4-trimethylpentane	For HPLC, ≥99 %	Merck, Darmstadt, Germany
Silica gel	Technical grade 40, 6-14 mesh	merck, Darmstadt, Germany
Anhydrous sodium sulfate	≥99.99 % trace metal basis	Merck, Darmstadt, Germany
NIST SRM 3133: Mercury (Hg) Standard Solution	/	NIST, Gaithersburg, MD, USA
^{196}Hg enriched elemental Hg	51.58 % ^{196}Hg	Isoflex, San Francisco, CA, USA
Type I purified water	Electrical resistivity 18.2 MΩ cm	Merck, Darmstadt, Germany

Table S2: Instruments used in the presented work

Description	Model	Producer
High-purity germanium (HPGe) coaxial-type detector	Model 7229P	Canberra Industries Inc., Meriden, CT, USA
High-purity germanium (HPGe) well-type detector	Model GCW6023/S	Canberra Industries Inc., Meriden, CT, USA
Cold vapor atomic absorption spectrometer	Model Hg-201 Semi-Automated Mercury Analyzer	Sanso Seisakusho Co., Ltd., Tokyo, Japan
Liquid evaporative generator for oxidized mercury	/	Optoseven Ltd. & VTT Ltd., Espoo, Finland
Amalgamation-atomic fluorescence spectrometer	Model PSA 10.525 Sir Galahad	P S Analytical, Orpington, UK
Temperature-controlled bath	Model R2	Grant Instruments Ltd., Cambridge, UK
Bell Jar elemental Hg calibrator	Model PSA 10.555	P S Analytical, Orpington, UK
Cavkit elemental Hg vapor generator	Model PSA 10.536	P S Analytical, Orpington, UK
Capillary gas chromatography atomic fluorescence spectrometry	Model PSA 10.725 with Agilent J&W, DB1, 15 m 0.53 mm ID, film thickness 1.50 µm	P S Analytical, Orpington, UK

Equation S1 was applied for calculation of both A_0 (activity at reference time) of the sample and A_0 of the standard. The recoveries were calculated using Equation S2.

Equation S1

$$A_{0,sample} = \frac{A_{sample} * \frac{\ln 2}{t_{1/2}}}{e^{-\left(\frac{t_{passed} * \ln 2}{t_{1/2}}\right)} * \left[1 - e^{-\left(\frac{t_{measurement} * \ln 2}{t_{1/2}}\right)}\right]}$$

Equation S2

$$R = \frac{A_{0,sample}}{A_{0,std.}} * \frac{m_{Hg,std.}}{m_{Hg,sample}} * 100$$

Where:

$A_{0,\,sample}$ is the sample activity at reference time t=0 [Bq],
$A_{0,\,std}$ is the standard activity at reference time t=0 [Bq],
A_{sample} is the sample activity at the time of measurement [Bq],
$t_{1/2}$ is the half-life of ^{197}Hg [s],
t_{passed} is the time passed since reference time t=0 till the start of measurement [s],
$t_{measurement}$ is the time passed during the measurement [s],
R is the recovery [%],
$m_{Hg,std.}$ is the mass of Hg used for standard [pg],
$m_{Hg\ sample}$ is the mass of Hg used for sample, assuming 100 % recovery [pg].

The dimensionless Henry's law constant can be calculated according to Equation S3.

Equation S3

$$k_{H'} = \frac{[Hg_{gas}]}{[Hg_{solution}]}$$

Where:
$k_{H'}$ is the dimensionless Henry's law constant,
$[Hg_{gas}]$ is the concentration of mercury in gas phase,
$[Hg_{solution}]$ is the concentration of mercury in liquid phase.

The true gas flow in the extractor stripping vessel, $\overline{Q_{(g)}}$ was calculated using Equation S4.

Equation S4

$$\overline{Q_{(g)}} = Q^{o}_{(g)} \times \frac{T \times p_0}{(\bar{p} - p_w) \times T_0}$$

Where:
T is the absolute temperature of the sample in the extractor,
$Q^{\circ}_{(g)}$ is the dry standard flow rate from the mass flow controller at reference conditions T_0 (293.15 K) and p_0 (1013.2 mbar),
$\bar{p}$ is the pressure of the headspace in the vessel,
p_w is the saturated vapor pressure of the KCl at temperature of the vessel.

Henry's law describes the relationship between the partial pressure of a gas and the amount of that gas species dissolved into a liquid phase. The ratio of the two is constant for a given system (temperature, gas species and liquid phase composition). For low gas-phase concentrations, the gas to liquid concentration ratio (in matrix independent units) can be used (Equation S3), with the constant of proportionality, $k_{H'}$, called the dimensionless Henry's law constant (HLC).(Saxholm et al., 2020)

Assuming equilibrium between elemental Hg in the aqueous and gas phases and considering Henry's law, the differential equation (Equation S5) can be applied, which describes the rate of decrease of Hg^0 dissolved in the aqueous phase as it is stripped out into the flowing gas.

Equation S5

$$\frac{dC_{aq}}{dt} = -\frac{\overline{Q_{(g)}} \times k_{H'} \times C_{aq}}{V_{solv}}$$

Where:
C_{aq} is the Hg concentration in the solvent,
V_{solv} is the volume of solvent in the extractor.

Solving Equation S5 gives Equation S6.

Equation S6

$$\frac{C_{aq}}{C_0} = e^{-\frac{\overline{Q_{(g)}} \times t \times k_{H'}}{V_{solv}}}$$

Equation S6 can be expressed as Equation S7 and Equation S8

Equation S7

$$C_{aq} = C_0 \times e^{-\alpha}$$

Where:

Equation S8

$$\alpha = \frac{\overline{Q_{(g)}} \times t \times k_{H'}}{V_{solv}} = \frac{V_{(g)} \times k_{H'}}{V_{solv}}$$

The amount of Hg collected during every extraction depends on the volume of gas and the volume of solution. During each successive extraction (n = 1, 2, 3 …) of the same period the concentration of mercury in solution can be calculated using Equation S9.

Equation S9

$$C_{aq}(n) = C_0 \times e^{-n*\alpha}$$

The mass of mercury collected from the gas phase, $m_{Hg}(n)$, during extraction n is the difference between the mass of Hg in solution after the extraction (n - 1) and the mass of Hg in solution after extraction n, which can be expressed as Equation S10.

Equation S10

$$m_{Hg}(n) = V_{solv} \times C_{aq}(n-1) - V_{aq} \times C_{aq}(n)$$

Equation S10 can also be expressed as Equation S11.

Equation S11

$$m_{Hg}(n) = V_{solv} \times C_0 \times (e^{\alpha} - 1) - e^{-n \times \alpha}$$

The natural logarithm of Equation S11 is expressed in Equation S12.

Equation S12

$$ln\left(m_{Hg}(n)\right) = -(n \times \alpha) + ln\left(V_{solv} \times C_0 \times (e^{\alpha} - 1)\right)$$

Therefore, a graph of $\ln\left(m_{Hg}(n)\right)$ against n has a slope of $-\alpha$ and an intercept of $\ln\left(V_{solv} \times C_0 \times (e^{\alpha} - 1)\right)$. If both V_{solv} and $V_{(g)}$ are known, the dimensionless HLC can be calculated from α using Equation S8.

Table S3 shows the temperature program that was used for determination of oxidized Hg in KCl trapping solutions by gas chromatography with atomic fluorescence detection (GC-AFS).

Table S3: GC-AFS temperature program.

Stage	Start temperature [°C]	Ramp [°C min^{-1}]	End temperature [°C]	Hold [min]
1	30	/	30	2
2	30	20	80	0
3	80	50	120	1
4	120	100	280	4

Table S4: Results of the stability test for the $^{197}Hg^{2+}$ (radiotracer) spike on KCl crystal. Low concentrations were loaded with less than 1 ng Hg per time period and high concentrations were loaded with more than 50 ng of Hg per time period. Low air flow experiments were performed with 100 mL min^{-1} air flow while high air flow experiments were performed with 400 mL min^{-1} flow.

Species	Concentration	Gas flow	Time period	0.0 - 0.5 h	0.5 – 1.0 h	1.0 - 1.5 h	1.5 – 2.0 h	2.0 – 2.5 h
$HgCl_2$	High	High	Average loss (%)	0.92	0.67	0.57	0.61	×
			SD (%)	0.52	0.46	0.14	0.23	×
			RSD	56.7	68.6	24.0	37.9	×
		Low	Average loss (%)	2.43	0.21	0.03	0.12	0.03
			SD (%)	1.45	0.26	0.03	0.10	0.03
			RSD	59.8	126	115	86.6	88.4
	Low	High	Average loss (%)	2.01	0.80	1.04	1.00	0.69
			SD (%)	1.25	1.07	1.50	1.70	1.04
			RSD	62.1	133	143	169	152
$HgBr_2$	High	High	Average loss (%)	0.04	0.01	0.02	0.02	0.00
			SD (%)	0.05	0.03	0.02	0.02	0.00
			RSD	104	199	100	118	0.00
		Low	Average loss (%)	0.02	0.09	0.04	0.00	×
			SD (%)	0.03	0.03	0.06	0.00	×
			RSD	173	31.9	173	509	×
	Low	High	Average loss (%)	0.95	0.17	0.03	0.13	0.00
			SD (%)	0.76	0.17	0.05	0.21	0.00
			RSD	80.1	103	173	154	173

Table S5. Results of the stability test for the calibrator loading of $^{197}Hg^{2+}$ (radiotracer) on KCl crystal. Low concentrations were loaded with less than 1 ng Hg per time period and high concentrations were loaded with more than 50 ng of Hg per time period. Low air flow experiments were performed with 100 mL min^{-1} air flow while high air flow experiments were performed with 400 mL min^{-1} flow.

Species	Concentration	Gas flow	Time period	0.0 - 0.5 h	0.5 – 1.0 h	1.0 - 1.5 h	1.5 – 2.0 h	2.0 – 2.5 h
$HgCl_2$	High	High	Average loss (%)	0.27	0.01	0.01	0.02	×
			SD (%)	0.27	0.00	0.01	0.02	×
			RSD	101	41.9	141	141	×
		Low	Average loss (%)	0.03	0.01	0.01	0.01	×
			SD (%)	0.02	0.01	0.02	0.01	×
			RSD	72.1	94.6	165	72.9	×
	Low	High	Average loss (%)	2.37	1.50	0.33	0.02	×
			SD (%)	0.61	1.06	0.56	0.02	×
			RSD	25.7	70.7	173	97.0	×
$HgBr_2$	High	High	Average loss (%)	0.04	0.01	0.01	0.01	×
			SD (%)	0.02	0.01	0.00	0.01	×
			RSD	41.7	70.3	18.9	43.7	×
		Low	Average loss (%)	0.03	0.02	0.02	0.02	×
			SD (%)	0.02	0.02	0.02	0.02	×
			RSD	78.2	103	85.1	82.2	×
	Low	High	Average loss (%)	1.86	0.19	0.10	0.18	×
			SD (%)	0.95	0.33	0.17	0.26	×
			RSD	51.4	173	173	147	×

Table S6. Results of the stability test for the $^{197}Hg^{2+}$ (radiotracer) spike on quartz wool impregnated with KCl. Low concentrations were loaded with less than 1 ng Hg per time period and high concentrations were loaded with more than 50 ng of Hg per time period. Low air flow experiments were performed with 100 mL min^{-1} air flow while high air flow experiments were performed with 400 mL min^{-1} flow.

Species	Concentration	Gas flow	Time period	0.0 - 0.5 h	0.5 – 1.0 h	1.0 - 1.5 h	1.5 – 2.0 h	2.0 – 2.5 h
$HgCl_2$	High	High	Average loss (%)	0.55	0.21	0.19	0.14	0.10
			SD (%)	0.22	0.09	0.18	0.10	0.09
			RSD	40.4	40.0	96.4	75.8	93.9
		Low	Average loss (%)	0.31	0.18	0.22	0.12	0.08
			SD (%)	0.17	0.13	0.28	0.08	0.10
			RSD	53.1	76.5	127	71.6	115
	Low	High	Average loss (%)	1.36	0.17	0.09	0.02	0.12
			SD (%)	0.47	0.27	0.10	0.04	0.05
			RSD	34.8	164	109	173	40.2
$HgBr_2$	High	High	Average loss (%)	0.21	0.07	0.03	0.02	0.02
			SD (%)	0.06	0.03	0.01	0.02	0.02
			RSD	31.2	47.8	44.7	122	121
		Low	Average loss (%)	0.23	0.18	0.03	0.02	0.01
			SD (%)	0.18	0.12	0.04	0.02	0.01
			RSD	77.1	68.6	131	90.5	86.9
	Low	High	Average loss (%)	1.59	0.32	0.25	0.11	0.08
			SD (%)	1.21	0.35	0.22	0.08	0.06
			RSD	76.1	107	87.3	74.6	75.1

Table S7. Results of the stability test for the calibrator loading of $^{197}Hg^{2+}$ (radiotracer) on quartz wool impregnated with KCl. Low concentrations were loaded with less than 1 ng Hg per time period and high concentrations were loaded with more than 50 ng of Hg per time period. Low air flow experiments were performed with 100 mL min^{-1} air flow while high air flow experiments were performed with 400 mL min^{-1} flow

Species	Concentration	Gas flow	Time period	0.0 - 0.5 h	0.5 – 1.0 h	1.0 - 1.5 h	1.5 – 2.0 h	2.0 – 2.5 h
$HgCl_2$	High	High	Average loss (%)	0.57	0.11	0.11	0.10	×
			SD (%)	0.07	0.11	0.13	0.04	×
			RSD	12.5	95.8	122	41.7	×
		Low	Average loss (%)	0.17	0.12	0.05	0.03	×
			SD (%)	0.15	0.11	0.07	0.03	×
			RSD	86.0	89.3	135	96.5	×
	Low	High	Average loss (%)	3.15	0.00	0.18	0.56	×
			SD (%)	0.67	0.00	0.32	0.72	×
			RSD	21.3	0.00	173	130	×
$HgBr_2$	High	High	Average loss (%)	0.12	0.00	0.02	0.01	×
			SD (%)	0.05	0.01	0.01	0.01	×
			RSD	46.0	173	70.9	104	×
		Low	Average loss (%)	0.30	0.03	0.05	0.02	×
			SD (%)	0.22	0.04	0.03	0.02	×
			RSD	74.8	140	59.7	120	×
	Low	High	Average loss (%)	2.38	0.15	0.15	0.17	×
			SD (%)	1.60	0.13	0.26	0.22	×
			RSD	67.2	86.6	173	129	×

3.4 Manuscript 4: Calibration Approach for Gaseous Oxidized Mercury Based on Nonthermal Plasma Oxidation of Elemental Mercury

Gačnik J., Živković I., Ribeiro Guevara S., Kotnik J., Berisha S., Vijayakumaran Nair S., Jurov A., Cvelbar U., Horvat M. (2022). Analytical Chemistry, 94, 8234-8240

Atmospheric mercury measurements carried out in recent decades have been subject to bias mainly due to metrological difficulties. One of the major constraints is an accurate and precise calibration of analytical equipment. Calibration approaches for GOM that use direct calibration with Hg^{II} species rather than indirect calibration with Hg^0 are scarce. Scarcity is most evident when considering GOM calibrations that are suitable for calibration at ambient GOM concentration levels. Even though attempts have been made to establish metrological traceability of GOM calibration (Seth N. Lyman, Gratz, et al., 2020), direct calibration of Hg^{II} species that is also metrologically traceable is non-existent.

In the present manuscript, we have developed a calibration approach for GOM based on the nonthermal plasma (NTP) oxidation of Hg^0 to Hg^{II} species (HgO, $HgCl_2$, and $HgBr_2$) in the presence of a reaction gas. The developed calibration consists of three steps: i) generation of a known amount of Hg^0, ii) oxidation of Hg^0 to Hg^{II} by NTP in the presence of reaction gas, and iii) thermal reduction of Hg^{II} to Hg^0. The first step is well established, while the second and third step had to be validated. Validation and proof of concept were done using the ^{197}Hg radiotracer. Using ^{197}Hg radiotracer, we studied the $Hg^0 \rightarrow Hg^{II}$ oxidation efficiency and $Hg^{II} \rightarrow Hg^0$ thermal reduction efficiency. Additionally, the uncertainty of the NTP calibration approach was evaluated. At the end, we attempted to experimentally identify the produced Hg^{II} species.

Firstly, we evaluated the thermal reduction efficiency. To promote thermal reduction, we tested 4 different catalysts: gold-coated silica, platinum wire, quartz wool, and Al_2O_3 (corundum). Al_2O_3 catalyst showed the best thermal reduction efficiencies, completely reducing Hg^{II} to Hg^0 (100% thermal reduction efficiency). Consequently, Al_2O_3 was implemented in the final NTP calibration design. Secondly, we studied the NTP oxidation efficiency by capturing NTP-produced Hg^{II} species in situ with the so-called "plasma trap" (KCl crystal and Al_2O_3 catalyst). Unconverted Hg^0 (breakthrough) was captured on the downstream Au trap. The oxidation efficiencies with the corresponding expanded standard uncertainty values were $100.5 \pm 4.7\%$ ($k = 2$) for 100 pg of HgO, $96.8 \pm 7.3\%$ ($k = 2$) for 250 pg of $HgCl_2$, and $77.3 \pm 9.4\%$ ($k = 2$) for 250 pg of $HgBr_2$. The oxidation of $HgBr_2$ was hindered by the electrolytic production of Br_2 reaction gas, which is tedious to handle and highly reactive. Finally, we used temperature-programmed desorption quadrupole mass spectrometry (TPD-QMS) to qualitatively confirm that we had indeed produced HgO, $HgCl_2$, and $HgBr_2$. By comparison to literature values for desorption temperatures and desorption temperatures of standards, we confirmed that the produced species were HgO, $HgCl_2$, and $HgBr_2$.

The developed NTP oxidation of Hg^0 to Hg^{II} species presents a viable approach for the calibration of GOM measurement instrumentation. Our calibration approach can reliably produce known quantities of HgO and $HgCl_2$, while further optimization is needed for $HgBr_2$ production. The presence of all produced species was qualitatively confirmed. Our calibration produces Hg^{II} species discretely ("batch-type" calibration); further work is planned to establish continuous production of Hg^{II} species since a continuous source will mostly likely be needed for the flue GOM gas calibration. Establishing traceability to SI

units could be possible through NIST SRM 3133, but this assumption has to be experimentally confirmed in the future.

In the present manuscript, my contribution consisted of performing the experimental work, evaluating the combined standard uncertainty of the developed calibration, preparing figures and tables, preparing early drafts for the journal cover art, and in the writing of the manuscript.

analytical chemistry

pubs.acs.org/ac Article

Calibration Approach for Gaseous Oxidized Mercury Based on Nonthermal Plasma Oxidation of Elemental Mercury

Jan Gačnik,[#] Igor Živković,[#] Sergio Ribeiro Guevara, Jože Kotnik, Sabina Berisha, Sreekanth Vijayakumaran Nair, Andrea Jurov, Uroš Cvelbar, and Milena Horvat*

Cite This: *Anal. Chem.* 2022, 94, 8234–8240 Read Online

ACCESS | Metrics & More | Article Recommendations | Supporting Information

Downloaded via INST JOZEF STEFAN on July 8, 2022 at 13:46:12 (UTC).
See https://pubs.acs.org/sharingguidelines for options on how to legitimately share published articles.

ABSTRACT: Atmospheric mercury measurements carried out in the recent decades have been a subject of bias largely due to insufficient consideration of metrological traceability and associated measurement uncertainty, which are ultimately needed for the demonstration of comparability of the measurement results. This is particularly challenging for gaseous Hg^{II} species, which are reactive and their ambient concentrations are very low, causing difficulties in proper sampling and calibration. Calibration for atmospheric Hg^{II} exists, but barriers to reliable calibration are most evident at ambient Hg^{II} concentration levels. We present a calibration of Hg^{II} species based on nonthermal plasma oxidation of Hg^0 to Hg^{II}. Hg^0 was produced by quantitative reduction of Hg^{II} in aqueous solution by $SnCl_2$ and aeration. The generated Hg^0 in a stream of He and traces of reaction gas (O_2, Cl_2, or Br_2) was then oxidized to different Hg^{II} species by nonthermal plasma. A highly sensitive ^{197}Hg radiotracer was used to evaluate the oxidation efficiency. Nonthermal plasma oxidation efficiencies with corresponding expanded standard uncertainty values were 100.5 ± 4.7% (k = 2) for 100 pg of HgO, 96.8 ± 7.3% (k = 2) for 250 pg of $HgCl_2$, and 77.3 ± 9.4% (k = 2) for 250 pg of $HgBr_2$. The presence of HgO, $HgCl_2$, and $HgBr_2$ was confirmed by temperature-programmed desorption quadrupole mass spectrometry (TPD-QMS). This work demonstrates the potential for nonthermal plasma oxidation to generate reliable and repeatable amounts of Hg^{II} compounds for routine calibration of ambient air measurement instrumentation.

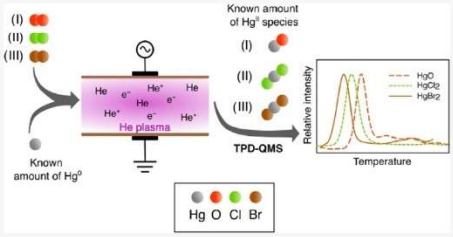

Atmospheric mercury is the largest pool of anthropogenic Hg.[1] Oxidized mercury (Hg^{II}) is present in the atmosphere either directly due to emissions or indirectly through the oxidation of elemental mercury. Hg^{II} can be methylated and bioaccumulated into the food chain after entering ecosystems via wet and dry deposition to aquatic and terrestrial environments.[2] The degree of dry and wet deposition in global Hg assessments can only be estimated by knowing the chemistry and composition of atmospheric Hg^{II} species.[3] Atmospheric Hg^{II} species are usually presented as operationally defined gaseous oxidized mercury (GOM), particulate-bound mercury (PBM), or reactive mercury (RM, GOM + PBM). Even though some Hg^{II} species, such as $HgCl_2$ and $HgBr_2$, have been identified in the atmosphere,[4,5] the exact composition of atmospheric Hg^{II} remains unknown; this points to the need for improved atmospheric mercury speciation.[6]

The first problems associated with atmospheric mercury speciation were identified more than a decade ago. The most commonly used procedure for atmospheric mercury speciation uses preconcentration on KCl-coated denuders that are subject to biases. Biases originate from the low GOM collection efficiency of denuders in the presence of ozone and high humidity.[7−10] Another analytical challenge is the correct calibration or lack thereof, as currently the calibration for GOM measurements is performed using Hg^0 vapor. Moreover, Hg^0 vapor concentration and its temperature dependence are described by an empirical equation that is not universally agreed upon.[11,12] Additionally, instruments should be calibrated directly with gaseous Hg^{II} species instead of Hg^0 to ensure a valid calibration.[13] Currently, the available calibrations for oxidized mercury species are based on either permeation[14,15] or liquid evaporation of Hg^{II} salts.[16,17] Although permeation calibrators are promising, they are still in the development stage, showing inconsistent results at permeation rates relevant to ambient Hg^{II} concentrations.[18] Liquid-evaporative calibrators perform well at flue gas Hg^{II} concentrations while having a biased low output at ambient Hg^{II} concentrations, mainly due to the adsorption and reactive nature of Hg^{II}.[19] Permeation and liquid-evaporative calibrators may also be subject to Hg^0 impurities.[14] No calibration is

Received: January 17, 2022
Accepted: May 18, 2022
Published: June 1, 2022

ACS Publications © 2022 The Authors. Published by American Chemical Society

https://doi.org/10.1021/acs.analchem.2c00260
Anal. Chem. 2022, 94, 8234–8240

currently available for PBM measurements. Due to the aforementioned problematics of atmospheric mercury speciation, measurement results are still a subject of biases and thus cannot be reliably evaluated as equivalent.

Validation of the calibration and, in general, validation of the methodology for atmospheric mercury speciation can be effectively assessed utilizing labeled Hg species. Although the use of Hg stable isotopes is prevalent in the literature,[20−24] radioactive isotopes offer certain advantages. The use of the ^{197}Hg radiotracer (half-life 2.671 days) enables validation at ambient concentrations due to its high specific activity and absence of blanks and contamination issues (^{197}Hg is not present in the nature).[19,25,26]

Nonthermal plasmas (NTP) differ from thermal and high-temperature plasmas in terms of the output energy conversion: in nonthermal plasmas, most of the energy is used to produce energetic electrons, while in thermal plasmas, the energy is also converted into heat.[27] NTP can be generated under near-ambient conditions (room temperature and atmospheric pressure) by means of corona discharges, dielectric barrier discharges (DBD), atmospheric pressure plasma jet (APPJ), micro hollow cathode discharges (MHCD), and many more, all having their own distinctive properties and applications.[28] To the best of the authors' knowledge, Chen et al.[29] were the first to employ NTP using DBD as a method for the oxidation of Hg^0 in flue gases. The method was found to be cost-effective with good oxidation efficiency (up to 80%) in the simulated flue gas mixture.[29] Oxidation reaction pathways,[30,31] the influence of flue gas composition[32,33] and the improvement of the Hg^0 oxidation efficiency by $CaCl_2$ treatment[34] were all investigated for the oxidation of Hg^0 in flue gases with NTP.

The use of DBD-NTP (hereinafter abbreviated as NTP) has so far been largely limited to the removal of Hg^0 from flue gases. In this paper, we report the development of a novel calibration system for gaseous Hg^{II} species based on the oxidation of Hg^0 to Hg^{II} by NTP. Using a highly selective and sensitive ^{197}Hg radiotracer, the newly developed calibration method was validated for use at ambient Hg^{II} concentrations.

1. EXPERIMENTAL SECTION

The validation experiments were performed using a ^{197}Hg radiotracer. The use of ^{197}Hg is not an essential part of the calibration but a useful tool that has been used for validation. For real-time calibration, the use of "normal" or nonradioactive Hg, such as National Institute of Standards and Technology (NIST) standard reference material (SRM) 3133, is intended. Real-time calibration instructions are described in the Supporting Information, Section S1, in the standard operating procedure (SOP) format.

All chemicals and instruments that were utilized in the following experiments are listed in the Supporting Information, Section S2.

1.1. Production of ^{197}Hg Radiotracer. ^{197}Hg radiotracer was used for the majority of performed experiments. Mercury enriched to 51.58% in ^{196}Hg isotope (0.15% natural abundance) was used for irradiation to produce a ^{197}Hg radiotracer. Enriched ^{196}Hg was diluted in 2% HNO_3 acid (v/v) solution and sealed into a quartz ampoule. By irradiating the ampoule with a high neutron flux (10^{13} cm^{-2} s^{-1}) for 12 h in the central channel (CC) of the 250 kW TRIGA Mark II research reactor (Jožef Stefan Institute, Ljubljana, Slovenia), ^{197}Hg ($t_{1/2}$ = 2.671 d) was formed via a neutron capture reaction (n,γ).[26] Similar reactions occur also for the formation of ^{199m}Hg ($t_{1/2}$ = 0.0296 d) from ^{198}Hg, ^{203}Hg ($t_{1/2}$ = 46.594 d) from ^{202}Hg, and ^{205}Hg ($t_{1/2}$ = 0.0036 d) from ^{204}Hg. Nevertheless, ^{199m}Hg, ^{203}Hg, and ^{205}Hg were never measured in our experiments due to their lower specific activity. Other Hg isotopes were unaffected by the neutron flux. After irradiation, the $^{197}Hg^{II}$(aq) stock solution was diluted to 100 pg mL^{-1} which was used as the working solution for the experiments.

1.2. Determining ^{197}Hg Using an HPGe Detector. The activity of ^{197}Hg was determined using two approaches, depending on the Hg collection protocol. The activity of ^{197}Hg collected on gold sorbent traps was measured by means of a coaxial-type HPGe detector, while in solutions, the activity was measured using a well-type HPGe detector. All activity measurements were relative to standards obtained from the irradiated solution in each experimental run. Peak area comparison of the sample and standard activity for the characteristic doublet peaks of γ-ray and X-ray emissions (67.0 + 68.8 and 77.3 + 78.1 keV) was performed using Genie 2000 Gamma analysis software. Oxidation and thermal reduction efficiencies were calculated as shown in the Supporting Information, Section S3.

Standards for the coaxial-type HPGe detector were obtained by a reduction of $^{197}Hg^{II}$(aq) to $^{197}Hg^0$(g), using a tin(II) chloride ($SnCl_2$) solution (100 mL, 2% $SnCl_2$ (w/v) and 0.5% HCl (v/v)). Produced $^{197}Hg^0$ was purged for 10 min with N_2 carrier gas (purity 4.7, flow rate of 1 L min^{-1}) and captured by a downstream gold trap to obtain a measurement standard. Gold traps were prepared out of gold-coated Al_2O_3 (corundum) as described in previous work.[35] To obtain standards for a well-type HPGe detector, triplicates of a Hg radiolabeled solution (8 mL, 2% HNO_3 (v/v)) were transferred into glass vials and measured by a well-type HPGe detector.

The values discussed in the Section 2 were obtained by comparing the sample activities to the standard activities. To determine the equivalence between the ^{197}Hg activity level and the Hg amount (including all Hg isotopes), the activity of stock $^{197}Hg^{II}$(aq) solution was connected to its concentration by cold vapor atomic absorption spectroscopy (CV-AAS) measurement (calibration against NIST SRM 3133).[36] The concentration of stock $^{197}Hg^{II}$(aq) solution was 93.3 μg mL^{-1} of Hg. CV-AAS measurements were performed before and after irradiation to ensure the stability of Hg concentration in the stock solution.

1.3. Production of Hg^{II} Species by Nonthermal Plasma. A simplified scheme of the experimental design is shown in Figure 2a. In the first step, Hg^0 was produced in a 250 mL impinger by the reduction of $^{197}Hg^{II}$(aq) working solution using $SnCl_2$ (as in Section 1.2.). From 1 to 2.5 mL of 100 pg mL^{-1} $^{197}Hg^{II}$(aq) working solution was used to produce 100−250 pg of Hg^0. This amount was chosen as it is sufficiently low to imitate ambient Hg levels while still assuring low measurement uncertainty of the activity measurement.

Produced Hg^0 was aerated from the reaction solution for 10 min using nitrogen gas (1400 mL min^{-1}), dried using a soda lime trap, and collected on the primary gold trap. The primary gold trap was then transferred to a separate setup that was used for the second step of NTP loading. In the second step, the primary gold trap was heated at 400 °C which released the trapped Hg^0 into the stream of He gas (gas flow of 370 mL

https://doi.org/10.1021/acs.analchem.2c00260
Anal. Chem. 2022, 94, 8234−8240

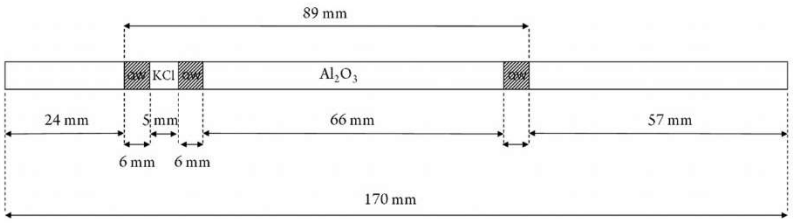

Figure 1. Design of the plasma trap, implemented for NTP oxidation of Hg^0 to Hg^{II} (QW—quartz wool).

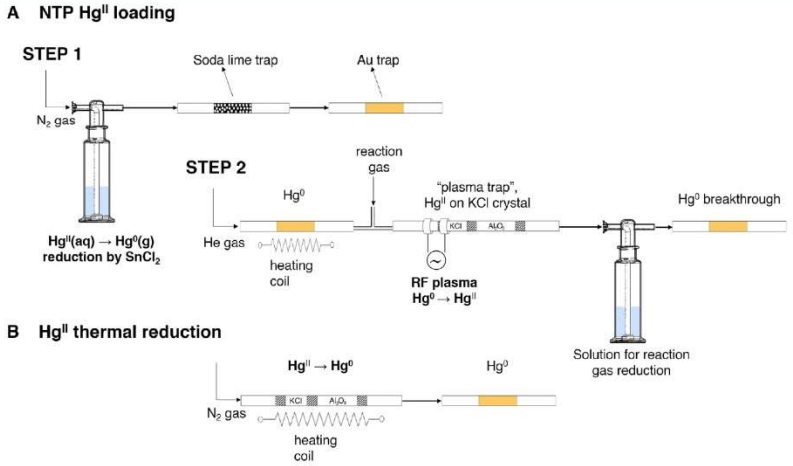

Figure 2. (A) Experimental setup for nonthermal plasma (NTP) loading of Hg^{II} species: in step 1, the gold trap is loaded with Hg^0 by purge and trap. In step 2, the loaded Hg^0 is desorbed from the gold trap and oxidized to Hg^{II} by NTP in a stream of helium and reaction gas mixture. (B) Experimental setup for Hg^{II} to Hg^0 thermal reduction and reduction efficiency studies: Hg^{II} loaded on the KCl is reduced to Hg^0 in the stream of N_2 by Al_2O_3 catalyst-assisted thermal reduction. The reduced Hg^0 is captured by the gold trap.

min^{-1}). Downstream, Hg^0 and He carrier gas were mixed with trace amounts of reaction gas (O_2, Cl_2, or Br_2). O_2 was obtained from a gas cylinder (purity 5.0), while Cl_2 and Br_2 were produced by electrolysis of 1 mol L^{-1} NaCl and KBr solution, respectively. More details regarding the electrolytic production of Cl_2 and Br_2 are available in the Supporting Information, Section S4. Reaction gas was mixed with He and Hg^0 downstream of the primary gold trap. The resulting gas mixture consisted of 99.2% of He and 0.8% of O_2, while for Cl_2 and Br_2, their relative flows were about 0.5% due to the partial solubility of Br_2 and Cl_2 in the KBr or NaCl electrolytic solution. In the mixture of He and the reaction gas, Hg^0 was then oxidized to Hg^{II} by NTP. Hg^{II} was captured on the spot by the KCl crystals, while traces of unoxidized fraction of Hg^0 (breakthrough) were collected on a gold trap. The oxidation efficiency was determined according to the analytical protocol described in Section 1.2. The most important parameter for the NTP oxidation system was the design of the dielectric quartz tube used as "plasma trap" shown in Figure 1. The use of Al_2O_3 catalyst is explained in Section 2.1.

NTP was ignited using a high-voltage high-frequency power generator by applying voltage to a pair of copper electrodes. Electrodes were made of 1 mm thick copper plates, which were cut into 10 mm wide strips and bent around the quartz tube. Such copper strips were separated 5 mm from each other when placed on the plasma trap. By controlling the input power (and indirectly voltage and current) of the generator, we controlled the NTP parameters. The obtained optimal parameters of the NTP generator were: average power applied to the electrodes of 180 μW, radiofrequency of 20 kHz, effective voltage of 345 V, effective current of 7.0 mA, and the phase angle between voltage and current of −101°. The presented values were measured for the gas combination of He and O_2, but they were similar for other gas mixtures.

1.4. Thermal Reduction of Hg^{II} to Hg^0 on Sorbent Traps. Traps with KCl crystal and tested catalyst material (or "plasma traps") were also used for the thermal reduction experiments to assure quantitative reduction. $^{197}Hg^{II}$ was loaded onto the KCl crystal part by spiking 10 μL of $^{197}Hg^{II}$(aq) in a 2% HNO_3 solution. The actual amount of Hg^{II} depended on the extent to which the radiotracer had already decayed and ranged between 100 and 500 pg. The design shown in Figure 2b was used to study the Hg^{II} thermal reduction efficiency.

https://doi.org/10.1021/acs.analchem.2c00260
Anal. Chem. 2022, 94, 8234−8240

Both the KCl crystal and the catalyst part were heated (ramped) from room temperature to 600 °C in 20 s. The trap was vented using N_2 carrier gas (flow rate of 370 mL min^{-1}) for 60 s after the end of heating to ensure complete downstream transport of $^{197}Hg^0$ to a gold trap. $^{197}Hg^0$ on the gold trap was measured using a γ coaxial detector.

Unconverted $^{197}Hg^{II}$ on the KCl trap was washed from the quartz tube and leached from the trap using a previously determined optimal washing solution (20 mL of 10% HNO_3 (v/v) + 5% HCl (v/v) solution). The washing solution (8 mL) was taken into the measurement vial, and the activity of the solution was measured with a γ well detector.

1.5. Analysis of Hg^{II} Species Using Temperature-Programmed Desorption. Indirect analysis of Hg^{II} species was performed on the basis of temperature-programmed desorption (TPD) using a quadrupole mass spectrometer (QMS) operating under a high vacuum. The experimental design of the TPD-QMS analysis of Hg was based on previous work.[37] Samples (<5 mg) loaded into a heating cell were heated to 750 °C at a rate of 10 °C min^{-1}. Heated desorbed atoms or molecules were then ionized at 70 eV using a cross-beam ion source followed by QMS separation based on mass-to-charge (m/z) ratio and detected using a secondary electron multiplier detector. Two different stable Hg isotopes were measured simultaneously, ^{200}Hg and ^{202}Hg. Data for ^{202}Hg were used to prepare TPD spectra for all analyzed Hg^{II} species. Hg^{II} species were determined indirectly because the direct determination of $^{202}HgX_n$ (X═O, Cl, or Br) is not possible; therefore, only ^{202}Hg was measured directly.

Using TPD-QMS, we measured two kinds of samples: Al_2O_3 (corundum) with Hg^{II} species loaded by NTP and Al_2O_3 mixed with Hg^{II} species standards. Hg^{II} species were loaded on Al_2O_3 using NTP as described in Section 1.3, with the only difference being that NIST 3133 was used instead of the ^{197}Hg radiotracer. Hg^{II} species standards were prepared using the so-called "wet preparation" method. For the wet preparation method, we used 100 mL of 1 mg mL^{-1} HgO, $HgCl_2$, and $HgBr_2$ solutions and added 0.5 g of Al_2O_3. The resulting solution containing insoluble Al_2O_3 was then stirred for 30 min, centrifuged, and air-dried. Al_2O_3 prepared in this way served as a Hg^{II} species standard for TPD-QMS.

2. RESULTS AND DISCUSSION

Initial results showed that the efficiency of NTP oxidation of Hg^0 to Hg^{II} could not be reliably estimated if the produced Hg^{II} was incompletely converted to Hg^0 by thermal reduction (Figure 2b). Therefore, we first tested various catalysts that could promote higher efficiency of thermal reduction of Hg^{II} to Hg^0. After selecting the most suitable catalyst, we examined the production of Hg^{II} by the NTP oxidation of Hg^0. Finally, we performed measurements using TPD-QMS with an attempt to confirm the presence of different Hg^{II} species that were produced by NTP oxidation. The order of presenting the results and discussion is therefore in the same sequence as described in the above paragraph.

2.1. Thermal Reduction of Hg^{II} to Hg^0 on Sorbent Traps. We studied the efficiency of thermal reduction for Hg^{II} loaded by spiking the plasma trap. Optimization of the thermal reduction was crucial to ensure reliable estimation of the NTP oxidation efficiency, which is discussed in Section 2.2. First results showed low reduction efficiencies; therefore, a set of different catalysts were used to promote the Hg^{II} thermal reduction. The catalysts were placed in the section of the "plasma trap" marked as "Al_2O_3" in Figure 1. Used catalysts were: Au-coated silica sand, densely packed platinum (Pt) wire, densely packed quartz wool, and Al_2O_3 (corundum, 0.60−0.85 mm grain size). The results of the experiments are shown in Table 1.

Table 1. Hg^{II} to Hg^0 Thermal Reduction, Hg^{II} Loaded by Spiking[a]

catalyst used	Hg^0 [%]	unconverted Hg^{II} [%]	mass balance [%]
none	88 (26)	25.6 (43)	113 (22)
Au-coated silica	38 (3)	61 (5)	99 (2)
Pt wire	39 (28)	49 (32)	88 (5)
quartz wool	86 (19)	15 (12)	101 (8)
Al_2O_3	101 (3)	<0.1	101 (3)

[a]Values are shown as averages of multiple replicates (replicates shown in Supporting Information, Section S5) with the repeatability standard deviation notation in the brackets.

When thermal reduction was not quantitative, Hg^{II} species were not completely reduced but partially desorbed from the plasma trap and deposited on the cooler parts of the tubing prior to reaching the gold trap. Initially, Pt wire as a catalyst showed promising results, but it was evident that with its reuse, the reduction efficiency decreased considerably between runs (1.92, 59.4, 64.8, and 71.5% of unconverted Hg^{II}, listed in consecutive runs: see Supporting Information, Section S5). The decrease in efficiency was attributed to the passivation of Pt. Quartz wool performed better than Pt wire, but Al_2O_3 was selected as the best catalyst, having the highest and most repeatable reduction efficiency (Table 1). Due to the knowledge gained from Hg^{II} reduction experiments, only the Al_2O_3 catalyst was implemented into the final NTP design.

2.2. Production of Hg^{II} Species by Nonthermal Plasma. The method of producing gaseous Hg^{II} species by NTP utilizes the oxidation of Hg^0 in plasma with oxidative gases and He carrier gas. The combination of plasma and oxidative gases seems to be effective in the quantitative production of gaseous Hg^{II} species under ambient air concentrations. The predicted Hg^{II} species that were produced were HgO using O_2 as a reaction gas, $HgCl_2$ using Cl_2 as a reaction gas, and $HgBr_2$ using Br_2 as a reaction gas. Whether those exact species were actually produced is discussed in Section 2.3. The validity of the calibration for Hg^{II} species by NTP oxidation was tested by evaluating the oxidation efficiency for each investigated oxidation reaction. Four to five replicate measurements were performed for each species to assess the oxidation efficiency (all replicates shown in the Supporting Information, Section S5). The corresponding standard uncertainty of the developed calibration was estimated according to the GUM and Eurachem guidelines.[38,39] Standard measurement uncertainties were assessed from all experimental data; repeatability contributed the most to the combined standard uncertainty for all three Hg^{II} species (relative contribution of 65, 81, and 94% for HgO, $HgCl_2$, and $HgBr_2$, respectively). The uncertainty contribution due to ^{197}Hg activity measurement was substantially lower, indicating that the use of ^{197}Hg is justified for the intended use. However, for the proper traceability to NIST 3133 (and as a consequence traceability to System of Units), the effects of blanks will be needed to be taken into account, as they will likely contribute significantly to the analytical signal and measurement uncertainty. This is especially true at very low

https://doi.org/10.1021/acs.analchem.2c00260
Anal. Chem. 2022, 94, 8234−8240

(ambient) Hg^{II} concentrations. The complete standard uncertainty estimation procedure is given in the Supporting Information, Section S6.

Resulting oxidation efficiencies with corresponding expanded standard uncertainty values were 100.5% ± 4.7% (k = 2) for 100 pg of HgO, 96.8% ± 7.3% (k = 2) for 250 pg of $HgCl_2$, and 77.3% ± 9.4% (k = 2) for 250 pg of $HgBr_2$. The provided masses refer to the amount of Hg^0 used for oxidation to Hg^{II}. Similar ambient-level masses of Hg^{II} as used in our work are usually sampled for atmospheric Hg speciation. For example, 125 min sample preconcentration using 8 L min^{-1} airflow of ambient air with 100 pg m^{-3} Hg^{II} concentration gives 100 pg of preconcentrated Hg^{II}.

While the oxidation efficiency values for HgO and $HgCl_2$ indicated almost quantitative oxidation, the oxidation efficiencies of $HgBr_2$ were considerably lower. There are two contrasting effects that might influence this observation. First, the low recoveries of $HgBr_2$ might be due to the electrolytic production of Br_2 gas. When Br_2 is produced from the electrolytic solution, it dissolves immediately, so a large amount of Br_2 must be produced to achieve a sufficiently high vapor pressure of aqueous Br_2. Otherwise, the small amount of Br_2 in the carrier gas seemed insufficient for the complete oxidization of Hg^0 in the NTP. Nevertheless, Br_2 and Cl_2 are highly reactive gases that can oxidize Hg^0 even prior to the NTP part of the setup, resulting in losses due to adsorption of Hg^{II} on walls prior to the NTP section. To reduce losses, the distance between T-split (mixing of $Cl_2(g)/Br_2(g)$ with $Hg^0(g)$) and NTP (Figure 2) had to be minimized. Of the two described effects (insufficient amount of Br_2 in the carrier gas and premature oxidation), we cannot assess which effect is more prevalent.

Due to the aforementioned properties of Cl_2 and Br_2, the highest recoveries and the lowest standard uncertainties were achieved using O_2 as a reaction gas, as it introduces the least complexity into the experimental setup due to its relative inertness and availability. Repeatability could be improved in the future by automating the presented NTP calibration system.

Comparison of the NTP calibration system with other available Hg^{II} calibration systems is difficult due to (i) scarce data on the system accuracy and precision, (ii) data usually available only for high Hg^{II} concentrations (>1 $\mu g\ m^{-3}$ of Hg), and (iii) lack of metrological traceability for the accuracy and precision data. Liquid evaporative calibrators developed by HovaCal, VTT & Optoseven, and Tekran (model 3315) are designed for use with high Hg^{II} concentrations. In our previous work, we evaluated the accuracy of a liquid-evaporative calibrator at near-ambient Hg^{II} concentration levels. The main conclusion was that while at the $\mu g\ m^{-3}$ level, the error ranged from 19 to 4% (depending on the duration of operation time), at the ng m^{-3} level, the error increased to as much as 63%. Additionally, the precision was unsatisfactory due to the time dependence of the calibrator output.[19] Therefore, the only calibration systems that can be compared to the NTP calibration system are those that were evaluated at ambient Hg^{II} concentration levels. As such, Hg^{II} permeation tubes are currently the only calibration system suitable for comparison. The permeation rates, their precision, and accuracy have been determined, but the data depended on measurement systems that can be subject to biases and are not traceable.[14] The design and dimensions of each individual permeation tube affect the permeation rate; consequently, each unit has to be assessed individually. Lyman et al.[18] attempted to establish the traceability of permeation tubes to the mass (and consequently to SI units), but low mass losses and weighing difficulties prevented reliable results.[18] High permeation rates (up to 30 pg s^{-1}) based on the gravimetric method matched the determined Hg concentrations to within 25%, but the agreement was worse for lower permeation rates.[18] The NTP approach for Hg^{II} calibration is accurate (no observed bias when calibration uncertainty is considered) for HgO and $HgCl_2$, while future optimization will be needed for $HgBr_2$ calibration accuracy and precision. Although traceability to SI units was not demonstrated within this paper, future work is planned on achieving SI traceability via NIST SRM 3133.

2.3. TPD-QMS Analysis of Produced Hg^{II} Species. In addition to the evaluation of NTP oxidation efficiency, we attempted to confirm the presence of each species on the plasma trap by indirect TPD-QMS measurement. The results of TPD-QMS measurements are shown in Figure 3. Figure 3a shows the temperature-programmed desorption of Hg^{II} species obtained by NTP oxidation, while Figure 3b shows the results for Hg^{II} species standards.

TPD-QMS peaks for Hg^{II} species loaded by NTP oxidation and Hg^{II} species standards were compared to identify which species were produced. To simplify the discussion, we indexed

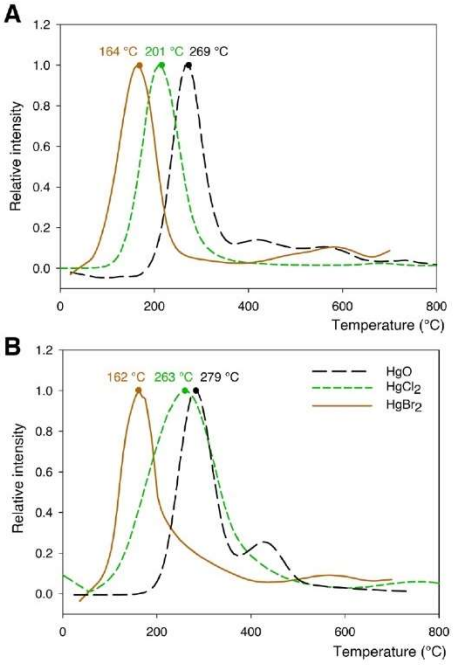

Figure 3. (A) Temperature-programmed desorption for three Hg^{II} species loaded on sorbent traps by NTP oxidation. (B) Results of the temperature-programmed desorption for Hg^{II} species standards. The temperatures indicated above the peaks are the temperatures of the highest signal intensity for each respective peak.

https://doi.org/10.1021/acs.analchem.2c00260
Anal. Chem. 2022, 94, 8234−8240

the temperatures of the highest signal intensity as follows: T_{HgO}, T_{HgCl_2}, and T_{HgBr_2} notations for HgO, $HgCl_2$, and $HgBr_2$, respectively, and "NTP" or "STD" notations for NTP-loaded Hg^{II} species or for Hg^{II} species standards. $T_{HgO,\ NTP}$ (269 °C) and $T_{HgO,\ STD}$ (279 °C) are similar as well as $T_{HgBr_2,\ NTP}$ (164 °C) and $T_{HgBr_2,\ STD}$ (162 °C). $T_{HgCl_2,\ NTP}$ (201 °C) and $T_{HgCl_2,\ STD}$ (263 °C) are different (Figure 3), which can be explained by the wider peaks obtained for Hg^{II} species standards. The wider peaks could originate from the wet deposition method of preparing Hg^{II} species standards (Hg^{II} aqueous phase chemistry), which is not entirely equivalent to the NTP-loaded Hg^{II} species (Hg^{II} gas-phase chemistry). Considerable hydrolysis of $HgCl_2$ in water and species transformation are possible, but those of higher halogenides (bromide and iodide) are less likely due to greater stability of these halogenides (several orders of magnitude lower solubility product constant K_{sp}).[40,41] Second, we compared the values obtained for NTP-loaded Hg^{II} species to the values from the literature. Literature values for temperature desorption of Hg^{II} species differ, mainly due to differences in the matrices to which Hg^{II} is bound. For HgO, the literature values for desorption temperature range from 240 to 310 °C for yellow HgO and from 550 to 600 °C for red HgO.[37,42] The temperature desorption diagram for NTP-loaded HgO agrees well with the literature data for yellow HgO, which serves as additional confirmation that the Hg^{II} produced was really HgO. For matrix-bound $HgCl_2$, the desorption temperature in the literature ranges between 190 and 250 °C,[37] which is similar to our results for NTP-loaded $HgCl_2$. The presence of Hg_2Cl_2 cannot be completely ruled out due to the fact that Hg_2Cl_2 and $HgCl_2$ have very similar desorption temperatures.[43] Nevertheless, desorption of Hg_2Cl_2 usually results in a doublet peak,[44] which is not seen in our results. For $HgBr_2$, there are not many data available for matrix-bound $HgBr_2$ but mostly for pure $HgBr_2$.[43] $HgBr_2$ is desorbed at lower temperatures than $HgCl_2$ and HgO, which is in agreement with our observations.[43] The limitation of our comparison to the literature values and to measured standards is that there is still a possibility that a similar but not yet tested Hg^{II} compound could have a similar temperature desorption range and therefore overlap with our presumably NTP-produced Hg^{II} species. Therefore, we can confirm the presence of presumed species with a high degree of confidence but not with absolute certainty.

3. CONCLUSIONS

Calibration using NTP oxidation of Hg^0 to Hg^{II} has proven to be a suitable way to achieve quantitative production of two gaseous Hg^{II} species: HgO and $HgCl_2$. They were produced with a degree of measurement uncertainty that we consider appropriate for ambient concentration calibration, as ambient Hg^{II} measurements are generally accompanied with higher uncertainty contributions (originating mostly from sampling). Quantitative production of $HgBr_2$ was limited by the high gaseous reactivity or aqueous solubility of Br_2 reaction gas. The presence of each produced Hg^{II} species was indirectly confirmed. Future research will focus on the use of NTP not only for sorbent traps but also for the calibration of denuders and the calibration of field measurements. Automation of the presented calibration could result in lower standard uncertainty due to improved repeatability.

■ ASSOCIATED CONTENT

Supporting Information

The Supporting Information is available free of charge at https://pubs.acs.org/doi/10.1021/acs.analchem.2c00260.

Standard operating procedure (SOP) for the developed calibration method (Section S1); list of chemicals and instruments used in validation work (Tables S1 and S2); calculation of the decay time-corrected peak areas for samples and standards (Equations 1 and 2); calculation of the oxidation or thermal reduction efficiency (Equation 3); electrolytic production of reaction gases Cl_2 and Br_2 (Figure S1); all replicates for the Hg^{II} thermal reduction (Table S3) and production of Hg^{II} species by NTP (Table S4); calculation of the combined standard uncertainty (Equations 4 to 18); and a calculation example for $HgCl_2$ species (Table S5) (PDF)

■ AUTHOR INFORMATION

Corresponding Author

Milena Horvat − *Department of Environmental Sciences, Jožef Stefan Institute, 1000 Ljubljana, Slovenia; Jožef Stefan International Postgraduate School, 1000 Ljubljana, Slovenia*; Email: milena.horvat@ijs.si

Authors

Jan Gačnik − *Department of Environmental Sciences, Jožef Stefan Institute, 1000 Ljubljana, Slovenia; Jožef Stefan International Postgraduate School, 1000 Ljubljana, Slovenia*; orcid.org/0000-0003-4453-4576

Igor Živković − *Department of Environmental Sciences, Jožef Stefan Institute, 1000 Ljubljana, Slovenia*; orcid.org/0000-0003-1774-1203

Sergio Ribeiro Guevara − *Laboratorio de Análisis por Activación Neutrónica, Centro Atómico Bariloche, 8400 Bariloche, Argentina*; orcid.org/0000-0001-7203-7687

Jože Kotnik − *Department of Environmental Sciences, Jožef Stefan Institute, 1000 Ljubljana, Slovenia; Jožef Stefan International Postgraduate School, 1000 Ljubljana, Slovenia*

Sabina Berisha − *Jožef Stefan International Postgraduate School, 1000 Ljubljana, Slovenia*

Sreekanth Vijayakumaran Nair − *Department of Environmental Sciences, Jožef Stefan Institute, 1000 Ljubljana, Slovenia; Jožef Stefan International Postgraduate School, 1000 Ljubljana, Slovenia*

Andrea Jurov − *Department of Gaseous Electronics, Jožef Stefan Institute, 1000 Ljubljana, Slovenia*

Uroš Cvelbar − *Jožef Stefan International Postgraduate School, 1000 Ljubljana, Slovenia; Department of Gaseous Electronics, Jožef Stefan Institute, 1000 Ljubljana, Slovenia*; orcid.org/0000-0002-1957-0789

Complete contact information is available at: https://pubs.acs.org/10.1021/acs.analchem.2c00260

Author Contributions

#J.G. and I.Ž. contributed equally to this work. All authors have given approval to the final version of the manuscript.

Notes

The authors declare no competing financial interest.

https://doi.org/10.1021/acs.analchem.2c00260
Anal. Chem. 2022, 94, 8234−8240

■ ACKNOWLEDGMENTS

This research was financially supported by: project no. 16ENV01 MercOx which has received funding from the EMPIR program co-financed by the Participating States and from the European Union's Horizon 2020 research and innovation program; project no. 689443 Integrated Global Observing Systems for Persistent Pollutants (IGOSP) funded by the European Commission in the framework of program "The European network for observing our changing planet (ERA-PLANET)"; project no. 860497 GMOS-Train which has received funding from the European Union's Horizon 2020 research and innovation program under the Marie Sklodowska-Curie; and Slovenian Research Agency (ARRS), grant numbers P1-0143 and PR-52044. The authors thank the TRIGA reactor staff at the Reactor Infrastructure Centre of the Jožef Stefan Institute for their availability and cooperation.

■ REFERENCES

(1) Driscoll, C. T.; Mason, R. P.; Chan, H. M.; Jacob, D. J.; Pirrone, N. *Environ. Sci. Technol.* **2013**, *47*, 4967−4983.
(2) Lyman, S. N.; Cheng, I.; Gratz, L. E.; Weiss-Penzias, P.; Zhang, L. *Sci. Total Environ.* **2020**, *707*, No. 135575.
(3) Zhang, L.; Wright, L. P.; Blanchard, P. *Atmos. Environ.* **2009**, *43*, 5853−5864.
(4) Deeds, D. A.; Ghoshdastidar, A.; Raofie, F.; Guérette, ÉA.; Tessier, A.; Ariya, P. A. *Anal. Chem.* **2015**, *87*, 5109−5116.
(5) Jones, C. P.; Lyman, S. N.; Jaffe, D. A.; Allen, T.; O'Neil, T. L. *Atmos. Meas. Tech.* **2016**, *9*, 2195−2205.
(6) Ariya, P. A.; Amyot, M.; Dastoor, A.; Deeds, D.; Feinberg, A.; Kos, G.; Poulain, A.; Ryjkov, A.; Semeniuk, K.; Subir, M.; Toyota, K. *Chem. Rev.* **2015**, *115*, 3760−3802.
(7) Lyman, S. N.; Jaffe, D. A.; Gustin, M. S. *Atmos. Chem. Phys.* **2010**, *10*, 8197−8204.
(8) Huang, J.; Gustin, M. S. *Environ. Sci. Technol.* **2015**, *49*, 6102−6108.
(9) Gustin, M. S.; Huang, J.; Miller, M. B.; Peterson, C.; Jaffe, D. A.; Ambrose, J.; Finley, B. D.; Lyman, S. N.; Call, K.; Talbot, R.; Feddersen, D.; Mao, H.; Lindberg, S. E. *Environ. Sci. Technol.* **2013**, *47*, 7295−7306.
(10) Cheng, I.; Zhang, L. *Environ. Sci. Technol.* **2017**, *51*, 855−862.
(11) Huber, M. L.; Laesecke, A.; Friend, D. G. *Ind. Eng. Chem. Res.* **2006**, *45*, 7351−7361.
(12) Brown, R. J. C.; Brown, A. S. *Analyst* **2008**, *133*, 1611−1618.
(13) Jaffe, D. A.; Lyman, S.; Amos, H. M.; Gustin, M. S.; Huang, J.; Selin, N. E.; Levin, L.; Ter Schure, A.; Mason, R. P.; Talbot, R.; Rutter, A.; Finley, B.; Jaeglé, L.; Shah, V.; McClure, C.; Ambrose, J.; Gratz, L.; Lindberg, S.; Weiss-Penzias, P.; Sheu, G. R.; Feddersen, D.; Horvat, M.; Dastoor, A.; Hynes, A. J.; Mao, H.; Sonke, J. E.; Slemr, F.; Fisher, J. A.; Ebinghaus, R.; Zhang, Y.; Edwards, G. *Environ. Sci. Technol.* **2014**, *48*, 7204−7206.
(14) Lyman, S.; Jones, C.; O'Neil, T.; Allen, T.; Miller, M.; Gustin, M. S.; Pierce, A. M.; Luke, W.; Ren, X.; Kelley, P. *Environ. Sci. Technol.* **2016**, *50*, 12921−12927.
(15) McClure, C. D.; Jaffe, D. A.; Edgerton, E. S. *Environ. Sci. Technol.* **2014**, *48*, 11437−11444.
(16) Schmäh, M. Method and Device for Producing a Gas-Vapor Mixture. German Patent DE102007004034B4; 2007.
(17) Saxholm, S.; Rajamäki, T.; Hämäläinen, J.; Hildén, P. *Meas. Sci. Technol.* **2020**, *31*, No. 034001.
(18) Lyman, S. N.; Gratz, L. E.; Dunham-cheatham, S. M.; Gustin, M. S.; Luippold, A. *Environ. Sci. Technol.* **2020**, *54*, 13379−13388.
(19) Gačnik, J.; Živković, I.; Guevara, S. R.; Jaćimović, R.; Kotnik, J.; Horvat, M. *Sensors* **2021**, *21*, 2501.
(20) Quétel, C. R.; Zampella, M.; Brown, R. J. C.; Ent, H.; Horvat, M.; Paredes, E.; Tunc, M. *Anal. Chem.* **2014**, *86*, 7819−7827.
(21) Quétel, C. R.; Zampella, M.; Brown, R. J. C. *TrAC, Trends Anal. Chem.* **2016**, *85*, 81−88.
(22) Srivastava, A.; Hodges, J. T. *Anal. Chem.* **2018**, *90*, 6781−6788.
(23) Srivastava, A.; Long, S. E.; Norris, J. E.; Bryan, C. E.; Carney, J.; Hodges, J. T. *Anal. Chem.* **2021**, *93*, 1050−1058.
(24) Long, S. E.; Kelly, W. R. *Anal. Chem.* **2002**, *74*, 1477−1483.
(25) Koron, N.; Bratkič, A.; Ribeiro Guevara, S.; Vahčič, M.; Horvat, M. *Appl. Radiat. Isot.* **2012**, *70*, 46−50.
(26) Guevara, S. R.; Horvat, M. *Anal. Methods* **2013**, *5*, 1996−2006.
(27) Nehra, V.; Kumar, A.; Dwivedi, H. K. *Int. J. Eng.* **2008**, *2*, 53−68.
(28) Moreau, M.; Orange, N.; Feuilloley, M. G. J. *Biotechnol. Adv.* **2008**, *26*, 610−617.
(29) Chen, Z.; Mannava, D. P.; Mathur, V. K. *Ind. Eng. Chem. Res.* **2006**, *45*, 6050−6055.
(30) Byun, Y.; Ko, K. B.; Cho, M.; Namkung, W.; Shin, D. N.; Lee, J. W.; Koh, D. J.; Kim, K. T. *Chemosphere* **2008**, *72*, 652−658.
(31) Byun, Y.; Koh, D. J.; Shin, D. N. *Chemosphere* **2011**, *83*, 69−75.
(32) Wang, Z. H.; Jiang, S. D.; Zhu, Y. Q.; Zhou, J. S.; Zhou, J. H.; Li, Z. S.; Cen, K. F. *Fuel Process. Technol.* **2010**, *91*, 1395−1400.
(33) An, J.; Shang, K.; Lu, N.; Jiang, Y.; Wang, T.; Li, J.; Wu, Y. *J. Hazard. Mater.* **2014**, *268*, 237−245.
(34) Zhang, J.; Duan, Y.; Zhao, W.; Zhu, C.; Zhou, Q.; Ding, W. *Plasma Chem. Plasma Process.* **2018**, *38*, 573−586.
(35) Gačnik, J.; Živković, I.; Ribeiro Guevara, S.; Jaćimović, R.; Kotnik, J.; De Feo, G.; Dexter, M.; Corns, W.; Horvat, M. *Atmos. Meas. Tech.* **2021**, *14*, 6619−6631.
(36) Akagi, H.; Nishimura, H. Speciation of Mercury in the Environment. In *Advances in Mercury Toxicology*; Suzuki, T.; Imura, N.; Clarkson, T. W., Eds.; Springer: US: Boston, 1991; pp 53−76.
(37) Pavlin, M.; Popović, A.; Jaćimović, R.; Horvat, M. *Open Chem.* **2018**, *16*, 544−555.
(38) BIPM. *Evaluation of Measurement Data - Guide to the Expression of Uncertainty in Measurement*; 2008..
(39) Ellison, S. L. R.; Williams, A. *Quantifying Uncertainty in Analytical Measurements*, 3rd ed.; 2012.
(40) Kozin, L. F.; Hansen, S. C. *Mercury Handbook: Chemistry, Applications and Environmental Impact*; Guminski, C., Ed.; The Royal Society of Chemistry, 2013.
(41) *Handbook of Chemistry and Physics*, 97th ed.; Haynes, W. M., Ed.; CRC Press, 2016.
(42) Sui, Z.; Zhang, Y.; Li, W.; Orndorff, W.; Cao, Y.; Pan, W. P. *J. Therm. Anal. Calorim.* **2015**, *119*, 1611−1618.
(43) Rumayor, M.; Diaz-Somoano, M.; Lopez-Anton, M. A.; Martinez-Tarazona, M. R. *Talanta* **2013**, *114*, 318−322.
(44) Lopez-Anton, M. A.; Yuan, Y.; Perry, R.; Maroto-Valer, M. M. *Fuel* **2010**, *89*, 629−634.

https://doi.org/10.1021/acs.analchem.2c00260
Anal. Chem. 2022, 94, 8234−8240

Supporting information

Calibration Approach for Gaseous Oxidized Mercury Based on Nonthermal Plasma Oxidation of Elemental Mercury

Jan Gačnik[1,2,‡], Igor Živković[1,‡], Sergio Ribeiro Guevara[3], Jože Kotnik[1,2], Sabina Berisha[2], Sreekanth Vijayakumaran Nair[1,2], Andrea Jurov[2,4], Uroš Cvelbar[2,4] and Milena Horvat[1,2,*]

[1]Department of Environmental Sciences, Jožef Stefan Institute, Jamova Cesta 39, 1000 Ljubljana, Slovenia

[2]Jožef Stefan International Postgraduate School, Jamova Cesta 39, 1000 Ljubljana, Slovenia

[3]Laboratorio de Análisis por Activación Neutrónica, Centro Atómico Bariloche, Av. Bustillo km 9.5, 8400 Bariloche, Argentina

[4]Department of Gaseous Electronics, Jožef Stefan Institute, Jamova Cesta 39, 1000 Ljubljana, Slovenia

‡J. G. and I. Ž. contributed equally to this work.

*E-mail: milena.horvat@ijs.si

Table of Contents

S1 - Standard operating procedure (SOP) for gaseous oxidized mercury species calibration by non-thermal plasma (NTP) oxidation of elemental mercury

1. *Foreword and scope of the method*

The calibration method is based on generation of a known amount of gaseous elemental mercury (Hg^0), its quantitative oxidation to gaseous oxidized mercury species (Hg^{II}) by NTP in the presence of reaction gas, Hg^{II} thermal reduction back to Hg^0, and its determination by cold vapor atomic fluorescence spectrometry (CV-AFS). The method is designed to be suitable for calibration of any commercially available atmospheric mercury speciation unit. In the presented SOP, the medium used for Hg^{II} collection is a sorbent trap (in the following sections named "plasma trap"; see Figure 1 of the article's main body for more information). Instead of a sorbent trap, commonly used atmospheric Hg speciation methods often utilize denuders or sorbent membranes. Although these Hg^{II} collection methods can be used for calibration instead of sorbent traps, their compatibility with our calibration was not validated in our work. The instructions provided in this SOP are fit-for-purpose regardless of the method used for Hg^{II} collection and regardless of the method used for mercury detection.

The intended amounts of Hg^{II} species produced using this method for calibration of ambient concentration levels of Hg^{II} are in the order of 50-100 pg. Therefore, ultra-trace analysis protocols have to be applied to prevent contaminations: keeping the laboratory clean, providing appropriate ventilation, and adequately washing glassware, tools, and containers.

2. *Safety precautions*

Follow universal precautions. Wear gloves, a lab coat, and safety glasses whilst handling chemicals. For handling the non-thermal plasma and its power supply unit, the safety rules for working with electrical equipment should be followed: turn off the power supply of the equipment before inspecting it; use only tools/equipment with non-conducting handles; avoid contacting the setup with wet hands and wet materials; do not store highly flammable chemicals near the electrical equipment; call expert electrician if the power supply or instrument keeps causing burn-out of fuses.

3. *Chemicals, materials, and equipment*

3.1 Chemicals and materials

- 65% nitric acid (HNO_3, Suprapur, Merck, Germany)
- 30% hydrochloric acid (HCl, Suprapur, Merck, Germany)
- Potassium permanganate ($KMnO_4$, analytical grade, Merck, Germany)
- Potassium chloride (KCl, Suprapur, Merck, Germany)
- Potassium hydroxide (KOH, analytical grade, Merck, Germany)
- Sodium thiosulfate ($Na_2S_2O_3$, analytical grade, Merck, Germany)
- Potassium bromate ($KBrO_3$, Suprapur, Merck)
- Potassium bromide (KBr, Suprapur, Merck)

- Tin(II) chloride dihydrate ($SnCl_2 \cdot 2H_2O$, analytical grade, Merck, Germany)
- Hydroxylammonium chloride ($NH_2OH \cdot HCl$, analytical grade, Merck, Germany)
- Gold(III) chloride hydrate ($HAuCl_4 \cdot xH_2O$, 99.995% trace metal basis, Merck, Germany)
- NIST SRM 3133: Mercury (Hg) Standard Solution (NIST, USA)
- Aluminum oxide, corundum (Al_2O_3, 0.60–0.85 mm grain size)
- Type I purified water (resistivity 18.2 MΩ cm)
- Quartz wool (Supelco, USA)

3.2 Equipment

- High-voltage high-frequency power generator (Information Unlimited, model Amazing PMV500, or similar)
- Cold vapor atomic fluorescence spectrometer (CV-AFS)

3.3 Preparation of reagents and materials

10% w/v $SnCl_2$ in 10% v/v HCl:

- Weigh accurately 10 g of $SnCl_2$ into a clean glass beaker using a plastic spatula (beaker and spatula are used only for $SnCl_2$).
- Add 10 mL of concentrated HCl directly to the $SnCl_2$ and transfer to a 100-mL volumetric flask. Mix and wait for complete dissolution of $SnCl_2$.
- Add Milli-Q water to the mark (100 mL).
- Purge the $SnCl_2$ solution with Hg-free nitrogen gas for two hours in order to obtain a mercury-free solution.

16% w/v $NH_2OH \cdot HCl$ solution:

- Weight 16 g of $NH_2OH \cdot HCl$ in a suitable glass bottle, add Milli-Q water to a 100-mL mark, and mix well.
- Add 20 µL of $SnCl_2$ solution and purge for 2 hours with Hg-free nitrogen gas.

10% w/v KOH:

- Dissolve 10 g of KOH in Milli-Q water to the final volume of 100 mL.
- Purge the KOH solution with nitrogen for two hours in order to obtain a mercury-free solution.

10% w/v $Na_2S_2O_3$:

- Dissolve 10 g of $Na_2S_2O_3$ in Milli-Q water to the final volume of 100 mL.
- Purge the $Na_2S_2O_3$ solution with nitrogen for two hours in order to obtain a mercury-free solution.

0.5% w/v $KMnO_4$ solution:

- Dissolve 0.5 g of $KMnO_4$ in Milli-Q water to the final volume of 100 mL.

Bromine monochloride (BrCl) oxidizing solution:

- Weigh 15 g of $KBrO_3$ and 11 g of KBr into a clean 1-liter glass bottle.
- Add 200 mL of Milli-Q water.
- Add 800 mL of concentrated HCl. The dilution has to be carried out in a well-ventilated fume hood to prevent exposure to toxic fumes released during dissolution of $KBrO_3$.
- Keep the bottle wrapped with aluminum foil.
- The prepared solution can be kept for an unlimited time if stored in darkness at 5 °C in a tightly closed Teflon or glass bottle.

Gold-coated corundum and gold trap preparation:

- Gold-coated corundum: Dissolve 1 g of $HAuCl_4 \cdot xH_2O$ in 10 mL of Milli-Q water and add 10 g of Al_2O_3. Evaporate the solution in an automatic rotary evaporator under reduced atmospheric pressure and then heat the remaining material at 500 °C for 4 h in an argon atmosphere.
- Gold trap preparation: Insert a small piece of quartz wool at the end of the longer part of the column. Then insert about 2 cm of gold-coated corundum. It is recommended to weigh the gold-coated corundum in order to obtain a better reproducibility between the traps. Insert a larger piece of quartz wool. Precondition the new trap by heating it at least 4 times before use.

Plasma trap preparation: shown in the main body of the article, in Figure 1.

Drying columns preparation: similar as for gold trap preparation, except that the gold-coated corundum is replaced with soda lime.

3.4 Mercury standard solutions (SRM NIST 3133)

Standard stock solution, 99.54 μg g^{-1} of Hg in 5% HNO_3: Important note: record the mass after each volume addition or subtraction step, otherwise the Hg mass concentration cannot be evaluated correctly. Fill a weighed 100-mL glass flask with 5% HNO_3 solution exactly to mark of 100 mL and remove 1 mL of the solution. Gently shake an ampoule of Standard Reference Material 3133, Mercury (Hg) Standard Solution for 2 minutes and open it according to the certificate. Take 1 mL of SRM solution with a pipette directly from the ampoule to the prepared glass flask containing acid solution. By doing so, a solution with an approximate Hg concentration of 99.54 μg g^{-1} is obtained (the exact value depends on the mass weighing). Cap the flask, shake it well and leave it on room temperature for 1 hour before further dilutions.

Intermediate and working standard solutions, 0.9954 μg g^{-1} of Hg in 5% HNO_3 and 0.9954 ng g^{-1} of Hg in 5% HCl: Prepare an intermediate Hg standard solution with the concentration of 0.9954 μg g^{-1} by 100-fold dilution of standard stock solution in the same manner as for standard stock solution. At the end, prepare a working Hg standard solution with the concentration of 0.9954 ng g^{-1} by 1000-fold dilution of the intermediate standard. The last dilution is made with 5% HCl solution instead of a 5% HNO_3 solution. Calculate the exact concentrations of the Hg standard solutions by taking into an account the exact mass of pipetted aliquots.

3.5 Cleaning glassware

Prior to use, thoroughly wash all laboratory glassware following the procedure:

- Allow the glass vessels to soak overnight in 2% Micro-90 detergent solution.
- Rinse the vessels thoroughly, first with tap water, and then with Milli-Q water.
- Rinse with 0.5% $KMnO_4$ solution.
- Rinse with water until the color of the $KMnO_4$ solution is no longer visible.
- Rinse with 2 mL of 16% $NH_2OH \cdot HCl$ solution.
- Rinse three times with Milli-Q water.
- Fill the vessels with 1% HCl solution and store in mercury-free storage facilities.
- Vessels should be emptied just before use for sample processing and allowed to dry at 60 °C.

4. NTP calibration protocol

As previously stated, the calibration method is comprised of three main steps: i) Hg^0 generation, ii) NTP oxidation of Hg^0 to Hg^{II} species in the presence of a reaction gas, and iii) thermal reduction of Hg^{II} species to Hg^0 with subsequent CV-AFS analysis. The second step has three different setup variations depending on the used reaction gas (O_2, Cl_2 or Br_2).

4.1 Hg^0 generation

Similar setup is used as in Figure 2a of the manuscript's main body.

- Provide a clean 250-mL glass impinger ("bubbler") and add 100 mL of Milli-Q water and 3 mL of 10% w/v $SnCl_2$ in 10% v/v HCl.
- Connect a drying column (soda lime trap) to the impinger gas exit and a gold trap downstream of the drying column.
- Add 100 pg of Hg from the working Hg standard solution. In the case of concentrations listed in the section 3.4, this means that 100.5 µL of working standard solution (Hg concentration of 0.9954 ng g^{-1}) needs to be pipetted directly to the impinger.
- As soon as the Hg standard is added, quickly close the impinger and connect it to a N_2 flow of 1 L min^{-1} for 10 minutes to purge the Hg^0 to the gold trap. Note: lower total volume of the solution in the impinger can be used together with a lower N_2 flow and shorter purging time since these parameters mostly depend on the shape, size, and design of the impinger.
- After 10 minutes, remove the Hg-loaded gold trap from the impinger and use it for the second step.

4.2 NTP oxidation of Hg^0 to Hg^{II} species

Similar setup is used as in Figure 2a of the manuscript's main body. Three different Hg^{II} species can be produced via NTP oxidation: HgO with O_2 reaction gas, $HgCl_2$ with Cl_2 reaction gas, and $HgBr_2$ with Br_2 reaction gas. Therefore, we can have three setups that marginally differ from each other.

- Assemble the following parts of the setup (similar as in Figure 2a in the manuscript's main body, going downstream in consecutive order): Hg-loaded gold trap, T-split for the introduction of reaction gas, plasma trap, and impinger with solution for reaction gas reduction. The reaction gas is obtained from i) O_2 gas cylinder for O_2 reaction gas and ii) electrolytic reaction for Cl_2 and Br_2 reaction gases (electrolysis described in section S4 of the Supplementary Information). The solution for reaction gas reduction is 50 mL of 10% w/v KOH for Cl_2 reaction gas and 50 mL of 10% w/v $Na_2S_2O_3$ for Br_2 reaction gas. In the case of O_2 reaction gas, the reduction of the reaction gas is not needed. The final flow of the gas mixture (He + reaction gas) should be 370 mL min^{-1}, where He represents >99% of the gas mixture and reaction gas represents <1% of the gas mixture.

- IMPORTANT NOTE: Cl_2 and Br_2 reaction gases are strong oxidants on their own (even without NTP). Therefore, it is important to release them into the system only when every part of the setup is gas-tight. Always connect the reaction gas the last (to avoid unnecessary reactions), after the whole setup is already on the flow of He gas.

- When the setup is assembled and under gas-tight He flow, connect the copper electrodes as shown on Figure 2a in the main text of the article, turn on the plasma driver and set it to these parameters: power applied to the electrodes of 180 μW, radiofrequency of 20 kHz, effective voltage of 345 V.

- After plasma is homogeneous, release the reaction gas flow and after approximately 10 seconds start heating the gold trap (e.g., using a heating coil) to 400 °C to release the Hg^0 from the trap.

- After heating is finished, wait for 60 s to ensure complete release of Hg^0 and then close the reaction gas flow and turn off plasma by turning off the plasma driver.

- After the reaction gas flow is closed and plasma driver is turned off, the setup can be safely disassembled. The produced Hg^{II} that is needed for further calibration is trapped on the plasma trap.

4.3 Thermal reduction of Hg^{II} species to Hg^0 and subsequent CV-AFS analysis

Similar setup is used as in Figure 2b of the manuscript's main body.

- Connect the plasma trap that is loaded with Hg^{II} species to a gold trap downstream.

- Connect both traps to the He flow of 370 mL min^{-1}.

- Heat the whole plasma trap (both KCl crystal part and Al_2O_3 catalyst) to >600 °C. The temperature should be achieved as fast as possible to avoid desorption of Hg^{II} and its re-deposition on cold spots of the system. For compete thermal reduction of Hg^{II} to Hg^0 (without Hg^{II} desorption), the plasma trap should be heated to >600 °C in under 20 s.

- After the heating is completed, wait for 60 seconds to ensure complete downstream transport of Hg^0 to the gold trap.

- The gold trap is now ready for the determination of mercury by double amalgamation CV-AFS measurement.[1]

S2 - Chemicals and instruments used in the validation work

Table S1. Chemicals used in the validation work.

Description of chemicals	Purity / type	Producer
65 % nitric acid (HNO_3)	For analysis	Supelco, Darmstadt, Germany
30 % hydrochloric acid (HCl)	Suprapur	Merck, Darmstadt, Germany
Tin(II) chloride dihydrate ($SnCl_2{\cdot}2H_2O$)	For analysis, max. 0.000001 % Hg	Merck, Darmstadt, Germany
Gold(III) chloride hydrate ($HAuCl_4{\cdot}xH_2O$)	99.995 % trace metal basis	Merck, Darmstadt, Germany
Potassium chloride (KCl) salt	Suprapur	Merck, Darmstadt, Germany
Mercury(II) oxide-yellow (HgO)	99.5 %	May & Baker, Essex, United Kingdom
Mercury(II) chloride ($HgCl_2$)	99.998 %	Merck, Darmstadt, Germany
Mercury(II) bromide ($HgBr_2$)	99.0 %	Merck, Darmstadt, Germany
NIST SRM 3133: Mercury (Hg) Standard Solution	9.954 mg g^{-1} ± 0.053 mg g^{-1}	NIST, Gaithersburg, MD, USA
^{196}Hg enriched elemental Hg	51.58 % ^{196}Hg	Isoflex, San Francisco, CA, USA
Type I purified water	Electrical resistivity 18.2 MΩ cm	Merck, Darmstadt, Germany

Table S2. Instruments used in the validation work.

Description of instruments	Model	Producer
High-voltage high-frequency power generator	Amazing PMV500	Information Unlimited, Amherst, NH, USA
High-voltage probe	Tektronix P6105A	Tektronix Inc., Beaverton, OR, USA
Electrical current monitor	Pearson 2877	Pearson Electronics Inc., Palo Alto, CA, USA
Oscilloscope	Picoscope 3204d	Pico Technology Ltd., Cambridgeshire, UK
High-purity germanium (HPGe) coaxial-type detector	Model 7229P	Canberra Industries Inc., Meriden, CT, USA
High-purity germanium (HPGe) well-type detector	Model GCW6023/S	Canberra Industries Inc., Meriden, CT, USA
Cold vapor atomic absorption spectrometer	Model Hg-201 Semi-Automated Mercury Analyzer	Sanso Seisakusho Co., Ltd., Tokyo, Japan
Quadrupole mass spectrometer (QMS)	Model QMS 700	Pfeiffer Vacuum Ltd., Asslar, Germany

S3 - Calculation of the decay time-corrected peak areas for samples and standards and the calculation of oxidation or thermal reduction efficiency

The peak area of the sample and standard activity had to be corrected for the decay since the start of irradiation. From the corrected peak areas for samples and standards, the oxidation or thermal reduction efficiencies were calculated as shown in the following paragraphs.

Eq. (1) was applied for calculation of both $A_{0,\,s}$ (sample peak area at reference time) and $A_{0,\,std}$ (standard peak area at reference time). If we insert the $A_{0,\,s}$ and $A_{0,\,std}$ values from Eq. (1) into the Eq. (2) (used for oxidation or thermal reduction efficiency calculation), we obtain Eq. (3).[2]

$$A_{0,i} = \frac{\mathrm{A}_i \cdot \frac{\ln 2}{t_{1/2}}}{e^{-\left(\frac{t_{passed}\cdot \ln 2}{t_{1/2}}\right)} \cdot \left[1 - e^{-\left(\frac{t_{measurement}\cdot \ln 2}{t_{1/2}}\right)}\right]} \tag{1}$$

where *i* is either sample (s) or standard (std).

$$\eta = \frac{A_{0,s}}{A_{0,std.}} \cdot 100 \cdot F_{dil} \cdot F_{rep} \tag{2}$$

$$\eta = \frac{A_s \cdot e^{-\left(\frac{t_{passed,std}\cdot \ln 2}{t_{1/2}}\right)} \cdot \left[1 - e^{-\left(\frac{t_{measurement,std}\cdot \ln 2}{t_{1/2}}\right)}\right]}{A_{std} \cdot e^{-\left(\frac{t_{passed,s}\cdot \ln 2}{t_{1/2}}\right)} \cdot \left[1 - e^{-\left(\frac{t_{measurement,s}\cdot \ln 2}{t_{1/2}}\right)}\right]} \cdot 100 \cdot F_{dil} \cdot F_{rep} \tag{3}$$

Where:
$A_{0,\,s}$ is the sample peak area at reference time t=0,
$A_{0,\,std}$ is the standard peak area at reference time t=0,
A_s is the sample peak area at the time of measurement,
A_{std} is the standard peak area at the time of measurement,
$t_{1/2}$ is the half-life of ^{197}Hg [s],
$t_{passed,\,s}$ is the time passed since reference time t=0 till the start of the sample measurement [s],
$t_{measurement,\,s}$ is the time passed during the sample measurement [s],
η is the oxidation or thermal reduction efficiency [%],
F_{dil} is the dilution factor,
F_{rep} is the repeatability factor (value of 1).

S4 - Electrolytic production of reaction gases Cl_2 and Br_2

Since Cl_2 and Br_2 are notoriously difficult to handle, they were produced in the laboratory just for the needs of our experiments. We used electrolysis of 1 M NaCl solution to produce Cl_2 and electrolysis of 1 M KBr solution to produce Br_2. 4.5 V battery was used as a power source for electrolysis. NaCl infused agar gel was used as a salt bridge to provide a closed electric circuit. The experimental setup for electrolytic production of Cl_2 and Br_2 is shown in Figure S1.

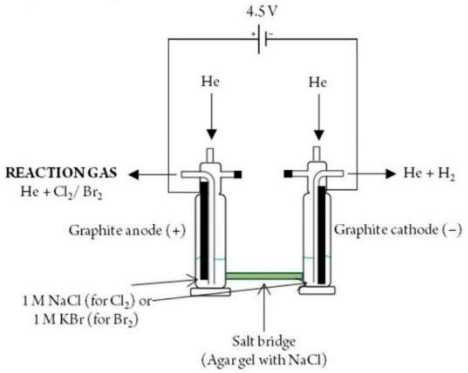

Figure S1. Experimental setup for electrolytic production of reaction gases Cl_2 and Br_2.

As Cl_2 and Br_2 are both water-soluble, the impinger solution containing the anode was always purged with He. This increased the amount of Cl_2 and Br_2 in the gas stream. As Br_2 immediately dissolves in the solution, it is not released into the gas stream until enough Br_2 is produced and its vapor pressure is sufficiently high.

S5 - All replicates for the Hg^{II} thermal reduction and production of Hg^{II} species by NTP.

Table S3. Hg^{II} to Hg^{0} thermal conversion, Hg^{II} loaded by spike, all replicates.

Catalyst used	Hg^{0}, thermal reduction efficiency [%]	Unconverted Hg^{II} [%]	Mass balance [%]
No catalyst	106	22.5	129
	69.1	28.6	97.7
Au-coated silica	34.5	65.5	100
	40.2	56.5	96.7
	39.0	61.0	100
Pt wire	80.2	1.92	82.1
	28.9	59.4	88.3
	26.5	64.8	91.3
	20.6	71.5	92.1
Quartz wool	98.0	5.33	103
	96.2	11.6	108
	64.7	27.8	92.5
Al_2O_3	106	<0.1	106
	102	<0.1	102
	97.4	<0.1	97.4
	98.6	<0.1	98.6
	99.1	<0.1	99.1

Table S4. Production of Hg^{II} species by NTP, all replicates.

Species used	Mass used [pg]	Unconverted Hg^{0} [%]	Hg^{II} on plasma trap, oxidation efficiency [%]
HgO	100	1.19	97.6
		2.22	101
		0.47	100
		2.26	102
		2.17	102
$HgCl_2$	250	2.30	93.2
		1.57	93.2
		1.60	99.7
		1.87	98.4
		3.71	99.3
$HgBr_2$	250	<0.1	79.3
		3.03	79.0
		1.91	68.8
		2.96	82.2

S6 - Calculation of the combined standard uncertainty for the proposed Hg^{II} species calibration

The uncertainty of the developed calibration was estimated according to the GUM and Eurachem guidelines.[3,4] The model used for uncertainty evaluation was shown in Eq. (3). To make the model clearer, we substituted the exponential terms:

$$EF_{p,std} = e^{-\left(\frac{t_{passed,std}\cdot \ln 2}{t_{1/2}}\right)} \quad (4)$$

$$EF_{p,s} = e^{-\left(\frac{t_{passed,s}\cdot \ln 2}{t_{1/2}}\right)} \quad (5)$$

$$EF_{m,std} = e^{-\left(\frac{t_{measurement,std}\cdot \ln 2}{t_{1/2}}\right)} \quad (6)$$

$$EF_{m,s} = e^{-\left(\frac{t_{measurement,s}\cdot \ln 2}{t_{1/2}}\right)} \quad (7)$$

This way, the model can be re-written as:

$$\eta = \frac{A_s \cdot EF_{p,std} \cdot \left[1 - EF_{m,std}\right]}{A_{std} \cdot EF_{p,s} \cdot \left[1 - EF_{m,s}\right]} \cdot 100 \cdot F_{dil} \cdot F_{rep} \quad (8)$$

The equations for the standard uncertainty of the exponential terms (e.g. $EF_{p,std}$) are as follows:

$$u\left(EF_{p,std}\right) = \frac{\partial\, EF_{p,std}}{\partial\, t_{1/2}} \cdot u\left(t_{1/2}\right) = EF_{p,std} \cdot \frac{ln2 \cdot t_{passed,std}}{\left(t_{1/2}\right)^2} \cdot u(t_{1/2}) \quad (9)$$

$$u\left(EF_{p,s}\right) = EF_{p,s} \cdot \frac{ln2 \cdot t_{passed,s}}{\left(t_{1/2}\right)^2} \cdot u(t_{1/2}) \quad (10)$$

$$u\left(EF_{m,std}\right) = EF_{m,std} \cdot \frac{ln2}{t_{1/2}} \cdot u(t_{measurement,std}) \quad (11)$$

$$u\left(EF_{m,s}\right) = EF_{m,s} \cdot \frac{ln2}{t_{1/2}} \cdot u(t_{measurement,s}) \quad (12)$$

Note that we assumed constant $t_{passed,\ std}$ and $t_{passed,\ s}$ to obtain Eq. (9) and Eq. (10) and constant $t_{1/2}$ to obtain Eq. (11) and Eq. (12). This assumption was made because in Eq. (9) and Eq. (10), the relative standard uncertainties of $t_{passed,\ std}$ and $t_{passed,\ s}$ were negligible in comparison to the relative standard uncertainty of $t_{1/2}$ (three orders of magnitude smaller relative standard uncertainties for $t_{passed,\ std}$ and $t_{passed,\ s}$ than for $t_{1/2}$). Similar assumption was made for Eq. (11) and Eq. (12); in this case, the relative standard uncertainty of $t_{1/2}$ was negligible in comparison to the relative standard uncertainty of $t_{measurement,\ std}$ and $t_{measurement,\ s}$.

The equation for obtaining standard uncertainties for A_s and A_{std} is calculated according to Poisson distribution with some adjustments due to background correction for the peak areas. The exact equation used for calculation is provided by the Genie 2000 gamma analysis software tool and is calculated automatically by the software, using Eq. (13).[5] Since ^{197}Hg has two doublet peaks in the activity measurement spectrum, the equation can be applied for both peaks, giving us two uncertainties u(A_1) and u(A_2). The standard uncertainty of the combined peaks (no overlapping of the peaks for our case) is calculated using Eq. (14).

$$u(A_i) = \sqrt{A_i + B_i \cdot \left(\frac{W_{p,i}}{W_{b,i}}\right)^2} \quad ; i = 1,2 \tag{13}$$

$$u(A) = \frac{1}{\sqrt{u(A_1)^2 + u(A_2)^2}} \quad ; A = A_s \text{ or } A_{std} \tag{14}$$

Where:
A_i is the sample peak area for the observed peak,
B_i is the background peak area for the observed peak,
$W_{p,i}$ is the spectral width of the sample peak region for the observed peak,
$W_{b,i}$ is the spectral width of the background peak region for the observed peak.

The last uncertainty components are present in F_{dil} and F_{rep}. u(F_{dil}) originates from two pipetting steps, one for the standard (5 mL pipette, u(V_{std})) and one for the sample (1 mL pipette, u(V_s)). Both u(V_{std}) and u(V_s) are calculated from uncertainty due to temperature influences (V_T) and uncertainty due to repeatability (V_{rep}); 10 replicate measurements) with Eq. (15). By combining both pipetting uncertainties, u(F_{dil}) is calculated with Eq. (16). F_{rep} value equals 1, but has to be included due to the components of the measurement procedure that influence the repeatability.

$$\frac{u(V_i)}{V_i} = \sqrt{\left(\frac{u(V_T)}{V_T}\right)^2 + \left(\frac{u(V_{i,rep})}{V_{i,rep}}\right)^2} \tag{15}$$

$$\frac{u(F_{dil})}{F_{dil}} = \sqrt{\sum_i \left(\frac{u(V_i)}{V_i}\right)^2} \tag{16}$$

where i is either sample (s) or standard (std).

u(F_{rep}) is the repeatability standard uncertainty and is calculated from the standard deviation of replicate oxidation efficiency measurements.

All listed uncertainty components are then used in calculation of combined standard measurement uncertainty by the law of uncertainty propagation. Combined standard measurement uncertainty is calculated as follows:

$$u_c(\eta) = \eta \cdot \sqrt{\begin{array}{l}\left(\frac{u(A_s)}{A_s}\right)^2 + \left(\frac{u(A_{std})}{A_{std}}\right)^2 + \left(\frac{u(EF_{p,s})}{EF_{p,s}}\right)^2 + \left(\frac{u(EF_{p,std})}{EF_{p,std}}\right)^2 \\ + \left(\frac{u(EF_{m,s})}{EF_{m,s}}\right)^2 + \left(\frac{u(EF_{m,std})}{EF_{m,std}}\right)^2 + \left(\frac{u(F_{dil})}{F_{dil}}\right)^2 + \left(\frac{u(F_{rep})}{F_{rep}}\right)^2\end{array}} \tag{17}$$

The expanded standard uncertainty is obtained by multiplication of the combined standard measurement uncertainty with a coverage factor, k (k=2) with Eq. (18).

$$U = u_c(\eta) \cdot k \tag{18}$$

Table S5. Example: calculation of the combined standard measurement uncertainty for $HgCl_2$ species calibration

Parameter, c	Value	Assumed distribution	Standard uncertainty, u(c)	Comment
$t_{passed,\ s}$	714166 s	rectangular	/	Assumed negligible
$t_{passed,\ std}$	700920 s	rectangular	/	
$t_{measurement,\ s}$	150 s	rectangular	0.029 s	Standard uncertainty value used only for the calculation of $u(EF_i)$
$t_{measurement,\ std}$	150 s	rectangular	0.029 s	
$t_{1/2}$	230904 s	rectangular	404 s	
A_s	2020	Poisson	23.8	Parameters and their standard uncertainties that were used in calculation of combined standard uncertainty using the simplified model in Eq. (8)
A_{std}	2144	Poisson	20.1	
$EF_{p,\ std}$	0.122	rectangular	4.49E-04	
$EF_{p,\ s}$	0.117	rectangular	4.40E-04	
$EF_{m,\ std}$	0.9995	rectangular	6.04E-06	
$EF_{m,\ s}$	0.9995	rectangular	4.95E-05	
F_{dil}	1	Gaussian	0.004	
F_{rep}	1	Gaussian	0.034	

	Relative standard uncertainty u(c, r)	$u^2(c, r)$	Relative contribution	Combined standard uncertainty	Expanded standard uncertainty, k=2
A_s	1.18E-02	1.39E-04	9.78%	0.036	0.073
A_{std}	9.36E-03	8.76E-05	6.18%		
$EF_{p,\ std}$	3.68E-03	1.36E-05	0.96%		
$EF_{p,\ s}$	3.75E-03	1.41E-05	0.99%		
$EF_{m,\ std}$	6.04E-06	3.65E-11	0.00%		
$EF_{m,\ s}$	4.95E-05	2.45E-09	0.00%		
F_{dil}	4.48E-03	2.01E-05	1.42%		
F_{rep}	3.38E-02	1.14E-03	80.68%		
$\eta = 0.97 \pm 0.07$ (k=2)					

Expanded standard uncertainty for the calibration of gaseous $HgCl_2$ by NTP oxidation is therefore 0.07 (k=2). Similar as for gaseous $HgCl_2$, we applied the above calculation for the uncertainty evaluation for gaseous HgO and gaseous $HgBr_2$. The expanded standard uncertainties amounted to 0.05 (k=2) for HgO and 0.09 (k=2) for $HgBr_2$.

References

(1) U.S. Environmental Protection Agency. EPA Method 1631, Revision E: Mercury in Water by Oxidation, Purge and Trap, and Cold Vapor Atomic Fluorescence. US Environmental Protection Agency 2002, p 38.
(2) Ribeiro Guevara, S.; Horvat, M. Stability and Behaviour of Low Level Spiked Inorganic Mercury in Natural Water Samples. *Anal. Methods* **2013**, 5 (8), 1996–2006. https://doi.org/10.1039/c3ay26496c.
(3) BIPM. *Evaluation of Measurement Data - Guide to the Expression of Uncertainty in Measurement*; 2008.
(4) Ellison, S. L. R.; Williams, A. Quantifying Uncertainty in Analytical Measurements, 3rd ed.; 2012.
(5) Zahn, G. S.; Genezini, F. A.; Moralles, M. Evaluation of Peak-Fitting Software for Gamma Spectrum Analysis. In *International Nuclear Atlantic Conference - INAC 2009*; Barros, R., Ed.; Rio de Janeiro, Brazil, 2011; pp 1083–1204.

Chapter 3

Conclusions

This dissertation focused on the metrology of atmospheric mercury species, specifically the sampling and calibration methods that are used for atmospheric Hg speciation. Such sampling and calibration methods already exist but are either i) limited in potential applications, ii) source of bias, iii) highly uncertain, or iv) not validated. As a consequence, results obtained from global atmospheric Hg measurements are often not comparable and metrologically traceable, which hinders interpretations and global mercury models. Therefore, we first evaluated three different GEM calibration approaches (Manuscript 1, Section 0) and a GOM calibration unit (Manuscript 2, Section 3.2). We then tested GOM sampling methods that are conventionally used for elevated flue gas GOM concentrations for potential use at ambient concentrations (Manuscript 3, Section 3.3). At the end, we used nonthermal plasma for oxidation of Hg^0 to Hg^{II} species. NTP oxidation of Hg^0 has previously been used for the removal of Hg from flue gas, while we applied it for GOM calibration approach (Manuscript 4, Section 0). The conclusions drawn from the mentioned manuscripts and their supporting materials are pointed out below and follow the hypotheses of the dissertation.

In most of our experiments, we used the ^{197}Hg radiotracer as a validation tool for the calibration and sampling methods for GOM. Accuracy and precision tests were done for a GOM evaporative calibrator and sorbent traps materials for GOM sampling - all performed with the ^{197}Hg radiotracer. The radiotracer enabled experiments at ambient or near-ambient concentration levels due to its selectivity and specificity, which confirmed our hypothesis. A major advantage over validation using isotope dilution ICP-MS is the absence of blanks, which often hinder the validation of atmospheric mercury speciation at low concentration levels. These favourable characteristics of the ^{197}Hg radiotracer were also used for validation and proof-of-concept in the development of a novel calibration approach for GOM using NTP oxidation.

In the comparison of different approaches for GEM calibration, we compared three GEM calibrations: VSL primary gas standard (SI traceable), JSI calibration via NIST SRM 3133 (SI traceable), and bell-jar calibration (traceable to the empirical equation). Their output was captured with two different sorbent trap materials: activated carbon and gold sorbents. The primary gas standard was used as a reference for the other two calibrations since it was previously well characterized. While the primary gas standard and the NIST SRM 3133 gave comparable results, the results of bell-jar calibration were statistically different. All sorbent materials for capturing the output of the calibrations gave comparable and consistent results. Ours has shown that sorbent traps can be effectively used as transfer standards for field calibration of measurement instrumentation. We observed agreement between the two SI traceable calibrations (VSL and JSI calibration) and disagreement between the SI traceable calibration and the bell-jar calibration. These results indicated

that the establishment of SI traceability for atmospheric Hg measurements is crucial for comparable measurement results.

Evaluation of the specificity and stability of sorbent trap materials and impinging solutions for GOM sampling showed that sampling conditions influence the behaviour of tested methods. We found that the losses of Hg^{II} during sampling with KCl sorbent materials are concentration-dependent. Low Hg^{II} concentrations resulted in higher relative losses than high Hg^{II} concentrations during exposures to airflow, indicating that findings from experiments that use high Hg^{II} concentrations cannot be generalized to all concentration levels. The specificity of the sorbent trap materials was decreased if the material was not fresh but previously reused. KCl sorbent materials were found to be feasible for ambient GOM sampling, since the specificity and stability of KCl sorbent materials were generally good.

The KCl impinging solution retained Hg^{II} well since we observed no Hg^{II} losses during simulated sampling conditions. On the other hand, the specificity was not satisfactory due to the solubility and oxidation of Hg^0 in the impinging solution, resulting in a large GOM overestimation bias. Theoretical calculations showed that the extent of the bias depended on the composition of atmospheric mercury (the ratio of GEM to GOM): the bias correlated positively with the relative GEM concentration. Due to the large GOM overestimation, KCl impinging solutions have proven unsuitable for ambient GOM sampling. Overall, we confirmed the hypothesis that losses and interconversions of Hg species during atmospheric sampling are largely dependent on sampling and atmospheric conditions. The results showed that different sampling methods have their own advantages and drawbacks; the use of an appropriate sampling method should be evaluated on a case-by-case basis.

Validation experiments for a GOM calibrator based on dynamic gas evaporation were conducted to assess the potential for the use of evaporative calibrators at ambient GOM concentrations. Previous work showed promising results and demonstrated accurate and precise outputs of the calibrator, but it was only done for high flue gas GOM concentrations. Our experiments on calibrator accuracy, stability, and precision have shown that all of these measures of calibrator behaviour decrease when going to near-ambient GOM concentration levels. We attributed this occurrence to the adsorption of Hg^{II} species on Teflon tubing, which was confirmed both experimentally (acid washing solutions for tubing) and theoretically (calculation of ΔH_{ads} by Langmuir isotherm). Efforts were made to reduce adsorption, but the results were not improved. We concluded that the tested evaporative calibrator is fit for the purpose of calibrations at elevated GOM concentrations, while this is not the case for ambient GOM concentrations – confirming our hypothesis. Since alternatives to such calibration at ambient concentrations also commonly succumb to problems with adsorption and instability, this pointed toward the need for the development of new calibration methods.

The knowledge gathered from the validation work for GOM analytical infrastructure indicated the need to develop new sampling and calibration methods focused on ambient concentration levels. Therefore, we developed a calibration approach for ambient GOM calibration that generates HgO, $HgCl_2$, and $HgBr_2$. The approach consisted of the generation of a known quantity of Hg^0, the quantitative oxidation of Hg^0 to Hg^{II} by nonthermal plasma in the presence of reaction gas, and the thermal reduction of Hg^{II} to Hg^0. Quantitative oxidation and thermal reduction were validated for HgO and $HgCl_2$, while further optimization of the setup is needed for $HgBr_2$. The presence of each species was confirmed by qualitative TPD-QMS analysis.

We used ^{197}Hg radiotracer in the development of the NTP calibration approach. Though the radiotracer enabled all of the validation work at ambient concentration levels, it is not an integral part of the calibration. For real-time calibration, the use of non-radioactive ("normal") mercury is intended. Instead of the radiotracer, mercury in the form of NIST

SRM 3133 could be used, which could provide SI traceability of the developed calibration. As the accuracy was high and the measurement uncertainty was suitable for ambient GOM calibration, this served to confirm our hypothesis that NTP calibration approach could provide SI traceable GOM calibration in the future. However, potential blank issues could prevent SI traceability, and further experimental validation is needed.

The traceable generation of HgO, $HgCl_2$, and $HgBr_2$ with nonthermal plasma oxidation of Hg^0 could open new possibilities for stable isotope measurements. We hypothesized that nonthermal plasma calibration is a suitable calibration method for Hg stable isotope measurements of Hg and its species in the atmosphere. Hg^{II} species can be generated by NTP from NIST SRM 3133. Since NIST SRM 3133 is also used as a standard for the stable isotope composition of Hg, the NTP calibration could serve as a standard for stable isotope measurements of Hg^{II} species. This confirms our hypothesis only in theory, but additional work is planned to confirm it experimentally as well. The same hypothesis was rejected for evaporative calibrators, as low accuracy and precision prevent their application for stable isotope calibration.

References

Ahn, M. C., Yi, S. M., Holsen, T. M., & Han, Y. J. (2011). Mercury wet deposition in rural Korea: Concentrations and fluxes. *Journal of Environmental Monitoring*, *13*(10), 2748–2754. https://doi.org/10.1039/c1em10014a

Amos, H. M., Jacob, D. J., Holmes, C. D., Fisher, J. A., Wang, Q., Yantosca, R. M., Corbitt, E. S., Galarneau, E., Rutter, A. P., Gustin, M. S., Steffen, A., Schauer, J. J., Graydon, J. A., St Louis, V. L., Talbot, R. W., Edgerton, E. S., Zhang, Y., & Sunderland, E. M. (2012). Gas-particle partitioning of atmospheric Hg(II) and its effect on global mercury deposition. *Atmospheric Chemistry and Physics*, *12*(1), 591–603. https://doi.org/10.5194/acp-12-591-2012

Amos, Helen M., Jacob, D. J., Streets, D. G., & Sunderland, E. M. (2013). Legacy impacts of all-time anthropogenic emissions on the global mercury cycle. *Global Biogeochemical Cycles*, *27*(2), 410–421. https://doi.org/10.1002/gbc.20040

Amouroux, D., Wasserman, J. C., Tessier, E., & Donard, O. F. X. (1999). Elemental mercury in the atmosphere of a tropical Amazonian forest (French Guiana). *Environmental Science and Technology*, *33*(17), 3044–3048. https://doi.org/10.1021/es990119b

Ariya, P. A., Amyot, M., Dastoor, A., Deeds, D., Feinberg, A., Kos, G., Poulain, A., Ryjkov, A., Semeniuk, K., Subir, M., & Toyota, K. (2015a). Mercury Physicochemical and Biogeochemical Transformation in the Atmosphere and at Atmospheric Interfaces: A Review and Future Directions. *Chemical Reviews*, *115*(10), 3760–3802. https://doi.org/10.1021/cr500667e

Ariya, P. A., Amyot, M., Dastoor, A., Deeds, D., Feinberg, A., Kos, G., Poulain, A., Ryjkov, A., Semeniuk, K., Subir, M., & Toyota, K. (2015b). Mercury Physicochemical and Biogeochemical Transformation in the Atmosphere and at Atmospheric Interfaces: A Review and Future Directions. *Chemical Reviews*, *115*(10), 3760–3802. https://doi.org/10.1021/cr500667e

ASTM International. (2008). *ASTM D6784-16, Standard Test Method for Elemental, Oxidized, Particle-Bound and Total Mercury in Flue Gas Generated from Coal-Fired Stationary Sources (Ontario Hydro Method)*. ASTM International. www.astm.org

Bash, J. O., Carlton, A. G., Hutzell, W. T., & Bullock, O. R. (2014). Regional air quality model application of the aqueous-phase photo reduction of atmospheric oxidized mercury by dicarboxylic acids. *Atmosphere*, *5*(1), 1–15. https://doi.org/10.3390/atmos5010001

Bieser, J., Slemr, F., Ambrose, J., Brenninkmeijer, C., Brooks, S., Dastoor, A., Desimone, F., Ebinghaus, R., Gencarelli, C. N., Geyer, B., Gratz, L. E., Hedgecock, I. M., Jaffe,

D., Kelley, P., Lin, C. J., Jaegle, L., Matthias, V., Ryjkov, A., Selin, N. E., … Pirrone, N. (2017). Multi-model study of mercury dispersion in the atmosphere: Vertical and interhemispheric distribution of mercury species. *Atmospheric Chemistry and Physics*, *17*(11), 6925–6955. https://doi.org/10.5194/acp-17-6925-2017

Britanica, T. editors of encyclopaedia. (1998). *heterogeneous reaction*. Encyclopedia Britannica. https://www.britannica.com/science/heterogeneous-reaction

Brown, A. S., Brown, R. J. C., Corns, W. T., & Stockwell, P. B. (2008). Establishing SI traceability for measurements of mercury vapour. *Analyst*, *133*(7), 946–953. https://doi.org/10.1039/b803724h

Brown, R. J. C., & Brown, A. S. (2008). Accurate calibration of mercury vapour measurements. *Analyst*, *133*(11), 1611–1618. https://doi.org/10.1039/b806860g

Brunke, E. G., Walters, C., Mkololo, T., Martin, L., Labuschagne, C., Silwana, B., Slemr, F., Weigelt, A., Ebinghaus, R., & Somerset, V. (2016). Mercury in the atmosphere and in rainwater at Cape Point, South Africa. *Atmospheric Environment*, *125*, 24–32. https://doi.org/10.1016/j.atmosenv.2015.10.059

Bu, X., Zhang, H., Lv, G., Lin, H., Chen, L., Yin, X., Shen, G., Yuan, W., Zhang, W., Wang, X., & Tong, Y. (2018). Comparison of Reactive Gaseous Mercury Collection by Different Sampling Methods in a Laboratory Test and Field Monitoring. *Environmental Science and Technology Letters*, *5*(10), 600–607. https://doi.org/10.1021/acs.estlett.8b00439

Calvert, J. G., & Lindberg, S. E. (2005). Mechanisms of mercury removal by O3 and OH in the atmosphere. *Atmospheric Environment*, *39*(18), 3355–3367. https://doi.org/10.1016/j.atmosenv.2005.01.055

Chen, L., Li, Y., Liu, C., Guo, L., & Wang, X. (2018). Wet deposition of mercury in Qingdao, a coastal urban city in China: Concentrations, fluxes, and influencing factors. *Atmospheric Environment*, *174*(August 2017), 204–213. https://doi.org/10.1016/j.atmosenv.2017.11.059

Cheng, C. M., Chen, C. W., Zhu, J., Chen, C. W., Kuo, Y. W., Lin, T. H., Wen, S. H., Zeng, Y. S., Liu, J. C., & Pan, W. P. (2009). Measurement of vapor phase mercury emissions at coal-fired power plants using regular and speciating sorbent traps with in-stack and out-of-stack sampling methods. *Energy and Fuels*, *23*(10), 4831–4839. https://doi.org/10.1021/ef900294s

Cheng, I., & Zhang, L. (2017). Uncertainty assessment of gaseous oxidized mercury measurements collected by atmospheric mercury network. *Environmental Science and Technology*, *51*(2), 855–862. https://doi.org/10.1021/acs.est.6b04926

Corns, W. T., Stockwell, P. B., Brown, R. J. C., & Brown, A. (2009). Determination of total mercury in ambient air using amalgamation with atomic fluorescence spectrometry. *IET*, *19*(5), 26–27.

de Foy, B., Tong, Y., Yin, X., Zhang, W., Kang, S., Zhang, Q., Zhang, G., Wang, X., & Schauer, J. J. (2016). First field-based atmospheric observation of the reduction of reactive mercury driven by sunlight. *Atmospheric Environment*, *134*, 27–39. https://doi.org/10.1016/j.atmosenv.2016.03.028

de Krom, I., Bavius, W., Ziel, R., Efremov, E., van Meer, D., van Otterloo, P., van Andel, I., van Osselen, D., Heemskerk, M., van der Veen, A. M. H., Dexter, M. A., Corns,

W. T., & Ent, H. (2021). Primary mercury gas standard for the calibration of mercury measurements. *Measurement: Journal of the International Measurement Confederation*, *169*, 108351. https://doi.org/10.1016/j.measurement.2020.108351

De Krom, I., Bavius, W., Ziel, R., Mcghee, E. A., Brown, R. J. C., Živković, I., Gačnik, J., Fajon, V., Kotnik, J., Horvat, M., & Ent, H. (2021). Comparability of calibration strategies for measuring mercury concentrations in gas emission sources and the atmosphere. *Atmospheric Measurement Techniques*, *14*(3), 2317–2326. https://doi.org/10.5194/amt-14-2317-2021

Deeds, D. A., Ghoshdastidar, A., Raofie, F., Guérette, É. A., Tessier, A., & Ariya, P. A. (2015). Development of a particle-trap preconcentration-soft ionization mass spectrometric technique for the quantification of mercury halides in air. *Analytical Chemistry*, *87*(10), 5109–5116. https://doi.org/10.1021/ac504545w

Deng, C., Tong, Y., Chen, L., Yuan, W., Sun, Y., Li, J., Wang, X., Zhang, W., Lin, H., Xie, H., & Bu, X. (2019). Impact of particle chemical composition and water content on the photolytic reduction of particle-bound mercury. *Atmospheric Environment*, *200*(May 2018), 24–33. https://doi.org/10.1016/j.atmosenv.2018.11.054

Driscoll, C. T., Mason, R. P., Chan, H. M., Jacob, D. J., & Pirrone, N. (2013). Mercury as a Global Pollutant: Sources, Pathways, and Effects. *Environmental Science and Technology*, *47*(10), 4967−4983. https://doi.org/dx.doi.org/10.1021/es305071v

Duan, L., Wang, X., Wang, D., Duan, Y., Cheng, N., & Xiu, G. (2017). Atmospheric mercury speciation in Shanghai, China. *Science of the Total Environment*, *578*, 460–468. https://doi.org/10.1016/j.scitotenv.2016.10.209

Dumarey, R., Brown, R. J. C., Corns, W. T., Brown, A. S., & Stockwell, P. B. (2010). Elemental mercury vapour in air: The origins and validation of the "Dumarey equation" describing the mass concentration at saturation. *Accreditation and Quality Assurance*, *15*(7), 409–414. https://doi.org/10.1007/s00769-010-0645-1

Dunham-Cheatham, S. M., Lyman, S., & Gustin, M. S. (2020). Evaluation of sorption surface materials for reactive mercury compounds. *Atmospheric Environment*, *242*(August), 117836. https://doi.org/10.1016/j.atmosenv.2020.117836

Ebinghaus, R., Jennings, S. G., Schroeder, W. H., Berg, T., Donaghy, T., Guentzel, J., Kenny, C., Kock, H. H., Kvietkus, K., Landing, W., Mühleck, T., Munthe, J., Prestbo, E. M., Schneeberger, D., Slemr, F., Sommar, J., Urba, A., Wallschläger, D., & Xiao, Z. (1999). International field intercomparison measurements of atmospheric mercury species at Mace Head, Ireland. *Atmospheric Environment*, *33*(18), 3063–3073. https://doi.org/10.1016/S1352-2310(98)00119-8

Ebinghaus, Ralf, Kock, H. H., Temme, C., Einax, J. W., Löwe, A. G., Richter, A., Burrows, J. P., & Schroeder, W. H. (2002). Antarctic springtime depletion of atmospheric mercury. *Environmental Science and Technology*, *36*(6), 1238–1244. https://doi.org/10.1021/es015710z

Electric Power Research Institute (EPRI). (2015). *Guidelines for Speciated Mercury Field Measurements*.

Engle, M. A., Sexauer Gustin, M., Lindberg, S. E., Gertler, A. W., & Ariya, P. A. (2005). The influence of ozone on atmospheric emissions of gaseous elemental mercury and reactive gaseous mercury from substrates. *Atmospheric Environment*, *39*(39 SPEC.

ISS.), 7506–7517. https://doi.org/10.1016/j.atmosenv.2005.07.069

Enrico, M., Roux, G. Le, Marusczak, N., Heimbürger, L. E., Claustres, A., Fu, X., Sun, R., & Sonke, J. E. (2016). Atmospheric Mercury Transfer to Peat Bogs Dominated by Gaseous Elemental Mercury Dry Deposition. *Environmental Science and Technology*, *50*(5), 2405–2412. https://doi.org/10.1021/acs.est.5b06058

Ent, H., Andel, I. Van, Heemskerk, M., Otterloo, P. Van, Bavius, W., Baldan, A., Horvat, M., Brown, R. J. C., & Quétel, C. R. (2014). A gravimetric approach to providing SI traceability for concentration measurement results of mercury vapor at ambient air levels. *Measurement Science and Technology*, *25*(11), 1–11. https://doi.org/10.1088/0957-0233/25/11/115801

Feddersen, D. M., Talbot, R., Mao, H., & Sive, B. C. (2012). Size distribution of particulate mercury in marine and coastal atmospheres. *Atmospheric Chemistry and Physics*, *12*(22), 10899–10909. https://doi.org/10.5194/acp-12-10899-2012

Feinberg, A. I., Kurien, U., & Ariya, P. A. (2015). The kinetics of aqueous mercury(II) reduction by sulfite over an array of environmental conditions. *Water, Air, and Soil Pollution*, *226*, 119. https://doi.org/10.1007/s11270-015-2371-0

Feng, X., Lu, J. Y., Hao, Y., Banic, C., & Schroeder, W. H. (2003). Evaluation and applications of a gaseous mercuric chloride source. *Analytical and Bioanalytical Chemistry*, *376*(7), 1137–1140. https://doi.org/10.1007/s00216-003-2034-7

Fitzgerald, W. F., & Gill, G. A. (1979). Subnanogram Determination of Mercury by Two-Stage Gold Amalgamation and Gas Phase Detection Applied to Atmospheric Analysis. *Analytical Chemistry*, *51*(11), 1714–1720. https://doi.org/10.1021/ac50047a030

Fu, X. W., Zhang, H., Yu, B., Wang, X., Lin, C. J., & Feng, X. B. (2015). Observations of atmospheric mercury in China: A critical review. *Atmospheric Chemistry and Physics*, *15*(16), 9455–9476. https://doi.org/10.5194/acp-15-9455-2015

Gačnik, J., Živković, I., Ribeiro Guevara, S., Jaćimović, R., Kotnik, J., De Feo, G., Dexter, M., Corns, W., & Horvat, M. (2021). Behaviour of KCl sorbent traps and KCl trapping solutions used for atmospheric mercury speciation: stability and specificity. *Atmospheric Measurement Techniques*, *14*(10), 6619–6631. https://doi.org/10.5194/amt-2021-153

Gačnik, J., Živković, I., Ribeiro Guevara, S., Jaćimović, R., Kotnik, J., & Horvat, M. (2021). Validating an evaporative calibrator for gaseous oxidized mercury. *Sensors*, *21*(7), 2501. https://doi.org/10.3390/s21072501

Gačnik, J., Živković, I., Ribeiro Guevara, S., Kotnik, J., Berisha, S., Vijayakumaran Nair, S., Jurov, A., Cvelbar, U., & Horvat, M. (2022). Calibration Approach for Gaseous Oxidized Mercury Based on Nonthermal Plasma Oxidation of Elemental Mercury. *Analytical Chemistry*, *94*(23), 8234–8240. https://doi.org/10.1021/acs.analchem.2c00260

Gårdfeldt, K., & Jonsson, M. (2003). Is bimolecular reduction of Hg(II) complexes possible in aqueous systems of environmental importance. *Journal of Physical Chemistry A*, *107*(22), 4478–4482. https://doi.org/10.1021/jp0275342

Gårdfeldt, K., Sommar, J., Strömberg, D., & Feng, X. (2001). Oxidation of atomic mercury by hydroxyl radicals and photoinduced decomposition of methylmercury in the

aqueous phase. *Atmospheric Environment*, *35*(17), 3039–3047. https://doi.org/10.1016/S1352-2310(01)00107-8

Ghoshdastidar, A. J., & Ariya, P. A. (2019). The Existence of Airborne Mercury Nanoparticles. *Scientific Reports*, *9*(1), 1–9. https://doi.org/10.1038/s41598-019-47086-8

Ghoshdastidar, A. J., Ramamurthy, J., Morissette, M., & Ariya, P. A. (2020). Development of methodology to generate, measure, and characterize the chemical composition of oxidized mercury nanoparticles. *Analytical and Bioanalytical Chemistry*, *412*(6), 1467. https://doi.org/10.1007/s00216-020-02397-y

Gustin, M., & Jaffe, D. (2010). Reducing the uncertainty in measurement and understanding of mercury in the atmosphere. *Environmental Science and Technology*, *44*(7), 2222–2227. https://doi.org/10.1021/es902736k

Gustin, M. S., Amos, H. M., Huang, J., Miller, M. B., & Heidecorn, K. (2015). Measuring and modeling mercury in the atmosphere: A critical review. *Atmospheric Chemistry and Physics*, *15*(10), 5697–5713. https://doi.org/10.5194/acp-15-5697-2015

Gustin, Mae Sexauer. (2011). Exchange of Mercury between the Atmosphere and Terrestrial Ecosystems. *Environmental Chemistry and Toxicology of Mercury*, *2*, 423–451. https://doi.org/10.1002/9781118146644.ch13

Gustin, Mae Sexauer, Dunham-Cheatham, S. M., Huang, J., Lindberg, S., & Lyman, S. N. (2021). Development of an Understanding of Reactive Mercury in Ambient Air: A Review. *Atmosphere*, *12*(1), 73. https://doi.org/10.3390/atmos12010073

Gustin, Mae Sexauer, Dunham-Cheatham, S. M., & Zhang, L. (2019). Comparison of 4 Methos for Measurement of Reactive, Gaseous Oxiize, an Particulate Bound Mercury. *Environmental Science and Technology*, *53*(24), 14489–14495. https://doi.org/10.1021/acs.est.9b04648

Gustin, Mae Sexauer, Dunham-Cheatham, S. M., Zhang, L., Lyman, S., Choma, N., & Castro, M. (2021). Use of Membranes and Detailed HYSPLIT Analyses to Understand Atmospheric Particulate, Gaseous Oxidized, and Reactive Mercury Chemistry. *Environmental Science and Technology*, *55*(2), 893–901. https://doi.org/10.1021/acs.est.0c07876

Gustin, Mae Sexauer, Huang, J., Miller, M. B., Peterson, C., Jaffe, D. A., Ambrose, J., Finley, B. D., Lyman, S. N., Call, K., Talbot, R., Feddersen, D., Mao, H., & Lindberg, S. E. (2013). Do we understand what the mercury speciation instruments are actually measuring? Results of RAMIX. *Environmental Science and Technology*, *47*(13), 7295–7306. https://doi.org/10.1021/es3039104

Gustin, Mae Sexauer, Pierce, A. M., Huang, J., Miller, M. B., Holmes, H. A., & Loria-Salazar, S. M. (2016). Evidence for different reactive Hg sources and chemical compounds at adjacent valley and high elevation locations. *Environmental Science and Technology*, *50*(22), 12225–12231. https://doi.org/10.1021/acs.est.6b03339

Hall, N. L., Dvonch, J. T., Marsik, F. J., Barres, J. A., & Landis, M. S. (2017). An artificial turf-based surrogate surface collector for the direct measurement of atmospheric mercury dry deposition. *International Journal of Environmental Research and Public Health*, *14*(2). https://doi.org/10.3390/ijerph14020173

Holmes, C. D., Jacob, D. J., Corbitt, E. S., Mao, J., Yang, X., Talbot, R., & Slemr, F.

(2010). Global atmospheric model for mercury including oxidation by bromine atoms. *Atmospheric Chemistry and Physics*, *10*(24), 12037–12057. https://doi.org/10.5194/acp-10-12037-2010

Holmes, Christopher D, Jacob, D. J., Mason, R. P., & Jaffe, D. A. (2009). Sources and deposition of reactive gaseous mercury in the marine atmosphere. *Atmospheric Environment*, *43*(14), 2278–2285. https://doi.org/10.1016/j.atmosenv.2009.01.051

Horowitz, H. M., Jacob, D. J., Zhang, Y., DIbble, T. S., Slemr, F., Amos, H. M., Schmidt, J. A., Corbitt, E. S., Marais, E. A., & Sunderland, E. M. (2017). A new mechanism for atmospheric mercury redox chemistry: Implications for the global mercury budget. *Atmospheric Chemistry and Physics*, *17*(10), 6353–6371. https://doi.org/10.5194/acp-17-6353-2017

Horvat, M., Lupšina, V., & Pihlar, B. (1991). Determination of total mercury in coal fly ash by gold amalgamation cold vapour atomic absorption spectrometry. *Analytica Chimica Acta*, *243*(C), 71–79. https://doi.org/10.1016/S0003-2670(00)82542-8

Huang, J., & Gustin, M. S. (2015a). Uncertainties of gaseous oxidized mercury measurements using KCl-coated denuders, cation-exchange membranes, and nylon membranes: Humidity influences. *Environmental Science and Technology*, *49*(10), 6102–6108. https://doi.org/10.1021/acs.est.5b00098

Huang, J., & Gustin, M. S. (2015b). Use of passive sampling methods and models to understand sources of mercury deposition to high elevation sites in the Western United States. *Environmental Science and Technology*, *49*(1), 432–441. https://doi.org/10.1021/es502836w

Huang, J., Miller, M. B., Edgerton, E., & Gustin, M. S. (2017). Deciphering potential chemical compounds of gaseous oxidized mercury in Florida, USA. *Atmospheric Chemistry and Physics*, *17*(3), 1689–1698. https://doi.org/10.5194/acp-17-1689-2017

Huang, J., Miller, M. B., Weiss-Penzias, P., & Gustin, M. S. (2013). Comparison of gaseous oxidized Hg measured by KCl-coated denuders, and nylon and cation exchange membranes. *Environmental Science and Technology*, *47*(13), 7307–7316. https://doi.org/10.1021/es4012349

Huber, M. L., Laesecke, A., & Friend, D. G. (2006). Correlation for the vapor pressure of mercury. *Industrial and Engineering Chemistry Research*, *45*(21), 7351–7361. https://doi.org/10.1021/ie060560s

Ippolito, S. J., Sabri, Y. M., & Bhargava, S. K. (2011). Measuring Gas Phase Mercury Emissions from Industrial Effluents. In *Environmental Chemistry and Toxicology of Mercury* (pp. 59–109). John Wiley & Sons. https://doi.org/https://doi.org/10.1002/9781118146644.ch3

IUPAC. (1997). *IUPAC Compendium of Chemical Terminology (the "Gold Book")* (A. D. McNaught & A. Wilkinson (eds.); 2nd editio). Blackwell Scientific Publications. https://doi.org/10.1351/goldbook.S05727

Jaffe, D. A., Lyman, S., Amos, H. M., Gustin, M. S., Huang, J., Selin, N. E., Levin, L., Ter Schure, A., Mason, R. P., Talbot, R., Rutter, A., Finley, B., Jaeglé, L., Shah, V., McClure, C., Ambrose, J., Gratz, L., Lindberg, S., Weiss-Penzias, P., … Edwards, G. (2014). Progress on understanding atmospheric mercury hampered by uncertain measurements. *Environmental Science and Technology*, *48*(13), 7204–7206.

https://doi.org/10.1021/es5026432

Jones, C. P., Lyman, S. N., Jaffe, D. A., Allen, T., & O'Neil, T. L. (2016). Detection and quantification of gas-phase oxidized mercury compounds by GC/MS. *Atmospheric Measurement Techniques*, *9*(5), 2195–2205. https://doi.org/10.5194/amt-9-2195-2016

Kalinchuk, V., Lopatnikov, E., & Astakhov, A. (2018). Gradient measurements of gaseous elemental mercury (Hg0) in the marine boundary layer of the northwest Sea of Japan (East Sea). *Environmental Pollution*, *237*, 1124–1136. https://doi.org/10.1016/j.envpol.2017.11.055

Kamp, J., Skov, H., Jensen, B., & Sørensen, L. L. (2018). Fluxes of gaseous elemental mercury (GEM) in the High Arctic during atmospheric mercury depletion events (AMDEs). *Atmospheric Chemistry and Physics*, *18*(9), 6923–6938. https://doi.org/10.5194/acp-18-6923-2018

Karthik, R., Paneerselvam, A., Ganguly, D., Hariharan, G., Srinivasalu, S., Purvaja, R., & Ramesh, R. (2017). Temporal variability of atmospheric Total Gaseous Mercury and its correlation with meteorological parameters at a high-altitude station of the South India. *Atmospheric Pollution Research*, *8*(1), 164–173. https://doi.org/10.1016/j.apr.2016.08.010

Kim, K. H., & Kim, M. Y. (2002). A decadal shift in total gaseous mercury concentration levels in Seoul, Korea: Changes between the late 1980s and the late 1990s. *Atmospheric Environment*, *36*(4), 663–675. https://doi.org/10.1016/S1352-2310(01)00470-8

Kim, P. R., Han, Y. J., Holsen, T. M., & Yi, S. M. (2012). Atmospheric particulate mercury: Concentrations and size distributions. *Atmospheric Environment*, *61*, 94–102. https://doi.org/10.1016/j.atmosenv.2012.07.014

Koenig, A. M., Sonke, J. E., Magand, O., Andrade, M., Moreno, I., Velarde, F., Forno, R., Gutierrez, R., Blacutt, L., Laj, P., Ginot, P., Bieser, J., Zahn, A., Slemr, F., & Dommergue, A. (2022). Evidence for Interhemispheric Mercury Exchange in the Pacific Ocean Upper Troposphere. *Journal of Geophysical Research: Atmospheres*, *127*(10), e2021JD036283. https://doi.org/10.1029/2021jd036283

Lai, S. O., Huang, J., Hopke, P. K., & Holsen, T. M. (2011). An evaluation of direct measurement techniques for mercury dry deposition. *Science of the Total Environment*, *409*(7), 1320–1327. https://doi.org/10.1016/j.scitotenv.2010.12.032

Lamborg, C. H., Hansel, C. M., Bowman, K. L., Voelker, B. M., Marsico, R. M., Oldham, V. E., Swarr, G. J., Zhang, T., & Ganguli, P. M. (2021). Dark Reduction Drives Evasion of Mercury From the Ocean. *Frontiers in Environmental Chemistry*, *2*. https://doi.org/10.3389/fenvc.2021.659085

Landis, M. S., Stevens, R. K., Schaedlich, F., & Prestbo, E. M. (2002). Development and Characterization of an Annular Denuder Methodology for the Measurement of Divalent Inorganic Reactive Gaseous Mercury in Ambient Air. *Environmental Science and Technology*, *36*(13), 3000–3009. https://doi.org/10.1021/es015887t

Lasorsa, B. K., Gill, G. A., & Horvat, M. (2012). Analytical Methods for Measuring Mercury in Water, Sediment, and Biota. In M. S. Bank (Ed.), *Mercury in the Environment: Pattern and Process* (First edit, pp. 27–54). University of California Press.

Laurier, F. J. G., Mason, R. P., Whalin, L., & Kato, S. (2003). Reactive gaseous mercury formation in the North Pacific Ocean's marine boundary layer: A potential role of halogen chemistry. *Journal of Geophysical Research: Atmospheres*, *108*(17), 1–12. https://doi.org/10.1029/2003jd003625

Lee, G. S., Kim, P. R., Han, Y. J., Holsen, T. M., Seo, Y. S., & Yi, S. M. (2016). Atmospheric speciated mercury concentrations on an island between China and Korea: Sources and transport pathways. *Atmospheric Chemistry and Physics*, *16*(6), 4119–4133. https://doi.org/10.5194/acp-16-4119-2016

Lee, S. J., Seo, Y. C., Jurng, J., & Lee, T. G. (2004). Removal of gas-phase elemental mercury by iodine- and chlorine-impregnated activated carbons. *Atmospheric Environment*, *38*(29), 4887–4893. https://doi.org/10.1016/j.atmosenv.2004.05.043

Lin, C. J., Gustin, M. S., Singhasuk, P., Eckley, C., & Miller, M. (2010). Empirical models for estimating mercury flux from soils. *Environmental Science and Technology*, *44*(22), 8522–8528. https://doi.org/10.1021/es1021735

Lin, C., & Pehkonen, S. O. (1998). Oxidation of elemental mercury by aqueous chlorine (HOCI/OCI-): Implications for tropospheric mercury chemistry. *J. Geophys. Res.*, *103*(D21), 28,093-28,102.

Lindberg, S. E., Brooks, S., Lin, C. J., Scott, K. J., Landis, M. S., Stevens, R. K., Goodsite, M., & Richter, A. (2002). Dynamic oxidation of gaseous mercury in the arctic troposphere at polar sunrise. *Environmental Science and Technology*, *36*(6), 1245–1256. https://doi.org/10.1021/es0111941

Liu, B., Keeler, G. J., Timothy Dvonch, J., Barres, J. A., Lynam, M. M., Marsik, F. J., & Morgan, J. T. (2010). Urban-rural differences in atmospheric mercury speciation. *Atmospheric Environment*, *44*(16), 2013–2023. https://doi.org/10.1016/j.atmosenv.2010.02.012

Liu, W., Xu, H., Liao, Y., Quan, Z., Li, S., Zhao, S., Qu, Z., & Yan, N. (2019). Recyclable CuS sorbent with large mercury adsorption capacity in the presence of SO2 from non-ferrous metal smelting flue gas. *Fuel*, *235*(May 2018), 847–854. https://doi.org/10.1016/j.fuel.2018.08.062

Liu, Y., Liu, G., Wang, Z., Guo, Y., Yin, Y., Zhang, X., Cai, Y., & Jiang, G. (2021). Understanding foliar accumulation of atmospheric Hg in terrestrial vegetation: Progress and challenges. *Critical Reviews in Environmental Science and Technology*. https://doi.org/10.1080/10643389.2021.1989235

Long, S. E., Norris, J. E., Carney, J., & Ryan, J. V. (2020). Provision of primary NIST traceability to support vapor phase mercury emissions monitoring of combustion sources using isotope dilution inductively coupled plasma mass spectrometry. *Atmospheric Pollution Research*, *11*(5), 909–919. https://doi.org/10.1016/j.apr.2020.02.003

Long, S. E., Norris, J. E., Carney, J., Ryan, V., Mitchell, G. D., & Dorko, W. D. (2020). Traceability of the output concentration of mercury vapor generators. *Atmospheric Pollution Research*, *11*(4), 639–645. https://doi.org/10.1016/j.apr.2019.12.012

Lu, J. Y., & Schroeder, W. H. (1999). Comparison of conventional filtration and a denuder-based methodology for sampling of particulate-phase mercury in ambient air. *Talanta*, *49*(1), 15–24. https://doi.org/10.1016/S0039-9140(98)00363-4

Luippold, A., Gustin, M. S., Dunham-Cheatham, S. M., & Zhang, L. (2020). Improvement of quantification and identification of atmospheric reactive mercury. *Atmospheric Environment*, *224*(January), 117307. https://doi.org/10.1016/j.atmosenv.2020.117307

Lyman, S., Jones, C., O'Neil, T., Allen, T., Miller, M., Gustin, M. S., Pierce, A. M., Luke, W., Ren, X., & Kelley, P. (2016). Automated calibration of atmospheric oxidized mercury measurements. *Environmental Science and Technology*, *50*(23), 12911–12927. https://doi.org/10.1021/acs.est.6b04211

Lyman, S. N., Jaffe, D. A., & Gustin, M. S. (2010). Release of mercury halides from KCl denuders in the presence of ozone. *Atmospheric Chemistry and Physics*, *10*(17), 8197–8204. https://doi.org/10.5194/acp-10-8197-2010

Lyman, Seth N., Cheng, I., Gratz, L. E., Weiss-Penzias, P., & Zhang, L. (2020). An updated review of atmospheric mercury. *Science of the Total Environment*, *707*, 135575. https://doi.org/10.1016/j.scitotenv.2019.135575

Lyman, Seth N., Gratz, L. E., Dunham-cheatham, S. M., Gustin, M. S., & Luippold, A. (2020). Improvements to the Accuracy of Atmospheric Oxidized Mercury Measurements. *Environmental Science and Technology*, *54*, 13379–13388. https://doi.org/10.1021/acs.est.0c02747

Lynam, M. M., Dvonch, J. T., Barres, J. A., Landis, M. S., & Kamal, A. S. (2016). Investigating the impact of local urban sources on total atmospheric mercury wet deposition in Cleveland, Ohio, USA. *Atmospheric Environment*, *127*, 262–271. https://doi.org/10.1016/j.atmosenv.2015.12.048

Lynam, M. M., Dvonch, J. T., Hall, N. L., Morishita, M., & Barres, J. A. (2015). Trace elements and major ions in atmospheric wet and dry deposition across central Illinois, USA. *Air Quality, Atmosphere and Health*, *8*(1), 135–147. https://doi.org/10.1007/s11869-014-0274-7

Lynam, M. M., & Keeler, G. J. (2002). Comparison of methods for particulate phase mercury analysis: Sampling and analysis. *Analytical and Bioanalytical Chemistry*, *374*(6), 1009–1014. https://doi.org/10.1007/s00216-002-1584-4

Lynam, M. M., Klaue, B., Keeler, G. J., & Blum, J. D. (2013). Using thermal analysis coupled to isotope dilution cold vapor ICP-MS in the quanti fi cation of atmospheric particulate phase mercury †. *Joirnal of Analytical Atomic Sprectrometry*, *28*, 1788–1795. https://doi.org/10.1039/c3ja50184a

Malcolm, E. G., Ford, A. C., Redding, T. A., Richardson, M. C., Strain, B. M., & Tetzner, S. W. (2009). Experimental investigation of the scavenging of gaseous mercury by sea salt aerosol. *Journal of Atmospheric Chemistry*, *63*(3), 221–234. https://doi.org/10.1007/s10874-010-9165-y

Malcolm, E. G., & Keeler, G. J. (2007). Evidence for a sampling artifact for particulate-phase mercury in the marine atmosphere. *Atmospheric Environment*, *41*(16), 3352–3359. https://doi.org/10.1016/j.atmosenv.2006.12.024

Mao, H., Ye, Z., & Driscoll, C. (2017). Meteorological effects on Hg wet deposition in a forested site in the Adirondack region of New York during 2000–2015. *Atmospheric Environment*, *168*, 90–100. https://doi.org/10.1016/j.atmosenv.2017.08.058

Mao, N., Antley, J., Cooper, M., Shah, N., Kadam, A., & Khalizov, A. (2021). Heterogeneous Chemistry of Mercuric Chloride on Inorganic Salt Surfaces. *Journal of*

Physical Chemistry A, *125*(18), 3943–3952. https://doi.org/10.1021/acs.jpca.1c02220

Marsik, F. J., Keeler, G. J., & Landis, M. S. (2007). The dry-deposition of speciated mercury to the Florida Everglades: Measurements and modeling. *Atmospheric Environment*, *41*(1), 136–149. https://doi.org/10.1016/j.atmosenv.2006.07.032

Mason, R. P., Hammerschmidt, C. R., Lamborg, C. H., Bowman, K. L., Swarr, G. J., & Shelley, R. U. (2017). The air-sea exchange of mercury in the low latitude Pacific and Atlantic Oceans. *Deep-Sea Research Part I: Oceanographic Research Papers*, *122*(February), 17–28. https://doi.org/10.1016/j.dsr.2017.01.015

McClure, C. D., Jaffe, D. A., & Edgerton, E. S. (2014). Evaluation of the KCl denuder method for gaseous oxidized mercury using HgBr2 at an in-service AMNet site. *Environmental Science and Technology*, *48*(19), 11437–11444. https://doi.org/10.1021/es502545k

Millhollen, A. G., Gustin, M. S., & Obrist, D. (2006). Foliar mercury accumulation and exchange for three tree species. *Environmental Science and Technology*, *40*(19), 6001–6006. https://doi.org/10.1021/es0609194

Moore, C. W., & Castro, M. S. (2012). Investigation of factors affecting gaseous mercury concentrations in soils. *Science of the Total Environment*, *419*, 136–143. https://doi.org/10.1016/j.scitotenv.2011.12.068

Munthe, J., Wängberg, I., Pirrone, N., Iverfeldt, Å., Ferrara, R., Ebinghaus, R., Feng, X., Gårdfeldt, K., Keeler, G., Lanzillotta, E., Lindberg, S. E., Lu, J., Mamane, Y., Prestbo, E., Schmolke, S., Schroeder, W. H., Sommar, J., Sprovieri, F., Stevens, R. K., … Urba, A. (2001). Intercomparison of methods for sampling and analysis of atmospheric mercury species. *Atmospheric Environment*, *35*(17), 3007–3017. https://doi.org/10.1016/S1352-2310(01)00104-2

Munthe, John. (1992). The aqueous oxidation of elemental mercury by ozone. *Atmospheric Environment Part A, General Topics*, *26*(8), 1461–1468. https://doi.org/10.1016/0960-1686(92)90131-4

Obrist, D., Agnan, Y., Jiskra, M., Olson, C. L., Colegrove, D. P., Hueber, J., Moore, C. W., Sonke, J. E., & Helmig, D. (2017). Tundra uptake of atmospheric elemental mercury drives Arctic mercury pollution. *Nature*, *547*(7662), 201–204. https://doi.org/10.1038/nature22997

Paige Wright, L., Zhang, L., & Marsik, F. J. (2016). Overview of mercury dry deposition, litterfall, and throughfall studies. *Atmospheric Chemistry and Physics*, *16*(21), 13399–13416. https://doi.org/10.5194/acp-16-13399-2016

Pal, B., & Ariya, P. A. (2004). Gas-phase HO•-initiated reactions of elemental mercury: Kinetics, product studies, and atmospheric implications. *Environmental Science and Technology*, *38*(21), 5555–5566. https://doi.org/10.1021/es0494353

Pandey, S. K., Kim, K. H., & Brown, R. J. C. (2011). Measurement techniques for mercury species in ambient air. *TrAC - Trends in Analytical Chemistry*, *30*(6), 899–917. https://doi.org/10.1016/j.trac.2011.01.017

Pehkonen, S. O., & Lin, C. J. (1998). Aqueous photochemistry of mercury with organic acids. *Journal of the Air and Waste Management Association*, *48*(2), 144–150. https://doi.org/10.1080/10473289.1998.10463661

Peleg, M., Tas, E., Obrist, D., Matveev, V., Moore, C., Gabay, M., & Luria, M. (2015).

Observational Evidence for Involvement of Nitrate Radicals in Nighttime Oxidation of Mercury. *Environmental Science and Technology*, *49*(24), 14008–14018. https://doi.org/10.1021/acs.est.5b03894

Petrov, P., Rajamäki, T., Corns, W. T., & Goenaga-Infante, H. (2020). Evaluating the performance of oxidized Hg reference gas generators in the range ng m−3 to μg m−3 by improved coupling with ICP-MS. *Atmospheric Environment: X*, *8*(100090). https://doi.org/10.1016/j.aeaoa.2020.100090

Pirrone, N., Cinnirella, S., Feng, X., Finkelman, R. B., Friedli, H. R., Leaner, J., Mason, R., Mukherjee, A. B., Stracher, G. B., Streets, D. G., & Telmer, K. (2010). Global mercury emissions to the atmosphere from anthropogenic and natural sources. *Atmospheric Chemistry and Physics*, *10*(13), 5951–5964. https://doi.org/10.5194/acp-10-5951-2010

Poluektov, N., Vitkun, R., & Zelyukova, Y. (1964). Determination of milligram amounts of mercury by atomic absorption in the gaseous phase. *Analytical Chemistry*, *19*(873).

Prestbo, E. M., & Bloom, N. S. (1995). Mercury Speciation Adsorption (MESA) Method for Combustion Flue Gas: Methodology, Artifacts, Intercomparison, and Atmospheric Implications. In D. B. Porcella, J. W. Huckabee, & B. Wheatley (Eds.), *Mercury as a Global Pollutant* (pp. 145–158). Springer, Dodrecht. https://doi.org/https://doi.org/10.1007/978-94-011-0153-0_17

Presto, A. A., & Granite, E. J. (2007). Impact of sulfur oxides on mercury capture by activated carbons. *100th Annual Conference and Exhibition of the Air and Waste Management Association 2007, ACE 2007*, *6*(18), 4234–4247.

Quétel, C. R., Zampella, M., & Brown, R. J. C. (2016). Temperature dependence of Hg vapour mass concentration at saturation in air: New SI traceable results between 15 and 30°C. *TrAC - Trends in Analytical Chemistry*, *85*, 81–88. https://doi.org/10.1016/j.trac.2015.12.010

Quétel, C. R., Zampella, M., Brown, R. J. C., Ent, H., Horvat, M., Paredes, E., & Tunc, M. (2014). International system of units traceable results of Hg mass concentration at saturation in air from a newly developed measurement procedure. *Analytical Chemistry*, *86*(15), 7819–7827. https://doi.org/10.1021/ac5018875

Ribeiro Guevara, S., Žižek, S., Repinc, U., Catán, S. P., Jaćimović, R., & Horvat, M. (2007). Novel methodology for the study of mercury methylation and reduction in sediments and water using 197Hg radiotracer. *Analytical and Bioanalytical Chemistry*, *387*(6), 2185–2197. https://doi.org/10.1007/s00216-006-1040-y

Rutter, A. P., Shakya, K. M., Lehr, R., Schauer, J. J., & Griffin, R. J. (2012). Oxidation of gaseous elemental mercury in the presence of secondary organic aerosols. *Atmospheric Environment*, *59*, 86–92. https://doi.org/10.1016/j.atmosenv.2012.05.009

Rutter, Andrew P., & Schauer, J. J. (2007). The impact of aerosol composition on the particle to gas partitioning of reactive mercury. *Environmental Science and Technology*, *41*(11), 3934–3939. https://doi.org/10.1021/es062439i

Ryan, J. V., & Keeney, R. M. (2004). *The Ontario Hydro Method for Speciated Mercury Measurements: Issues and Considerations*. https://cfpub.epa.gov/si/si_public_record_Report.cfm?Lab=NRMRL&dirEntryId

=83795

Saiz-Lopez, A., Acuña, A. U., Trabelsi, T., Carmona-García, J., Dávalos, J. Z., Rivero, D., Cuevas, C. A., Kinnison, D. E., Sitkiewicz, S. P., Roca-Sanjuán, D., & Francisco, J. S. (2019). Gas-Phase Photolysis of Hg(I) Radical Species: A New Atmospheric Mercury Reduction Process. *Journal of the American Chemical Society*, *141*(22), 8698–8702. https://doi.org/10.1021/jacs.9b02890

Saiz-Lopez, A., Sitkiewicz, S. P., Roca-Sanjuán, D., Oliva-Enrich, J. M., Dávalos, J. Z., Notario, R., Jiskra, M., Xu, Y., Wang, F., Thackray, C. P., Sunderland, E. M., Jacob, D. J., Travnikov, O., Cuevas, C. A., Acuña, A. U., Rivero, D., Plane, J. M. C., Kinnison, D. E., & Sonke, J. E. (2018). Photoreduction of gaseous oxidized mercury changes global atmospheric mercury speciation, transport and deposition. *Nature Communications*, *9*(1), 1–9. https://doi.org/10.1038/s41467-018-07075-3

Sakata, M., & Marumoto, K. (2004). Dry Deposition Fluxes and Deposition Velocities of Trace Metals in the Tokyo Metropolitan Area Measured with a Water Surface Sampler. *Environmental Science and Technology*, *38*(7), 2190–2197. https://doi.org/10.1021/es030467k

Sasmaz, E., Kirchofer, A., Jew, A. D., Saha, A., Abram, D., Jaramillo, T. F., & Wilcox, J. (2012). Mercury chemistry on brominated activated carbon. *Fuel*, *99*, 188–196. https://doi.org/10.1016/j.fuel.2012.04.036

Saxholm, S., Rajamäki, T., Hämäläinen, J., & Hildén, P. (2020). Dynamic calibration method for reactive gases. *Measurement Science and Technology*, *31*, 034001. https://doi.org/10.1088/1361-6501/ab4d68

Schmäh, M. (2007). *Method and device for producing a gas-vapor mixture (German patent DE102007004034B4)* (Patent No. 102007004034B4). German Patent and Trademark Office. https://patents.google.com/patent/DE102007004034B4/en

Schmidt, J. A., Jacob, D. J., Horowitz, H. M., Hu, L., Sherwen, T., Evans, M. J., Liang, Q., Suleiman, R. M., Oram, D. E., Le Breton, M., Percival, C. J., Wang, S., Dix, B., & Volkamer, R. (2016). Modeling the observed tropospheric BrO background: Importance of multiphase chemistry and implications for ozone, OH, andmercury. *Journal of Geophysical Research*, *121*(19), 11819–11835. https://doi.org/10.1002/2015JD024229

Schroeder, W. H., & Munthe, J. (1998). Atmospheric mercury - An overview. *Atmospheric Environment*, *32*(5), 809–822. https://doi.org/10.1016/S1352-2310(97)00293-8

Selin, N. E. (2009). Global biogeochemical cycling of mercury: A review. *Annual Review of Environment and Resources*, *34*, 43–63. https://doi.org/10.1146/annurev.environ.051308.084314

Si, L., & Ariya, P. A. (2011). Aqueous photoreduction of oxidized mercury species in presence of selected alkanethiols. *Chemosphere*, *84*(8), 1079–1084. https://doi.org/10.1016/j.chemosphere.2011.04.061

Si, L., & Ariya, P. A. (2018). Recent advances in atmospheric chemistry of mercury. *Atmosphere*, *9*(2), 1–18. https://doi.org/10.3390/atmos9020076

Spolaor, A., Angot, H., Roman, M., Dommergue, A., Scarchilli, C., Vardè, M., Del Guasta, M., Pedeli, X., Varin, C., Sprovieri, F., Magand, O., Legrand, M., Barbante, C., & Cairns, W. R. L. (2018). Feedback mechanisms between snow and atmospheric

mercury: Results and observations from field campaigns on the Antarctic plateau. *Chemosphere*, *197*, 306–317. https://doi.org/10.1016/j.chemosphere.2017.12.180

Sprovieri, F., Pirrone, N., Bencardino, M., D'Amore, F., Angot, H., Barbante, C., Brunke, E. G., Arcega-Cabrera, F., Cairns, W., Comero, S., Del Carmen Diéguez, M., Dommergue, A., Ebinghaus, R., Bin Feng, X., Fu, X., Elizabeth Garcia, P., Manfred Gawlik, B., Hageström, U., Hansson, K., … Zhang, H. (2017). Five-year records of mercury wet deposition flux at GMOS sites in the Northern and Southern hemispheres. *Atmospheric Chemistry and Physics*, *17*(4), 2689–2708. https://doi.org/10.5194/acp-17-2689-2017

Sprovieri, F., Pirrone, N., Bencardino, M., D'Amore, F., Carbone, F., Cinnirella, S., Mannarino, V., Landis, M., Ebinghaus, R., Weigelt, A., Brunke, E. G., Labuschagne, C., Martin, L., Munthe, J., Wängberg, I., Artaxo, P., Morais, F., De Melo Jorge Barbosa, H., Brito, J., … Norstrom, C. (2016). Atmospheric mercury concentrations observed at ground-based monitoring sites globally distributed in the framework of the GMOS network. *Atmospheric Chemistry and Physics*, *16*(18), 11915–11935. https://doi.org/10.5194/acp-16-11915-2016

Sprovieri, F., Pirrone, N., Landis, M. S., & Stevens, R. K. (2005). Oxidation of gaseous elemental mercury to gaseous divalent mercury during 2003 polar sunrise at Ny-Alesund. *Environmental Science and Technology*, *39*(23), 9156–9165. https://doi.org/10.1021/es050965o

Srivastava, A., & Hodges, J. T. (2018). Development of a High-Resolution Laser Absorption Spectroscopy Method with Application to the Determination of Absolute Concentration of Gaseous Elemental Mercury in Air. *Analytical Chemistry*, *90*(11), 6781–6788. https://doi.org/10.1021/acs.analchem.8b00757

Srivastava, A., Long, S. E., Norris, J. E., Bryan, C. E., Carney, J., & Hodges, J. T. (2021). Comparison of Primary Laser Spectroscopy and Mass Spectrometry Methods for Measuring Mass Concentration of Gaseous Elemental Mercury. *Analytical Chemistry*, *93*(2), 1050–1058. https://doi.org/10.1021/acs.analchem.0c04002

Stamenkovic, J., & Gustin, M. S. (2009). Nonstomatal versus stomatal uptake of atmospheric mercury. *Environmental Science and Technology*, *43*(5), 1367–1372. https://doi.org/10.1021/es801583a

Steffen, A., Ariya, P., Scherz, C., Temme, C., Ferrari, C., Cobbett, F., Bottenheim, J., Aspmo, K., Lean, D., Skov, H., Poulain, A., Amyot, M., Brooks, S., Gardfeldt, K., Sommar, J., Dommergue, A., Dastoor, A., Douglas, T., Berg, T., … Ebinghaus, R. (2010). A synthesis of atmospheric mercury depletion event chemistry linking atmosphere, snow and water. *Atmospheric Chemistry and Physics Discussions*, *7*(4), 10837–10931. https://doi.org/10.5194/acpd-7-10837-2007

Stergaršek, A., Horvat, M., Kotnik, J., Tratnik, J., Frkal, P., Kocman, D., Jaćimović, R., Fajon, V., Ponikvar, M., Hrastel, I., Lenart, J., Debeljak, B., & Čujež, M. (2008). The role of flue gas desulphurisation in mercury speciation and distribution in a lignite burning power plant. *Fuel*, *87*(17–18), 3504–3512. https://doi.org/10.1016/j.fuel.2008.06.003

Stratton, W. J., & Lindberg, S. E. (1995). Use of a refluxing mist chamber for measurement of gas-phase mercury(II) species in the atmosphere. *Water, Air, & Soil Pollution*,

80(1–4), 1269–1278. https://doi.org/10.1007/BF01189790

Subir, M., Ariya, P. A., & Dastoor, A. P. (2011). A review of uncertainties in atmospheric modeling of mercury chemistry I. Uncertainties in existing kinetic parameters - Fundamental limitations and the importance of heterogeneous chemistry. *Atmospheric Environment*, *45*(32), 5664–5676. https://doi.org/10.1016/j.atmosenv.2011.04.046

Subir, M., Ariya, P. A., & Dastoor, A. P. (2012). A review of the sources of uncertainties in atmospheric mercury modeling II. Mercury surface and heterogeneous chemistry - A missing link. *Atmospheric Environment*, *46*, 1–10. https://doi.org/10.1016/j.atmosenv.2011.07.047

Švehla, J., Žídek, R., Ružovič, T., Svoboda, K., & Kratzer, J. (2019). Simple approaches to on-line and off-line speciation analysis of mercury in flue gases with detection by atomic absorption spectrometry: A pilot study. *Spectrochimica Acta - Part B Atomic Spectroscopy*, *156*(May), 51–58. https://doi.org/10.1016/j.sab.2019.05.002

Swartzendruber, P. C., Jaffe, D. A., & Finley, B. (2009). Development and first results of an aircraft-based, high time resolution technique for gaseous elemental and reactive (oxidized) gaseous mercury. *Environmental Science and Technology*, *43*(19), 7484–7489. https://doi.org/10.1021/es901390t

Tacey, S. A., Szilvási, T., Xu, L., Schauer, J. J., & Mavrikakis, M. (2018). The role of iron-oxide aerosols and sunlight in the atmospheric reduction of Hg(II) species: A DFT+U study. *Applied Catalysis B: Environmental*, *234*(March), 347–356. https://doi.org/10.1016/j.apcatb.2018.04.049

Tacey, S. A., Xu, L., Mavrikakis, M., & Schauer, J. J. (2016). Heterogeneous Reduction Pathways for Hg(II) Species on Dry Aerosols: A First-Principles Computational Study. *Journal of Physical Chemistry A*, *120*(13), 2106–2113. https://doi.org/10.1021/acs.jpca.5b12769

Talbot, R., Mao, H., Feddersen, D., Smith, M., Youn Kim, S., Barkley, S., Haase, K., Ambrose, J., Zhou, Y., & Russo, R. (2011). Comparison of Particulate Mercury Measured with Manual and Automated Methods. *Atmosphere*, *2*(1), 1–20. https://doi.org/10.3390/atmos2010001

Tang, H., Duan, Y., Zhu, C., Cai, T., Li, C., & Cai, L. (2017). Theoretical evaluation on selective adsorption characteristics of alkali metal-based sorbents for gaseous oxidized mercury. *Chemosphere*, *184*, 711–719. https://doi.org/10.1016/j.chemosphere.2017.06.039

Tang, H., Li, C., Duan, Y., Zhu, C., & Cai, L. (2019). Combined experimental and theoretical studies on adsorption mechanisms of gaseous mercury(II) by calcium-based sorbents: The effect of unsaturated oxygen sites. *Science of the Total Environment*, *656*, 937–945. https://doi.org/10.1016/j.scitotenv.2018.11.460

Tang, Y., Wang, S., Wu, Q., Liu, K., Wang, L., Li, S., Gao, W., Zhang, L., Zheng, H., Li, Z., & Hao, J. (2018). Recent decrease trend of atmospheric mercury concentrations in East China: The influence of anthropogenic emissions. *Atmospheric Chemistry and Physics*, *18*(11), 8279–8291. https://doi.org/10.5194/acp-18-8279-2018

Tekran. (n.d.). *Model 3400-CAL Elemental & Oxidized Mercury Generator*. Retrieved July 7, 2022, from https://www.tekran.com/products/flue-gas-cem/system-calibration/

Tekran Inc. (1998). *Tekran, Model 2357A - Principles of Operation.*

Thermo Fisher Scientific. (2014). *Mercuric Chloride Generator (Instruction Manual).* https://www.thermofisher.com/si/en/home.html

Tong, Y., Eichhorst, T., Olson, M. R., McGinnis, J. E., Turner, I., Rutter, A. P., Shafer, M. M., Wang, X., & Schauer, J. J. (2013). Atmospheric photolytic reduction of Hg(ii) in dry aerosols. *Environmental Sciences: Processes and Impacts*, *15*(10), 1883–1888. https://doi.org/10.1039/c3em00249g

Tong, Y., Eichhorst, T., Olson, M. R., Rutter, A. P., Shafer, M. M., Wang, X., & Schauer, J. J. (2014). Comparison of heterogeneous photolytic reduction of Hg(II) in the coal fly ashes and synthetic aerosols. *Atmospheric Research*, *138*, 324–329. https://doi.org/10.1016/j.atmosres.2013.11.015

Travnikov, O., Angot, H., Artaxo, P., Bencardino, M., Bieser, J., D'Amore, F., Dastoor, A., De Simone, F., DIéguez, M. C., Dommergue, A., Ebinghaus, R., Bin Feng, X., Gencarelli, C. N., Hedgecock, I. M., Magand, O., Martin, L., Matthias, V., Mashyanov, N., Pirrone, N., … Yang, X. (2017). Multi-model study of mercury dispersion in the atmosphere: Atmospheric processes and model evaluation. *Atmospheric Chemistry and Physics*, *17*(8), 5271–5295. https://doi.org/10.5194/acp-17-5271-2017

U.S. Environmental Protection Agency. (2002). *EPA Method 1631, Revision E: Mercury in Water by Oxidation, Purge and Trap, and Cold Vapor Atomic Fluorescence: Vol. Revision E* (p. 38). US Environmental Protection Agency.

U.S. Environmental Protection Agency. (2017). *Method 30A — Determination of Total Vapor Phase Mercury Emissions from Stationary Sources (Instrumental Analyzer Procedure).* https://www.epa.gov/emc

UN Environment. (2019). *Global mercury assessment 2018* (pp. 1–258). https://www.unep.org/resources/publication/global-mercury-assessment-2018

Unagar, A., Hashmi, A., Tiwari, A. K., Jawak, S. D., Desai, B., Urba, A., & Qureshi, A. (2021). Coast of Eastern Antarctica as the source of atmospheric mercury during austral summer. *Atmospheric Pollution Research*, *12*(12), 101226. https://doi.org/10.1016/j.apr.2021.101226

United States Environmental Protection Agency (U.S. EPA). (1996). *Method 29 – Metals Emissions from Stationary Sources.*

United States Environmental Protection Agency (U.S. EPA). (1999). Chapter IO-5, Sampling and analysis for atmospheric mercury, US EPA. In *Compendium of Methods for the Determination of Inorganic Compounds in Ambient Air.*

Urba, A., Kvietkus, K., Sakalys, J., Xiao, Z., & Lindqvist, O. (1995). A New Sensitive and Portable Mercury Vapor Analyzer Gardis-1A. *Water, Air, and Soil Pollution*, *80*, 1305–1309. https://doi.org/10.1007/978-94-011-0153-0_148

Van Loon, L., Mader, E., & Scott, S. L. (2000). Reduction of the aqueous mercuric ion by sulfite: UV spectrum of HgSO3 and its intramolecular redox reaction. *Journal of Physical Chemistry A*, *104*(8), 1621–1626. https://doi.org/10.1021/jp994268s

Veiga, M. M., Angeloci-Santos, G., & Meech, J. A. (2014). Review of barriers to reduce mercury use in artisanal gold mining. *Extractive Industries and Society*, *1*(2), 351–361. https://doi.org/10.1016/j.exis.2014.03.004

Wang, S., Holsen, T. M., Huang, J., & Han, Y.-J. (2013). Evaluation of various methods to measure particulate bound mercury and associated artifacts. *Atmospheric Chemistry and Physics Discussions*, *13*(4), 8585–8614. https://doi.org/10.5194/acpd-13-8585-2013

Wang, Z., & Pehkonen, S. O. (2004). Oxidation of elemental mercury by aqueous bromine: Atmospheric implications. *Atmospheric Environment*, *38*(22), 3675–3688. https://doi.org/10.1016/j.atmosenv.2004.02.059

Weiss-Penzias, P. S., Gay, D. A., Brigham, M. E., Parsons, M. T., Gustin, M. S., & ter Schure, A. (2016). Trends in mercury wet deposition and mercury air concentrations across the U.S. and Canada. *Science of the Total Environment*, *568*, 546–556. https://doi.org/10.1016/j.scitotenv.2016.01.061

White, E. M., Landis, M. S., Keeler, G. J., & Barres, J. A. (2013). Investigation of mercury wet deposition physicochemistry in the Ohio River Valley through automated sequential sampling. *Science of the Total Environment*, *448*, 107–119. https://doi.org/10.1016/j.scitotenv.2012.12.046

Xie, J., Qu, Z., Yan, N., Yang, S., Chen, W., Hu, L., Huang, W., & Liu, P. (2013). Novel regenerable sorbent based on Zr-Mn binary metal oxides for flue gas mercury retention and recovery. *Journal of Hazardous Materials*, *261*, 206–213. https://doi.org/10.1016/j.jhazmat.2013.07.027

Xu, H., Xie, J., Ma, Y., Qu, Z., Zhao, S., Chen, W., Huang, W., & Yan, N. (2015). The cooperation of FeSn in a MnOx complex sorbent used for capturing elemental mercury. *Fuel*, *140*, 803–809. https://doi.org/10.1016/j.fuel.2014.10.004

Xu, L., Chen, J., Yang, L., Niu, Z., Tong, L., Yin, L., & Chen, Y. (2015). Characteristics and sources of atmospheric mercury speciation in a coastal city, Xiamen, China. *Chemosphere*, *119*, 530–539. https://doi.org/10.1016/j.chemosphere.2014.07.024

Yang, X., Jiskra, M., & Sonke, J. E. (2019). Experimental rainwater divalent mercury speciation and photoreduction rates in the presence of halides and organic carbon. *Science of the Total Environment*, *697*, 133821. https://doi.org/10.1016/j.scitotenv.2019.133821

Ye, Z., Mao, H., Lin, C. J., & Youn Kim, S. (2016). Investigation of processes controlling summertime gaseous elemental mercury oxidation at midlatitudinal marine, coastal, and inland sites. *Atmospheric Chemistry and Physics*, *16*(13), 8461–8478. https://doi.org/10.5194/acp-16-8461-2016

Yu, B., Yang, L., Wang, L., Liu, H., Xiao, C., Liang, Y., Liu, Q., Yin, Y., Hu, L., Shi, J., & Jiang, G. (2020). New evidence for atmospheric mercury transformations in the marine boundary layer from stable mercury isotopes. *Atmospheric Chemistry and Physics*, *20*(16), 9713–9723. https://doi.org/10.5194/acp-20-9713-2020

Yuan, W., Sommar, J., Lin, C. J., Wang, X., Li, K., Liu, Y., Zhang, H., Lu, Z., Wu, C., & Feng, X. (2019). Stable Isotope Evidence Shows Re-emission of Elemental Mercury Vapor Occurring after Reductive Loss from Foliage. *Environmental Science and Technology*, *53*(2), 651–660. https://doi.org/10.1021/acs.est.8b04865

Zhang, H., Fu, X. W., Lin, C. J., Wang, X., & Feng, X. B. (2015). Observation and analysis of speciated atmospheric mercury in Shangri-La, Tibetan Plateau, China. *Atmospheric Chemistry and Physics*, *15*(2), 653–665. https://doi.org/10.5194/acp-15-

653-2015

Zhang, Hui, Fu, X., Wang, X., & Feng, X. (2019). Measurements and Distribution of Atmospheric Particulate-Bound Mercury: A Review. *Bulletin of Environmental Contamination and Toxicology*, *103*(1), 48–54. https://doi.org/10.1007/s00128-019-02663-5

Zhang, L., Zhou, P., Cao, S., & Zhao, Y. (2019). Atmospheric mercury deposition over the land surfaces and the associated uncertainties in observations and simulations: A critical review. *Atmospheric Chemistry and Physics*, *19*(24), 15587–15608. https://doi.org/10.5194/acp-19-15587-2019

Zhang, X., Siddiqi, Z., Song, X., Mandiwana, K. L., Yousaf, M., & Lu, J. (2012). Atmospheric dry and wet deposition of mercury in Toronto. *Atmospheric Environment*, *50*, 60–65. https://doi.org/10.1016/j.atmosenv.2011.12.062

Zhang, Y., Jacob, D. J., Horowitz, H. M., Chen, L., Amos, H. M., Krabbenhoft, D. P., Slemr, F., St. Louis, V. L., & Sunderland, E. M. (2016). Observed decrease in atmospheric mercury explained by global decline in anthropogenic emissions. *Proceedings of the National Academy of Sciences of the United States of America*, *113*(3), 526–531. https://doi.org/10.1073/pnas.1516312113

Zhou, H., Zhou, C., Hopke, P. K., & Holsen, T. M. (2018). Mercury wet deposition and speciated mercury air concentrations at rural and urban sites across New York state: Temporal patterns, sources and scavenging coefficients. *Science of the Total Environment*, *637–638*, 943–953. https://doi.org/10.1016/j.scitotenv.2018.05.047

Živković, I., Berisha, S., Kotnik, J., Jagodic, M., & Horvat, M. (2020). Traceable determination of atmospheric mercury using iodinated activated carbon traps. *Atmosphere*, *11*(8), 1–14. https://doi.org/10.3390/ATMOS11080780

Živković, I., Humphreys, M. P., Achterberg, E. P., Dumousseaud, C., Woodward, E. M. S., Bojanić, N., Šolić, M., Bratkič, A., Kotnik, J., Vahčič, M., Obu Vazner, K., Begu, E., Fajon, V., Shlyapnikov, Y., & Horvat, M. (2022). Enhanced mercury reduction in the South Atlantic Ocean during carbon remineralization. *Marine Pollution Bulletin*, *178*, 113644. https://doi.org/10.1016/j.marpolbul.2022.113644

Bibliography

Publications Related to the Thesis

Journal Articles

De Krom, I., Bavius, W., Ziel, R., Mcghee, E. A., Brown, R. J. C., Živković, I., Gačnik, J., Fajon, V., Kotnik, J., Horvat, M., & Ent, H. (2021). Comparability of calibration strategies for measuring mercury concentrations in gas emission sources and the atmosphere. *Atmospheric Measurement Techniques*, *14*(3), 2317–2326. https://doi.org/10.5194/amt-14-2317-2021

Gačnik, J., Živković, I., Ribeiro Guevara, S., Jaćimović, R., Kotnik, J., De Feo, G., Dexter, M., Corns, W., & Horvat, M. (2021). Behaviour of KCl sorbent traps and KCl trapping solutions used for atmospheric mercury speciation: stability and specificity. *Atmospheric Measurement Techniques*, *14*(10), 6619–6631. https://doi.org/10.5194/amt-2021-153

Gačnik, J., Živković, I., Ribeiro Guevara, S., Jaćimović, R., Kotnik, J., & Horvat, M. (2021). Validating an evaporative calibrator for gaseous oxidized mercury. *Sensors*, *21*(7), 2501. https://doi.org/10.3390/s21072501

Gačnik, J., Živković, I., Ribeiro Guevara, S., Kotnik, J., Berisha, S., Vijayakumaran Nair, S., Jurov, A., Cvelbar, U., & Horvat, M. (2022). Calibration Approach for Gaseous Oxidized Mercury Based on Nonthermal Plasma Oxidation of Elemental Mercury. *Analytical Chemistry*, *94*(23), 8234–8240. https://doi.org/10.1021/acs.analchem.2c00260

Conference Paper

Gačnik, J., Ribeiro Guevara, S., Kotnik, J., Živković, I., & Horvat, M. (2019). Evaluation of calibration and sampling methods of gaseous oxidized mercury in air using the 197Hg radiotracer. 14th International Conference on Mercury as a Global Pollutant, ICMGP 2019, 8-13 September 2019, Krakow, Poland. https://mercury2019krakow.com/public/files/ICMGP2019-abstract-volume.pdf

Gačnik, J., Saxholm, S., Igor, Ž., Ribeiro Guevara, S., Jaćimović, R., Rajamäki, T., Kotnik, J., & Horvat, M. (2021). Validation of an evaporative calibrator for gaseous oxidized mercury. CIM 2021, 20th International Metrology Congress, 7-9 September 2021, Lyon, France. https://www.cim2021.com/files/programmes/CIM2021-PapersAbstract-V1.pdf

Gačnik, J., Živković, I., Kotnik, J., Božič, D., Maaire Gyengne, F., BerishaA, S., Tassone, A., Naccarato, A., Pirrone, N., Sprovieri, F., & Horvat, M. (2022). Comparison of yearly atmospheric mercury monitoring with passive sampling, biomonitoring and active measurements. Reducing Mercury Emissions to Achieve a Greener World : 15th International Conference on Mercury as a Global Pollutant (ICMGP), 24- 29 July 2022, Virtual Event. https://app.swapcard.com/widget/event/icmgp-2022/planning/UGxhbm5pbmdfOTUxNjIw

Gačnik, J., Živković, I., Kotnik, J., Vijayakumaran Nair, S., Cvelbar, U., & Horvat, M. (2022). Validation of Sampling Methods for Gaseous Oxidized Mercury Using Traceable Calibration Procedure. Reducing Mercury Emissions to Achieve a Greener World : 15th International Conference on Mercury as a Global Pollutant (ICMGP), 24th - 29th July 2022, Virtual Event. https://app.swapcard.com/event/icmgp-2022/planning/UGxhbm5pbmdfOTUxNjA5

Gačnik, J., Živković, I., Ribeiro Guevara, S., Kotnik, J., Vijayakumaran Nair, S., Jurov, A., Cvelbar, U., Andron, T. D., & Horvat, M. (2022). Development of a Traceable Calibration for Gaseous Oxidized Mercury Species Based on Non-Thermal Plasma Approach. Reducing Mercury Emissions to Achieve a Greener World : 15th International Conference on Mercury as a Global Pollutant (ICMGP), 24th - 29th July 2022, Virtual Event. https://app.swapcard.com/event/icmgp-2022/planning/UGxhbm5pbmdfOTU2MTgx

Gačnik, J., Živković, I., Vijayakumaran Nair, S., Kotnik, J., Jurov, A., & Horvat, M. (2022). Gaseous oxidized mercury calibration by non-thermal plasma. 14th CEM 2022, Emission Monitoring, 2-4 March 2022 : Virtual Meeting. https://www.ilmexhibitions.com/cem/abstract/Gaseous+oxidized+mercury+calibration+by+non-thermal+plasma/1275/

Horvat, M., Živković, I., Gačnik, J., Kotnik, J., Ribeiro Guevara, S., Fettig, I., Rajamäki, T., Petrov, P., de Krom, I., Amouroux, D., Tessier, E., Donard, O. F. X., del Rocio Arvizu, M., Corns, W. T., Hedgecock, I. M., Naccarato, A., Pirrone, N., Sprovieri, F., Moeseler, R., & Can, S. (2019). Traceability of oxidized mercury measurements in air. AGU 100, Fall Meeting, Washington, D.C., 9-13 December 2019. https://agu.confex.com/agu/fm19/meetingapp.cgi/Paper/501506

Kotnik, J., Živković, I., Gačnik, J., Jurov, A., Cvelbar, U., & Horvat, M. (2019). Novel plasma oxidized mercury source. 14th International Conference on Mercury as a Global Pollutant, ICMGP 2019, 8-13 September 2019, Krakow, Poland.

Tulasi, D., Gačnik, J., Fajon, V., Živković, I., Adotey, D., Serfor-Armani, Y., & Horvat, M. (2019). Speciation of mercury in fish, water and sedimet from ponds in artisanal and small scale gold mining communities of South Western Ghana. 14th International Conference on Mercury as a Global Pollutant, ICMGP 2019, 8-13 September 2019, Krakow, Poland. https://mercury2019krakow.com/public/files/ICMGP2019-abstract-volume.pdf

Vijayakumaran Nair, S., Gačnik, J., Živković, I., & Horvat, M. (2022). Gas-phase Photoreduction and Losses of HgII from KCl-coated Denuders Used for Sampling Gaseous Oxidised Mercury Species. Reducing Mercury Emissions to Achieve a Greener World : 15th International Conference on Mercury as a Global Pollutant

(ICMGP), 24th - 29th July 2022, Virtual Event. https://app.swapcard.com/event/icmgp-2022/planning/UGxhbm5pbmdfOTU2MTg0

Vijayakumaran Nair, S., Gačnik, J., Živković, I., Kotnik, J., Koenig, A. M., Ljubič Mlakar, T., & Horvat, M. (2022). Mercury Emission and Speciation in the Vicinity of Salonit Anhovo Cement Plant in Western Slovenia. Reducing Mercury Emissions to Achieve a Greener World : 15th International Conference on Mercury as a Global Pollutant (ICMGP), 24th - 29th July 2022, Virtual Event. https://app.swapcard.com/event/icmgp-2022/planning/UGxhbm5pbmdfOTUxNTcz

Živković, I., Gačnik, J., Jozić, S., Kotnik, J., Šolić, M., & Horvat, M. (2022). Normalized wet deposition of total mercury reflects concentration gradient in surface seawater. Goldschmidt 2022 : Honolulu, Hawai'i, USA and Online, 10-15 July 2022. https://conf.goldschmidt.info/goldschmidt/2022/meetingapp.cgi/Paper/11806

Biography

The author of this dissertation Jan Gačnik was born on July 2, 1994 in Novo mesto, Slovenia. He finished his primary school in Žužemberk, Slovenia and high school at Gymnasium Novo mesto, Novo mesto, Slovenia. In 2013, he started his undergraduate studies in "Chemistry" at the Faculty of Chemistry and Chemical Technology, Ljubljana, Slovenia and received his BSc degree in chemistry in 2016. In the same year, he enrolled in the graduate program "Chemistry" at the same faculty. During undergraduate and graduate studies, he collaborated with the Department of Environmental Sciences at Jožef Stefan Institute, where he was trained in analytical chemistry and radiochemistry. He also obtained a certificate for working with open radioactive sources at the Milan Čopič Nuclear Training Centre. After successfully defending his master's thesis entitled "Development and optimization of methods for determination of ^{90}Sr in water samples" he received his MSc degree in chemistry in 2018. Following the master's degree, he started his PhD studies in the same year at the Jožef Stefan International Postgraduate School, Ljubljana, Slovenia, under the supervision of Asst. Prof. Dr. Jože Kotnik and Prof. Dr. Milena Horvat.

The majority of the experimental work was conducted in the facilities of the Department of Environmental Sciences, Jožef Stefan Institute. The candidate visited and collaborated with international researchers from research institutes such as the Dutch Metrology Institute (Delft, Netherlands), LGC Group Ltd. (Teddington, United Kingdom), University of Nevada, Reno (Reno, Nevada, United States of America) and more. His research focuses on atmospheric mercury and with special emphasis on the metrology of atmospheric mercury species. His first goal was to evaluate the currently used methodology for atmospheric mercury speciation. The evaluation was made possible by cooperation with Bariloche Atomic Centre (Bariloche, Argentina), where the candidate acquired the knowledge to work with the ^{197}Hg radiotracer. This knowledge was also used in the development of a novel approach for the calibration of gaseous oxidized mercury species. Additionally, his work has been presented to international audiences at several conferences related to metrology, mercury as a global contaminant, and gaseous pollutant measurements.